UNIVERSITÉ DE TOURS

ÉCOLE DOCTORALE « Santé, Sciences Biologiques et Chimie du Vivant »

ÉQUIPE de RECHERCHE « EA 6295 Nanomédicaments et nanosondes »

THÈSE présentée par :

Sanaa BEN DJEMAA

soutenue le : **24 octobre 2019**

pour obtenir le grade de : **Docteur de l'université de Tours**

Discipline/ Spécialité : Sciences de la Vie et de la Santé

Nanovectorisation de siRNA pour le traitement du cancer du sein triple négatif

THÈSE dirigée par :

Mme MUNNIER Emilie	Maître de conférences-HDR, Université de Tours
Mme ALLARD-VANNIER Emilie	Maître de conférences-HDR, Université de Tours

RAPPORTEURS :

M. MONTIER Tristan	Professeur des universités-praticien hospitalier, Université de Brest
M. BLANQUART Christophe	Chargé de recherche-HDR, Université de Nantes

---

JURY :

Mme ALLARD-VANNIER Emilie	Maître de conférences-HDR, Université de Tours
M. BLANQUART Christophe	Chargé de recherche-HDR, Université de Nantes
M. MONTIER Tristan	Professeur des universités-praticien hospitalier, Université de Brest
Mme MUNNIER Emilie	Maître de conférences-HDR, Université de Tours
M. LAGARCE Frederic	Professeur des universités-praticien hospitalier, Université d'Angers
Mme PICHON Chantal	Professeur des universités, Université d'Orléans

MEMBRE INVITE :

Mme. DAVID Stéphanie	Maître de conférences, Université de Tours

Remerciements

Je tiens tout d'abord à remercier les membres du jury d'avoir accepté d'évaluer ce travail de thèse.

Cette thèse n'aurait pas été possible sans l'aide et le soutien apportés par de nombreuses personnes avec lesquelles j'ai eu la chance d'interagir au cours de ces dernières années. Je tiens donc, à travers ces quelques mots, à leur exprimer ma reconnaissance.

Je tiens à remercier notre chef d'équipe Pr. Igor Chourpa pour m'avoir accueillie dans son équipe et de m'avoir donné l'opportunité de réaliser ma thèse dans le laboratoire.

Un très grand merci à ma directrice de thèse Dr. Emilie Munnier, ma co-directrice de thèse Dr. Emilie Allard-Vannier et mon encadrante Dr. Stéphanie David. Merci de m'avoir accordé votre confiance pour mener à bien ces travaux, pour vos conseils, pour toutes les connaissances que vous m'avez transmises et pour la liberté que vous m'avez laissée. Merci pour ces trois ans.

Je voudrais remercier Le Pr. Stefania Galdiero et le Dr. Annarita Falanga, de l'université de Naples, pour ces trois ans de collaboration, pour leur disponibilité et pour le peptide que vous nous avez fourni.

J'exprime mes remerciements à :

Dr. Katel Hervé-Aubert, notre chimiste et experte des SPION, pour sa disponibilité, ses conseils et pour le temps qu'elle a consacré pour me transmettre son savoir-faire.

Dr. Martin Soucé pour sa disponibilité et de m'avoir aidé à réaliser des analyses HPLC.

Dr. Laurie Lajoie, Dr. Audrey Oudin et Steven Nedellec de m'avoir accueillie dans leurs laboratoires et m'avoir aidé pour la réalisation de la cytométrie/imagerie en flux, la RT-qPCR et l'imagerie confocale, respectivement.

Je tiens également à remercier tous les membres, permanents et non permanents, de l'équipe Nanomédicaments et Nanosondes, pour leur bienveillance et leur soutien.

L'ambiance de travail que j'ai connu au cours de ces trois ans de thèse a été dépendante de la présence des personnes qui m'ont entouré au quotidien, sans donner des noms (vous êtes très nombreux), et surtout de leur bonne humeur. Merci pour les discussions intéressantes et les

moins intéressantes, les pauses, les blagues, les soirées et tous les bons moments partagés ensemble.

Enfin, je voudrais remercier toute personne ayant cru en moi …

Résumé

Dans l'optique d'améliorer le traitement du cancer du sein triple négatif (CSTN), les objectifs de ces travaux de thèse sont : i) d'optimiser la formulation d'un nanovecteur de siRNA fonctionnalisé par un peptide membranotrope (CS-MSN) pour augmenter son efficacité de transfection et pour avoir des caractéristiques compatibles avec une administration par voie systémique, ii) étudier ses voies d'internalisation et son trafic et devenir intracellulaire et iii) valider son efficacité sur un modèle cellulaire de CSTN. L'optimisation de la formulation des CS-MSN a abouti à un nanovecteur d'une taille d'environ 170 nm avec une charge de surface légèrement positive. Les CS-MSN ont montré une capacité à protéger les siRNA contre la dégradation en présence de sérum sans toxicité remarquable sur les cellules. L'entrée des CS-MSN dans les cellules est augmentée par la présence du peptide gH625 à leur surface et elle implique une voie d'endocytose clathrines et cavéoles dépendante. Les CS-MSN ont montré une capacité à échapper à la dégradation par les vésicules endo-lysosomales, cet échappement étant facilité par la présence du peptide gH625. Cet échappement résulte en une inhibition de 73 % de l'expression de la protéine GFP et une réduction significative de l'ARNm et de la protéine Bcl-xL.

Mots clés : nanovecteur, siRNA, transfection, trafic intracellulaire, peptide gH625, polymères

Abstract

In order to improve the treatment of triple negative breast cancer (TNBC), the objectives of this work are: i) to optimize the formulation of a siRNA nanovector (CS-MSN) functionalized by a cell-penetrating peptide to increase its transfection efficiency and to obtain features compatible with a systemic administration, ii) to investigate its internalization mechanisms and pathways and its intracellular trafficking and iii) to validate its efficiency on a TNBC cell model. The optimization of CS-MSN formulation resulted in a nanovector with a size of about 170 nm with a slightly positive surface charge. CS-MSN showed an ability to protect siRNA against degradation in the presence of serum without remarkable cell toxicity. The entry of CS-MSN in cells is enhanced by the presence of the membranotropic peptide gH625 on their surface and involves clathrin- and caveolae-mediated endocytosis pathway. CS-MSN showed an ability to escape degradation in endo-lysosomal vesicles, facilitated by the gH625 peptide. This endosomal escape results in 73 % of inhibition of the GFP protein expression and a significant reduction of Bcl-xL mRNA and protein.

Keywords: nanovecteor, siRNA, transfection, intracellular trafficking, gH625 peptide, polymers

Table des matières

Remerciements……..……1
Résumé…….....3
Abstract……..……4
Table des matières……...5
Liste des tableaux……7
Liste des figures……...8
Listes des annexes……10

Introduction……..……...11
1. Le cancer, une urgence sanitaire……11
1.1. Le cancer du sein……...11
1.2. Les cancers du sein triple négatif……..13
2. L'expression génique et sa régulation……...13
2.1. Les étapes de l'expression génique……13
2.2. Régulation de l'expression génique par le mécanisme d'ARN interférence……....16
2.3. Petits ARN interférents (siRNA)……...17
3. Développement des stratégies thérapeutiques basées sur les siRNA pour le traitement du cancer……..……19
3.1. Limites d'utilisation des siRNA……20
3.2. Nanovectorisation des siRNA……...21
3.2.1. Les nanovecteurs lipidiques…….……..22
3.2.2. Les nanovecteurs polymères……..…23
3.2.3. Les nanovecteurs peptidiques……24
3.2.4. Les nanovecteurs hybrides à cœur inorganique…….25
3.3. Les essais cliniques de nanovecteurs de siRNA pour le traitement des cancers……...25
4. Internalisation et trafic intracellulaire de nanovecteurs de siRNA……29
4.1. Voies d'internalisation…… ……..29
4.1.1. Les voies d'entrée médiées par endocytose : ……29
4.1.2. Les voies d'entrée indépendantes de l'endocytose : ……32
4.2. Trafic intracellulaire……..33
Objectifs de la thèse……...38

Première partie : Nanovecteurs polymères de siRNA assemblés électrostatiquement……40

Publication 1: Versatile electrostatically assembled polymeric siRNA nanovectors: can they overcome the limits of siRNA tumor delivery?.....41

Deuxième partie : Développement, caractérisation et évaluation in vitro d'un nanovecteur magnétique pour la délivrance des siRNA…….58

Publication 2: Formulation and in vitro evaluation of a siRNA delivery nanosystem decorated with gH625 peptide for triple negative breast cancer theranosis……..59

Troisième partie : Internalisation, trafic intracellulaire et devenir de nanovecteur de siRNA..73

Publication 3: gH625 cell-penetrating peptide promote the endosomal escape of nanovectorized siRNA in triple negative breast cancer cells…….75

Quatrième partie : Efficacité du nanovecteur de siRNA sur le gène cible codant pour la protéine Bcl-xL……..93

Observations complémentaires et discussion……..117

Conclusion……..134

Bibliographie……...137

Annexes……...160

Liste des tableaux

Tableau I. Nanovecteurs de siRNA anticancéreux en essais cliniques (78,79)……28
Tableau II. Séquences des siRNA utilisées……...96
Tableau III. Protocole de la rétrotranscription……..97
Tableau IV. Protocole de la PCR……..99
Tableau V. Programme de la PCR……99
Tableau VI. Séquences des amorces de gènes Bcl-xL et GAPDH utilisées……100
Tableau VII. Protocole de la qPCR……..100
Tableau VIII. Programme de la qPCR……100
Tableau IX. Taille, indice de polydispersité (PDI), potentiel zêta (ZP) et osmolarité des CS-MSN préparés pour une application in vitro ou in vivo……..104

Liste des figures

Figure 1. Les étapes de l'expression génique de l'ADN jusqu'à la protéine……..15
Figure 2. Illustration des différentes étapes de la production des siRNA endogènes et du déclenchement de la dégradation de l'ARNm cible par le mécanisme d'ARNi……19
Figure 3. Représentation schématique de la structure des nanovecteurs lipidiques (d'après Granot et al. 2017 et Kong et al. 2013 (53,54)……..23
Figure 4. Représentation schématique de la structure des nanovecteurs polymères……....24
Figure 5. Illustration de l'entrée des nanovecteurs par macropinocytose, par endocytose médiée par les clathrines et par endocytose cavéole-dépendante ainsi que du trafic associé à chaque voie (modifiée d'après Hillaireau et Couvreur, 2009 (84))……32
Figure 6. Illustration schématique de l'effet pompe à proton (modifiée d'après Bus et al., 2018 (96))……...34
Figure 7. Représentation de l'effet parapluie induit par certains polymères (modifiée d'après Nguyen et Szoka, 2012 (97))……35
Figure 8. Illustration de la formation de pores transitionnels au niveau de la membrane endosomale induit par certains polymères (modifiée d'après Bus et al., 2018 (96))……..36
Figure 9. Illustration de l'échappement endosomal par fusion de liposome avec la membrane endosomale……37
Figure 10. Gel d'agarose pour évaluer la complexation des siRNA dans les CS-MSN et la libération des siRNA en présence de la solution d'héparine (A) pour une application in vitro ou (B) in vivo……104
Figure 11. Gel d'agarose pour vérifier la rétrotranscription des ARN en ADNc et l'amplification par PCR…….. 105
Figure 12. Gel d'agarose pour vérifier l'amplification de l'ADN par PCR en utilisant les amorces A) N°1 et B) N°2……106
Figure 13. Courbes de calibration des amorces N°1 des gènes A) Bcl-xL et B) GAPDH et des amorces N°2 des gènes C) Bcl-xL et D) GAPDH……106
Figure 14. Expression de la protéine Bcl-xL normalisée par rapport à l'expression de la protéine GAPDH dans des cellules MDA-MB-231 traitées ou non avec l'Oligofectamine™ préparé avec les différentes séquences des siRNA (1, 2 ou 3) ou le mélange de trois séquences, à une concentration en siRNA de 50 nM……...……107
Figure 15. Expression de l'ARNm Bcl-xL relative à l'expression de l'ARNm GAPDH dans des cellules MDA-MB-231 traitées ou non avec l'Oligofectamine™ préparé avec les différentes séquences des siRNA (1, 2 ou 3) ou le mélange de trois séquences, à une concentration en siRNA de 50 nM……..108
Figure 16. Viabilité cellulaire des cellules MDA-MB-231 traitées ou non avec H2O2, siRNA anti-Bcl-xL libres, Oligofectamine™ ou CS-MSN (50nM) pendant 24 h, 48 h, 72 h ou 96 h …….....109
Figure 17. Evaluation de l'expression de la protéine Bcl-xL dans des cellules MDA-MB-231 traitées ou non avec l'Oligofectamine™ ou les CS-MSN à une concentration de 50 nM en siRNA……..110
Figure 18. Evaluation de l'expression de la protéine Bcl-xL dans des cellules MDA-MB-231 traitées ou non avec des CS-MSN à différentes concentrations (50, 100 ou 200 nM)……..111

Figure 19. Expression de l'ARNm Bcl-xL relative à l'expression de l'ARNm GAPDH dans des cellules MDA-MB-231 traitées on non avec l'Oligofectamine™ ou des CS-MSN à différentes concentrations (50, 100 ou 200 nM en siRNA)……112
Figure 20. Image en échographie d'une tumeur orthotopique de cancer du sein triple négatif chez la souris après injection intraveineuse d'un agent de contraste……113
Figure 21. Taux d'évolution de la masse des souris comparé au jour 0……114
Figure 22. Chromatogramme HPLC des CS-FNP avant et après dialyse pour la détection du peptide gH625 libre……120
Figure 23. Images des cellules MDA-MB-231 incubées avec des CS-MSN marqués avec la cyanine 5.5 (bleu, ligne de haut) ou la sulfocyanine 5 (rouge, ligne de bas) et préparés avec des siRNA conjugués à l'Alexa Fluor 488, et obtenues par imagerie en flux AMNIS®……....121
Figure 24. Illustration schématique des types d'interactions entre les différents composants du nanovecteur……122

Listes des annexes

Annexe 1 : Fluorescence Microscopy as a Tool for Nanomedicine-Cell Interactions Study: Input of Particle Design and of Analytical Strategy……..161
Annexe 2 : siRNA delivery system based on magnetic nanovectors: Characterization and stability evaluation……..165
Annexe 3 : Stealth magnetic nanocarriers of siRNA as platform for breast cancer theranostics ……173
Annexe 4 : Magnetic nanocarriers for the specific delivery of siRNA: Contribution of breast cancer cells active targeting for down-regulation efficiency……183
Annexe 5: Curriculum Vitae……193

Introduction

1. Le cancer, une urgence sanitaire

Plusieurs études ont montré que le cancer est l'une des maladies les plus fréquentes dans le monde. Le GLOBOCAN 2018 de l'Agence Internationale pour la Recherche sur le Cancer (International Agency for Research on Cancer, IARC), affirme qu'en 2018 le nombre de nouveaux cas de cancer a augmenté pour atteindre 18,1 millions de cas avec 9,6 millions de décès, soit une augmentation de 4 millions et de 1,4 millions, respectivement, en 6 ans (1,2). Outre, en se basant sur les changements démographiques, le vieillissement et la croissance de la population mondiale, le nombre de nouveaux cas est estimé à 29,4 millions en 2040 (3). L'augmentation rapide du nombre de cas de cancer représente un fardeau lourd pour l'économie et la santé publique. En effet, en 2008 le coût de la prise en charge du cancer dans l'Union européenne est estimé à 126 milliards d'euros (4).

Le terme cancer désigne une maladie caractérisée par la croissance et la division rapides et la prolifération incontrôlable de cellules anormales au niveau d'un organe, liées à une dérégulation de mécanismes qui assurent la survie normale d'un organisme (5). Les cellules cancéreuses ont une capacité à ignorer la signalisation cellulaire normale et à influer sur leur environnement. En effet, elles sont capables de contourner le fonctionnement des cellules normales voisines et de la vascularisation pour assurer leur survie. L'environnement qu'elles créent autour d'elles favorise une angiogenèse accélérée pour garantir un apport nutritionnel continu et suffisant pour la formation et la croissance d'une tumeur. Cette tumeur a la capacité d'altérer les tissus hôtes et leurs fonctionnements normaux. La situation peut s'aggraver encore plus quand certaines cellules se détachent de la masse tumorale et migrent vers d'autres organes dans le corps à travers la circulation sanguine ou le système lymphatique pour donner naissance à des foyers secondaires appelés métastases.

1.1. Le cancer du sein

Le cancer du sein est le cancer féminin le plus commun dans le monde. Il est le cancer le plus diagnostiqué chez la femme et il représente 24,4 % des cas de cancers, c'est-à-dire qu'environ 1 nouveau cas de cancer chez la femme dans le monde sur 4 est un cancer du sein. En 2018, il représente le premier cancer au niveau de prévalence, le deuxième cancer au niveau

de l'incidence et le cinquième au niveau de la mortalité. Durant l'année 2018, ce cancer a causé 627 000 décès, soit 6,6 % des cas de décès causés par le cancer (1,6).

Le cancer du sein est une tumeur maligne qui se développe au niveau de la glande mammaire. Dans la majorité des cas, ce cancer est un adénocarcinome (95 %), c'est-à-dire qu'il se développe à partir d'un épithélium glandulaire. Ce type se devise lui-même en deux sous-types : le cancer canalaire, le plus fréquent, qui prend naissance dans le revêtement des canaux galactophores du sein et le cancer lobulaire qui prend naissance dans les glandes productrices de lait. Les cancers du sein sont associés à plusieurs facteurs de risques comme l'obésité, la contraception hormonale ou les traitements hormonaux, les grossesses tardives, la ménopause tardive, la consommation d'alcool, le diabète de type 2, l'absence d'activité physique, les antécédents familiaux de cancer du sein. L'augmentation du risque de cancer du sein peut être aussi liée à certaines mutations génétiques notamment au niveau des gènes BRCA1, BRCA2 et p53. Cependant, ces mutations sont rares et ne représentent qu'un faible pourcentage de l'ensemble des cancers du sein. Malgré la bonne connaissance de ces facteurs de risque, il est difficile d'identifier des facteurs spécifiques dans la majorité des cas de ce cancer (7).

En se basant sur le profil immunohistochimique, on distingue les sous-types moléculaires de cancer du sein suivants :

- Luminal A : il est caractérisé par la présence des récepteurs hormonaux (récepteurs aux estrogènes (ER+) et/ou à la progestérone (PR+)) et l'absence de récepteur 2 du facteur de croissance épidermique humain (HER2-). Ce type croît lentement, a le meilleur pronostic et répond bien à l'hormonothérapie.
- Luminal B : ce sous-type est caractérisé par la présence des récepteurs hormonaux (ER+ et/ou PR+) et d'HER2. Ce type croît légèrement plus vite que le type précédent, présente un pronostic plus défavorable et est généralement traité par l'association de l'hormonothérapie et de la chimiothérapie.
- HER2 + : il est caractérisé par l'absence des récepteurs hormonaux (ER- et/ou PR-) et par la surexpression d'HER2. Ces cancers tendent à croître plus rapidement que les cancers luminaux ce qui engendre un mauvais pronostic. Cependant, ils sont souvent traités avec succès avec des thérapies qui ciblent la protéine HER2.
- Triple négatif ou aussi appelé type basal : ce sous-type est caractérisé par l'absence de récepteurs hormonaux (ER- et/ou PR-) et d'HER2 (HER2-). Ce type est plus commun chez les femmes avec des mutations de gène BRCA1 et il a un très mauvais pronostic (8).

1.2. Les cancers du sein triple négatifs

Les cancers du sein triple négatifs (CSTN) représentent environ 20 % des cancers du sein. Ils sont classés parmi les formes les plus agressives et sont associés à un mauvais pronostic. Malgré leur appartenance au même groupe, les cancers du sein triple négatifs sont très hétérogènes et ils peuvent être encore classés dans plusieurs sous-groupes selon leurs profils cliniques, histopathologiques, moléculaires et génétiques (9). L'absence de récepteurs hormonaux et de récepteurs spécifiques (tels que HER2) fait que la croissance de ces cancers est indépendante de la stimulation hormonale et d'HER2. Cela indique qu'il est improbable que ces cancers répondent aux traitements hormonaux, notamment le tamoxifène et les inhibiteurs de l'aromatase (10,11), ainsi que les traitements qui ciblent HER2 tels que le trastuzumab (Herceptin®) (12,13), le pertuzumab (Perjeta®) (14), le T-DM1 ou ado-trastuzumab emtansine (Kadcyla®) (15), le neratinib (Nerlynx®) (16) ou le lapatinib (Tykerb®) (17). Ce caractère ainsi que l'hétérogénéité moléculaire limitent le choix des traitements. Les traitements du CSTN actuellement utilisés sont la chirurgie, la radiothérapie et la chimiothérapie (le paclitaxel, la doxorubicine, le cisplatine, la capecitabine) (18,19). Malgré l'hétérogénéité moléculaire, le traitement systémique standard du CSTN suit le même principe général que les autres types de cancer du sein (20). De plus, ces traitements manquent de spécificité, de sélectivité et d'efficacité et engendrent plusieurs effets secondaires indésirables. Il y a donc nécessité de rechercher de nouvelles thérapies pour ce type de cancer.

2. L'expression génique et sa régulation

2.1. Les étapes de l'expression génique

Le caractère commun de tous les cancers est la dérégulation de l'expression de certains gènes ou l'expression/surexpression de certains oncogènes. Il est donc important de connaître le fonctionnement de la cellule et le processus de l'expression génique pour comprendre les mécanismes de sa régulation. L'ADN est connu pour être le support de l'information génique, alors que les protéines sont connues comme étant des effecteurs responsables du fonctionnement des cellules. Le passage de l'ADN vers la protéine nécessite certaines étapes.

Brièvement, la première étape est la transcription et elle se déroule au niveau du noyau. D'abord, un complexe enzymatique appelé ARN polymérase repère le promoteur qui se trouve au début de la région à transcrire au niveau de l'ADN (le gène), initie son débobinage et la séparation des deux brins ce qui facilite l'accès au brin matrice (ou anti-sens). Ensuite, une

molécule d'ARN est synthétisée par l'addition de ribonucléotides d'une manière complémentaire à la matrice d'ADN (Figure 1). Une fois la transcription terminée, un ARN pré-messager simple brin se détache et subit des étapes de maturation (ajout d'une coiffe protectrice à l'extrémité 5', queue poly-adénylation à l'extrémité 3' et épissage) pour donner un ARN messager (ARNm). Cet ARNm quitte le noyau vers le cytoplasme via les pores de la membrane nucléaire.

La deuxième étape est la traduction et elle aboutit à la production de la protéine à partir d'une matrice d'ARNm. La production de la protéine se fait à partir d'un enchainement d'acides aminés initialement associés à des ARN de transfert (ARNt) exprimant des anticodons complémentaires aux codons (un codon est formé par trois nucléotides) de la séquence de l'ARNm. Cette étape se déroule ainsi : un complexe de pré-initiation, formé par la petite sous-unité ribosomique et des facteurs d'initiation, se fixe sur l'ARNm et le scanne jusqu'à l'arrivée au niveau d'un codon d'initiation AUG. À ce niveau, ce complexe recrute la grande sous-unité ribosomique déclenchant la traduction. Un ribosome contient trois sites permettant de couvrir trois codons en même temps. Le premier est le site A (pour « amino acid ») qui permet la reconnaissance de l'anticodon au niveau de l'ARNt (chargé avec un acide aminé) et sa fixation sur le codon correspondant au niveau de l'ARNm. Ensuite, le ribosome se déplace d'un codon ce qui permet de déplacer le premier ARNt au site P (pour polypeptide) libérant le site A pour la fixation d'un deuxième ARNt amenant un deuxième acide aminé spécifique. Le premier acide aminé se lie au deuxième avec une liaison peptidique et se détache de son ARNt. Le ribosome se déplace encore d'un codon, le premier ARNt est dans le site E (pour « exit ») et le site A est à nouveau libre permettant la fixation d'un troisième ARNt. Avec la fixation de ce dernier, le premier ARNt se libère du site E, et ainsi de suite (Figure 1). Ce processus se poursuit jusqu'à ce qu'un codon STOP (UAA, UGA ou UAG) arrive au niveau du site A. Cela met fin à la traduction et induit la séparation de deux sous-unités ribosomiques et le détachement de la séquence des acides aminés néoformés et de l'ARNm traduit (21).

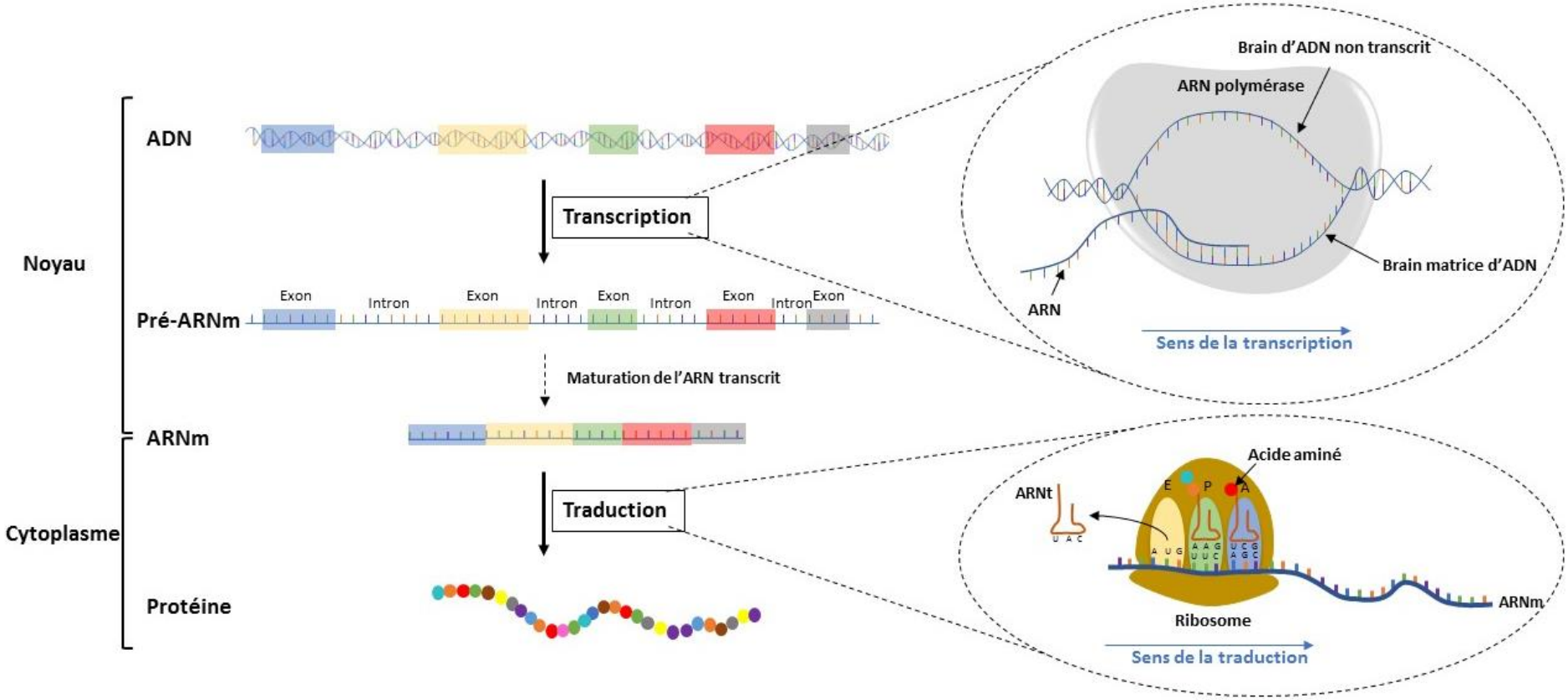

Figure 1. Les étapes de l'expression génique de l'ADN jusqu'à la protéine

Plusieurs mécanismes et acteurs sont impliqués dans la régulation de l'expression génique au cours de ces différentes étapes. Selon le niveau de la régulation, on distingue :

- La régulation transcriptionnelle : elle implique des facteurs de transcriptions et des séquences régulatrices qui contrôlent l'activité des promoteurs (22).
- La régulation post-transcriptionnelle : elle agit sur le transcrit (pré-ARNm ou ARNm) à un ou plusieurs niveaux et elle a pour objectif d'empêcher sa traduction (23).
- La régulation traductionnelle : l'objectif de cette régulation est de contrôler le niveau de la traduction, par exemple, en inhibant la fixation ou le déplacement des ribosomes.
- La régulation post-traductionnelle : il s'agit, principalement, de contrôler l'abondance et l'activité des protéines en régulant leurs fonctions et/ou leur stabilité (24).

2.2. Régulation de l'expression génique par le mécanisme d'ARN interférence

Un processus cellulaire naturel qui permet la régulation physiologique post-transcriptionnelle de l'expression des gènes est le mécanisme d'ARN interférence (ARNi). Ce mécanisme a été découvert en premier chez des plantes par l'équipe de Jorgensen en 1990. Dans le but d'augmenter l'expression de la chalcone synthase pour intensifier la coloration des pétales de pétunia, ils ont introduit des copies supplémentaires du gène. Contrairement à ce qui était attendu, cette manipulation a provoqué un blanchissement des fleurs (25). Dans ce cas, l'excès du gène a stimulé un mécanisme de régulation pour corriger cette perturbation. Quelques années plus tard, le même mécanisme a été décrit chez un nématode Caenorhabditis elegans par Fire et Mello qui ont étudié l'inhibition des gènes par les ARN exogènes. Ce travail leur a d'ailleurs permis de décrocher le prix Nobel de physiologie et de médecine en 2006 (26). Ensuite, il a été démontré qu'un processus similaire se produit aussi dans les cellules de mammifères (27). L'ARNi est une extinction génétique spécifique induite par une courte séquence non codante d'ARN tel que les petits ARN en épingle à cheveux (shRNA), les microARN (miRNA), piwi-interaction ARN (piRNA) et les petits ARN interférents (siRNA). Ces séquences d'ARN permettent l'inhibition de l'expression de l'ARNm cible. Bien que ces ARN agissent d'une manière similaire, les siRNA offrent la meilleure spécificité et sont les plus utilisés dans le développement des traitements contre le cancer (28). Pour mieux comprendre le mécanisme d'ARNi l'exemple du mécanisme faisant intervenir les siRNA sera développé.

2.3. Petits ARN interférents (siRNA)

Initialement chez les mammifères, les siRNA ont été considérés d'origine exogènes (dérivés des virus), transposons ou déclencheurs de transgènes. Plus récemment, des études ont déterminé des sources endogènes de ces séquences d'acides nucléiques (29,30), malgré l'absence d'ARN polymérase ARN dépendante. Les siRNA endogènes (endo-siRNA) sont des petites séquences d'ARN non-codants double brins parfaitement appariés d'environ 21 nucléotides. Ils dérivent des ARN précurseurs double brins générés par une transcription classique par l'ARN polymérase II, principalement. La formation de la structure double brin est due à la présence de séquences palindromiques en tandem sur le brin, c'est-à-dire des séquences de nucléotides se lisant dans le même ordre dans les deux sens (exemple : ACCGGT – TGGCCA), qui permettent l'appariement des nucléotides du même brin d'ARN et le repliement de ce dernier sur lui-même pour former des structures intramoléculaires. Ces duplexes sont clivés par l'endonucléase Dicer-2, de type ribonucléase III, pour donner des petites séquences, les endo-siRNA. Certaines de ces endo-siRNA sont complémentaires à des ARNm codant pour des protéines particulières, ce qui suggère un rôle dans la régulation de leur expression. Ces complexes siRNA-Dicer sont ensuite pris en charge par des protéines cytoplasmiques (exemple : TRBP et Argonaute 2 (Ago2)) pour former le précurseur du complexe enzymatique RISC (RNA-induced silencing complex). À ce niveau, le duplex siRNA est dissocié en un brin sens (appelé aussi brin passager), dégradé par des RNases cytoplasmiques, et un brin antisens (appelé aussi brin guide), pris en charge par Ago2 qui présente la partie active (ou le cœur) du complexe RISC, induisant ainsi l'activation de ce complexe enzymatique (29,31). La sélection du brin guide se fait par la protéine Ago2 qui choisit le brin le moins stable thermodynamiquement au niveau de son extrémité 5', et induit la dégradation de l'autre brin (32). Une fois le complexe RISC actif, son action est guidée par le brin antisens qui va permettre de diriger ce complexe enzymatique vers les séquences complémentaires de l'ARNm. L'hybridation parfaite du siRNA avec la séquence correspondante sur le brin de l'ARNm au niveau de la protéine Ago2 déclenche le mécanisme d'ARNi : clivage médié par l'endonucléase Ago2 de l'ARNm entre les bases 10 et 11 relatives à l'extrémité 5' du brin guide du siRNA (33) (Figure 2).

Des études *in vitro* et *in vivo* ont montré que ce mécanisme d'ARNi peut être utilisé pour atténuer ou supprimer l'expression de divers gènes (34–37). À l'issue de cette révélation, plusieurs siRNA synthétiques sont produits avec des séquences spécifiques pour inhiber l'expression des gènes cibles par simple introduction dans les cellules d'intérêt. Cette procédure

implique des mécanismes uniquement cytoplasmiques sans les étapes nucléaires de la production.

Les siRNA synthétiques se présentent généralement sous forme d'un duplex de 19 à 23 paires de base avec deux nucléotides non-appariés aux extrémités 3'. Ces siRNA sont directement délivrés dans le compartiment cytoplasmique pour s'associer avec Dicer qui recrute, comme décrit précédemment, les protéines nécessaires pour former le précurseur du complexe RISC (38,39). Le mécanisme d'ARNi médié par ces siRNA peut se dérouler indépendamment de l'endonucléase Dicer (40). Dans ce cas, le duplex de siRNA est pris en charge essentiellement par les protéines TRBP et Ago2. Dans un premier temps, la protéine TRBP s'associe au brin le plus stable thermodynamiquement, alors que la protéine Ago2 se lie à celui le moins stable (le brin guide), déclenchant ensuite la séparation des deux brins, la dégradation du brin passager et l'activation du complexe RISC (41). La suite de ce processus est la même que celui des endo-siRNA (Figure 2). La fragmentation de l'ARNm par le complexe enzymatique RISC induit la libération des séquences générées dans le cytoplasme et leur dégradation par des nucléases non spécifiques. Le complexe RISC peut ainsi continuer son action d'extinction en s'hybridant sur une autre séquence d'ARNm grâce au brin guide du siRNA.

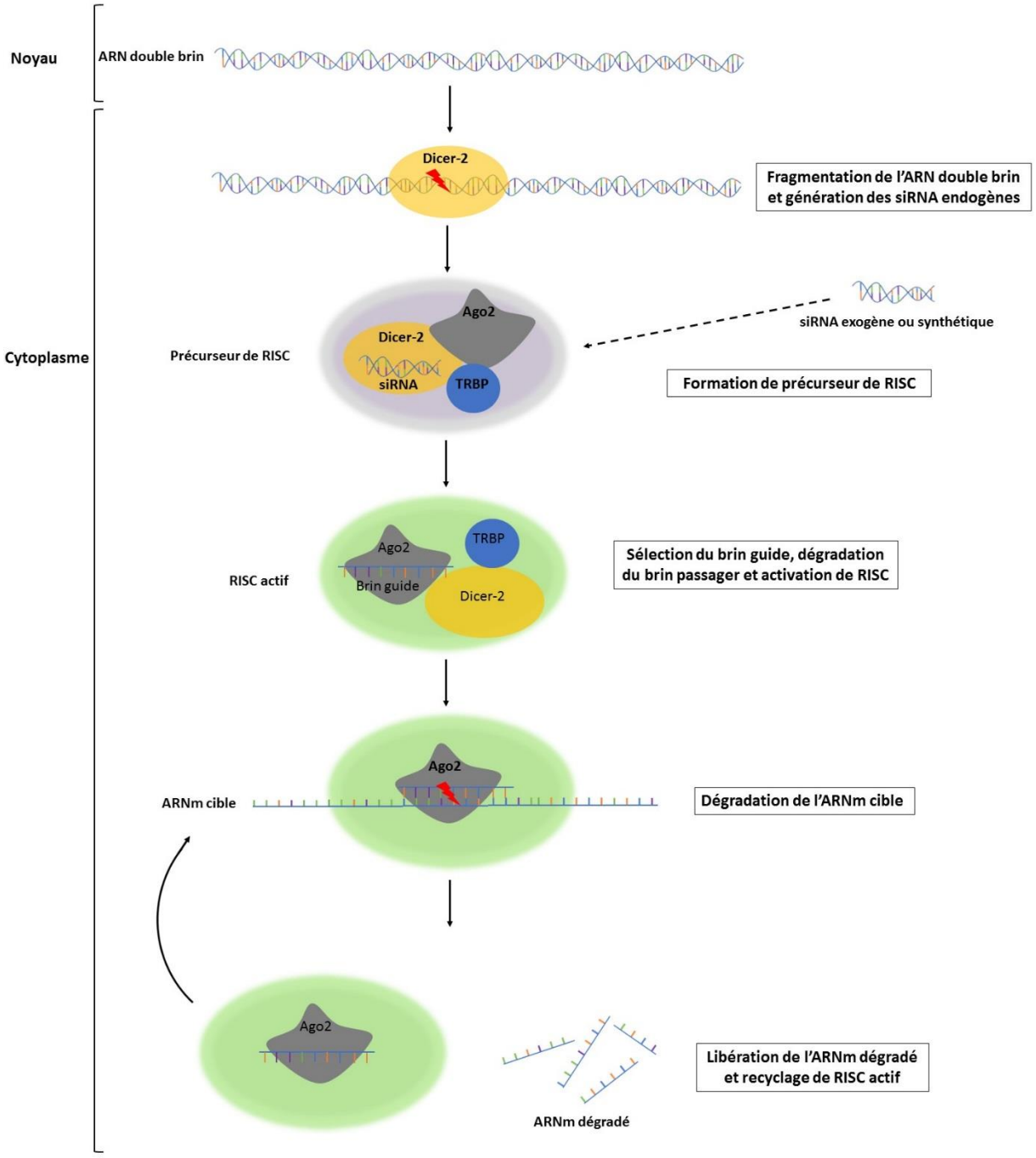

Figure 2. Illustration des différentes étapes de la production des siRNA endogènes et du déclenchement de la dégradation de l'ARNm cible par le mécanisme d'ARNi.

3. Développement des stratégies thérapeutiques basées sur les siRNA pour le traitement du cancer

La découverte et la compréhension du mécanisme d'ARNi a permis de prendre conscience de son rôle dans la régulation post-transcriptionnelle de l'expression génique. Ce

mécanisme endogène a inspiré la communauté scientifique pour inhiber l'expression de gènes cibles d'une manière spécifique en utilisant des petites séquences d'acides nucléiques exogènes. Ainsi, l'utilisation de ces molécules s'avère intéressante pour des études diverses telles que la recherche de biomarqueurs pour le diagnostic de certaines maladies (42), la recherche de nouvelles cibles thérapeutiques (43) ou le développement d'une stratégie thérapeutique (44).

Parmi les maladies concernées par l'application de cette stratégie thérapeutique, le cancer représente la cible la plus visée. En oncologie, il est connu que le développement d'un cancer et la croissance tumorale sont principalement liés à une dérégulation de l'expression génique provoquée par l'accumulation de mutations de certains groupes de gènes : une expression d'oncogènes ou de mutants oncogènes et/ou une surexpression des gènes impliqués dans la multiplication et la croissance cellulaire (exemple : les gènes anti-apoptotiques ou les régulateurs du cycle cellulaire) (45–47). Dans ce cas, le rétablissement du niveau basal de l'expression de ces gènes au niveau de la tumeur pourrait résoudre ce problème. Ainsi, le mécanisme d'ARNi semble être une stratégie thérapeutique prometteuse et les siRNA, grâce à leur spécificité, de bons candidats (48). Conceptuellement, une thérapie anticancéreuse basée sur l'utilisation de l'ARNi consiste à introduire les séquences nucléotidiques candidates dans les cellules cancéreuses pour bloquer l'expression des gènes cibles et induire la mort cellulaire.

3.1. Limites d'utilisation des siRNA

Il s'avérait, depuis les premiers essais *in vitro* et *in vivo*, qu'il était optimiste de penser qu'il suffise d'utiliser la bonne séquence de siRNA pour obtenir une extinction de l'expression du gène cible. Malgré les divers avantages de l'utilisation des siRNA pour les thérapies anticancéreuses, de nombreuses études ont mis en évidence plusieurs contraintes à surmonter pour obtenir une efficacité satisfaisante une fois administrés par voie systémique (32). Ces difficultés sont principalement dues aux caractéristiques des siRNA tels que la faible stabilité, la charge négative, l'hydrophilicité ainsi que la taille (qui est, en même temps, faible favorisant l'élimination rapide de la circulation sanguine et importante empêchant le transport passif à travers des membranes). De plus, la présence de freins biologiques, tels que les RNases, le système immunitaire, la clairance rénale, l'environnement tumoral, limite leur arrivée au niveau de site d'action et donc freine leur action thérapeutique (48).

La compréhension des limites de l'utilisation des siRNA dans un environnement biologique (*in vitro* ou *in vivo*) a incité les chercheurs à développer diverses approches pour les surmonter. Ces approches peuvent être classées en deux groupes :

- La modification chimique des siRNA : elle consiste à appliquer des changements à la séquence de siRNA ou à rajouter des groupements à ces extrémités pour augmenter sa stabilité et éviter sa dégradation.
- Le chargement des siRNA dans des constructions nanométriques leur permettant une protection contre la dégradation et facilitant leur délivrance dans les cellules cancéreuses.

3.2. Nanovectorisation des siRNA

Dans ces travaux de thèse, on s'intéresse plus particulièrement à la deuxième approche, nommée nanovectorisation des siRNA. C'est une mise en forme galénique particulière, nécessaire pour profiter de l'action thérapeutique des siRNA. Elle consiste à inclure ces siRNA dans un nanosystème qui permet i) d'obtenir des caractéristiques physico-chimiques meilleures que celles des siRNA seuls et conformes aux exigences de la voie d'administration et ii) d'apporter des propriétés demandées pour une efficacité thérapeutique élevée (résistance à la dégradation par les nucléases, temps de circulation long, capacité à franchir les barrières biologiques …). Dans ces nanovecteurs, les siRNA peuvent être associés à différentes molécules avec divers types de liaisons.

Durant les deux dernières décennies, un arsenal de divers nanovecteurs a été développé pour répondre aux exigences de la délivrance des siRNA, introduisant ainsi une nouvelle classe thérapeutique. On distingue deux classes principales de nanovecteurs : les nanovecteurs viraux et les nanovecteurs non-viraux ou synthétiques. Ici on s'intéresse à la deuxième classe. Pour simplifier la lecture, le terme nanovecteur est utilisé dans le reste de ce manuscrit pour désigner les nanovecteurs synthétiques.

Selon la nature des composants utilisés, on distingue plusieurs groupes de nanovecteurs de siRNA. Chaque groupe possède des caractéristiques, des propriétés physico-chimiques et des propriétés de surface déterminées par les types, les structures et l'organisation des matériaux qui le composent. En ce sens, la considération de ces éléments ainsi que la maîtrise des caractéristiques et des propriétés des nanovecteurs lors de la conception permettent d'obtenir une formulation efficace pour surmonter les barrières biologiques et optimiser les effets obtenus.

3.2.1. Les nanovecteurs lipidiques

Ce groupe de nanovecteurs est basé sur l'utilisation de lipides. Les nanovecteurs lipidiques sont parmi les premiers nanovecteurs à être développés et étudiés et ils sont les plus utilisés dans les applications *in vitro*, *in vivo* et dans les essais cliniques (49). Depuis des années, ces nanovecteurs sont utilisés pour le transport de molécules pharmaceutiques grâce à leurs propriétés intéressantes, telles que leur composition proche de celle de la membrane cellulaire, permettant de faciliter l'entrée des molécules à transporter. Actuellement, les nanovecteurs lipidiques représentent le groupe le plus commercialisé. Au sein de ces nanovecteurs, les siRNA peuvent être complexés avec plusieurs types de liaisons. Généralement, cette liaison dépend de la charge et de la nature des lipides utilisés. Par exemple, dans la majorité des cas, les lipides cationiques sont utilisés pour former des interactions électrostatiques avec les siRNA, alors que les lipides neutres et anioniques sont liés avec les liaisons covalentes. Les lipides anioniques sont peu utilisés dans la délivrance des siRNA à cause de leur immunogénicité et leur difficulté à pénétrer la membrane cellulaire chargée négativement. Cependant quelques études ont tenté de les combiner avec des composants cationiques (lipides ou polymères cationiques) (50,51). Selon la structure et la composition, on distingue différents nanovecteurs lipidiques qui peuvent être groupés en trois classes (Figure 3) :

- Les liposomes : ce sont des auto-assemblages sphériques de bicouche lipidique délimitant un cœur hydrophile.
- Les lipoplexes : ce sont des complexes formés spontanément par interactions entre les lipides chargés positivement et les siRNA.
- Les nanoparticules lipidiques : ils se présentent sous forme d'une monocouche sphérique de lipides avec un cœur hydrophobe. Les charges positives se présentent en surface de ces nanoparticules et elles permettent la complexation des siRNA (52).

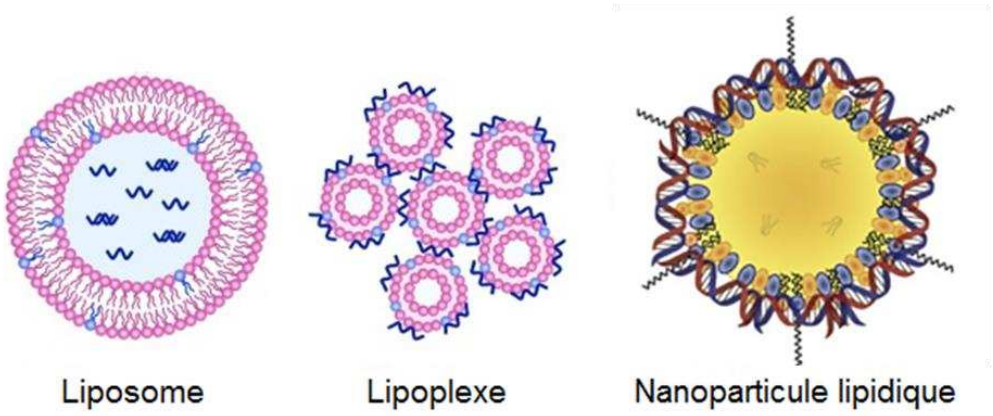

Figure 3. Représentation schématique de la structure des nanovecteurs lipidiques (d'après Granot *et al.* 2017 et Kong *et al.* 2013 (53,54).

Les nanovecteurs lipidiques de siRNA montrent une efficacité de transfection très élevée *in vitro*. Cependant leur application *in vivo* reste limitée par des problèmes de stabilité en présence de protéines sériques et par des problèmes de toxicité qui sont principalement associés aux lipides cationiques.

3.2.2. Les nanovecteurs polymères

Les nanovecteurs polymères sont largement étudiés pour le transport et la délivrance de gènes, notamment de siRNA. Ces systèmes sont connus par leur biodégradabilité, leur stabilité colloïdale élevée et leur capacité à prolonger la demi-vie des siRNA dans l'environnement biologique (55). Différents types de polymères sont utilisés dans la conception de ces nanovecteurs tels que les polymères naturels (chitosan, cyclodextrine, ...) et les polymères synthétiques (polyéthylèneimine (PEI), dendrimères, …) qui peuvent être des polymères cationiques (poly-arginine, poly-lysine, …) ou non-cationiques (polyéthylène glycol (PEG), poly(d,l-lactide-co-glycolide (PLGA)). La majorité de ces nanovecteurs sont développés à partir des polymères cationiques qui peuvent i) lier les siRNA par interactions électrostatiques, ii) faciliter l'internalisation dans la cellule grâce aux interactions avec la membrane cellulaire chargée négativement et iii) favoriser l'échappement endosomal en raison de leur charge positive (56,57). Ces nanovecteurs polymères peuvent être classés en trois groupes selon l'organisation des polymères et la structure obtenue (Figure 4) :

- Les polyplexes : ce sont des complexes formés spontanément par interactions entre les polymères chargés positivement et les siRNA
- Les micelles : ce sont des structures cœur/ enveloppe nanométriques formées par auto-assemblage de copolymères amphiphiles. Ces micelles permettent de séparer le milieu

intérieur hydrophobe du milieu extérieur hydrophile en suivant une organisation qui permet d'orienter les têtes polaires hydrophiles vers le solvant et les queues hydrophobes vers le centre des micelles.

- Les nanocapsules : elles présentent une coque polymère et un cœur permettant l'encapsulation des siRNA (58).

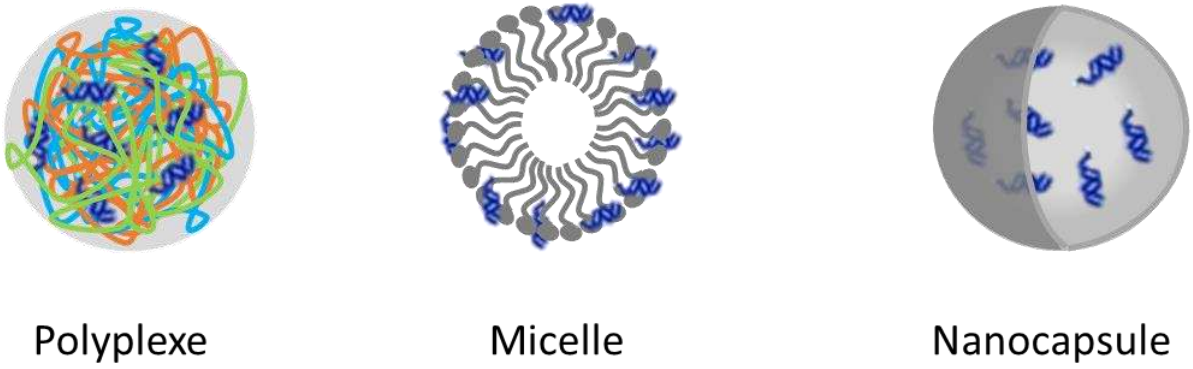

Figure 4. Représentation schématique de la structure des nanovecteurs polymères

Cependant, l'application clinique de ces nanovecteurs est limitée par des problèmes de toxicité associés aux polymères cationiques. En effet, la densité élevée de charge positive provoque des dommages au niveau de la membrane plasmique, induisant la mort cellulaire. Par ailleurs, l'association avec d'autres polymères neutres tels que le PEG permet de masquer les charges négatives et diminuer cette toxicité (55).

3.2.3. Les nanovecteurs peptidiques

Les peptides se montrent bons candidats pour associer et véhiculer des molécules, notamment les siRNA, grâce à leurs capacités de polymorphisme intéressantes. En effet, les peptides ont une certaine flexibilité structurale qui permet la modification de leur conformation et favorise donc l'adaptation aux conditions environnementales (59,60). Les approches actuelles de délivrance des siRNA médiées par les peptides peuvent être divisées en deux catégories principales : i) la complexation non covalente par des interactions électrostatiques et ii) l'association via des liaisons covalentes (60). Les peptides les plus utilisés pour la vectorisation des siRNA sont les peptides de pénétration cellulaire. Ces sont des petites séquences de 10 à 30 acides aminés, caractérisés par leur charge positive autorisant l'établissement des interactions électrostatiques avec les charges anioniques des groupements phosphates des siRNA. Selon leur polarité, ils sont classés en deux groupes : peptides

amphipatiques et peptides hydrophobes, et dans les deux cas ils contiennent au moins un groupement hydrophobe qui facilite l'interaction avec la membrane cellulaire. Ces peptides sont connus pour leur capacité à entrer dans les cellules par translocation directe dans le cytosol ou par une voie d'endocytose (59,61). Ces séquences de faible poids moléculaire peuvent assurer des fonctions multiples telles que la complexation des siRNA, le ciblage actif, la pénétration dans les cellules et la perturbation des endosomes (62).

3.2.4. Les nanovecteurs hybrides à cœur inorganique

Ce groupe de nanovecteurs est basé sur l'utilisation de structures inorganiques qui représentent le cœur des nanovecteurs. Ce cœur peut être construit à partir de divers métaux tels que l'oxyde de fer, l'or, l'argent, le cobalt, le nickel, et il nécessite un traitement de surface pour apporter des fonctions chimiques permettant la complexation des siRNA chargés négativement. Les siRNA peuvent être conjugués directement à la partie métallique ou, plus fréquemment, associés à un revêtement polymère ou lipidique présent à la surface des particules inorganiques (63,64).

L'avantage de l'utilisation de matériaux inorganiques est que leurs propriétés permettent leur suivi avec différentes techniques d'imagerie telles que l'imagerie par résonance magnétique (IRM) pour l'oxyde de fer (65,66), la fluorescence pour les quantums dots (65,67) ou la luminescence pour les particules d'or (68). De plus, le cœur magnétique pourrait être utilisé pour faciliter leur accumulation au niveau du site tumoral en utilisant le guidage magnétique ou pour détruire les cellules cancéreuses par hyperthermie (69–71).

En dépit de leur caractère théranostique, ces nanovecteurs restent moins adoptés et moins étudiés pour la délivrance des siRNA que ceux des autres groupes en raison de certains défauts de la partie inorganique, tels que la toxicité associée aux métaux, ou de la mauvaise compréhension de leurs mécanismes de métabolisation et d'excrétion par le corps (72).

3.3. Les essais cliniques de nanovecteurs de siRNA pour le traitement des cancers

Les ARNi thérapeutiques, notamment les siRNA, deviennent attractifs dans la recherche de thérapies anticancéreuses. Le premier essai clinique basé sur l'utilisation des siRNA nanovectorisés a été conduit par Calando pharmaceuticals en 2008 sur 24 patients présentant différents cancers. L'objectif de la phase I de cette étude était d'évaluer la toxicité et la tolérance

de ce nanovecteur de siRNA (CALAA-01) administré par voie intraveineuse, déterminer sa pharmacocinétique et de fournir des premières preuves de son efficacité en évaluant la réponse tumorale. CALAA-01 est un nanovecteur de siRNA polymère à base de cyclodextrine qui cible la sous-unité M2 de ribonucléotide réductase. Les effets indésirables majeurs de ce nanovecteur chez l'Homme étaient une hypersensibilité et des séquelles de réponses immunitaires aiguës (bouffées vasomotrices, fièvre, fatigue, etc.). CALAA-01 était éliminé rapidement de la circulation sanguine, principalement par les reins, à cause de son interaction avec la barrière de filtration rénale. Les biopsies tumorales de patients atteints de mélanome, obtenues après traitement, montrent une localisation intracellulaire du nanovecteur en quantité corrélée avec la dose administrée. De plus, une réduction de l'expression de l'ARNm cible et la présence des fragments de ces ARNm, témoignant de l'action des siRNA, ont été détectés (73,74). Le deuxième essai clinique était mené par Alnylam Pharmaceuticals en 2009 sur 41 patients âgés de 18 ans ou plus et présentant un cancer du foie. Dans cette étude, la tolérance et l'efficacité d'un nanovecteur lipidique (LNP) chargé avec des siRNA thérapeutiques dirigés contre le facteur de croissance de l'endothélium vasculaire (VEGF) et la kinésine KSP (kinesin spindle protein), ont été évaluées. Les résultats obtenus ont montré une bonne tolérance pour ce traitement administré par voie systémique. L'analyse des biopsies tumorales a permis la détection de ces nanoparticules lipidiques, indiquant une accumulation dans la tumeur. Une inhibition spécifique de ces protéines cibles (VEGF et KSP) a été observée ainsi qu'une régression complète des métastases hépatiques (75). Ces études représentent une preuve de concept pour l'application d'une thérapie basée sur le potentiel des siRNA pour le traitement des cancers et une base pour les recherches dans ce domaine. Un exemple de nanovecteur de siRNA qui mérite d'être cité, même si ce n'est pas pour le traitement de cancers, est le patisiran (ONPATTRO®). Il représente le premier médicament basé sur l'action thérapeutiqu des siRNA mis sur le marché en 2018. Ce traitement est prescrit dans le contexte de l'amyloïdose héréditaire à transthyrétine (hATTR). L'ONPATTRO® est un nanovecteur lipidique constitué de lipides cationiques, de lipides fusogéniques et de PEG. Le siRNA utilisé dans ce traitement cible l'ARNm de la transthyrétine. Une mutation au niveau du gène codant pour cette protéine est responsable du développement de cette maladie (76).

Avec l'amélioration de la compréhension de leur mécanisme d'action, le nombre d'essais utilisant des siRNA pour le traitement de cancer a augmenté depuis 2008 pour compter aujourd'hui 20 études (77). Le Tableau I présente quelques exemples de nanovecteurs de siRNA anticancéreux en essais cliniques (phase I et II). Les études présentées dans ce tableau sont

conduites sur différents types de cancers solides. Dans ces études, des nanovecteurs lipidiques ou polymères avec des siRNA qui ciblent différentes protéines sont testés dans l'objectif de déterminer leur biodistribution et leur pharmacocinétique et d'évaluer leur toxicité/ tolérance et leur efficacité sur les tumeurs.

Tableau I. Nanovecteurs de siRNA anticancéreux en essais cliniques (78,79).

Nom	Compagnie	Type de nanovecteur	Protéine cible	Type de cancer	Phase	Identifiant	Statut
ALN-VSP02	Alnylam Pharmaceuticals	Lipidique	VEGF et KSP	Tumeurs solides	I	NCT01158079	Terminé
Atu027	Silence Therapeutics GmbH	Lipidique	Protéine kinase N3	Tumeurs solides	I	NCT00938574	Terminé
				Cancer du pancréas	II	NCT01808638	Terminé
CALAA-01	Calando Pharmaceuticals	Polymère	Sous-unité M2 de ribonucléotide réductase	Tumeurs solides	I	NCT00689065	Terminé
DCR-MYC	Dicerna Pharmaceuticals, Inc	Lipidique	MYC	Tumeurs solides	I	NCT02110563	Terminé
				Cancer du foie	I/ II	NCT02314052	Terminé
siG12D LODER	Silenseed Ltd	Polymère	KrasG12D	Cancer du pancréas	I	NCT01188785	Terminé
					II	NCT01676259	En cours
siRNA-EphA2-DOPC	M.D. Anderson Cancer Center	Lipidique	EphA2	Cancers avancés	I	NCT01591356	En cours
TKM-080301	National Cancer Institute	Lipidique	Polo-like kinase 1 (PLK1)	Cancer du foie	I	NCT01437007	Terminé

4. Internalisation et trafic intracellulaire de nanovecteurs de siRNA

Un aspect des nanovecteurs de siRNA le moins étudié est leur mécanisme d'internalisation et leur trafic et devenir intracellulaire. Bien qu'il soit communément admis que l'entrée de ces nanovecteurs suit, dans la majorité des cas, une voie impliquant l'endocytose, les mécanismes spécifiques de cette internalisation restent peu investigués. En raison de son importance, les études récentes sur les nanovecteurs de siRNA s'orientent de plus en plus vers cette direction.

À cause de la complexité des mécanismes d'internalisation et du trafic intracellulaire des nanovecteurs, il est difficile de construire une image complète regroupant tous les évènements et les processus qui se déroulent au niveau de la membrane cellulaire et à l'intérieur de la cellule. Les mécanismes d'entrée mis en place par les cellules et le trafic intracellulaire dépendent, fortement, de divers paramètres tels que le type de cellules ainsi que les composants et les caractéristiques physico-chimiques des nanovecteurs (taille, potentiel zêta, forme, chimie de la surface ...).

4.1. Voies d'internalisation

La membrane plasmique représente une barrière séparant l'intérieur de la cellule de son environnement externe. Ses propriétés et sa composition lui donnent un caractère majeur, la sélectivité. Cette sélectivité rend l'étape d'entrée des nanovecteurs dans la cellule un défi à relever. Cette entrée implique un processus hautement contrôlé et des interactions complexes avec la membrane cytoplasmique. Généralement, les interactions se font au niveau des régions spécifiques de la membrane comme les régions riches en clathrine, cavéoline 1, radeaux lipidiques, récepteurs, etc (80). Cette interaction peut être décisive pour la voie d'entrée à emprunter.

Dans cette section, nous présentons les voies d'entrée qui peuvent être impliquées dans l'internalisation des nanovecteurs de siRNA. On distingue plusieurs types de voies pouvant être classées en deux groupes : les voies d'entrées médiées par l'endocytose et celles qui sont indépendantes de l'endocytose.

4.1.1. Les voies d'entrée médiées par endocytose :

- Endocytose médiée par les clathrines

C’est une voie largement étudiée et qui se produit dans toutes les cellules de mammifères dans des régions spécifiques de la membrane plasmique riches en clathrines. Elle représente la voie principale d'absorption d'éléments nutritifs essentiels, tels que les lipoprotéines de basse densité (LDL) et la transferrine. L'induction de cette voie nécessite une liaison spécifique entre la clathrine et son ligand au niveau des régions spécifiques, qui représentent 1 à 2 % de la surface de la membrane plasmique. Cette liaison déclenche la formation de vésicules à clathrines, typiquement d’environ 120 nm, par invagination et fermeture de ces puits recouverts de clathrines. La fermeture des vésicules à clathrines est provoquée par la dynamine, une grande GTPase. La clathrine induit le bourgeonnement des vésicules intracellulaires. Ensuite, des protéines d'assemblage, telles que l’adaptine, la dynamine et de nombreuses protéines de rab assurent la formation des vésicules et favorisent leur internalisation et leur trafic. Ces vésicules évoluent en endosomes et finissent par fusionner avec les lysosomes (Figure 5) (81–84).

- Endocytose médiée par les cavéoles

L'expression de la protéine cavéoline 1 à la surface des cellules induit la formation d'une invagination d'environ 60 nm de diamètre, appelée cavéole. Les cavéoles sont présentes dans de nombreux types cellulaires et délimitent des microdomaines riches en cholestérol et en sphingolipides dans une membrane plasmique avec diverses molécules de signalisation et transporteurs membranaires. L'endocytose médiée par les cavéoles est impliquée dans le trafic de nombreuses molécules, telles que l'acide folique, le cholestérol et l'albumine, capables de se lier à la protéine cavéoline 1 présentée à la surface de la cavéole. Ces molécules sont transportées à l'intérieur de la cellule via des vésicules qui migrent à travers le cytoplasme en utilisant une cascade de transduction de signalisation (82,85). Deux trafics de ces vésicules sont possibles : une voie qui rejoint celle des vésicules à clathrine et qui finit par fusion avec les lysosomes ou une voie qui permet l’évolution des vésicules à cavéoles en cavéosomes (Figure 5). La deuxième voie implique des vésicules dépourvues d’enzymes de dégradation, ce qui représente un trafic de choix pour plusieurs pathogènes. Le développement de nanovecteurs qui utilise cette voie d’entrée peut donc être avantageux pour contourner la voie de dégradation lysosomale et pour la délivrance des agents thérapeutiques (84). Certaines molécules transportées par ce processus, telles que l'acide folique, sont utilisées pour fonctionnaliser des nanovecteurs pour une délivrance ciblée d'acides nucléiques (86).

- Endocytose indépendante des clathrines et cavéoles

Cette voie comprend plusieurs portails d'entrée qui sont tous issus de domaines membranaires hydrophobes riches en cholestérol et en glycosphingolipides, appelés radeaux lipidiques. L'endocytose indépendante de la clathrine et des cavéoles se produit généralement dans les cellules dépourvues de clathrine et de cavéoline 1 mais dépendante de la présence ou non du cholestérol. Ce processus résulte en une invagination de la membrane cellulaire dans des régions spécialisées (radeaux). Ces voies d'entrée peuvent être régulées par plusieurs effecteurs. En se basant sur ces effecteurs, les voies indépendantes de la cavéole et de la clathrine sont actuellement classées en différents sous-groupes : dépendante d'Arf6 (ADP-ribosylation factor 6), dépendante de la flotilline, dépendante de Cdc42 (Cell division control protein 42) et dépendante de RhoA (Ras homolog gene family, member A). Certaines de ces voies sont également médiées par la dynamine (82,87).

- Macropinocytose

La macropinocytose est un cas particulier d'endocytose indépendante de la clathrine, de la cavéole et de la dynamine. C'est une voie d'endocytose non sélective qui se produit dans plusieurs types cellulaires en réponse à la stimulation avec des facteurs de croissance. Ce mécanisme implique le réarrangement du cytosquelette d'actine qui déclenche la formation des plis au niveau de la membrane plasmique, puis la formation de larges vésicules (0,5 – 10 µm) (85). Ces vacuoles, appelées aussi macropinosomes, permettent d'engloutir le fluide et les nutriments du milieu extracellulaire (Figure 5) (87).

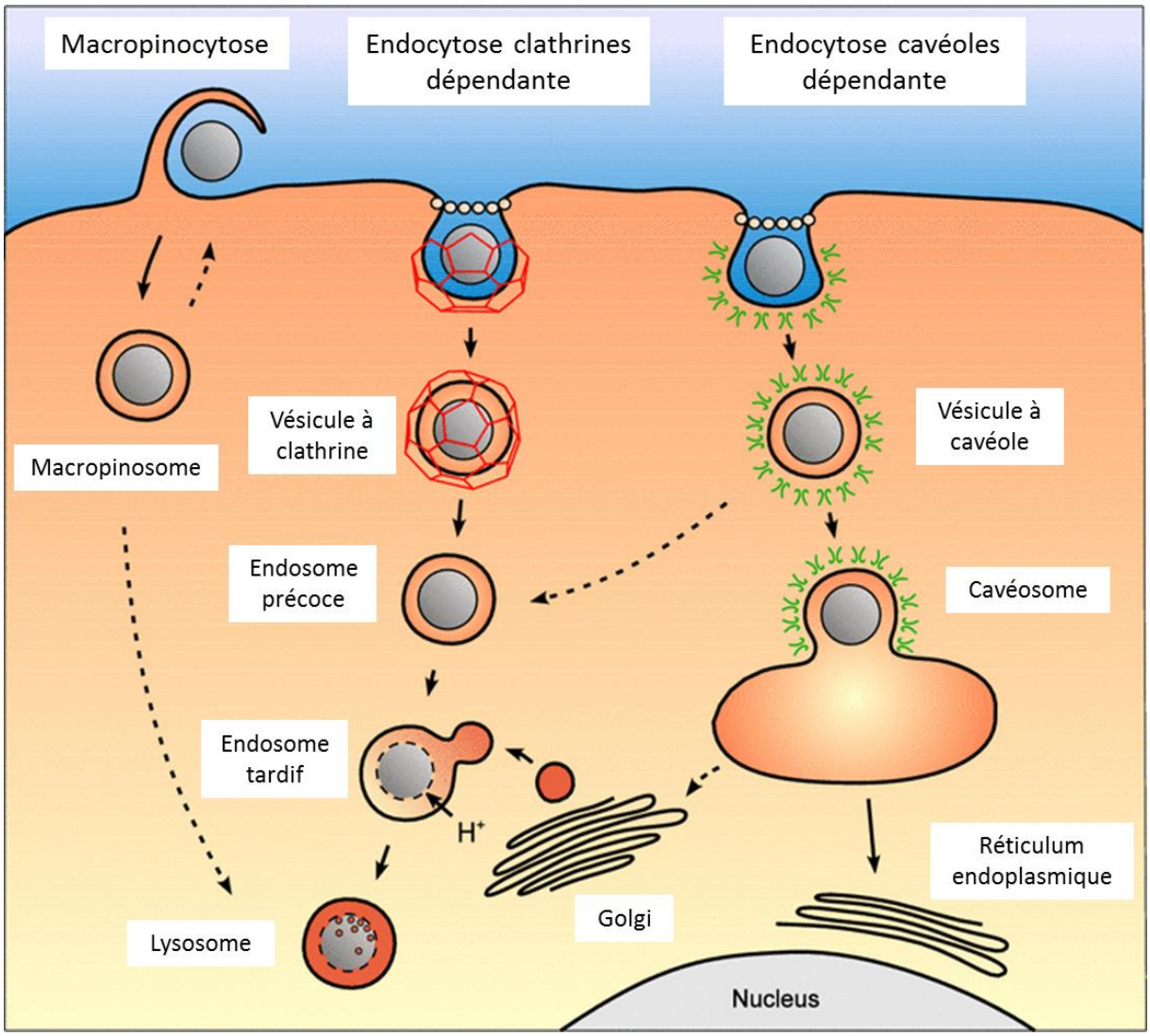

Figure 5. Illustration de l'entrée des nanovecteurs par macropinocytose, par endocytose médiée par les clathrines et par endocytose cavéole-dépendante ainsi que du trafic associé à chaque voie (modifiée d'après Hillaireau et Couvreur, 2009 (84)).

4.1.2. Les voies d'entrée indépendantes de l'endocytose :

- Transcytose

La transcytose est une voie d'internalisation indépendante de l'endocytose et de l'énergie qui se produit par passage direct des molécules dans le cytosol. Cette voie dépend de la nature et des caractéristiques de la molécule (taille, charge, polarité …) et elle représente aussi la voie principale pour le passage des agents thérapeutiques à travers la barrière hématoencéphalique et l'entrée dans le système nerveux central (88). Certains peptides tels que les peptides de pénétration cellulaires sont connus pour leur capacité à franchir la membrane cellulaire via ce processus. Ce passage permet de transporter ces molécules directement dans le

cytoplasme en évitant le passage endosomal et diminuant, ainsi, la probabilité de la dégradation dans les vésicules endo-lysosomales. Pour cela, plusieurs études récentes de développement de nanovecteurs de siRNA ont adopté cette stratégie et fonctionnalisé la surface de leurs nanovecteurs avec des peptides de pénétration cellulaire (89,90).

- Fusion membranaire

Cette voie d'entrée est réservée aux nanovecteurs lipidiques ou contenant des lipides au niveau de leur surface d'interaction avec les cellules. Ce processus implique la fusion des composants lipidiques des nanovecteurs avec la bicouche lipidique de la membrane cellulaire. Ce phénomène est typique des cellules dépourvues de clathrine et de cavéoline à leur surface telles que de nombreuses cellules cancéreuses humaines (86). Cette stratégie est souvent considérée comme une voie rapide pour la délivrance intracellulaire puisque la fusion membranaire se produit en moins de 2 minutes à 37°C. Cette fusion induit une libération directe de l'agent thérapeutique nanovectorisé (tel que les siRNA) dans le cytosol (91,92). Parmi les lipides utilisés dans la conception et le développement des nanovecteurs, certains, tels que le cholestérol, sont plus connus que d'autres (tels que la phosphatidyl choline (93)) pour leur rôle dans la fusion membranaire.

4.2. Trafic intracellulaire

Une fois internalisés par les cellules, les nanovecteurs de siRNA subissent un transport et suivent un trafic pour atteindre leur destination. Ce transport et ce trafic sont appropriés à la voie d'entrée utilisée. Par exemple, durant l'internalisation via une voie d'endocytose, les nanovecteurs sont, la plupart du temps, confinés dans des vésicules issues de la membrane cellulaire, telles que les endosomes. Ces vésicules sont transportées vers l'intérieur des cellules par des mécanismes complexes à travers les filaments d'actine (80).

Au vu des caractéristiques des nanovecteurs, leur passage par les endosomes est une étape très probable pour leur internalisation. Cependant, une fois dans ces vésicules, ils peuvent être exposés à la dégradation endolysosomale qui peut inhiber leurs effets biologiques et thérapeutiques. Plus longtemps ils y restent, plus la probabilité qu'ils soient dégradés dans ce compartiment augmente (94). En conséquence, pour accomplir leur mission, les nanovecteurs de siRNA doivent éviter cette dégradation, franchir la barrière endosomale et passer dans le cytosol. Les propriétés physico-chimiques, la composition et la conception de nanovecteurs peuvent être des facteurs influençant leurs capacités à échapper les endosomes et déterminant

les mécanismes impliqués dans ce processus. On distingue quatre mécanismes d'échappement endosomal principaux :

- L'effet pompe à proton : ce phénomène est induit par des composants de nanovecteurs ayant la capacité de se protoner (c'est-à-dire gagner des charges positives) lors de l'acidification des endosomes. Cette propriété caractérise, principalement, les composants cationiques tels que certains polymères, lipides ou peptides. Cette protonation permet d'augmenter le flux entrant des protons (H^+) et, par conséquent, le flux des ions chlorure (Cl^-) ce qui induit le gonflement de l'endosome et sa rupture (Figure 6) (94,95).

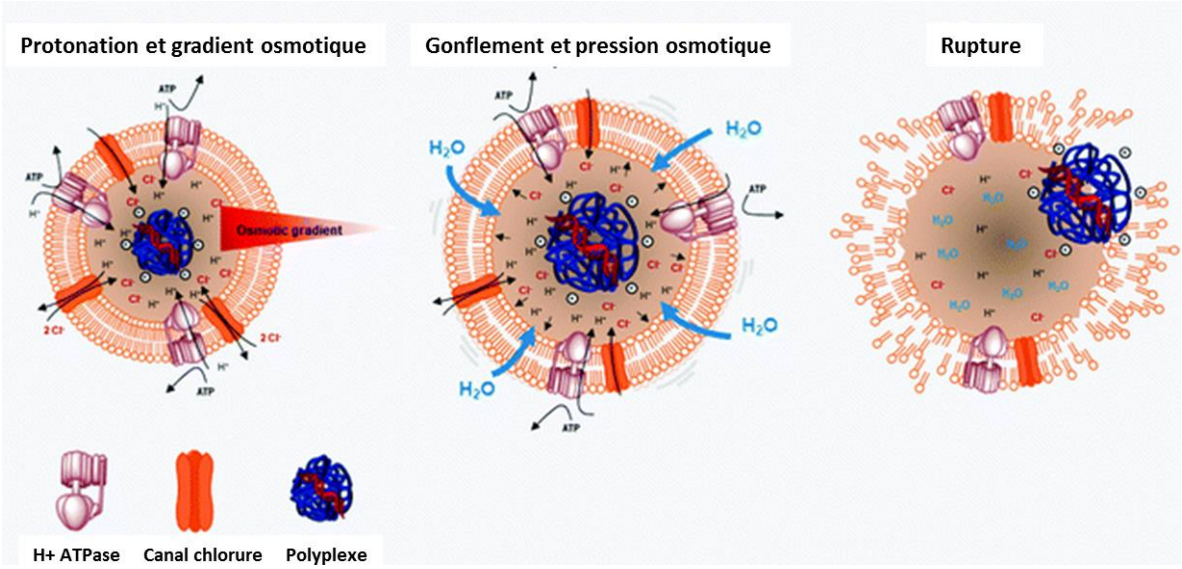

Figure 6. Illustration schématique de l'effet pompe à proton (modifiée d'après Bus *et al.*, 2018 (96)).

- L'effet parapluie : cet effet est la conséquence de l'effet précédent. La protonation des molécules dans les endosomes cause une répulsion entre les groupements avec une densité élevée de charge positive induisant l'augmentation du volume occupé par la molécule. En association avec l'effet pompe à proton, l'effet parapluie conduit à la rupture de l'endosome (Figure 7) (96,97).

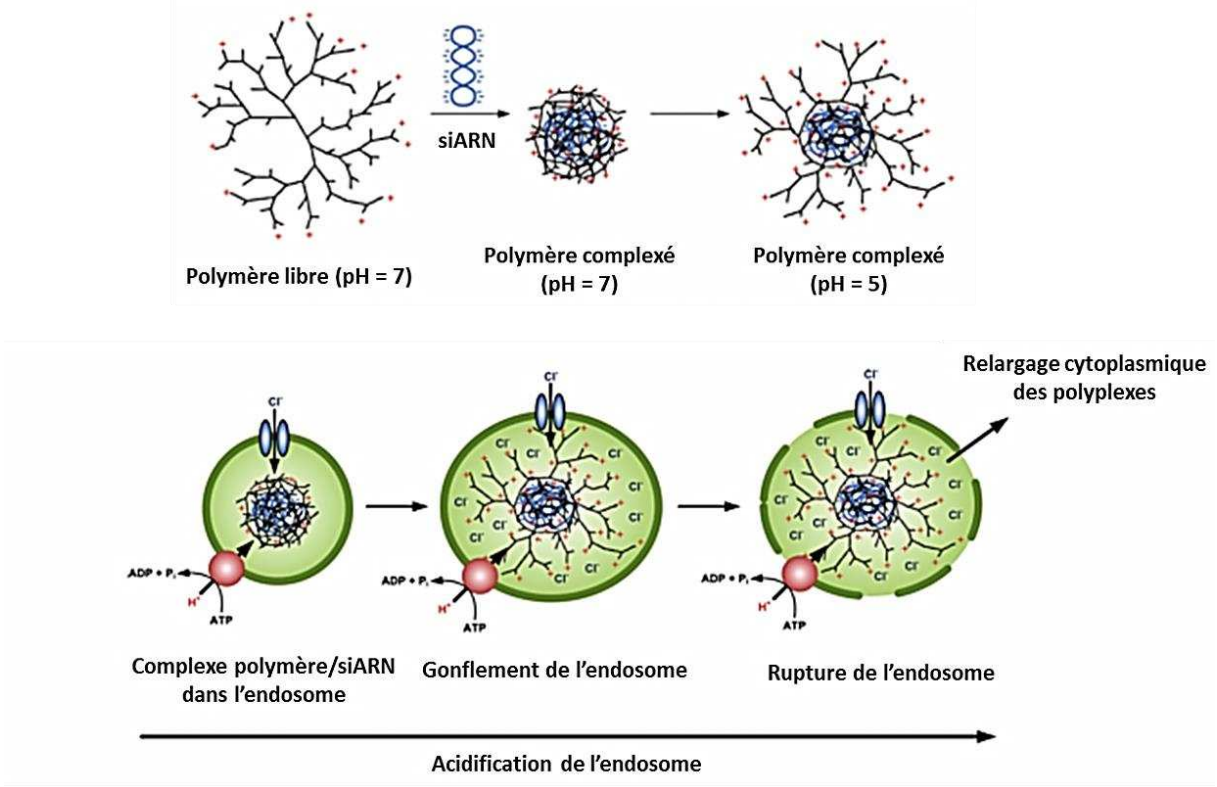

Figure 7. Représentation de l'effet parapluie induit par certains polymères (modifiée d'après Nguyen et Szoka, 2012 (97)).

- La formation des pores transitionnels : il s'agit d'un processus conduit par des composants de nanovecteurs capables d'interagir avec la membrane interne des endosomes tels que certains lipides et peptides. Cette interaction induit une perturbation locale de la membrane cellulaire et la formation de petits pores transitionnels permettant le passage des siRNA seuls (après la libération) ou les nanovecteurs de siRNA vers le cytosol (96,98). Il a été aussi rapporté que la formation de pores peut être aussi le résultat des effets pompe à proton et parapluie, et que la rupture complète des endosomes est peu probable (Figure 8) (96).

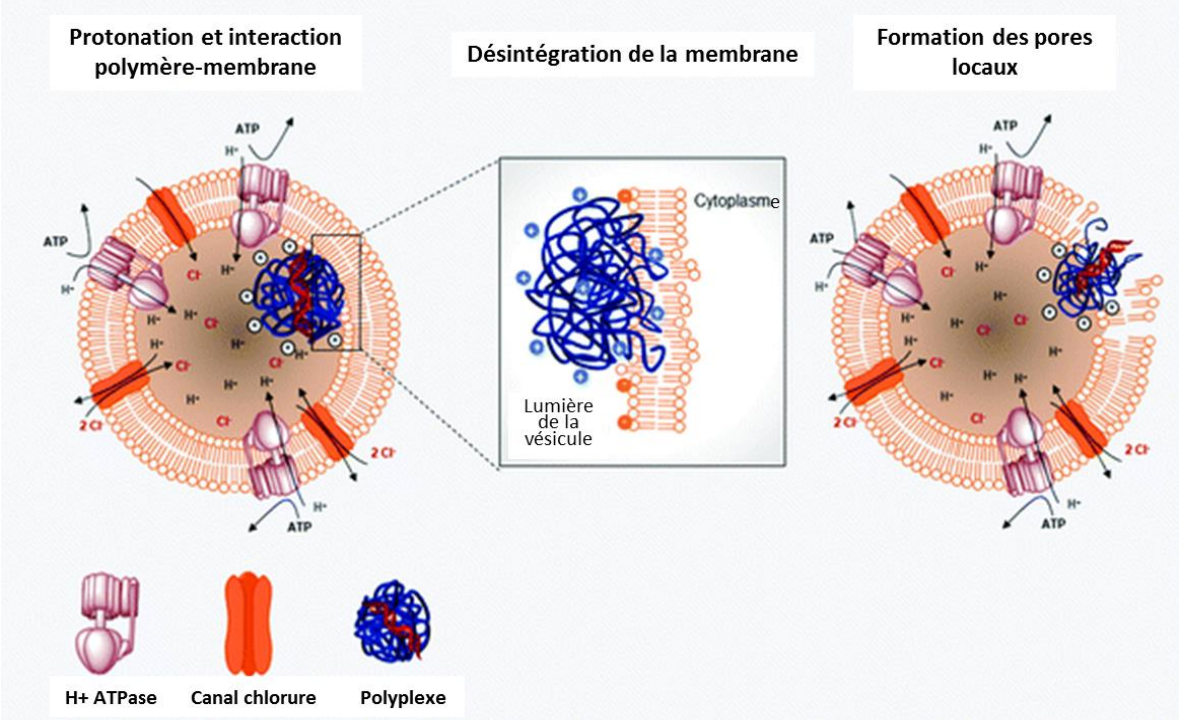

Figure 8. Illustration de la formation de pores transitionnels au niveau de la membrane endosomale induit par certains polymères (modifiée d'après Bus *et al.*, 2018 (96)).

- Fusion : ce mécanisme se produit en présence de certains lipides ou peptides dits fusogéniques. Pour les lipides, il s'agit de leur fusion avec les lipides de la membrane endosomale d'une manière comparable à celle utilisée au cours de l'internalisation par fusion. Cette fusion induit la libération du contenu du nanovecteur dans le cytosol (Figure 9) (99–101). Pour les peptides, il s'agit d'une insertion dans la membrane lipidique grâce à la présence de domaines spécifiques et au changement de structure du peptide en hélice alpha déclenché par le pH acide (62,95).

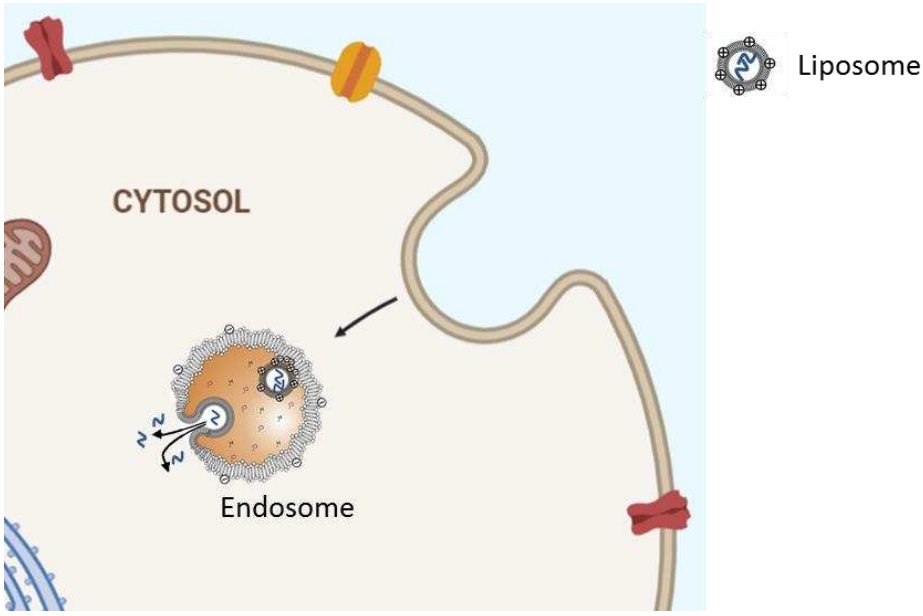

Figure 9. Illustration de l'échappement endosomal par fusion de liposome avec la membrane endosomale.

A l'heure actuelle, des études précliniques et des essais cliniques démontrent l'intérêt et le potentiel des siRNA pour le traitement des cancers. Malgré les progrès achevés depuis la découverte des mécanismes d'ARNi et le début du développement des nanovecteurs, le nanovecteur idéal est encore recherché. Afin que cette nouvelle classe thérapeutique soit appliquée pour le traitement de cancers, un nombre croissant de recherche et d'investigations sont attendues.

Objectifs de la thèse

Dans l'optique de concevoir un nanosystème pour la délivrance d'agents thérapeutiques pour traiter le cancer du sein triple négatif, une nanoplateforme (appelée cell-penetrating peptide (CPP)-capped stealth fluorescent nanoparticles, CS-FNP) à base de nanoparticules d'oxydes de fer superparamagnétiques (SPION), développée au sein de notre laboratoire, a été choisie (102). Les SPION sont intéressants pour leurs propriétés d'imagerie qui facilitent leur suivi *in vitro* (par microscopie électronique en transmission, MET) et *in vivo* (par imagerie par résonance magnétique, IRM). Ces SPION sont marquées avec un fluorochrome proche infra-rouge pour un suivi par imagerie de fluorescence. Pour augmenter la stabilité colloïdale et la furtivité de cette nanoplateforme, un polymère neutre, le PEG_{5000}, est greffé à la surface des SPION. Un ligand biologique, le peptide membranotrope gH625, est utilisé pour fonctionnaliser les CS-FNP. Ce peptide gH625 est un domaine d'interaction membranaire dérivé du virus d'herpès simplex de type 1, développé par l'équipe du Pr. Galdiero à l'université de Naples (103). Ce peptide a montré une capacité élevée à franchir la membrane cellulaire et les barrières biologiques, seul ou conjugué à d'autres molécules, et à délivrer des molécules thérapeutiques en intracellulaire (90,104–106).

Les objectifs de ces travaux de thèse sont : i) le développement d'un nanovecteur théranostique de siRNA, à partir de cette nanoplateforme, compatible avec une administration systémique pour le traitement du cancer du sein triple négatif, ii) l'étude des mécanismes d'internalisation et la détermination du trafic et du devenir intracellulaire de ces nanovecteurs et iii) l'évaluation *in vitro* de l'effet biologique de cette délivrance.

Pour le développement de ce nanovecteur permettant la transfection de siRNA, nous nous sommes basés sur une conception rationnelle des différents ingrédients composants le nanovecteur. Nous souhaitons développer un nanovecteur avec des étapes de formulation simples et rapides et qui offre une complexation efficace assurant une rétention et une protection optimales des siRNA. Par ailleurs, nous souhaitons utiliser une stratégie autorisant l'association de plusieurs composants dont chacun assure un rôle et une fonction précise. Cette stratégie doit permettre d'obtenir un nanovecteur multifonctionnel avec une certaine versatilité dans sa composition afin de pouvoir l'adapter aux conditions et aux exigences de son utilisation. Pour développer ce nanovecteur (CPP-capped stealth magnetic siRNA nanovector, CS-MSN), nous

nous sommes servis des CS-FNP développés par notre équipe pour former le cœur des CS-MSN. A ces CS-FNP, nous y avons associé des polymères cationiques (chitosan et poly-L-arginine) de façon électrostatique pour la complexation et la protection des siRNA et pour faciliter l'internalisation cellulaire et l'échappement endosomal. Une formulation de nanovecteurs dont les caractéristiques sont maîtrisées (taille inférieure à 200 nm, charge légèrement positive …) offre des avantages non seulement en termes d'internalisation au niveau de la cellule, mais aussi des avantages pour l'administration intraveineuse et l'accumulation par effet EPR (Enhanced Permeability and Retention effect) au niveau tumoral.

Les étapes de développement et d'optimisation de ce nanovecteur de siRNA doivent prendre en considération les critères évoqués précédemment (caractéristiques physico-chimiques et rétention/protection des siRNA) ainsi que la sécurité de l'utilisation de ce nanovecteur et l'effet biologique pour obtenir une efficacité de transfection élevée.

Cette thèse se présente en quatre parties :

- **La première partie** est **une étude bibliographique** de l'état de l'art, traitant les nanovecteurs à base de polymères avec ou sans une partie inorganique, décorés ou non avec des peptides et associant les siRNA d'une manière électrostatique.
- **La deuxième partie** présente les étapes de développement et d'optimisation de la formulation des CS-MSN ainsi qu'une étude biologique qui a permis d'évaluer la toxicité de la formulation de ce nanovecteur, d'optimiser le protocole de transfection et de fournir une preuve de concept pour l'efficacité des CS-MSN *in vitro*.
- **La troisième partie** est consacrée à l'étude des mécanismes et des voies d'entrée des nanovecteurs ainsi que de leur trafic et devenir intracellulaire en mettant l'accent sur le rôle du peptide gH625 dans chaque étape de cette étude.
- **La quatrième partie** est une évaluation de l'efficacité des CS-MSN à inhiber l'expression d'un gène cible, Bcl-xL, avec une mise en place de la technique de RT-qPCR et d'un modèle orthotopique de cancer du sein triple négatif chez la souris.

Ces travaux sont suivis d'une **discussion générale** des résultats obtenus dans les différentes parties de cette thèse.

Première partie : Nanovecteurs polymères de siRNA assemblés électrostatiquement

Publication 1: Versatile electrostatically assembled polymeric siRNA nanovectors: can they overcome the limits of siRNA tumor delivery?

Publiée dans « International Journal of Pharmaceutics », 2019

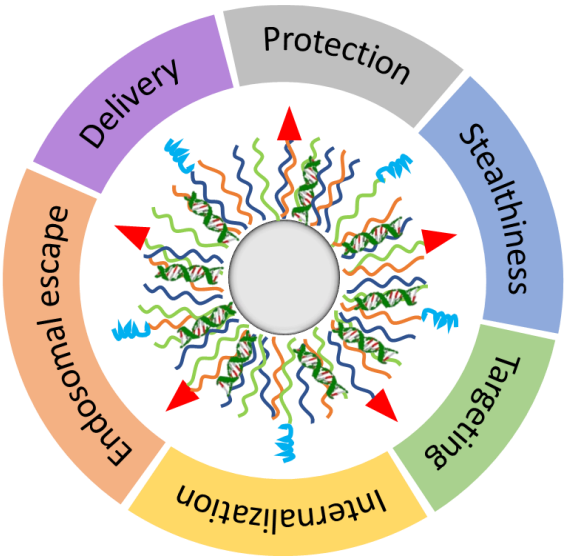

Préambule de la publication 1

Dans l'objectif de traiter les cancers, l'utilisation des siRNA semble être une stratégie prometteuse. Cependant, plusieurs barrières limitent leur application en clinique. Pour surmonter ces difficultés, différentes approches telles que la modification chimique des siRNA ou leur association à des molécules pour améliorer leur délivrance, ont été développées. A partir de la deuxième approche, un arsenal de nanovecteurs de siRNA est décrit dans la littérature. Deux classifications de nanovecteurs sont possibles : selon la nature des composants (lipidiques, polymères, peptidiques ou hybrides (contenant une partie organique et une partie inorganique)) ou selon le type de liaison des siRNA avec ces composants (liaisons covalentes ou liaisons électrostatiques).

La variété des nanovecteurs de siRNA existants étant grande, cette revue s'est focalisée sur les nanovecteurs à base de polymères avec ou sans une partie inorganique, décorés ou non avec des peptides et associant les siRNA d'une manière électrostatique. La littérature démontre que dans une conception rationnelle chaque composant doit être bien choisi et joue un rôle bien défini, soit à l'extérieur de la cellule (complexation, protection, furtivité, ciblage) soit au niveau de la cellule (internalisation, échappement endosomal, action sur l'expression du gène cible). Cet article de synthèse présente les difficultés de l'administration des siRNA et discute la capacité de ce groupe de nanovecteurs à délivrer efficacement les siRNA au niveau de leur cible en mettant l'accent sur les atouts de ces nanovecteurs par rapport à chaque défi (dégradation des siRNA, clairance rénale, faible accumulation au niveau de cite tumorale, faible internalisation par les cellules tumorales, difficulté à accéder au cytosol).

International Journal of Pharmaceutics 567 (2019) 118432

Contents lists available at ScienceDirect

International Journal of Pharmaceutics

journal homepage: www.elsevier.com/locate/ijpharm

Versatile electrostatically assembled polymeric siRNA nanovectors: Can they overcome the limits of siRNA tumor delivery?

S. Ben Djemaa, E. Munnier, I. Chourpa, E. Allard-Vannier, S. David*

Université de Tours, EA6295 Nanomédicaments et Nanosondes, 31 Avenue Monge, 37200 Tours, France

ARTICLE INFO

Keywords:
siRNA delivery
Electrostatically assembled polymeric siRNA nanovectors (EPSN)
Nanovector design
Intracellular trafficking
Protein down-regulation

ABSTRACT

The application of small interfering RNA (siRNA) cancer therapeutics is limited by several extra- and intracellular barriers including the presence of ribonucleases that degrade siRNA, the premature clearance, the impermeability of the cell membrane, or the difficulty to escape endo-lysosomal degradation. Therefore, several delivery systems have emerged to overcome these limitations and to successfully deliver siRNA to the tumor site. This review is focused on polymer-based siRNA nanovectors which exploit the negative charge of siRNA, representing a major challenge for siRNA delivery, to their advantage by loading siRNA via electrostatic assembly. These nanovectors are easy to prepare and to adapt for an optimal gene silencing efficiency. The ability of electrostatically assembled polymeric siRNA nanovectors (EPSN) to improve the half-life of siRNA, to favor the specificity of the delivery and the accumulation in tumor and to enhance the cellular uptake and endosomal escape for an efficient siRNA delivery will be discussed. Finally, the influence of the versatility of the structure of these nanovectors on the protein down-regulation will be evaluated.

1. Introduction

Since the 1990s and the discovery of post-transcriptional gene extinction in plants (Ratcliff et al., 1997), the mechanism of RNA interference (RNAi) has gained scientists' interest worldwide. This discovery has provided hope for the treatment of many severe diseases like cancers, autoimmune diseases, dominant genetic disorders and viral infections (Ferrari et al., 2012). RNAi is a natural phenomenon of sequence-specific gene silencing mediated by short sequences of non-coding endogenous RNA such as small hairpin RNA (shRNA), micro RNA (miRNA) and small interfering RNA (siRNA), considered as regulation systems of gene expression and RNA-based gene-silencing molecules (Carthew et al., 2009). The use of RNAi is linked to the transfer of genetic material into damaged cells, in order to ensure a targeted molecular intervention and achieve a higher level of specific action than conventional cytotoxic chemotherapy (Jabir et al., 2012). Basically, thanks to the potency and the selectivity for the silencing of specific genes, RNAi-based therapy could treat any human disease caused by the over-expression of one or few genes (Aagaard and Rossi, 2007). Over the past few years, different approaches have been developed based on this strategy to inhibit the expression of certain genes, called oncogenes, coding for over-expressed proteins that are implicated in tumor growth (Haussecker, 2014). Among these small nucleic acids, it is generally accepted that siRNA sequences, of 21–23 nucleotides, offers the best combination of specificity and potency as therapeutics and are the most used in the development of anticancer treatments (Ferrari et al., 2012; Resnier et al., 2013)

Following the demonstration of RNAi in mammalian cells in 2001 (Elbashir et al., 2001), several studies have quickly concentrated on specific gene silencing of siRNA to exploit this powerful mechanism to interfere with cancer-causing or cancer-promoting genes to develop a new class of drugs. In 2003, Song et *al.* presented the first *in vivo* evidence of RNAi-based therapeutic efficacy to protect mice from liver failure and fibrosis. By using siRNA duplexes targeting gene Fas, they demonstrated a specific decrease of mRNA level and protein expression of Fas in mice hepatocytes, after intravenous injections using a modified

Abbreviations: siRNA, small interfering RNA; EPSN, electrostatically assembled polymeric siRNA nanovectors; RNAi, RNA interference; shRNA, small hairpin RNA; miRNA, micro RNA; TLR, Toll-like receptor; N/P ratio, the molar ratio between the number of positive charges of polymer's amino groups and that of negative charges of siRNA's phosphate groups; SPION, superparamagnetic iron oxide nanoparticles; PEG, polyethylene glycol; PEI, Polyethylenimine; IL-4R, Interleukin-4 receptor; IL-4RPep-1, Interleukin-4 receptor binding peptide 1; CPP, cell-penetrating peptide; DMAEMA, [2-(dimethylamino) ethyl methacrylate]; BMA, butyl methacrylate; b-pDPB, b-(dimethylaminoethyl methacrylate-co-propylacrylic acid-co-butyl methacrylate); pD-b-pDPB, poly[dimethylaminoethyl methacrylate-b-(dimethylaminoethyl methacrylate-co-propylacrylic acid co-butyl methacrylate)]; CS-MSN, CPP-capped stealth magnetic siRNA nanovector

* Corresponding author.
E-mail address: stephanie.david@univ-tours.fr (S. David).

https://doi.org/10.1016/j.ijpharm.2019.06.023
Received 29 March 2019; Received in revised form 4 June 2019; Accepted 10 June 2019
Available online 11 June 2019
0378-5173/ © 2019 Published by Elsevier B.V.

hydrodynamic transfection method (Song et al., 2003). Today, some siRNA-based therapies for cancer treatment are in clinical trial phases (Nikam and Gore, 2018; Tabernero et al., 2013; Tatiparti et al., 2017). For example, Silenseed Ltd performed the phase I clinical trial of its siRNA-based treatment (siG12D-LODER) against pancreatic cancer. SiG12D-LODER target the oncogene KRAS that is implicated in cancer growth. This trial was completed in 2014 and showed high safety and tolerability profiles of this treatment in patients. This therapy is currently in Phase II trial which aims to evaluate the efficacy of the combination of siG12D-LODER with standard chemotherapy treatment (Gemcitabine + nab-paclitaxel) by measuring progression-free survival in patients (Kaczmarek et al., 2017). The first siRNA-based therapy, ONPATTRO® (patisiran), was approved by the Food and Drug Administration (FDA) and the European Medicines Agency (EMA) in August 2018 for the treatment of polyneuropathy of hereditary transthyretin-mediated amyloidosis in adult patients (Al Shaer et al., 2019; Rizk and Tüzmen, 2017). This approval presents a great achievement in nanomedicine discovery and development and provides hope for the progress toward an anti-cancer application.

Despite the therapeutic potency of siRNA, *in vitro* and *in vivo* trials revealed extra- and intracellular barriers difficult to overcome by naked siRNA. Therefore, different delivery systems have been exploited to increase the therapeutic potency of siRNA *in vivo*. The first part of this revue will present these barriers and the principle of siRNA nanovectorization. The second part of the review will focus on electrostatically assembled polymeric siRNA nanovectors (EPSN). First, the design of EPSN to overcome these barriers will be discussed, second, the parameters that have to be taken into account to evaluate the protein down-regulation efficiency will be presented and illustrated with currently studied EPSN.

2. siRNA delivery: Challenges and nanovectorization

2.1. Extra- and intracellular barriers for naked siRNA

The limitations of naked siRNA are due to their properties (charge, hydrophilicity, size, sensitivity to degradation …) which represent hurdles in each step of the trafficking of siRNA, extra- and intracellularly (Fig. 1). For example, in the blood or in biological environment, presence of enzymes such as ribonucleases affects the siRNA stability and involves their rapid degradation (Gavrilov and Saltzman, 2012). Even if siRNA escape enzymatic degradation in blood, their small size favors their rapid elimination by renal clearance. Therefore, the accumulation of siRNA in target site is a big challenge. Furthermore, the characteristics of the tumor tissue, such as i) the heterogeneous blood flow distribution and poor perfusion of inner region of solid tumor, ii) the dense intercellular matrix in this region, and iii) high hypoxia, acidity and interstitial fluid pressure, due to dysfunctional tumor lymphatics (Forster et al., 2017; Gillies et al., 1999; Heldin et al., 2004), restrict the uniform delivery of nanovectors to the tumors in sufficient quantities (Jain and Stylianopoulos, 2010). Once in the tumor site, siRNA must reach their target cells that express or overexpress the gene(s) of interest. Nevertheless, naked siRNA do not have the ability to distinguish target cells and they can act in the same way on normal cells and defective cells including unwanted off-target effects (Wang et al., 2017). Moreover, the negative charge of siRNA phosphate groups and their hydrophilicity limit their ability to cross cell membranes, because of the electrostatic repulsions between siRNA and the cell surface, negatively charged as well, and the impermeability of the lipid bilayer to hydrophilic molecules (Dominska and Dykxhoorn, 2010; Reischl and Zimmer, 2009; Videira et al., 2014). The small amount of siRNA that overcomes previously mentioned challenges and is internalized into cells must escape endosomal/lysosomal degradation in order to reach the cytosol where its targets are present (Gavrilov and Saltzman, 2012). In addition to these limitations, the immunogenicity of siRNA represents another concern associated with *in vivo* administration. In fact, Reynolds *et al.* reported that siRNA can activate the innate immune system by inducing the expression of associated genes such as interferons or interferon-inducible genes. They demonstrated that this activation is cell type- and siRNA length-dependent (Reynolds et al., 2006). Other studies showed that certain siRNA can be recognized by some Toll-like receptors (TLR) such as TLR3, 7 and 8. This recognition can trigger interferon pathway responses (Behlke, 2006). The activation of this pathway results in the induction of the apoptosis and the cell death (from 20% to 60% of cell death) (Reynolds et al., 2006). The consequence of the association of previously presented limitations of the use of naked siRNA is an unsatisfactory effect *in vitro* as well as *in vivo*. It is, therefore, necessary to develop delivery systems with suitable properties to overcome all these challenges.

2.2. Nanovectorization for siRNA delivery

Because of the challenges mentioned above, many approaches were adopted to develop various galenic forms of siRNA-based medicine, in order to exploit the powerful effect of siRNA in anticancer therapies. One promising approach is the loading of siRNA in a nanovector. This strategy, called siRNA nanovectorization, consists in associating siRNA to suitable materials to obtain a nano-sized vector able to effectively

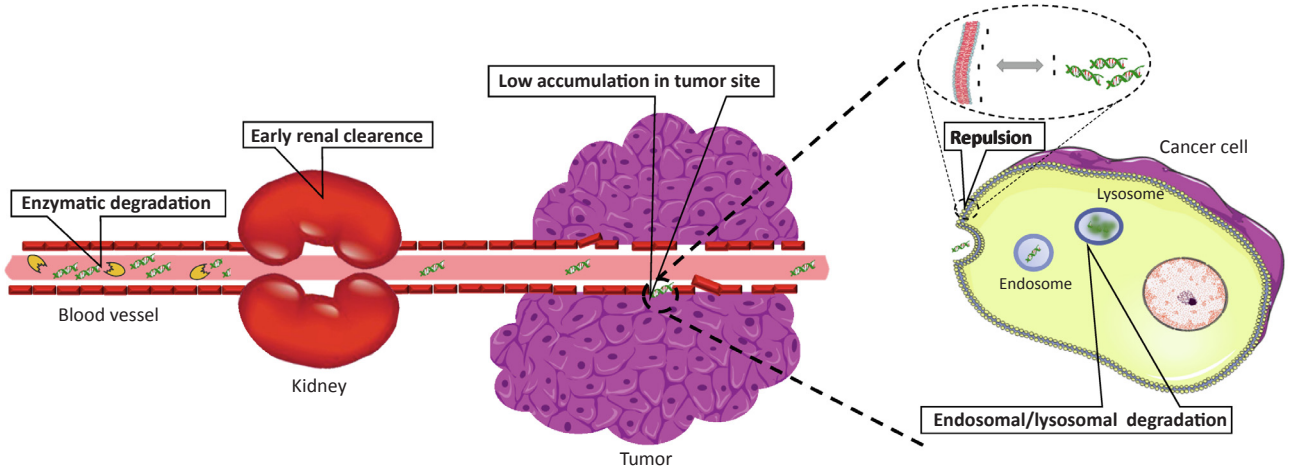

Fig. 1. Illustration of extra- and intra-cellular biological barriers for siRNA-based cancer therapy. Extracellular barriers: enzymatic degradation in the blood, early elimination by the kidney, low accumulation in the tumor site, and repulsion at the surface of the cell membrane. Intracellular barriers: endosomal entrapment and endo-lysosomal degradation.

convey siRNA toward their target (Ferrari et al., 2012; Resnier et al., 2013). Nanovectors are developed to carry and deliver drugs, oligonucleotides, peptides or other desired cargos to target tissues. Various nanosystems have been used for siRNA delivery in biomedical applications. At the present time, a relatively extensive arsenal of nanovectors has been proposed to administer siRNA without interfering with their silencing efficiency (Ozcan et al., 2015). In literature several types of nanovectors are described, including organic (lipid-based, polymer-based, peptide-based) (Resnier et al., 2013) and inorganic ones (based on the use of iron oxide, gold, quantum dots, …) (Conde et al., 2014). These nanovectors can be associated with siRNA using various methods: 1) conjugation, which needs chemical intervention and consists in covalently attaching siRNA to the nanovector components (Ding et al., 2014, 2012; Muratovska and Eccles, 2004), 2) encapsulation that is based on the loading of siRNA into a protective shell (liposomes or micelles, for instance) (Chen et al., 2012; David et al., 2012; Mokhtarieh et al., 2018) and 3) electrostatic bonds which aim to complex negatively charged siRNA with positively charged nanovector components (Bruniaux et al., 2017; Guruprasath et al., 2017; Liu et al., 2011).

3. Electrostatically assembled polymeric siRNA nanovectors (EPSN)

The common cause of the different challenges of siRNA delivery is their anionic character. This property generally considered as a disadvantage can be used to complex siRNA electrostatically and then at the same time create a nanosystem and hide the charge. Electrostatic complexation can be achieved with cationic polymers, peptides/proteins or cationic lipids. This review will more particularly relate to siRNA polymer-based nanovectors which are less described in the review literature than siRNA lipid-based nanovectors. We will distinguish four groups of EPSN: (A) EPSN containing only polymers and siRNA, (B) EPSN decorated with peptides, (C) EPSN containing an inorganic core, and (D) EPSN containing an inorganic core and decorated with peptides (Fig. 2).

Electrostatic interaction has several advantages such as the ease and the rapidity of nanovector formulation. The use of electrostatic association avoids siRNA chemical modification and purification procedures that could affect their biological activity (Cavallaro et al., 2017; Conde et al., 2014). Electrostatic interactions need positively charged components in the nanovector to bind negatively charged siRNA. The stability of such an assembly depends on the number of charged groups on the molecules, therefore on the pH and the ionic strength of the environment. This strategy to load siRNA in nanovectors might be advantageous for the release of therapeutic agent. In fact, pH-sensitive components such as polymers or peptides are usually used for this assembly. This property can be useful at two levels: 1) in the tumor site and 2) in endosomes. As tumor tissues exhibit an acidic environment with a pH significantly lower than that of normal tissues, these components can allow a smart release. For example, the change of the pH induces a modification in the polymer charge density, leading to a pretty localized release of siRNA in the target site (Shakiba et al., 2017). In endosomes, the pH-variation is also exploited for facilitating the release of siRNA from nanovectors (Creusat et al., 2012, 2010; Nguyen and Szoka, 2012). This process is known as endosomal escape and will be more discussed later. Furthermore, the tumor environment is, often also characterized by hypoxia and the enrichment with free radical species. This difference can be exploited as well for siRNA delivery by using hypoxia-sensitive polymers (Perche et al., 2014). Many studies for siRNA nanovector development adopt these strategies of formulation.

Despite the ease and the speed of the preparation of electrostatically assembled nanovectors, their development needs serious work on the optimization of the formulation. Indeed, a critical point is the stability of these complexes in biological environment. As the electrostatic association between siRNA and cationic components is low, these complexes may disassemble too early if the formulation is not optimized (Creusat et al., 2010; Creusat and Zuber, 2008). Therefore, to successfully complex siRNA with polymers, there are some parameters to consider such as the components ratio and concentration (Richards Grayson et al., 2006). One can distinguish two types of ratio described in literature: i) charge ratio which represents the molar ratio between the number of positive charges of polymers (for instance, those of amino groups) and that of negative charges of siRNA phosphate groups (N/P ratio) (Guruprasath et al., 2017; Werfel et al., 2017), and ii) mass ratio which represents the ratio between the mass of polymer and that of siRNA (Corbet et al., 2016; Veiseh et al., 2010). These ratios are usually optimized at the beginning of each siRNA nanovector development to determine the best formulation. The complexation efficiency is often evaluated by gel retardation assay using ethidium bromide, as nucleic acid intercalant (Liu et al., 2011; Veiseh et al., 2011b, 2010). In fact, with this technique, free siRNA appear as fluorescent bands, while no fluorescence is detected if they are complexed and not accessible to ethidium bromide.

siRNA can also be complexed with polymers surrounding an inorganic core or support (Ben Djemaa et al., 2018; Guruprasath et al., 2017; Pittella et al., 2011). In this case another ratio appears which defines the quantity of the inorganic part used in the nanovector. The presence of the inorganic core can be advantageous for the formulation. In fact, it has been demonstrated that the use of the inorganic core

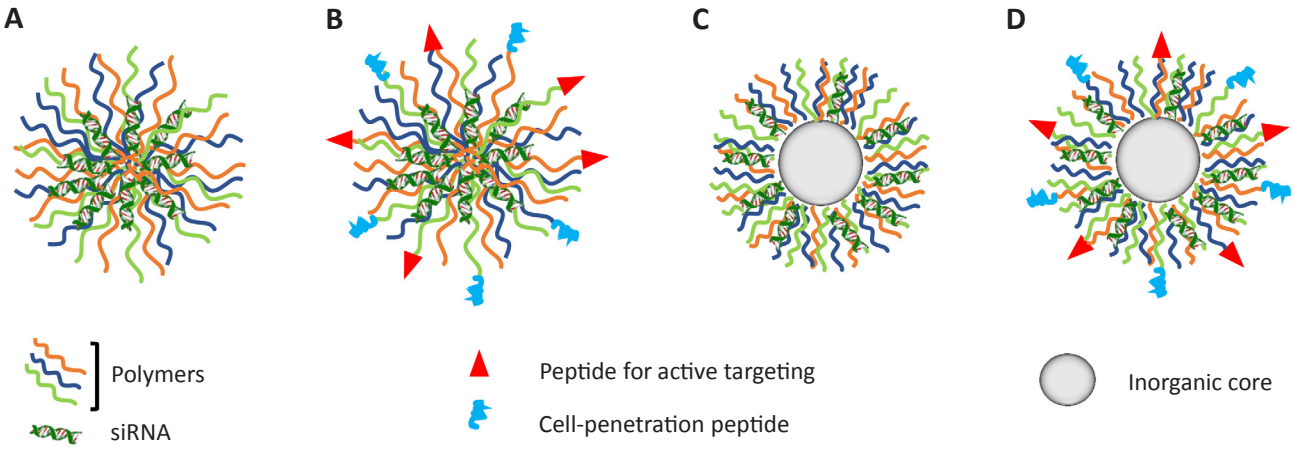

Fig. 2. Schematic presentation of electrostatic assembled polymer-based siRNA nanovectors (EPSN): (A) containing only polymers and siRNA, (B) decorated with peptides, (C) containing an inorganic core, and (D) containing an inorganic core and decorated with peptides.

(based on superparamagnetic iron oxide nanoparticles (SPION)) plays an important role in the stability and the control of the size of the final nanovector. Addition of an inorganic core to the formulation decreased the size and the polydispersity index of the complexes from 213 nm to 175 nm and from 0.43 to 0.34, respectively (Ben Djemaa et al., 2018). Moreover, Xie *et al.* developed hybrid nanoparticles based on calcium phosphate core for the electrostatic loading and delivery of siRNA. These nanoparticles exhibited efficient siRNA loading and enhanced colloidal and serum stability (Xie et al., 2014). Apart from their role in the formulation and the transport of siRNA, some inorganic cores such as quantum dots (Derfus et al., 2007; Pan et al., 2010), gold nanoparticles (Jaganathan et al., 2014; Rosi et al., 2006; Song et al., 2010) or magnetic nanoparticles (Lu et al., 2007; Sun et al., 2008), can also be used as diagnostic tools. They allow the monitoring and the study of the distribution of inorganic nanovectors [45,46] using fluorescence, fluorescent energy transfer (Fan et al., 2003) or magnetic resonance imaging (Pan et al., 2010; Sosnovik et al., 2008). Therefore, the choice of this inorganic part of the nanovectors is of great interest.

As an example of electrostatically assembled siRNA nanovectors, Pitella *et al.* presented a nanosystem based on a stable core of calcium phosphate nanoparticles coated with polyethylene glycol (PEG) and a charge-conversional polymer for the delivery of siRNA. This nanovector was prepared by simple mixing of the components at a determined concentration and was confirmed to possess excellent siRNA loading (about 80% of dose) (Pittella et al., 2011). Yet, Miteva and coworkers used two diblock polymers based on polyethylene glycol (PEG-b-pDPB) and polydimethylaminoethyl (pD-b-pDPB), for the nanovectorization of siRNA. Results showed a high cytoplasmic release and bioavailability in triple negative breast cancer cells (MDA-MB-231) due to the high intracellular unpackaging of the complex, quantified by FRET (Miteva et al., 2015). This electrostatic interaction shows a good balance between the siRNA complexation and release which present a suitable feature for siRNA delivery.

Certainly, this strategy of siRNA nanovectors formulation has many advantages but the electrostatic assembly results in less controlled structures in terms of components organization and nanovector size due to the poor control of their interactions and the formation of electrostatic bonds. One question rises here: are these siRNA nanovectors able to accomplish their mission to successfully transport siRNA through biological barriers and efficiently deliver them into tumor site to down-regulate the targeted gene(s) in cancer cells?

The main goal of siRNA nanovectors development is to improve the efficiency of used siRNA to down-regulate targeted genes. Therefore, to obtain a successful siRNA gene silencing, the nanovector must provide a) the protection of siRNA and the suitable stealthiness, b) the specific recognition of target cells or tissues, c) the capacity to cross cell membranes and d) the ability to escape endosomes and to deliver siRNA into the cytosol (Fig. 3).

3.1. Design rationale of EPSN to overcome extracellular barriers

One of the principal needs of siRNA nanovectorization is to protect siRNA from biodegradation and to delay their elimination via clearance organs. Therefore, two properties can be brought to siRNA in order to improve the chance to reach their therapeutic target: physico-chemical stability and immune stealthiness.

3.1.1. Protection from enzymatic degradation and premature clearance

Actually, the presence of enzymes such as ribonucleases in biological environment threatens siRNA integrity and shortens their plasma half-life (Behlke, 2006). To solve this problem, one strategy is the electrostatic binding of siRNA with polymers. Table 1 presents some of the most used polymers in the development of siRNA delivery nanovectors. Polymers, especially biocompatible ones, have been considered as attractive materials for molecules delivery because of their interesting features (Gary et al., 2007; Tan et al., 2011; Venditti, 2017). In fact, polymers and polymer-based siRNA nanovectors show high colloidal stability in biological environment (Veiseh et al., 2011a) and have the ability to increase the half-life of siRNA in serum by limiting the accessibility of enzymes and molecules to siRNA (Arnold et al., 2017).

Cationic polymers are widely used for siRNA nanovector development strategies thanks to the presence of multiple positive charges per molecule and their ability to bind siRNA electrostatically (Liu et al., 2014; Veiseh et al., 2011b). In our previously published results, we showed that naked siRNA were degraded in the presence of a low percentage of serum (5%) after 4 h and in the presence of ribonuclease A within 30 min. However, the use of two cationic polymers, chitosan and poly-L-arginine, in a siRNA nanovector offers a complete complexation and provides a protection of siRNA even in a high amount of serum (50%) or in the presence of ribonuclease A during 4 h (Ben Djemaa et al., 2018; Bruniaux et al., 2017).

Another example of cationic polymers classically used and studied for gene delivery/therapy is Polyethylenimine (PEI). PEI is a synthetic macromolecule consisting of a repeating amine and ethyl unit, with a high cationic charge density able to condense spontaneously, via electrostatic interaction, anionically charged siRNA and increase their stability in biological medium (Boussif et al., 1995). In their study, Liu and colleagues have successfully complexed siRNA with Alkyl-PEI. This complexation results in a high siRNA protection from enzymatic degradation in the presence of 50% of serum at 37 °C, evaluated by a qualitative gel retardation assay (Liu et al., 2011). In addition to protect the siRNA from the degradation and the early elimination, these polymers are able to condense nucleic acid and increase the size of the complex, compared to the size of naked siRNA, to avoid the clearance of siRNA, while their size remain suitable for gene delivery (Arnold et al., 2017; Parmar et al., 2018; Videira et al., 2014).

In most cases, the limitation of the use of cationic polymers with a high charge density, such as PEI, poly-arginine and poly-lysine, is the relative toxicity (Lv et al., 2006). Different studies reported that this toxicity depends on a set of factors such as the molecular weight, the dose and the degree of branching. In their study, Fischer and coworkers showed that the use of low molecular weight PEI (10 KDa) with a low degree of branching offers a good alternative for classic PEI and shows low cytotoxicity (Fischer et al., 1999). Ohsaki et al. reported that the use of poly-L-lysine with dendritic structure and several types of branch units did not show any significant toxicity in Hela cells (Ohsaki et al., 2002). One strategy used to reduce the toxicity is the chemical modification of these polymers such as lipid-substitution (Landry et al., 2012; Parmar et al., 2018), covalent conjugation (Foillard et al., 2011) or structural modification (Chiper et al., 2017; Fröhlich et al., 2012). Another strategy is the association of another polymer or copolymer like chitosan (Shim and Kwon, 2010), polyethylene glycol (Mi et al., 2005) or poly-(γ-benzyl l-glutamate) (Tian et al., 2007).

3.1.2. Increase of the immune stealthiness of siRNA

One of the major bottlenecks of the use of siRNA is their immunogenicity and their negative charge. These limitations underline the importance of an improved strategy for the delivery of siRNA. The complexation of siRNA with polymers could be an approach to overcome this challenge. Takeshita and coworkers used atelocollagen for the intravenous delivery of siRNA in a bone tumor metastasis model in mice. After the injection of a control naked siRNA or atelocollagen-siRNA complex, they evaluated the stimulation of the innate immune responses and they showed that the association of siRNA with this polymer did not result in an increase in the level of interferon (Takeshita et al., 2005). Moreover, the association of siRNA to polymers could neutralize their negative charge. As an example, the electrostatic assembly of siRNA with Alkyl-PEI or with a complex of polymers and peptide result in neutral zeta potential of the nanovectors around −2.6 or −0.01 mV, respectively (Liu et al., 2011; Veiseh et al., 2011b). However, the use of several cationic polymers or highly positively

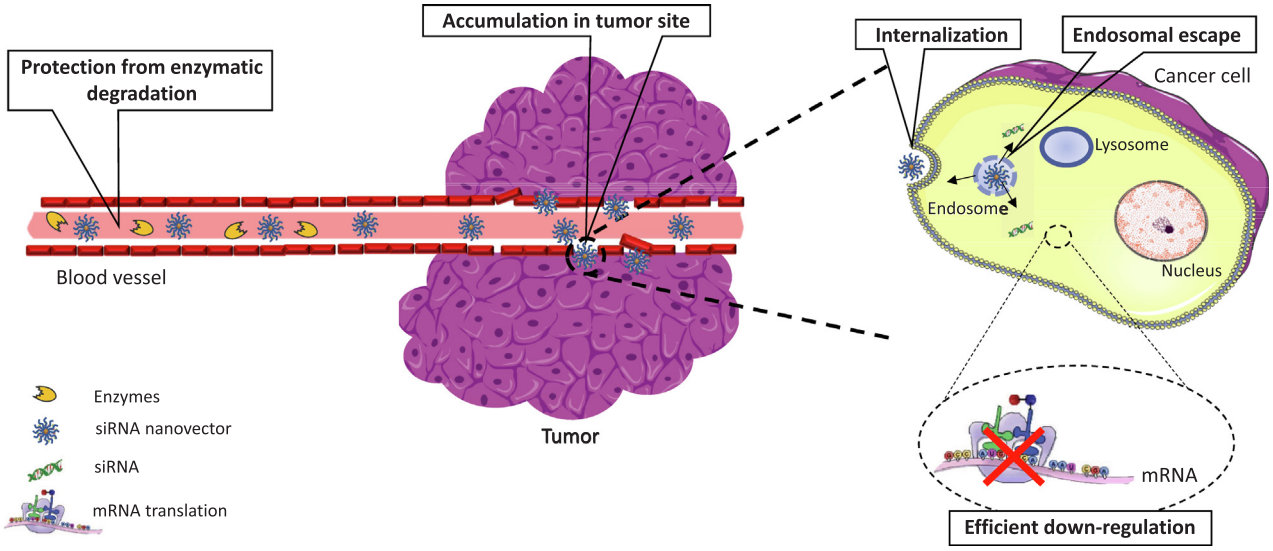

Fig. 3. Schematic presentation showing features of EPSN for efficient siRNA delivery after systemic administration. EPSN protect siRNA from enzymatic degradation in the blood. Thanks to their stealthiness, the extension of the circulation time and their characteristics, the accumulation in the tumor site is increased. The internalization of EPSN occurs by different routes, mostly via an endocytic pathway. When internalized by endocytosis, EPSN's components promote the endosomal escape of siRNA and avoid their lysosomal degradation to gain access to the cytosol where they use the mechanism of RNAi to down-regulate the expression of the target gene.

charged polymers results in unwanted high density of positive charges. In fact, a high positive surface charge induces the interaction with negatively charged plasmatic molecules and the formation of large aggregates that can be recognized by the innate immune system and promotes their elimination (Resnier et al., 2013). In EPSN containing an inorganic core, the association of neutral polymers such as PEG or polyvinylpyrrolidone (Pan et al., 2018) is often chosen to mask charges and to increase the stealthiness of siRNA nanovectors (Arnold et al., 2017). Neutral polymers are usually attached by covalent interaction to the inorganic core of the nanovector (Veiseh et al., 2011b), to cationic polymers (Xie et al., 2014) or to both of those (Veiseh et al., 2010). For example, in one study, the use of polylysine to develop a siRNA nanovector for the targeting of breast tumor-initiating cells yielded in positive zeta potential of 19 mV. In contrary, the addition of PEG to polylysine in another siRNA nanovector resulted in a surface charge of 0.5 mV. By masking the surface charge of nanovectors, PEG is able to avoid siRNA nanovectors' binding to plasma proteins, prolong their systemic circulation time, prevent their recognition by the immune system and promote their accumulation due to the enhanced permeability and retention (EPR) effect in different types of tumors (Jabir et al., 2012; Owens III and Peppas, 2006). Sun *et al.* showed that PEGylation of their polymeric siRNA nanovector using PEG_{5k} or PEG_{6K} prolonged the circulation time in the blood 4-fold compared to free siRNA, by preventing protein adsorption on the surface (Sun et al., 2015).

3.1.3. Targeting of cancer cells

One additional major flaw of naked siRNA is their lack of specific recognition of target cells. Thus, it is unlikely that siRNA can be accumulated with a high concentration and for a sufficient period of time for deep penetration in the core of the tumor. To take advantage of enhanced permeability and retention (EPR) effect that allows the accumulation in the tumoral site by passive targeting, siRNA can be associated to polymers to obtain complexes with adequate properties (50 nm < size < 250 nm and neutral charge) (Resnier et al., 2013). In this case, the obtained EPSN remain compatible with an intravenous administration (Arnold et al., 2017; Videira et al., 2014). In some cancers whose cells do not express any specific marker or receptor, this passive targeting is the only hope for tumor accumulation of the nanovectors.

When active targeting is possible, one can improve the cellular specificity of siRNA nanovectors and increase their accumulation in the tumor. Therefore, biological ligands such as antibodies (anti-HER2 (Goren et al., 1996), anti-CD19 (Menezes et al., 1998)), peptides (Schmohl et al., 2017), vitamins (folate) (Dohmen et al., 2012), growth factors, enzymes are associated to nanovectors (Prokop and Davidson, 2008). Mostly, ligands are chosen for their high ability to target selectively some specific extracellular molecules (such as receptors) overexpressed in some tumor types (An et al., 2015; Lee et al., 2016a,b). This review focuses on the use of peptides for the functionalization of EPSN, as these ligands can be useful at various levels during the extra- and/ or intracellular trafficking of the siRNA nanovector. Peptides are able to allow the active targeting of tumors as described above and/ or to participate in the cellular trafficking which will be discussed in the following sections of this review.

Peptides, or polyamines, are short chains containing < 50 amino acids monomers linked by amide bonds and are structurally similar to proteins. Peptides can be found naturally or synthetically and have the potential for the stabilization and biofunctionalization of nanoparticles (Conde et al., 2014; Zhang et al., 2016). Peptides can be associated with siRNA nanovectors by electrostatic or covalent bonds (Corbet et al., 2016; Jiang et al., 2012; Muratovska and Eccles, 2004; Wang et al., 2009). Table 2 presents some of the most used peptides in the functionalization of siRNA nanovectors. Some peptides can be selectively addressed to membrane molecules on the surface of specific cells (Conde et al., 2014; Schmohl et al., 2017). Thus, the use of these peptides in siRNA nanovectors could guide and improve the interactions with cell surfaces. In order to treat cancer, Guruprasath and colleagues presented an example of the functionalization of siRNA nanovectors with peptide for active targeting. In this study, they demonstrated a specific interaction of their siRNA nanovector functionalized with Interleukin-4 receptor (IL-4R)-binding peptide 1 (IL4RPep-1) with the IL-4R up-regulated on cancer cells. Furthermore, they showed an efficient accumulation in tumor, 3-fold more than with nanovectors without peptide (Guruprasath et al., 2017).

To enhance the targeting and the penetration in the tumor site, a rational design of nanovectors that considers tumors characteristics and the properties of their microenvironment, mentioned in Section 2.1., is needed. As solid tumors exhibit low interstitial pH, many pH-sensitive nanovectors were developed to deliver siRNA to tumors using pH-

Table 1
Examples of the most used polymers in electrostatically assembled polymer-based siRNA nanovectors.

Polymer	Abbreviation	Charge	MW	References
Chitosan	CS	Cationic	110–250 KDa	Chen et al. (2012); Huh et al. (2010); Sun et al. (2016); Veiseh et al. (2010); Xie et al. (2014)
Atelocollagen	ATCOL	Cationic	300 KDa	Minakuchi et al. (2004); Mu et al. (2009)
Polyethylenimine	PEI	Cationic	1.2 – 25 KDa	Huh et al. (2010); Liu et al. (2011); Mok et al. (2010); Veiseh et al. (2011b, 2010)
Poly-arginine/poly-L-arginine	pArg/PLR	Cationic	10–70 KDa	Ben Djemaa et al. (2018); Bruniaux et al. (2017); Kim et al. (2009); Veiseh et al. (2011b)
Poly-lysine/poly-L-lysine	pLys /PLL	Cationic	10–70 KDa	Cavalieri et al. (2015); Jaganathan et al. (2014); Veiseh et al. (2011b)
Poly-alpha-glutamate	PGA	Cationic	7 KDa	Krivitsky et al. (2018)
Poly-amidoamine	PAMAM	Cationic	20–80 KDa	Liu et al. (2014); Liu and Peng (2016)
Polyaspartamide-1,2-diaminoethane	PAsp(DET)	Cationic		Pittella et al. (2011)
Poly(dimethylaminoethyl methacrylate)	pDMAEMA	Cationic	12 KDa	Lee et al. (2018); Miteva et al. (2015)
Poly[dimethylaminoethyl methacrylate-b-(dimethylaminoethyl methacrylate-co-propylacrylic acidco-butyl methacrylate)]	pD-b-pDPB	Cationic	32 KDa	Miteva et al. (2015)
Hyaluronic acid	HA	Anionic	19–50 KDa	Kim et al., 2009; Yin et al., 2016)
Poly-D,L-lactic-co-glycolic acid	PLGA	Anionic	66–107 KDA	Chen et al. (2012)
Polyethylene glycol	PEG	Neutral	2–12 KDa	Cavalieri et al. (2015); Pittella et al. (2011); Sun et al. (2016); Veiseh et al. (2011b, 2010); Werfel et al. (2017)

Table 2
Examples of the most used peptides for the functionalization of electrostatically assembled polymer-based siRNA nanovectors.

Peptide	Abbreviation	Origin	Family	Sequence	Target	Reference
Oligo-arginine	R8, R9, R11, …	Synthetic peptide	Cell-penetrating peptide	Rn (n = 8, 9, 11 …)	Not identified	Liu et al. (2014)
Trans-activated transcription	TAT	Protein transduction domain of human immunodeficiency virus type 1	Cell-penetrating peptide	GRKKRRQRRRPPQ	No data	Malhotra et al. (2013)
Penetratin	P	Homeodomain of the Drosophila homeoprotein Antennapedia	Cell-penetrating peptide	CRQIKIWFQNRRMKWKK	No data	Muratovska and Eccles (2004)
gH625	gH625	Glycoprotein H of Herpes simplex virus type 1	Cell-penetrating peptide	HGLASTLTRWAHYNALIRAF	Not identified	Ben Djemaa et al. (2018)
Transportan	TP 10	Galanin and mastoparan	Cell-penetrating peptide	GWTLNSAGYLLGKINLKALAALAKKIL	No data	Pärnaste et al. (2017)
Chlorotoxin	CTX	Scorpion-derived peptide	Tumor-targeting peptide	MCMPCFTTDHQMARKCDDCCGGKGRGKCYGPQCLCR	affinity to a vast majority of brain tumors, prostate, skin and colorectal cancers	Mok et al. (2010); Veiseh et al. (2010)
Arginine-glycine-aspartate	RGD	Synthetic	Receptor-recognition motif	RGD	Tumor endothelial cells	Huang et al. (2015); Ragelle et al. (2015); Wang et al. (2009)
IL-4 receptor- binding peptide	IL4RPep-1	Synthetic	Peptide	CRKRLDRNC	IL-4 receptor	Guruprasath et al. (2017)
RRRVVVVVV	R3V6	Synthetic	Cell-penetrating peptide	RRRVVVVVV	Not identified	Oh and Lee (2014)
Bombesin	BN	Skin of an European frog	Peptide	QRLGNQWAVGHLM	Gastrin-releasing peptide receptors	Wang et al. (2009)

sensitive peptides for instance (Mok et al., 2010; Zhu et al., 2015). In addition, the formulation of hypoxia-sensitive nanovectors using, for example, hypoxia-responsive polymers or hypoxia-targeted polymers can be used to benefit from the hypoxia in tumor site (Kang et al., 2016; Perche et al., 2016). Perche and colleagues synthesized hypoxia-sensitive polymers to develop a nanovector for the delivery of siRNA in tumors. They showed that these polymers respond to the hypoxia-stimulation by detaching PEG from the complexes to enhance the accessibility and the targeting of tumor cells (Perche et al., 2014). In tumors, the deep penetration of nanovectors can also be achieved by the application of an external magnetic field thanks to the presence of iron magnetic nanoparticles in the formulation of the nanovector (Scherer et al., 2002).

3.2. Design rationale of EPSN to overcome intracellular barriers

3.2.1. Cellular uptake of EPSN

As the plasma membrane is negatively charged, it is important to load siRNA in positively charged or neutral nanosystems. Therefore, EPSN can be a good candidate for the nanovectorization of siRNA and an asset for the intracellular delivery. Thanks to the positive charge density of cationic polymers, they can easily favor the interaction with the cell membrane and facilitate the passage into the intracellular compartment (Cavallaro et al., 2017).

3.2.1.1. Internalization by endocytosis. As siRNA nanovectors are bigger than 1 kDa, cells use a variety of specialized internalization mechanisms to adapt their entry (Bareford and Swaan, 2007). Various internalization mechanisms can be observed depending on nanovector characteristics and the nature of its components. Endocytosis is the principal pathway implicated in the entry of nanoparticles into cells. This process involves the transport of extracellular molecules/particles into cells by vesicles derived from the invagination of the plasma membrane. Generally, endocytosis occurs by different mechanisms which can be categorized in two groups: phagocytosis (to clear large pathogens or large cell debris) characterize only mammalian specialized cells like macrophage, while pinocytosis (the uptake of fluid and solutes) takes place in all cells. There are four pinocytosis mechanisms differing with regard to the size of the endocytic vesicle, the nature of the molecule and the mechanism of vesicle formation: 1) clathrin-mediated endocytosis (vesicles ~120 nm), 2) caveolae-mediated endocytosis (vesicles ~60 nm), 3) clathrin- and caveolae-independent endocytosis (vesicles ~90 nm) and 4) macropinocytosis (vesicles > 1 μm) (Conner and Schmid, 2003; Marsh and McMahon, 1999) (Fig. 4).

For EPSN constituted of siRNA complexed to polymers with or without inorganic core (Fig. 2A and C), passive endocytosis is expected. Werfel *et al.* showed that cells treated with siRNA nanovector prepared with a combination of [2-(dimethylamino) ethyl methacrylate] (DMAEMA) copolymerized with butyl methacrylate (BMA) and pre-conjugation of PEG and DMAEMA (DB-PD ternary si-NPs), with a zeta potential of 18 mV, exhibited a high fluorescence intensity of nanoparticles. This result showed the ability of this cationic block of polymer to enhance the cell internalization of the siRNA nanovector (Werfel et al., 2017). Similarly, Cavalieri and colleagues designed a siRNA nanovector prepared with poly-L-lysin and PEG for the silencing of the anti-apoptotic gene, survivin, in prostate cancer cells. In this study, they showed that a rapid cell uptake of the siRNA nanovector occurred within 2 h in almost 100% of cells. Moreover, they observed, using deconvolution fluorescence microscopy, that the siRNA nanovector was internalized by endocytosis (Cavalieri et al., 2015).

The functionalization of the surface of EPSN with peptides can help to enhance passage through the membrane mediated by active endocytosis (Azevedo et al., 2018) (Fig. 2B and D). Some peptides used for the functionalization of siRNA nanovectors are able to recognize specific molecules on the cell membrane such as receptors. Upon binding to these molecules, the entry of associated siRNA nanovector occurs by receptor-mediated endocytosis. This internalization pathway is largely used for active targeted siRNA delivery. In this process, receptors are considered as mediators between cells and extracellular molecules/particles, they play a crucial role in cellular internalization by ensuring high specific interaction. Although numerous mechanisms of ligand-receptor internalization exist, all occur by ligand-stimulated manner. Briefly, the binding of ligand, held on nanovectors surface, to the extracellular domain elicits the receptor phosphorylation. Following this step, the phosphorylated receptor-ligand binary complex or only the phosphorylated receptor is internalized (Allen, 2002). In the case of nanovectors, it is requested to be receptor-ligand internalization. Depending on ligand nature and cell type, intracellular processing of ligand can differ. Although internalized ligands (likewise peptide functionalized nanovectors) commonly end into endosomal compartment, receptor is recycled back to the cell membrane (Lodish et al., 2000; Prokop and Davidson, 2008). Indeed, in endosomes, the recruitment of vacuolar ATPase pump causes vesicles acidification by the entry of H^+ ions. The acidic pH induces a conformational change of receptors, often resulting in a ligand-receptor dissociation (Bareford and Swaan, 2007). This mechanism can be considered as the best entry route for a high targeting specificity and an efficient cellular uptake of nanovectors. As an example for this entry pathway, Guruprasath and coworkers functionalized their siRNA nanovector by IL-4 receptor-binding peptide (IL4RPep-1) to target IL-4R for the delivery of anti-Bcl-xL siRNA. Results showed a high accumulation of the siRNA nanovector in the tumor and a specific internalization by IL-4 receptor-mediated endocytosis (Guruprasath et al., 2017).

3.2.1.2. Internalization mediated by transcytosis. EPSN can also be decorated with some peptides to enhance the internalization thanks to their ability to cross the cell membrane by a non-endocytic pathway, transcytosis (Fig. 2B and D). It is particularly interesting when active targeting is not possible, like when the cells do not over-express any specific receptor.

Transcytosis is a mechanism allowing to cross the cell membrane in an energy independent way. It depends on the size, the charge and the nature of nanovector surface components and on the nanovector concentration (Tuma and Hubbard, 2003). Peptide-functionalized nanovectors, in particular those conjugated to cell-penetrating peptides (CPP), have various internalization mechanisms. CPP are short peptide sequences of about thirty amino acids positively charged and are known for their ability to cross the lipid membrane by translocation mediated with their hydrophobic sequence and directly enter the cytosol (Rothbard et al., 2004). Briefly, the amphipathic character and the easy change of CPP structure from α-helices to β-sheets provide this peptide a high degree of conformational flexibility. This property has a key role in CPP translocation capacity. CPP – mediated transcytosis is induced by CPP hydrophobic extremity, so-called membrane perturbing/interacting domain. This extremity initiates lipid destabilization of cell membranes which permits the fusion with lipid bilayer in order to gain the cytoplasmic compartment (Galdiero et al., 2015). These short amphipathic peptides are emerging as attractive gene delivery tools and they can be associated with other molecules of different nature such as polymers (Wang et al., 2014). One example of the application of such a short peptide was published by Oh *et al.* who used the CPP R3V6 associated by electrostatic manner to deliver siRNA against sphingosine-1-phosphate lyase (S1PLyase) and recombinant high mobility group box-1 box A peptide (HMGB1A) into LA-4 lung epithelial cells in animal model. The presence of R3V6 increases the cell entry of the nanovector (Oh and Lee, 2014). Despite the absence of specific tumor recognition, this study showed that the use of CPP improves siRNA delivery, indicating the participation of the EPR effect. Once nanovectors are accumulated, the CPP intervenes to enhance the deep penetration into tumor cells. Veiseh and coworkers have evaluated PEG-modified iron oxide nanoparticles coated with an oligo-arginine and loaded with

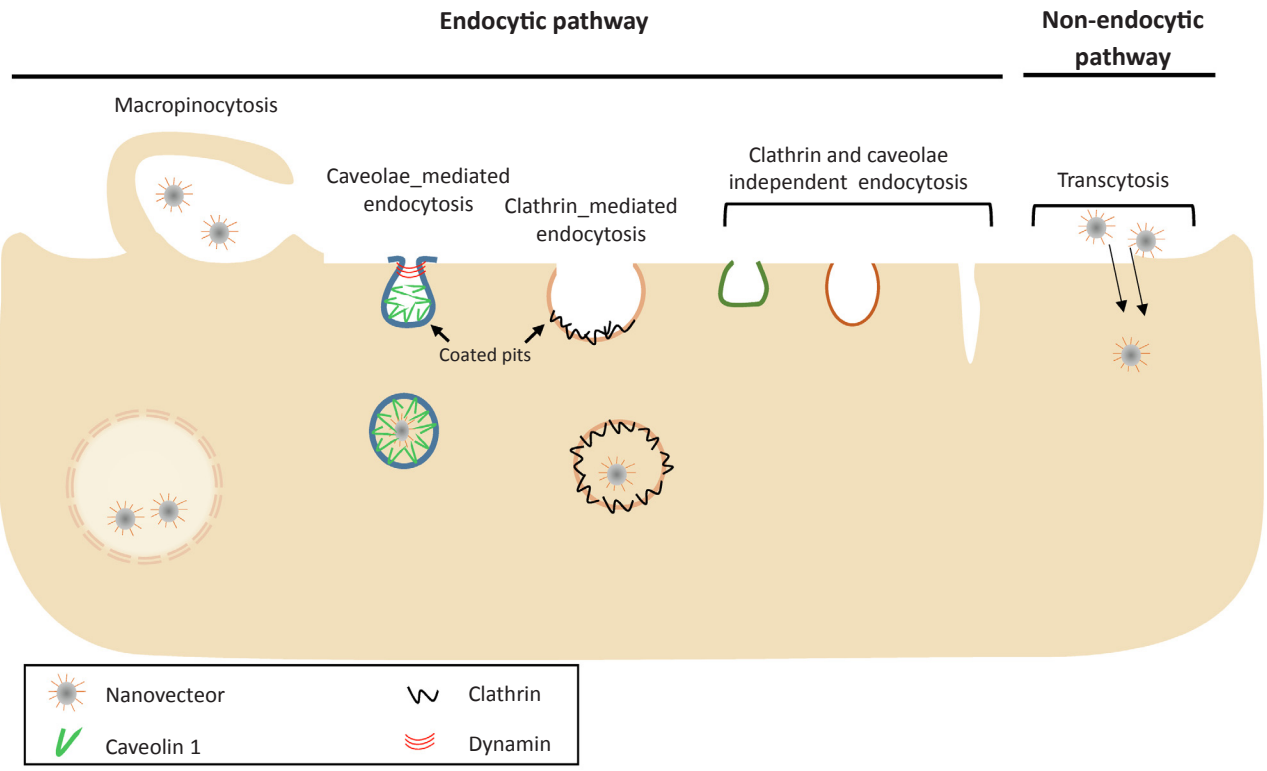

Fig. 4. Schematic illustration of the different entry pathways of nanovectors. EPSN can be internalized via endocytic (macropinocytosis, caveolae-mediated endocytosis, clathrin-mediated endocytosis or clathrin and caveolae-independent endocytosis) or non-endocytic (transcytosis) pathway.

siRNA (size about 50 nm) for their cellular entry pathway in three types of cancer cells. Results showed an enhanced internalization of this siRNA nanovectors by transcytosis without the formation of endocytic vesicles (Veiseh et al., 2011b).

3.2.2. Endosomal escape

Due to their endosomal buffering ability, cationic polymers can facilitate the endosomal escape of siRNA. Most EPSN are internalized by endocytosis, more precisely pinocytosis (Corbet et al., 2016; Xie et al., 2014; Yin et al., 2016). Briefly, after immobilization on the cell surface, nanovectors are encompassed in vesicles derived from local invagination of the cell membrane. After vesicles formation, nanovectors are attracted into cell inside newly formed endosomes (Wang et al., 2010). In this stage, the challenge of siRNA nanovectors is to escape endosomes before their fusion with lysosomes to avoid degradation and to pass into the cytosol. At this level, cationic polymers could be good candidates for this challenge. In 1997, Behr and others introduced the concept of the proton sponge and hypothesized that polymers such as PEI, polylysine and polyarginine could buffer the acidity of endosomes and induce their rupture (Behr, 1997). Afterward, this concept was more studied and developed. To summarize, endosomes acidification causes two complementary and simultaneous effects. The first is the so-called "proton sponge effect" which consists of a massive entry of water following a high concentration of hydrogen chloride (HCl) caused by the stimulation of the flow of chloride ions after the increase of the H^+ ions density in endosomes. The second is the consequence of the acidification of the endosomes and is called the umbrella effect that occurs by the capture of positive charges by cationic components of nanovectors, inducing thus an increase in the volume occupied by these molecules caused by the repulsions between groups of the same charge. These two phenomena combined allow the lysis of the endosomes (Nguyen and Szoka, 2012) and promote the passage of nanovectors and/ or siRNA into the cytosol. Recently, the proton sponge hypothesis was discussed on the part of the lysis of the endosomal membrane. Several studies showed that this complete rupture is highly unlikely and that in the presence of cationic polymers, the endosomal escape is promoted by the interaction of polymers' amino groups and the inner side of the membrane. This interaction causes a local membrane destabilization which leads a transient formation of "nanoscale holes" which could explain the endosomal escape (Jonker et al., 2017; Rehman et al., 2013; Schubert et al., 2018; Trützschler et al., 2018). In their study, Xie *et al.* used an inorganic core of calcium phosphate and a polymer coating (PEG and modified chitosan) to nanovectorize siRNA. They demonstrated that the nanovector was internalized mainly by macropinocytosis with the contribution of clathrin- and caveolae-mediated endocytosis. Using fluorescently labeled siRNA loaded in their nanovector, endosomal-lysosomal tracker and confocal laser scanning microscopy, they observed colocalization between the fluorophore associated to siRNA and that of the tracker after 3 h of nanovector incubation with cells. However, after 6 h the colocalization of these fluorescent signals was decreased, and fluorescent siRNA was detected in the cytoplasm. Authors explained this observation by the dissociation of the calcium phosphate core from polymers due to the protonation of amino groups of PEG-chitosan in the acidic environment. This process leads to the swelling of endosomes and then the release of siRNA into the cytoplasm (Xie et al., 2014). Table 3 shows the entry pathway of nanovectors and the studies performed to investigate the endosomal escape by indicating the used techniques and the main results.

3.3. Evaluation of protein down-regulation efficiency

The efficiency of siRNA nanovectors is evaluated by the cellular and/or the molecular responses of treated cells or tissues and it depends on the used siRNA. The evaluation of the molecular response can reflect the efficiency of the nanovector even if there is no cellular effect of the used siRNA. Molecular responses are the inhibition of the targeted mRNA expression and consequently a decrease in the expression of the associated protein. In the development phase of a nanovector, model

Table 3
Internalization pathways and endosomal escape studies of electrostatically assembled polymer-based siRNA nanovectors.

Entry pathway	Nanovector	Techniques used for endosomal studies	Main result	Refs.
Receptor-mediated endocytosis	NP-siRNA-CTX	Fluorescence microscopy Endosomal integrity assay: calcein	Nanovectors are able to escape endosomes	Veiseh et al. (2010)
	$HA-^{PTX}PSR_{siRNA}$	Confocal microscopy	Decrease of the colocalization of nanovectors with lysotracker after 24 h compared to 2 h	Yin et al. (2016)
	IL-4R-targeted BPEI-SPION/siRNA	Confocal microscopy	Nanovectors are detected in early endosomes. After 24 h nanovectors are detected in late endosomes, lysosomes and cytosol	Guruprasath et al. (2017)
	9R/DG-QDs	Confocal microscopy	No colocalization between nanovectors and lysosomes after 28 h of cell treatment and nanovectors are localized in the cytosol	Zhu et al. (2015)
Macropinocytosis	PEG-CMCS/CaP hybrid anionic nanoparticles	Confocal microscopy	Nanovectors escape endosomes and pass in cytosol	Xie et al. (2014)
Non-specified endocytosis	PEG-polyanion/siRNA/CaP hybrid nanoparticles	Confocal microscopy	Nanovectors escape endosomes and pass in cytosol	Pittella et al. (2011)
	Mixed micelles	Confocal microscopy	Low colocalization with lysotracker	Miteva et al. (2015)
	NPEG – PLLs	Flow cytometry Confocal microscopy	Decrease of the colocalization of nanovectors with lysosomes after 24 h	Cavalieri et al. (2015)
	Ternary siRNA polyplexes	Confocal microscopy	Low colocalization with endosomes and cytosolic dispersion	Werfel et al. (2017)

NP: nanoparticles; **CTX**: chlorotoxin; **HA**: hyaluronic acid; **PTX**: Paclitaxel; **PSR**: Octyl modified polyethyleneimine containing disulfide linkages; **IL-4R**: interleukin 4 receptor; **BPEI**: branched PEI; **SPION**: superparamagnetic iron oxide nanoparticles; **DG**: 2-deoxyglucose; **QDs**: quantum dots; **PEG**: polyethylene glycol; **CMCS**: carboxymethyl chitosan; **CaP**: calcium phosphate; **PLL**: poly-L-lysin.

siRNA (or reporter siRNA) targeting GFP or luciferase are widely used because they are convenient, relatively inexpensive, and gives quantitative and rapid measurements. These siRNA are commonly used as a tool to study gene expression at the transcriptional level and they give a molecular response due to the inhibition of the GFP or the luciferase protein and the extinction of their signals, easily detected by flow cytometry (for GFP) or luminescence (for luciferase) analysis. In the validation phase, the cellular response is usually an induction of cell death and it is detected by cytotoxicity (WST-1, MTT, LDH, …) or apoptosis assays (Annexin V- FITC / PI assay, DNA laddering, …). The used siRNA usually target mRNA of genes implicated in different functions needed for tumor process such as cell survival (survivin (Cavalieri et al., 2015)), apoptosis control (Bcl-2 family (Guruprasath et al., 2017)), cell cycle control, tumoral growth and angiogenesis (HIF 1α (Zhu et al., 2015)), tumor cells migration, metastasis (VEGF (Chen et al., 2014)), etc. The efficiency of a nanovector depend on a) the nanovector design and composition, b) the chosen cellular model and the corresponding target protein and c) the chosen therapeutic scheme. Tables 4 and 5 give an overview of some examples of existing versatile polymeric nanovectors which efficiently down-regulate protein expression.

3.3.1. Influence of the nanovector design and composition

To obtain a high gene silencing, it is necessary to carefully design the siRNA nanovector considering all the challenges presented above. Veiseh and colleagues developed a nanovector for nucleic acid delivery based on the use of a magnetic nanoplatform of SPION core coated with a copolymer of chitosan-grafted-PEG and PEI. In this nanosystem, the use of the combination of chitosan and PEG stabilized the nanovector. Cationic PEI was incorporated into this coating to protect and complex, by electrostatic interaction, negatively charged oligonucleotide (Veiseh et al., 2009). In a following study, they improved the specific targeting of the nanovector using a biological ligand, the chlorotoxin peptide. The addition of this peptide enhanced the cell internalization of the siRNA nanovector by receptor-mediated endocytosis pathway and its ability to escape endosomes (Veiseh et al., 2010). This nanovector exhibited a high accumulation in the tumor, after systemic administration, and showed an increased transfection efficiency in a mouse model of glioma compared to nanovectors without chlorotoxin peptide (Kievit et al., 2010). This nanovector is a good example of siRNA nanovector in which components were well chosen and each one has a key role and a specific function.

Several studies showed that the chosen polymers could affect the stability, the trafficking and, therefore, the efficiency of the siRNA nanovector. For example, siRNA nanovectors containing PEG as a neutral polymer to increase their colloidal stability and their stealthiness show, generally, a transfection efficiency higher than 60% (Cavalieri et al., 2015; Miteva et al., 2015; Werfel et al., 2017; Xie et al., 2014). Veiseh and coworkers evaluated PEG-modified iron oxide nanoparticles coated with either polyarginine, polylysine or PEI for their ability in promoting gene knockdown by siRNA delivery. They demonstrated that the transfection efficiency depended on the used cationic polymer. In fact, it was inferior to 40% by using polylysine or PEI as the only cationic polymer in the formulation. However, the replacement of these two polymers by polyarginine increases the efficiency of the nanovector to 68% (Veiseh et al., 2011b). In other studies, the use of PEI and polylysine in siRNA nanovectors with more complex structures showed a high down-regulation efficiency. For example, the use of PEI with chitosan, PEG and a small peptide (Ragelle et al., 2015) or with SPIONs, chitosan, PEG and chlorotoxin peptide (Veiseh et al., 2010) result in, respectively, 80% and 62% of GFP down-regulation. Similarly, the use of polylysine with modified PEG (Cavalieri et al., 2015) or with PEG, polyarginine and quantum dots (Zhu et al., 2015) results in 60% of transfection efficiency.

3.3.2. Influence of the cellular model and the corresponding target protein

Model cells used to evaluate the down-regulation efficiency of

Table 4
Electrostatically assembled polymer-based siRNA nanovectors studied *in vitro*.

Nanovector	Composition	Cells	Target gene	siRNA concentration	Treatment time (h)	Silencing efficiency (%)	Reference
ternary siRNA polyplexes	DMAEMA, BMA, PEG, siRNA	MDA-MB-231 NIH3T3 MSC	Luciferase	100 nM	24	85	Werfel et al. (2017)
PEG-polyanion/siRNA/CaP hybrid nanoparticles	CaP, PEG, CCP, siRNA	ApanC-1	Luciferase	60 nM	3	82	Pittella et al. (2011)
Mixed micelles	PEG-b-pDPB, pD-b-pDPB, siRNA	MDA-MB-231	Luciferase	100 nM	24	80	Miteva et al. (2015)
Alkyl-PEI2k-IO/siRNA	Iron oxide, Alkyl-PEI, siRNA	4 T1	Luciferase	6 pM	3	80	Liu et al. (2011)
RGDp NP	Integrin-arginine-glycine-aspartate, PEG, chitosan, PEI, siRNA	H1299	GFP	100 nM	4	80	Ragelle et al. (2015)
PEG-CMCS/CaP hybrid anionic nanoparticles	PEG, carboxymethyl chitosan, calcium, phosphate, siRNA	Hep G2	Luciferase hTERT	100 nM	48	79 60	Xie et al. (2014)
RGDp R1 NP	PEG, chitosan, RGDp, siRNA	H1299 SiHa	GFP ASCT2 MCT1	100 nM	6	70	Corbet et al. (2016)
NP-pArg-siRNA	SPION, PEG, pArg, siRNA	C6 MCF7 TC2	GFP	No data	8	68	Veiseh et al. (2011b)
NP-siRNA-CTX	SPION, PEG, chitosan, PEI, chlorotoxin, siRNA	C6	GFP	225 nM	2	62	Veiseh et al. (2010)
NPEG − PLLs	NPEG-PLL, siRNA	PC-3	Survivine	31 nM	120	60	Cavalieri et al. (2015)
HA-$^{PTX}PSR_{siRNA}$	PEI, hyaluronic acid, siRNA (HA-PTX_PSR-siRNA)	A549	PIK1	80 nM	6	60	Yin et al. (2016)
9R/DG-QDs	2-deoxyglucose (DG), PEG, lipoic acid- lysine- 9-poly-d-arginine (LA–Lys–9R), QDs, siRNA	Hep G2	GLUT1 HIF_1 α	50 nM	2	60	Zhu et al. (2015)
NP-pLys-siRNA	SPION, PEG, pLys, siRNA	C6 MCF7 TC2	GFP	No data	8	39	Veiseh et al. (2011b)
NP-PEI-siRNA	SPION, PEG, PEI, siRNA	C6 MCF7 TC2	GFP	No data	8	32	Veiseh et al. (2011b)

DMAEMA: [2-(dimethylamino) ethyl methacrylate]; **BMA**: butyl methacrylate; **PEG**: polyethylene glycol; **CaP**: calcium phosphate; **CCP**: charge-conversional polymer; **b-pDPB**: b-(dimethylaminoethyl methacrylate-co-propylacrylic acid-co-butyl methacrylate); **pD-b-pDPB:** poly[dimethylaminoethyl methacrylate-b-(dimethylaminoethyl methacrylate-co-propylacrylic acidco-butyl methacrylate)]; **IO**: iron oxide; **PEI**: polyethyleneimine; **RGDp**: arginine-glycine-aspartate peptide; **NP**: nanoparticles; **CMCS**: carboxymethyl chitosan; **hTERT**: human telomerase reverse transcriptase; **pArg**: polyarginine; **SPION**: superparamagnetic iron oxide nanoparticles; **CTX**: chlorotoxin; **PLL**: poly-L-lysin; **HA**: hyaluronic acid; **PTX**: Paclitaxel; **PSR**: Octyl modified polyethyleneimine containing disulfide linkages; **DG**: 2-deoxyglucose; **QDs**: quantum dots; **pLys**: polylysin.

Table 5
Electrostatically assembled polymer-based siRNA nanovectors studied *in vivo*.

Nanovector	Composition	Model	Target gene	siRNA dose	Administration protocol (number of injection)	Administration route	Silencing efficiency (%)	Reference
HA-$^{PTX}PSR_{siRNA}$	PEI, hyaluronic acid, siRNA (HA-PTX_PSR-siRNA)	4 T1-Fluc cells BALB/c nude mice	PIK1	0.5 mg/kg	3	Intravenously	60	Yin et al. (2016)
Alkyl-PEI2k-IO/siRNA	Iron oxide, Alkyl-PEI, siRNA	A549 cells Athymic nude mice	Luciferase	250 pg/kg	1 day/2, for 34 days	Intratumorally	60	Liu et al. (2011)
ternary siRNA polyplexes	DMAEMA, BMA, PEG, siRNA	L231 cells Athymic nude mice	Luciferase	1 mg/kg	2	Intravenously	59	Werfel et al. (2017)
PEG-CMCS/CaP hybrid anionic nanoparticles	PEG, carboxymethyl chitosan, calcium, phosphate, siRNA	HepG2 cells BALB/c nude mice	Luciferase hTERT	1.2 mg/kg	2	Intravenously	57	Xie et al. (2014)
IL-4R-targeted BPEI-SPION/siRNA	SPION, PEI, IL4RPep1, siRNA	MDA-MB231 cells BALB/c nude mice	Bcl-xL	0.15 mg/kg	3/week for 4 weeks	Intravenously	40	Guruprasath et al. (2017)
RGDp R1 NP	PEG, chitosan, RGDp, siRNA	SiHa cells NMRI nude mice	ASCT2 MCT1	2 mg/kg	2/week for 2 weeks	Intravenously Peritumoral	60	Corbet et al. (2016)
9R/DG-QDs	2-deoxyglucose (DG), PEG, lipoic acid- lysine- 9-poly-d-arginine (LA–Lys–9R), QDs, siRNA	HepG2 cells Kunming mice	HIF_1α	3 mg/kg	8 (1 day/2)	Intravenously	No data	Zhu et al. (2015)

HA: hyaluronic acid; **PTX**: Paclitaxel; **PSR**: Octyl modified polyethyleneimine containing disulfide linkages; **PEI**: polyethyleneimine; **IO**: iron oxide; **DMAEMA**: [2-(dimethylamino) ethyl methacrylate]; **BMA**: butyl methacrylate; **PEG**: polyethylene glycol; **CMCS**: carboxymethyl chitosan; **CaP**: calcium phosphate; **hTERT**: human telomerase reverse transcriptase; **IL-4R**: interleukin 4 receptor; **SPION**: superparamagnetic iron oxide nanoparticles; **BPEI**: branched PEI; **RGDp**: arginine-glycine-aspartate peptide; **DG**: 2-deoxyglucose; **QDs**: quantum dots.

siRNA nanovectors are always chosen to be representative of the targeted cancer type (Table 4). The cellular responses towards gene therapies depend on the cell type. In this context, Veiseh *et al.* evaluated *in vitro* the transfection efficiency of EPSN based on the use of PEGylated superparamagnetic iron oxide nanoparticles (SPION) polyarginine in cell lines expressing GFP representative of glioma, breast cancer and colon adenocarcinoma: C6, MCF7, and TC2 respectively. These nanovectors appear to be significantly more efficient to down-regulate the expression of the GFP in MCF7 cells (68.2%), followed by C6 cells (52.9%) and TC2 cells (24%) (Veiseh et al., 2011b). Similarly, Werfel and coworkers showed that the transfection efficiency of a siRNA nanovector formulated using DMAEMA, BMA and PEG as polymers and siRNA anti luciferase at a concentration of 100 nM varies in three cell lines: MDA-MB-231, NIH3T3 and mesenchymal stem cell (MSC), but it was higher than 80% in all the cell lines (Werfel et al., 2017).

As we mentioned above, generally, in the development stage of siRNA nanovectors it is easier to use a model gene, but then it is necessary to evaluate the silencing potential of the siRNA nanovector on a target gene, usually related to the tumor process (Tables 4 and 5). However, the modification of the target protein leads, sometimes, to a variable down-regulation efficiency dependent on the protein. For example, Xie *et al.* evaluated the transfection efficiency of a siRNA nanovector prepared with an inorganic core of calcium phosphate nanoparticles and a coating of PEG grafted carboxymethyl chitosan on HepG2 model cells expressing luciferase at a siRNA concentration of 100 nM. The incubation of this nanovector prepared with siRNA anti-luciferase leads to 79% of silencing efficacy. However, the evaluation of the therapeutic potential of siRNA delivery targeting hTERT gene results in only 60% and almost 50% of inhibition in the targeted mRNA and protein level (Xie et al., 2014). This study showed a loss of down-regulation efficiency of at least 20% between the model gene and the gene of interest.

3.3.3. Influence of the therapeutic scheme

3.3.3.1. Dose of siRNA. The dose or the concentration of siRNA is one of the important parameters to consider for successful gene transfection and satisfactory gene silencing (Tables 4 and 5). The determination of the adequate siRNA quantity requires an optimization step. Ragelle and colleagues performed a transfection of cells with an EPSN at different siRNA concentrations (from 12.5 nM to 200 nM). They showed that at low concentration (12.5–50 nM) the gene silencing of GFP was lower than 40% and it increased significantly up to 150 nM of siRNA to achieve almost 90%. However, no significant increase in the silencing efficiency was observed at concentrations above 150 nM (Ragelle et al., 2015). Moreover, the used concentration of siRNA depends on the used nanovector. In fact, by using different EPSN the same down-regulation efficiency can be achieved, but with different siRNA concentrations. For example, to obtain 80% of silencing of luciferase in breast cancer cells, Liu and colleagues used 6 pmol of siRNA loaded in a nanovector based on iron oxide nanoparticles and alkyl-PEI (Liu et al., 2011). However, for the same luciferase silencing efficiency (80%), Miteva *et al.* used a siRNA nanovector prepared with two polymer blocks (PEG-b-pDPB et pD-b-pDPB) at a siRNA concentration of 100 nM (Miteva et al., 2015), much higher than the previous study. Likewise, the intravenous administration of vectorized siRNA (with DMAEMA, BMA and PEG) in a xenograft mouse cancer model at a concentration of 1 mg/kg resulted in 59% of efficiency (Werfel et al., 2017). Yet, Corbet *et al.* obtained almost the same efficiency (60%) by injecting by the same route a siRNA nanovector prepared with two polymers, PEG and chitosan, and functionalized with the peptide RGD in a xenograft mouse cancer model at a dose twice as high (2 mg/kg) (Corbet et al., 2016). Therefore, the dose of siRNA must be adapted to the used system. That means that it is not the use of more siRNA that increases the silencing efficiency of the nanovector as shown in these two following studies. Ragelle *et al.* showed a knockdown of targeted gene expression (GFP) of 80% using their siRNA nanovector composed of three polymers: PEG, chitosan and PEI, and functionalized with RGD peptide in GFP model cells, at a siRNA concentration of 100 nM (Ragelle et al., 2015). However, Veiseh *et al.* used more than twice as much siRNA in a nanovector based on SPION, PEGylated chitosan and PEI and functionalized with a tumor-targeting peptide to obtain a GFP silencing efficiency of 62% (Veiseh et al., 2010).

3.3.3.2. Treatment time and administration protocol. For an efficient siRNA transfection *in vitro*, it is important to consider a sufficient treatment time, long enough for the internalization of the siRNA nanovector (Table 4). As an example, Cavalieri and colleagues exposed PC-3 cells to a nanovector prepared with anti-survivin siRNA for 72 h. After this treatment time, they obtained a negligible down-regulation of the protein survivin (< 10%). The increase of the incubation time of siRNA nanovector with cells from 72 h to 120 h resulted in a marked silencing in the targeted gene (almost 60%) (Cavalieri et al., 2015). Similarly, in a previous study published by our team, it was shown that the optimization of the treatment time of MDA-MB-231 cells expressing GFP with CS-MSN could improve the inhibition efficiency of the expression of GFP. An increase of the silencing of the targeted protein up to 4 h of treatment and the prolongation of this time did not improve the efficiency (Ben Djemaa et al., 2018). For *in vivo* studies, the treatment time can be translated by the administration protocol (i.e. number of injections and interval between injections). Many administration protocols with different numbers of injections and different administration schemes were described in the literature (Table 5). Tingjie *et al.* injected a siRNA nanovector 17 times (every other day for 34 days) (Yin et al., 2016). However, Werfel and colleagues administered their siRNA nanovector twice with an interval of 24 h (Werfel et al., 2017). In both studies, they obtained almost 60% of efficiency.

3.3.3.3. Routes of administration. The choice of the administration route depends on the accessibility of the tumors. In fact, for the tumors with deep localization such as liver cancer (Xie et al., 2014; Zhu et al., 2015), the only way to get access to them is through intravenous administration. However, it is possible to use both systemic or local administration (intravenous or intra-/*peri*-tumoral (Liu et al., 2011)) for the easy to access tumors such as breast cancer. For the intravenous administration, siRNA nanovectors have to overcome all biological barriers described in Section 2.1. However, by using the intratumoral injection the nanovector is directly administrated into the tumor and only the cellular barriers needed to be overcome. Various routes of administration depending on the cancer type have been used (Table 5). In research from Xie and coworkers, the intravenous injection of siRNA at 1.2 mg/kg loaded in a nanovector composed of polymers and calcium phosphate core, in a xenograft liver cancer model showed an inhibition of approximative 60% in tumor growth (Xie et al., 2014). As an example of local treatment, the intratumoral administration of vectorized siRNA at 250 pmol was applied by Liu *et al.* in xenograft breast cancer model for *in vivo* evaluation of the down-regulation efficiency of luciferase. Results showed a significant reduction of the luciferase expression in the tumor (Liu et al., 2011). Yet, for the treatment of xenograft carcinoma mouse model, Corbet and colleagues used both intravenous and peritumoral route to deliver a combination of vectorized therapeutic siRNA. This treatment led to a dramatic tumor growth inhibition (about 60%) upon peritumoral but also systemic administration.

4. Summary and concluding remarks

In summary, an interesting approach to overcome the extra- and intracellular barriers for the delivery of naked siRNA is the use of electrostatically assembled polymer-based nanovectors. One advantage of EPSN is their versatility due to their easy and rapid preparation. Nevertheless, the development of EPSN require a careful optimization

(amount of the different components, siRNA complexation; physico-chemical characteristics). To obtain a high efficacy, each component has to be well-chosen and plays a specific role to overcome these barriers: (i) polymers complex and protect siRNA from enzymatic degradation and premature clearance, (ii) neutral polymers increase the immune stealthiness and the circulation time in blood (iii) cationic polymers are implicated in the cellular internalization and in the endosomal escape, (iv) targeting peptides and cell-penetrating peptides enhance the tumor targeting and the uptake respectively, and (v) an inorganic core can be used for diagnostic purpose and to improve the physico-chemical characteristics. In addition, adequate properties of EPSN can enhance the accumulation in the tumor site due to the EPR effect.

Furthermore, the siRNA sequences need to be carefully chosen for an efficient silencing and to avoid the off-target effect of siRNA. Besides the formulation of EPSN, the silencing efficiency of EPSN depends on other factors related to the application of the treatment such as cell line, targeted protein, siRNA dose, treatment time, administration route, etc.

In conclusion, EPSN have proved their ability to successfully deliver siRNA into tumor cells and appear as a promising tool for cancer treatment. However, there is still much progress needed to reach clinical trials and achieve this goal.

Acknowledgments

This work was supported by the “Institut National du Cancer (INCa)”, the “Fondation ARC” and the “Ligue Nationale Contre le Cancer (LNCC)”, France (ARC_INCa_LNCC_7636, EVASION project and INTERACTION project), the “Région Centre-Val de Loire” and the “Cancéropole Grand Ouest” (MATURE project).

Declaration of Competing Interest

Authors declare that there are no conflicts of interest in the present manuscript.

References

Aagaard, L., Rossi, J.J., 2007. RNAi therapeutics: principles, prospects and challenges. Adv. Drug Deliv. Rev. 59, 75–86. https://doi.org/10.1016/j.addr.2007.03.005.

Al Shaer, D., Al Musaimi, O., Albericio, F., de la Torre, B., Al Shaer, D., Al Musaimi, O., Albericio, F., de la Torre, B.G., 2019. 2018 FDA tides harvest. Pharmaceuticals 12, 52. https://doi.org/10.3390/ph12020052.

Allen, T.M., 2002. Ligand-targeted therapeutics in anticancer therapy. Nat. Rev. Cancer 2, 750–763. https://doi.org/10.1038/nrc903.

An, S., He, D., Wagner, E., Jiang, C., 2015. Peptide-like polymers exerting effective glioma-targeted siRNA delivery and release for therapeutic application. Small 11, 5142–5150. https://doi.org/10.1002/smll.201501167.

Arnold, A.E., Czupiel, P., Shoichet, M., 2017. Engineered polymeric nanoparticles to guide the cellular internalization and trafficking of small interfering ribonucleic acids. J. Control. Release 259, 3–15. https://doi.org/10.1016/j.jconrel.2017.02.019.

Azevedo, C., Macedo, M.H., Sarmento, B., 2018. Strategies for the enhanced intracellular delivery of nanomaterials. Drug Discov. Today 23, 944–959. https://doi.org/10.1016/J.DRUDIS.2017.08.011.

Bareford, L.M., Swaan, P.W., 2007. Endocytic mechanisms for targeted drug delivery. Adv. Drug Deliv. Rev. 59, 748–758. https://doi.org/10.1016/j.addr.2007.06.008.

Behlke, M.A., 2006. Progress towards in vivo use of siRNAs. Mol. Ther. 13, 644–670. https://doi.org/10.1016/J.YMTHE.2006.01.001.

Behr, J.-P., 1997. The proton sponge: a trick to enter cells the viruses did not exploit. Chim. Int. J. Chem. 51, 34–36.

Ben Djemaa, S., David, S., Hervé-Aubert, K., Falanga, A., Galdiero, S., Allard-Vannier, E., Chourpa, I., Munnier, E., 2018. Formulation and in vitro evaluation of a siRNA delivery nanosystem decorated with gH625 peptide for triple negative breast cancer theranosis. Eur. J. Pharm. Biopharm. 131, 99–108. https://doi.org/10.1016/j.ejpb.2018.07.024.

Boussif, O., Lezoualc'ht, F., Zanta, M.A., Mergnyt, D., Schermant, D., Demeneixt, B., Behr, J.-P., 1995. A versatile vector for gene and oligonucleotide transfer into cells in culture and in vivo: polyethylenimine. Biochemistry.

Bruniaux, J., Djemaa, S. Ben, Hervé-Aubert, K., Marchais, H., Chourpa, I., David, S., Ben Djemaa, S., Hervé-Aubert, K., Marchais, H., Chourpa, I., David, S., 2017. Stealth magnetic nanocarriers of siRNA as platform for breast cancer theranostics. Int. J. Pharm. 532, 660–668. https://doi.org/10.1016/j.ijpharm.2017.05.022.

Carthew, Richard W., Sontheimer, E.J., Carthew, R.W., Sontheimer, E.J., 2009. Origins and mechanisms of miRNAs and siRNAs. Cell 136, 642–655. https://doi.org/10.1016/j.cell.2009.01.035.

Cavalieri, F., Beretta, G.L., Cui, J., Braunger, J.A., Yan, Y., Richardson, J.J., Tinelli, S., Folini, M., Zaffaroni, N., Caruso, F., 2015. Redox-sensitive PEG-polypeptide nanoporous particles for survivin silencing in prostate cancer cells. Biomacromolecules 16, 2168–2178. https://doi.org/10.1021/acs.biomac.5b00562.

Cavallaro, G., Sardo, C., Craparo, E.F., Porsio, B., Giammona, G., 2017. Polymeric nanoparticles for siRNA delivery: production and applications. Int. J. Pharm. 525, 313–333. https://doi.org/10.1016/J.IJPHARM.2017.04.008.

Chen, M., Gao, S., Dong, M., Song, J., Yang, C., Howard, K.A., Al, C.E.T., 2012. Chitosan/siRNA nanoparticles encapsulated in PLGA nanofibers for siRNA delivery. ACS Nano 4835–4844.

Chen, Y., Gu, H., Zhang, D.S.-Z., Li, F., Liu, T., Xia, W., 2014. Highly effective inhibition of lung cancer growth and metastasis by systemic delivery of siRNA via multimodal mesoporous silica-based nanocarrier. Biomaterials 35, 10058–10069. https://doi.org/10.1016/J.BIOMATERIALS.2014.09.003.

Chiper, M., Tounsi, N., Kole, R., Kichler, A., Zuber, G., 2017. Self-aggregating 1.8 kDa polyethylenimines with dissolution switch at endosomal acidic pH are delivery carriers for plasmid DNA, mRNA, siRNA and exon-skipping oligonucleotides. J. Control. Release 246, 60–70. https://doi.org/10.1016/J.JCONREL.2016.12.005.

Conde, J., Dias, J.T., Grazú, V., Moros, M., Baptista, P.V., de la Fuente, J.M., 2014. Revisiting 30 years of biofunctionalization and surface chemistry of inorganic nanoparticles for nanomedicine. Front. Chem. 2, 1–27. https://doi.org/10.3389/fchem.2014.00048.

Conner, S.D., Schmid, S.L., 2003. Regulated portals of entry into the cell. Nature 422, 37–44. https://doi.org/10.1038/nature01451.

Corbet, C., Ragelle, H., Pourcelle, V., Vanvarenberg, K., Marchand-Brynaert, J., Préat, V., Feron, O., 2016. Delivery of siRNA targeting tumor metabolism using non-covalent PEGylated chitosan nanoparticles: identification of an optimal combination of ligand structure, linker and grafting method. J. Control. Release 223, 53–63. https://doi.org/10.1016/j.jconrel.2015.12.020.

Creusat, G., Rinaldi, A.S., Weiss, E., Elbaghdadi, R., Remy, J.S., Mulherkar, R., Zuber, G., 2010. Proton sponge trick for ph-sensitive disassembly of polyethylenimine-based sirna delivery systems. Bioconjug. Chem. 21, 994–1002. https://doi.org/10.1021/bc100010k.

Creusat, G., Thomann, J.-S., Maglott, A., Pons, B., Dontenwill, M., Guérin, E., Frisch, B., Zuber, G., 2012. Pyridylthiourea-grafted polyethylenimine offers an effective assistance to siRNA-mediated gene silencing in vitro and in vivo. J. Control. Release 157, 418–426. https://doi.org/10.1016/J.JCONREL.2011.10.007.

Creusat, G., Zuber, G., 2008. Self-Assembling polyethylenimine derivatives mediate efficient siRNA delivery in mammalian cells. ChemBioChem 9, 2787–2789. https://doi.org/10.1002/cbic.200800540.

David, S., Resnier, P., Guillot, A., Pitard, B., Benoit, J.-P., Passirani, C., 2012. siRNA LNCs – a novel platform of lipid nanocapsules for systemic siRNA administration. Eur. J. Pharm. Biopharm. 81, 448–452. https://doi.org/10.1016/J.EJPB.2012.02.010.

Derfus, A.M., Chen, A.A., Min, D.-H., Ruoslahti, E., Bhatia, S.N., 2007. Targeted quantum dot conjugates for siRNA delivery. Bioconjug. Chem. 18, 1391–1396. https://doi.org/10.1021/bc060367e.

Ding, Y., Wang, W., Feng, M., Wang, Y., Zhou, J., Ding, X., Zhou, X., Liu, C., Wang, R., Zhang, Q., 2012. A biomimetic nanovector-mediated targeted cholesterol-conjugated siRNA delivery for tumor gene therapy. Biomaterials 33, 8893–8905. https://doi.org/10.1016/j.biomaterials.2012.08.057.

Ding, Y., Wang, Y., Zhou, J., Gu, X., Wang, W., Liu, C., Bao, X., Wang, C., Li, Y., Zhang, Q., 2014. Direct cytosolic siRNA delivery by reconstituted high density lipoprotein for target-specific therapy of tumor angiogenesis. Biomaterials 35, 7214–7227. https://doi.org/10.1016/j.biomaterials.2014.05.009.

Dohmen, C., Fröhlich, T., Lächelt, U., Röhl, I., Vornlocher, H.-P., Hadwiger, P., Wagner, E., 2012. Defined folate-PEG-siRNA conjugates for receptor-specific gene silencing. Mol. Ther. – Nucleic Acids 1, e7. https://doi.org/10.1038/MTNA.2011.10.

Dominska, M., Dykxhoorn, D.M., 2010. Breaking down the barriers: siRNA delivery and endosome escape. J Cell Sci 123, 1183–1189. https://doi.org/10.1242/jcs.066399.

Elbashir, S.M., Harborth, J., Lendeckel, W., Yalcin, A., Weber, K., Tuschl, T., 2001. Duplexes of 21-nucleotide RNAs mediate RNA interference in cultured mammalian cells. Nature 411, 494–498. https://doi.org/10.1038/35078107.

Fan, C., Wang, S., Hong, J.W., Bazan, G.C., Plaxco, K.W., Heeger, A.J., 2003. Beyond superquenching: Hyper-efficient energy transfer from conjugated polymers to gold nanoparticles. Proc. Natl. Acad. Sci. U. S. A. 100, 6297–6301. https://doi.org/10.1073/pnas.1132025100.

Ferrari, M., Sun, T., Shen, H., Gilmore, J.H., 2012. Nanovector delivery of siRNA for cancer therapy. Cancer Gene Ther. 19, 1883–1889. https://doi.org/10.1038/cgt.2012.22.

Fischer, D., Bieber, T., Li, Y., Elsässer, H.P., Kissel, T., 1999. A novel non-viral vector for DNA delivery based on low molecular weight, branched polyethylenimine: effect of molecular weight on transfection efficiency and cytotoxicity. Pharm. Res. 16, 1273–1279. https://doi.org/10.1023/A:1014861900478.

Foillard, S., Zuber, G., Doris, E., 2011. Polyethylenimine–carbon nanotube nanohybrids for siRNA-mediated gene silencing at cellular level. Nanoscale 3, 1461. https://doi.org/10.1039/c0nr01005g.

Forster, J.C., Harriss-Phillips, W.M., Douglass, M.J., Bezak, E., 2017. A review of the development of tumor vasculature and its effects on the tumor microenvironment. Hypoxia (Auckland, N.Z.) 5, 21–32. https://doi.org/10.2147/HP.S133231.

Fröhlich, T., Edinger, D., Kläger, R., Troiber, C., Salcher, E., Badgujar, N., Martin, I., Schaffert, D., Cengizeroglu, A., Hadwiger, P., Vornlocher, H.-P., Wagner, E., 2012. Structure–activity relationships of siRNA carriers based on sequence-defined oligo (ethane amino) amides. J. Control. Release 160, 532–541. https://doi.org/10.1016/J.JCONREL.2012.03.018.

Galdiero, S., Falanga, A., Morelli, G., Galdiero, M., 2015. gH625: A milestone in

understanding the many roles of membranotropic peptides. Biochim. Biophys. Acta – Biomembr. 1848, 16–25. https://doi.org/10.1016/j.bbamem.2014.10.006.
Gary, D.J., Puri, N., Won, Y.-Y., 2007. Polymer-based siRNA delivery: perspectives on the fundamental and phenomenological distinctions from polymer-based DNA delivery. J. Control. Release 121, 64–73. https://doi.org/10.1016/J.JCONREL.2007.05.021.
Gavrilov, K., Saltzman, W.M., 2012. Therapeutic siRNA: principles, challenges, and strategies. Yale J. Biol. Med. 85, 187–200.
Gillies, R.J., Schornack, P.A., Secomb, T.W., Raghunand, N., 1999. Causes and effects of heterogeneous perfusion in tumors. Neoplasia 1, 197–207.
Goren, D., Horowitz, A.T., Zalipsky, S., Woodle, M.C., Yarden, Y., Gabizon, A., 1996. Targeting of stealth liposomes to erbB-2 (Her/2) receptor: in vitro and in vivo studies. Br. J. Cancer 74, 1749–1756.
Guruprasath, P., Kim, J., Gunassekaran, G.R., Chi, L., Kim, S., Park, R.-W., Kim, S.-H., Baek, M.-C., Bae, S.M., Kim, S.Y., Kim, D.-K., Park, I.-K., Kim, W.-J., Lee, B., 2017. Interleukin-4 receptor-targeted delivery of Bcl-xL siRNA sensitizes tumors to chemotherapy and inhibits tumor growth. Biomaterials 142, 101–111. https://doi.org/10.1016/j.biomaterials.2017.07.024.
Haussecker, D., 2014. Current issues of RNAi therapeutics delivery and development. J. Control. Release 195, 49–54. https://doi.org/10.1016/j.jconrel.2014.07.056.
Heldin, C.-H., Rubin, K., Pietras, K., Östman, A., 2004. High interstitial fluid pressure – an obstacle in cancer therapy. Nat. Rev. Cancer 4, 806–813. https://doi.org/10.1038/nrc1456.
Huang, Y., Wang, X., Huang, W., Cheng, Q., Zheng, S., Guo, S., Cao, H., Liang, X.J., Du, Q., Liang, Z., 2015. Systemic administration of siRNA via cRGD-containing Peptide. Sci. Rep. 5, 12458. https://doi.org/10.1038/srep12458.
Huh, M.S., Lee, S.Y., Park, S., Lee, Seulki, Chung, H., Lee, Sojin, Choi, Y., Oh, Y.K., Park, J.H., Jeong, S.Y., Choi, K., Kim, K., Kwon, I.C., 2010. Tumor-homing glycol chitosan/polyethylenimine nanoparticles for the systemic delivery of siRNA in tumor-bearing mice. J. Control. Release 144, 134–143. https://doi.org/10.1016/j.jconrel.2010.02.023.
Jabir, N.R., Tabrez, S., Ashraf, G.M., Shakil, S., Damanhouri, G.A., Kamal, M.A., 2012. Nanotechnology-based approaches in anticancer research. Int. J. Nanomed. 7, 4391–4408. https://doi.org/10.2147/IJN.S33838.
Jaganathan, H., Mitra, S., Srinivasan, S., Dave, B., Godin, B., 2014. Design and in vitro evaluation of layer by layer siRNA nanovectors targeting breast tumor initiating cells. PLoS One 9, e91986. https://doi.org/10.1371/journal.pone.0091986.
Jain, R.K., Stylianopoulos, T., 2010. Delivering nanomedicine to solid tumors. Nat. Rev. Clin. Oncol. 7, 653–664. https://doi.org/10.1038/nrclinonc.2010.139.
Jiang, T., Zhang, Z., Zhang, Y., Lv, H., Zhou, J., Li, C., Hou, L., Zhang, Q., 2012. Dual-functional liposomes based on pH-responsive cell-penetrating peptide and hyaluronic acid for tumor-targeted anticancer drug delivery. Biomaterials 33, 9246–9258. https://doi.org/10.1016/j.biomaterials.2012.09.027.
Jonker, C., de Heus, C., Faber, L., ten Brink, C., Potze, L., Fermie, J., Liv, N., Klumperman, J., 2017. An adapted protocol to overcome endosomal damage caused by polyethylenimine (PEI) mediated transfections. Matters 3, e201711000012. https://doi.org/10.19185/matters.201711000012.
Kaczmarek, J.C., Kowalski, P.S., Anderson, D.G., 2017. Advances in the delivery of RNA therapeutics: from concept to clinical reality. Genome Med. 9, 60. https://doi.org/10.1186/s13073-017-0450-0.
Kang, L., Fan, B., Sun, P., Huang, W., Jin, M., Wang, Q., Gao, Z., 2016. An effective tumor-targeting strategy utilizing hypoxia-sensitive siRNA delivery system for improved anti-tumor outcome. Acta Biomater. 44, 341–354. https://doi.org/10.1016/J.ACTBIO.2016.08.029.
Kievit, F.M., Veiseh, O., Fang, C., Bhattarai, N., Lee, D., Ellenbogen, R.G., Zhang, M., 2010. Chlorotoxin labeled magnetic nanovectors for targeted gene delivery to glioma. ACS Nano 4, 4587–4594. https://doi.org/10.1021/nn1008512.
Kim, E.J., Shim, G., Kim, K., Kwon, I.C., Oh, Y.K., Shim, C.K., 2009. Hyaluronic acid complexed to biodegradable poly L-arginine for targeted delivery of siRNAs. J. Gene Med. 11, 791–803. https://doi.org/10.1002/jgm.1352.
Krivitsky, A., Polyak, D., Scomparin, A., Eliyahu, S., Ofek, P., Tiram, G., Kalinski, H., Avkin-Nachum, S., Feiner Gracia, N., Albertazzi, L., Satchi-Fainaro, R., 2018. Amphiphilic poly(α)glutamate polymeric micelles for systemic administration of siRNA to tumors. Nanomedicine Nanotechnology. Biol. Med. 14, 303–315. https://doi.org/10.1016/j.nano.2017.10.012.
Landry, B., Aliabadi, H.M., Samuel, A., Gül-Uludağ, H., Jiang, X., Kutsch, O., Uludağ, H., 2012. Effective non-viral delivery of siRNA to acute myeloid leukemia cells with lipid-substituted polyethylenimines. PLoS One 7, e44197. https://doi.org/10.1371/journal.pone.0044197.
Lee, D.-J., He, D., Kessel, E., Padari, K., Kempter, S., Lächelt, U., Rädler, J.O., Pooga, M., Wagner, E., 2016a. Tumoral gene silencing by receptor-targeted combinatorial siRNA polyplexes. J. Control. Release 244, 280–291. https://doi.org/10.1016/J.JCONREL.2016.06.011.
Lee, D.-J., Kessel, E., Edinger, D., He, D., Klein, P.M., Voith von Voithenberg, L., Lamb, D.C., Lächelt, U., Lehto, T., Wagner, E., 2016b. Dual antitumoral potency of EG5 siRNA nanoplexes armed with cytotoxic bifunctional glutamyl-methotrexate targeting ligand. Biomaterials 77, 98–110. https://doi.org/10.1016/J.BIOMATERIALS.2015.11.004.
Lee, J.E., Lee, K., Nam, J.A., Kim, A., Lee, S.Y., Lee, M.S., Kim, N.W., Yin, Y., Park, J.W., Park, S.Y., Jeong, J.H., 2018. Cellular delivery of siRNA using Poly(2-dimethylaminoethyl methacrylate)- functionalized graphene oxide nano-wrap. Macromol. Res. 26, 1115–1122. https://doi.org/10.1007/s13233-019-7017-4.
Liu, C., Liu, X., Rocchi, P., Qu, F., Iovanna, J.L., Peng, L., 2014. Arginine-terminated generation 4 PAMAM dendrimer as an effective nanovector for functional siRNA delivery in vitro and in vivo. Bioconjug. Chem. 25, 521–532. https://doi.org/10.1021/bc4005156.
Liu, G., Xie, J., Zhang, F., Wang, Z.-Y., Luo, K., Zhu, L., Quan, Q.-M., Niu, G., Lee, S., Ai, H., Chen, X., 2011. N-Alkyl-PEI functional iron oxide nanocluster for efficient siRNA delivery**. Small 7, 2742–2749. https://doi.org/10.1002/smll.201100825.
Liu, X., Peng, L., 2016. Dendrimer nanovectors for siRNA delivery. Methods Mol. Biol. 1364, 127–142. https://doi.org/10.1007/978-1-4939-3112-5_11.
Lodish, H., Berk, A., Zipursky, S.L., Matsudaira, P., Baltimore, D., Darnell, J., 2000. Receptor-Mediated Endocytosis and the Sorting of. Internalized Proteins.
Lu, A.-H., Salabas, E.L., Schüth, F., 2007. Magnetic nanoparticles: synthesis, protection, functionalization, and application. Angew. Chem. Int. Ed. Engl. 46, 1222–1244. https://doi.org/10.1002/anie.200602866.
Lv, H., Zhang, S., Wang, B., Cui, S., Yan, J., 2006. Toxicity of cationic lipids and cationic polymers in gene delivery. J. Control. Release Off. J. Control. Release Soc. 114, 100–109. https://doi.org/10.1016/j.jconrel.2006.04.014.
Malhotra, M., Tomaro-Duchesneau, C., Saha, S., Prakash, S., 2013. Intranasal, siRNA delivery to the Brain by TAT/MGF tagged PEGylated chitosan nanoparticles. J. Pharm. 2013, 1–10. https://doi.org/10.1155/2013/812387.
Marsh, M., McMahon, H.T., 1999. The structural era of endocytosis. Science 285, 215–220.
de Menezes, D.E.L., Pilarski, L.M., Allen, T.M., 1998. In vitro and in vivo targeting of immunoliposomal doxorubicin to human B-Cell Lymphoma. Cancer Res. 58, 3320–3330.
Mi, R.P., Ki, O.H., In, K.H., Myung, H.C., Jae, W.N., Yun, J.C., Chong, S.C., 2005. Degradable polyethylenimine-alt-poly(ethylene glycol) copolymers as novel gene carriers. J. Control. Release 105, 367–380. https://doi.org/10.1016/j.jconrel.2005.04.008.
Minakuchi, Y., Takeshita, F., Kosaka, N., Sasaki, H., Yamamoto, Y., Kouno, M., Honma, K., Nagahara, S., Hanai, K., Sano, A., Kato, T., Terada, M., Ochiya, T., 2004. Atelocollagen-mediated synthetic small interfering RNA delivery for effective gene silencing in vitro and in vivo. Nucleic Acids Res. 32, e109. https://doi.org/10.1093/nar/gnh093.
Miteva, M., Kirkbride, K.C., Kilchrist, K.V., Werfel, T.A., Li, H., Nelson, C.E., Gupta, M.K., Giorgio, T.D., Duvall, C.L., 2015. Tuning PEGylation of mixed micelles to overcome intracellular and systemic siRNA delivery barriers. Biomaterials 38, 97–107. https://doi.org/10.1016/j.biomaterials.2014.10.036.
Mok, H., Veiseh, O., Fang, C., Kievit, F.M., Wang, F.Y., Park, J.O., Zhang, M., 2010. PH-sensitive siRNA nanovector for targeted gene silencing and cytotoxic effect in cancer cells. Mol. Pharm. 7, 1930–1939. https://doi.org/10.1021/mp100221h.
Mokhtarieh, A.A., Lee, J., Kim, S., Lee, M.K., 2018. Preparation of siRNA encapsulated nanoliposomes suitable for siRNA delivery by simply discontinuous mixing. Biochim. Biophys. Acta – Biomembr. 1860, 1318–1325. https://doi.org/10.1016/J.BBAMEM.2018.02.027.
Mu, P., Nagahara, S., Makita, N., Tarumi, Y., Kadomatsu, K., Takei, Y., 2009. Systemic delivery of siRNA specific to tumor mediated by atelocollagen: combined therapy using siRNA targeting Bcl-xL and cisplatin against prostate cancer. Int. J. Cancer 125, 2978–2990. https://doi.org/10.1002/ijc.24382.
Muratovska, A., Eccles, M.R., 2004. Conjugate for efficient delivery of short interfering RNA (siRNA) into mammalian cells. FEBS Lett. 558, 63–68. https://doi.org/10.1016/S0014-5793(03)01505-9.
Nguyen, J., Szoka, F.C., 2012. Nucleic acid delivery: the missing pieces of the puzzle? Acc. Chem. Res. 45, 1153–1162. https://doi.org/10.1021/ar3000162.
Nikam, R.R., Gore, K.R., 2018. Journey of siRNA: clinical developments and targeted delivery. Nucleic Acid Ther. 28, 209–224. https://doi.org/10.1089/nat.2017.0715.
Oh, B., Lee, M., 2014. Combined delivery of HMGB-1 box A peptide and S1PLyase siRNA in animal models of acute lung injury. J. Control. Release 175, 25–35. https://doi.org/10.1016/j.jconrel.2013.12.008.
Ohsaki, M., Okuda, T., Wada, A., Hirayama, T., Niidome, T., Aoyagi, H., 2002. In vitro gene transfection using dendritic poly(L-lysine). Bioconjug. Chem. 13, 510–517. https://doi.org/10.1021/bc015525a.
Owens III, D.E., Peppas, N.A., 2006. Opsonization, biodistribution, and pharmacokinetics of polymeric nanoparticles. Int. J. Pharm. 307, 93–102. https://doi.org/10.1016/j.ijpharm.2005.10.010.
Ozcan, G., Ozpolat, B., Coleman, R.L., Sood, A.K., Lopez-Berestein, G., Medicine, R., 2015. Preclinical and clinical development of siRNA-based therapeutics. Adv. Drug Deliv. Rev. 87, 108–119. https://doi.org/10.1016/j.addr.2015.01.007.
Pan, J., Ruan, W., Qin, M., Long, Y., Wan, T., Yu, K., Zhai, Y., Wu, C., Xu, Y., 2018. Intradermal delivery of STAT3 siRNA to treat melanoma via dissolving microneedles. Sci. Rep. 8, 1117. https://doi.org/10.1038/s41598-018-19463-2.
Pan, X., Thompson, R., Meng, X., Wu, D., Xu, L., 2010. Tumor-targeted RNA-interference: functional non-viral nanovectors. Am. J. Cancer Res. 1, 25–42.
Parmar, M.B., Bahadur, R., Lö, R., Uludağ, H., 2018. Additive polyplexes to undertake siRNA therapy against CDC20 and survivin in breast cancer cells. Biomacromolecules 19 (11), 4193–4206. https://doi.org/10.1021/acs.biomac.8b00918.
Pärnaste, L., Arukuusk, P., Langel, K., Tenson, T., Langel, Ü., 2017. The formation of nanoparticles between small interfering RNA and amphipathic cell-penetrating peptides. Mol. Ther. Nucleic Acids 7, 1–10. https://doi.org/10.1016/j.omtn.2017.02.003.
Perche, F., Biswas, S., Patel, N.R., Torchilin, V.P., 2016. Hypoxia-responsive copolymer for siRNA delivery. Methods Mole. Biol. 139–162. https://doi.org/10.1007/978-1-4939-3148-4_12.
Perche, F., Biswas, S., Wang, T., Zhu, L., Torchilin, V.P., 2014. Hypoxia-targeted siRNA delivery. Angew. Chemie – Int. Ed. 53, 3362–3366. https://doi.org/10.1002/anie.201308368.
Pittella, F., Zhang, M., Lee, Y., Kim, H.J., Tockary, T., Osada, K., Ishii, T., Miyata, K., Nishiyama, N., Kataoka, K., 2011. Enhanced endosomal escape of siRNA-incorporating hybrid nanoparticles from calcium phosphate and PEG-block charge-conversional polymer for efficient gene knockdown with negligible cytotoxicity. Biomaterials 32, 3106–3114. https://doi.org/10.1016/j.biomaterials.2010.12.057.

Prokop, A., Davidson, J.M.J., 2008. Nanovehicular intracellular delivery systems. J. Pharm. Sci. 97, 3518–3590. https://doi.org/10.1002/jps.21270.
Ragelle, H., Colombo, S., Pourcelle, V., Vanvarenberg, K., Vandermeulen, G., Bouzin, C., Marchand-Brynaert, J., Feron, O., Foged, C., Préat, V., 2015. Intracellular siRNA delivery dynamics of integrin-targeted, PEGylated chitosan-poly(ethylene imine) hybrid nanoparticles: a mechanistic insight. J. Control. Release 211, 1–9. https://doi.org/10.1016/j.jconrel.2015.05.274.
Ratcliff, F., Harrison, B.D., Baulcombe, D.C., 1997. A similarity between viral defense and gene silencing in plants. Science (80) 276, 1558–1560. https://doi.org/10.1126/science.276.5318.1558.
Rehman, Z., ur Hoekstra, D., Zuhorn, I.S., 2013. Mechanism of polyplex- and lipoplex-mediated delivery of nucleic acids: Real-time visualization of transient membrane destabilization without endosomal lysis. ACS Nano 7, 3767–3777. https://doi.org/10.1021/nn3049494.
Reischl, D., Zimmer, A., 2009. Drug delivery of siRNA therapeutics: potentials and limits of nanosystems. Nanomedicine Nanotechnology. Biol. Med. 5, 8–20. https://doi.org/10.1016/J.NANO.2008.06.001.
Resnier, P., Montier, T., Mathieu, V., Benoit, J.-P.P., Passirani, C., 2013. A review of the current status of siRNA nanomedicines in the treatment of cancer. Biomaterials 34, 6429–6443. https://doi.org/10.1016/j.biomaterials.2013.04.060.
Reynolds, A., Anderson, E.M., Vermeulen, A., Fedorov, Y., Robinson, K., Leake, D., Karpilow, J., Marshall, W.S., Khvorova, A., 2006. Induction of the interferon response by siRNA is cell type- and duplex length-dependent. RNA 12, 988–993. https://doi.org/10.1261/rna.2340906.
Richards Grayson, A.C., Doody, A.M., Putnam, D., 2006. Biophysical and structural characterization of polyethylenimine-mediated siRNA delivery in vitro. Pharm. Res. 23, 1868–1876. https://doi.org/10.1007/s11095-006-9009-2.
Rizk, M., Tüzmen, Ş., 2017. Update on the clinical utility of an RNA interference-based treatment: focus on Patisiran. Pharmgenomics. Pers. Med. 10, 267–278. https://doi.org/10.2147/PGPM.S87945.
Rosi, N.L., Giljohann, D.A., Thaxton, C.S., Lytton-Jean, A.K.R., Han, M.S., Mirkin, C.A., 2006. Oligonucleotide-modified gold nanoparticles for intracellular gene regulation. Science 312, 1027–1030. https://doi.org/10.1126/science.1125559.
Rothbard, J.B., Jessop, T.C., Lewis, R.S., Murray, B.A., Wender, P.A., 2004. Role of membrane potential and hydrogen bonding in the mechanism of translocation of guanidinium-rich peptides into cells. J. Am. Chem. Soc. 126, 9506–9507. https://doi.org/10.1021/ja0482536.
Scherer, F., Anton, M., Schillinger, U., Henke, J., Bergemann, C., Krüger, A., Gänsbacher, B., Plank, C., 2002. Magnetofection: enhancing and targeting gene delivery by magnetic force in vitro and in vivo. Gene Ther. 9, 102–109. https://doi.org/10.1038/sj.gt.3301624.
Schmohl, K.A., Gupta, A., Grünwald, G.K., Trajkovic-Arsic, M., Klutz, K., Braren, R., Schwaiger, M., Nelson, P.J., Ogris, M., Wagner, E., Siveke, J.T., Spitzweg, C., 2017. Imaging and targeted therapy of pancreatic ductal adenocarcinoma using the theranostic sodium iodide symporter (NIS) gene. Oncotarget 8, 33393–33404. https://doi.org/10.18632/oncotarget.16499.
Schubert, U.S., Traeger, A., Bus, T., 2018. The great escape: how cationic polyplexes overcome the endosomal barrier. J. Mater. Chem. B 6, 6904–6918. https://doi.org/10.1039/C8TB00967H.
Shakiba, A., Zenasni, O., Marquez, M.D., Lee, T.R., 2017. Advanced drug delivery via self-assembled monolayer-coated nanoparticles. AIMS Bioeng. 4, 275–299. https://doi.org/10.3934/bioeng.2017.2.275.
Shim, M.S., Kwon, Y.J., 2010. Efficient and targeted delivery of siRNA in vivo. FEBS J. 277, 4814–4827. https://doi.org/10.1111/j.1742-4658.2010.07904.x.
Song, E., Lee, S.-K., Wang, J., Ince, N., Ouyang, N., Min, J., Chen, J., Shankar, P., Lieberman, J., 2003. RNA interference targeting Fas protects mice from fulminant hepatitis. Nat. Med. 9, 347–351. https://doi.org/10.1038/nm828.
Song, W.-J., Du, J.-Z., Sun, T.-M., Zhang, P.-Z., Wang, J., 2010. Gold nanoparticles capped with polyethyleneimine for enhanced sirna delivery. Small 6, 239–246. https://doi.org/10.1002/smll.200901513.
Sosnovik, D.E., Nahrendorf, M., Weissleder, R., 2008. Magnetic nanoparticles for MR imaging: agents, techniques and cardiovascular applications. Basic Res. Cardiol. 103, 122–130. https://doi.org/10.1007/s00395-008-0710-7.
Sun, C.-Y.Y., Shen, S., Xu, C.-F.F., Li, H.-J.J., Liu, Y., Cao, Z.-T.T., Yang, X.-Z.Z., Xia, J.-X.X., Wang, J., 2015. Tumor acidity-sensitive polymeric vector for active targeted siRNA delivery. J. Am. Chem. Soc. 137, 15217–15224. https://doi.org/10.1021/jacs.5b09602.
Sun, C., Lee, J.S.H., Zhang, M., 2008. Magnetic nanoparticles in mr imaging and drug delivery. Adv. Drug Deliv. Rev. 60, 1252–1265. https://doi.org/10.1016/j.addr.2008.03.018.
Sun, P., Huang, W., Jin, M., Wang, Q., Fan, B., Kang, L., Gao, Z., 2016. Chitosan-based nanoparticles for survivin targeted siRNA delivery in breast tumor therapy and preventing its metastasis. Int. J. Nanomed. 11, 4931–4945. https://doi.org/10.2147/IJN.S105427.
Tabernero, J., Shapiro, G.I., LoRusso, P.M., Cervantes, A., Schwartz, G.K., Weiss, G.J., Paz-Ares, L., Cho, D.C., Infante, J.R., Alsina, M., Gounder, M.M., Falzone, R., Harrop, J., White, A.C.S., Toudjarska, I., Bumcrot, D., Meyers, R.E., Hinkle, G., Svrzikapa, N., Hutabarat, R.M., Clausen, V.A., Cehelsky, J., Nochur, S.V., Gamba-Vitalo, C., Vaishnaw, A.K., Sah, D.W.Y., Gollob, J.A., Burris, H.A., 2013. First-in-humans trial of an RNA interference therapeutic targeting VEGF and KSP in cancer patients with liver involvement. Cancer Discov. 3, 406–417. https://doi.org/10.1158/2159-8290.CD-12-0429.
Takeshita, F., Minakuchi, Y., Nagahara, S., Honma, K., Sasaki, H., Hirai, K., Teratani, T., Namatame, N., Yamamoto, Y., Hanai, K., Kato, T., Sano, A., Ochiya, T., 2005. Efficient delivery of small interfering RNA to bone-metastatic tumors by using atelocollagen in vivo. Proc. Natl. Acad. Sci. USA 102, 12177–12182. https://doi.org/10.1073/pnas.0501753102.
Tan, S.J., Kiatwuthinon, P., Roh, Y.H., Kahn, J.S., Luo, D., 2011. Engineering nanocarriers for siRNA delivery. Small 7, 841–856. https://doi.org/10.1002/smll.201001389.
Tatiparti, K., Sau, S., Kashaw, S.K., Iyer, A.K., 2017. siRNA delivery strategies: a comprehensive review of recent developments. Nanomater. (Basel, Switzerland) 7. https://doi.org/10.3390/nano7040077.
Tian, H., Xiong, W., Wei, J., Wang, Y., Chen, X., Jing, X., Zhu, Q., 2007. Gene transfection of hyperbranched PEI grafted by hydrophobic amino acid segment PBLG. Biomaterials 28, 2899–2907. https://doi.org/10.1016/j.biomaterials.2007.02.027.
Trützschler, A.K., Bus, T., Reifarth, M., Brendel, J.C., Hoeppener, S., Traeger, A., Schubert, U.S., 2018. Beyond gene transfection with methacrylate-based polyplexes – the influence of the amino substitution pattern. Bioconjug. Chem. 29, 2181–2194. https://doi.org/10.1021/acs.bioconjchem.8b00074.
Tuma, P.L., Hubbard, A.L., 2003. Transcytosis: crossing cellular barriers. Physiol. Rev. 83, 871–932. https://doi.org/10.1152/physrev.00001.2003.
Veiseh, O., Kievit, F.M., Ellenbogen, R.G., Zhang, M., 2011a. Cancer cell invasion: treatment and monitoring opportunities in nanomedicine. Adv. Drug Deliv. Rev Target Cell Movement Tumor Cardiovascular Diseases 63, 582–596. https://doi.org/10.1016/j.addr.2011.01.010.
Veiseh, O., Kievit, F.M., Fang, C., Mu, N., Jana, S., Leung, M.C., Mok, H., Ellenbogen, R.G., Park, J.O., Zhang, M., 2010. Chlorotoxin bound magnetic nanovector tailored for cancer cell targeting, imaging, and siRNA delivery. Biomaterials 31, 8032–8042. https://doi.org/10.1016/j.biomaterials.2010.07.016.
Veiseh, O., Kievit, F.M., Mok, H., Ayesh, J., Clark, C., Fang, C., Leung, M., Arami, H., Park, J.O., Zhang, M., 2011b. Cell transcytosing poly-arginine coated magnetic nanovector for safe and effective siRNA delivery. Biomaterials 32, 5717–5725. https://doi.org/10.1016/j.biomaterials.2011.04.039.
Veiseh, O., Sun, C., Fang, C., Bhattarai, N., Gunn, J., Kievit, F., Du, K., Pullar, B., Lee, D., Ellenbogen, R.G., Olson, J., Zhang, M., 2009. Specific targeting of brain tumors with an optical/magnetic resonance imaging nanoprobe across the blood-brain barrier. Cancer Res. 69, 6200–6207. https://doi.org/10.1158/0008-5472.CAN-09-1157.
Venditti, I., 2017. Morphologies and functionalities of polymeric nanocarriers as chemical tools for drug delivery: a review. J. King Saud Univ. – Sci. https://doi.org/10.1016/j.jksus.2017.10.004.
Videira, M., Arranja, A., Rafael, D., Gaspar, R., 2014. Preclinical development of siRNA therapeutics: towards the match between fundamental science and engineered systems. Nanomedicine Nanotechnology. Biol. Med. 10, 689–702. https://doi.org/10.1016/j.nano.2013.11.018.
Wang, F., Wang, Y., Zhang, X., Zhang, W., Guo, S., Jin, F., 2014. Recent progress of cell-penetrating peptides as new carriers for intracellular cargo delivery. J. Control. Release 174, 126–136. https://doi.org/10.1016/j.jconrel.2013.11.020.
Wang, J., Lu, Z., Wientjes, M.G., Au, J.L.-S., 2010. Delivery of siRNA therapeutics: barriers and carriers. AAPS J. 12, 492–503. https://doi.org/10.1208/s12248-010-9210-4.
Wang, T., Shigdar, S., Shamaileh, H. Al, Gantier, M.P., Yin, W., Xiang, D., Wang, L., Zhou, S.-F., Hou, Y., Wang, P., Zhang, W., Pu, C., Duan, W., 2017. Challenges and opportunities for siRNA-based cancer treatment. Cancer Lett. 387, 77–83. https://doi.org/10.1016/J.CANLET.2016.03.045.
Wang, X.-L., Xu, R., Wu, X., Gillespie, D., Jensen, R., Lu, Z.-R., 2009. Targeted systemic delivery of a therapeutic siRNA with a multifunctional carrier controls tumor proliferation in mice. Mol. Pharm. 6, 738–746. https://doi.org/10.1021/mp800192d.
Werfel, T.A., Jackson, M.A., Kavanaugh, T.E., Kirkbride, K.C., Miteva, M., Giorgio, T.D., Duvall, C., 2017. Combinatorial optimization of PEG architecture and hydrophobic content improves ternary siRNA polyplex stability, pharmacokinetics, and potency in vivo. J. Control. Release 255, 12–26. https://doi.org/10.1016/j.jconrel.2017.03.389.
Xie, Y., Qiao, H., Su, Z., Chen, M., Ping, Q., Sun, M., 2014. PEGylated carboxymethyl chitosan/calcium phosphate hybrid anionic nanoparticles mediated hTERT siRNA delivery for anticancer therapy. Biomaterials 35, 7978–7991. https://doi.org/10.1016/j.biomaterials.2014.05.068.
Yin, T., Liu, J., Zhao, Z., Dong, L., Cai, H., Yin, L., Zhou, J., Huo, M., 2016. Smart nanoparticles with a detachable outer shell for maximized synergistic antitumor efficacy of therapeutics with varying physicochemical properties. J. Control. Release 243, 54–68. https://doi.org/10.1016/j.jconrel.2016.09.036.
Zhang, W., Müller, K., Kessel, E., Reinhard, S., He, D., Klein, P.M., Höhn, M., Rödl, W., Kempter, S., Wagner, E., 2016. Targeted siRNA delivery using a lipo-oligoaminoamide nanocore with an influenza peptide and transferrin shell. Adv. Healthc. Mater. 5, 1493–1504. https://doi.org/10.1002/adhm.201600057.
Zhu, H., Zhang, S., Ling, Y., Meng, G., Yang, Y., Zhang, W., 2015. PH-responsive hybrid quantum dots for targeting hypoxic tumor siRNA delivery. J. Control. Release 220, 529–544. https://doi.org/10.1016/j.jconrel.2015.11.017.

Deuxième partie : Développement, caractérisation et évaluation *in vitro* d'un nanovecteur magnétique pour la délivrance des siRNA

Publication 2: Formulation and in vitro evaluation of a siRNA delivery nanosystem decorated with gH625 peptide for triple negative breast cancer theranosis

Publiée dans « European Journal of Pharmaceutics and Biopharmaceutics », 2018

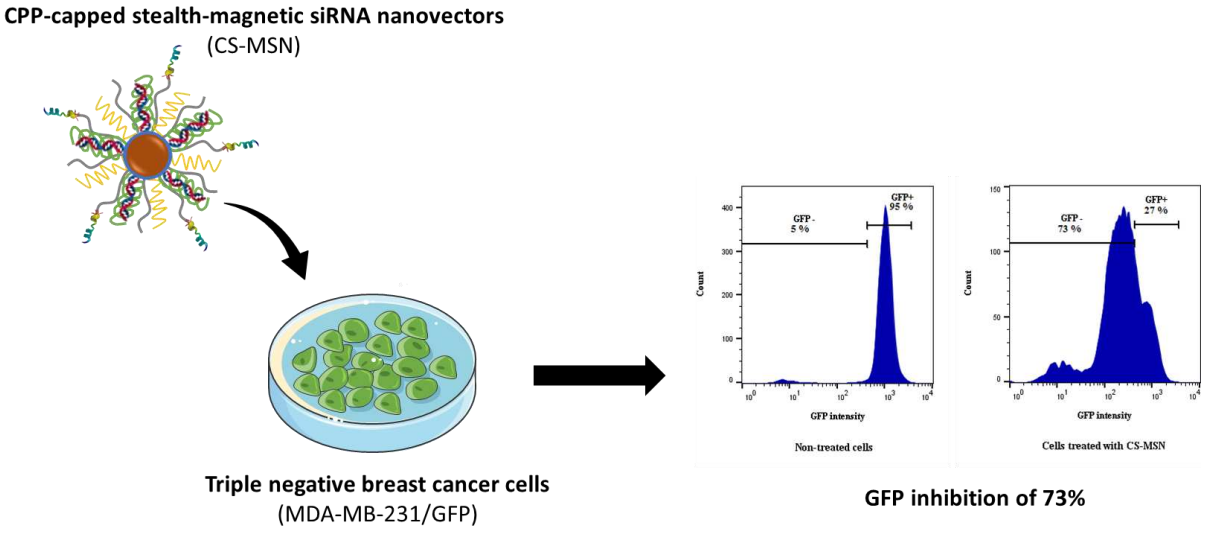

Préambule de la publication 2

Depuis la découverte du pouvoir thérapeutique des siRNA et la compréhension des limites de leur utilisation, plusieurs chercheurs se sont mis à développer de nouvelles approches pour essayer de surmonter ces difficultés. Une stratégie prometteuse est d'associer les siRNA à d'autres molécules capables de les complexer, les protéger contre la dégradation enzymatique et les délivrer au niveau du site cible. Cette approche est nommée la nanovectorisation des siRNA. Elle consiste à concevoir un nanovecteur à partir des composants qui ont des caractéristiques et des propriétés utiles pour aider les siRNA à réussir leur mission.

Une nanoplateforme à base de nanoparticules d'oxydes de fer superparamagnétiques (SPION) marquées avec un fluorochrome proche infra-rouge (la cyanine 5), stabilisées avec du polyéthylène glycol (PEG_{5000}) et fonctionnalisées avec un peptide membranotrope gH625, a été développée préalablement dans notre laboratoire. En se basant sur l'utilisation de cette nanoplateforme, nous avons développé un nanovecteur de siRNA pour améliorer le traitement du cancer du sein triple négatif. Pour obtenir ce nanovecteur, nous avons utilisé des polymères cationiques (chitosan et poly-L-arginine) pour la complexation et la protection des siRNA. Chaque composant de ce nanovecteur a un rôle et une fonction spécifique : les SPION représentent le cœur du nanovecteur et permettent le suivi en IRM ; le PEG apporte une stabilité colloïdale et une certaine furtivité ; le peptide gH625 favorise l'entrée dans les cellules ; les polymères cationiques permettent la complexation et la protection des siRNA et favorisent l'entrée, l'échappement endosomal et la délivrance des siRNA dans le cytosol.

La première partie de cette étude présente les étapes de l'optimisation et la caractérisation de la formulation des CS-MSN, en variant les quantités de polymères cationiques par rapport à la quantité des siRNA utilisée. Cette optimisation est basée sur des mesures de taille et de potentiel zêta ainsi que sur l'évaluation de la complexation et de la rétention en présence et en l'absence de différentes concentrations de sérum. Les CS-MSN ont une taille d'environ 175 nm avec un potentiel zêta de 14 mV. Ces caractéristiques physico-chimiques sont intéressantes pour l'utilisation *in vitro* et pour l'administration *in vivo* par voie intraveineuse. Nous avons montré que chaque composant de ce nanovecteur a un rôle bien déterminé et une fonction essentielle dans la formulation.

En appliquant les CS-MSN sur les cellules en présence de siRNA contrôle, la formulation de ce nanovecteur se montre pas ou peu cytotoxique même à une concentration

supérieure à celle utilisée pour traiter les cellules. De plus, les CS-MSN ont été internalisés rapidement (4 h) par une lignée de cellules de cancer du sein triple négatif (MDA-MB-231). Cette internalisation a abouti à une inhibition de 73 % de l'expression de la protéine GFP (green fluorescent protein) dans des cellules exprimant cette protéine, en utilisant des CS-MSN préparés avec des siRNA anti-GFP. Cette inhibition est significativement plus importante que celle d'un agent de transfection commercial, l'Oligofectamine™.

European Journal of Pharmaceutics and Biopharmaceutics 131 (2018) 99–108

Contents lists available at ScienceDirect

European Journal of Pharmaceutics and Biopharmaceutics

journal homepage: www.elsevier.com/locate/ejpb

Research paper

Formulation and *in vitro* evaluation of a siRNA delivery nanosystem decorated with gH625 peptide for triple negative breast cancer theranosis

Sanaa Ben Djemaa[a], Stephanie David[a,*], Katel Hervé-Aubert[a], Annarita Falanga[b], Stefania Galdiero[b], Emilie Allard-Vannier[a], Igor Chourpa[a], Emilie Munnier[a]

[a] EA6295 Nanomédicaments et Nanosondes, Université de Tours, 31 Avenue Monge, 37200 Tours, France
[b] Department of Pharmacy, CIRPEB – University of Naples "Federico II", Via Mezzocannone 16, 80134 Napoli, Italy

ARTICLE INFO

Keywords:
SPION
Chitosan
Poly-L-arginine
Cell-penetrating peptide
Nanovector
Down-regulation

ABSTRACT

The development of an efficient small interfering RNA (siRNA) delivery system has held scientists interest since the discovery of the RNA interference mechanism (RNAi). This strategy gives hope for the treatment of many severe diseases. Herein, we developed hybrid nanovectors able to deliver siRNA to triple negative breast cancer cells. The nanovectors are based on PEGylated superparamagnetic iron oxide nanoparticles (SPION) functionalized with gH625 peptide, chitosan and poly-L-arginine. Every component has a key role and specific function: SPION is the core scaffolding the nanovector; PEG participates in the colloidal stability and the immune stealthiness; gH625 peptide promotes the nanovector internalization into cancer cells; cationic polymers provide the siRNA protection and favor siRNA endosomal escape and delivery to cytosol. The formulation was optimized by varying the amount of each compound. The efficacy of the siRNA retention and protection were investigated in the presence of high concentration of serum. Optimized nanovectors show a high uptake by MDA-MB-231 cells. The resulting down regulation of GFP expression was 73 ± 3% with our nanovector compared to 59 ± 8% obtained with the siRNA-Oligofectamine™ complex in the same conditions.

1. Introduction

Triple negative breast cancer (TNBC) is classified as one of the most aggressive forms of breast cancer and is generally associated with high tumor grade and a poor survival. TNBC is characterized by the absence of estrogen receptor, progesterone receptor and human epidermal growth factor receptor 2 [1]. The lack of these receptors deprives the TNBC of the benefits of specific therapy targeting these proteins [2]. That is one of the reasons why no effective targeted therapy is available for TNBC and its treatment presents a major clinical challenge [3]. To combat this disease and to reduce female mortality, novel approaches have to be developed.

One promising strategy which has provided hope for the treatment of various severe diseases like cancer is based on the use of small interfering RNA (siRNA) [4–6]. This strategy emerged after the demonstration of the mechanism of RNA interference (RNAi) in mammalian cells in 2001 [7]. SiRNA are double-stranded RNA of 21–25 nucleotides in length, which act with specificity on post-transcriptional gene extinction. SiRNA have a high ability to recognize complementary mRNAs and to guide the associated cytosolic RNA-induced silencing complex (RISC). This association leads to the mRNA degradation and consequently the inhibition of gene expression [8]. For cancer treatment, this strategy is used to induce the down-regulation of genes coding for proteins implicated in cancer cells proliferation and tumor growth [9]. However, when siRNA are administrated in systemic circulation there are some limitations. Indeed, the negative charge of siRNA limits their ability to cross cell membranes and the presence of enzymes in the blood, such as ribonucleases, affects siRNA stability and leads to their rapid degradation [10]. Consequently, it is necessary to develop a delivery system to protect siRNA, prolong their blood

Abbreviations: SiRNA, small interfering RNA; RNAi, RNA interference; SPION, superparamagnetic iron oxide nanoparticles; PEG, polyethylene glycol; GFP, green fluorescent protein; TNBC, triple negative breast cancer; CPP, cell-penetrating peptide; CS-FNP, CPP-capped stealth fluorescent nanoparticles; CS-MSN, CPP-capped stealth magnetic siRNA nanovectors; N, amine groups; P, phosphate groups; Cs, chitosan; PLR, poly-L-arginine; MR, mass ratio; N_{CS}/P, the molar ration of the positive charges of chitosan amine groups and the negative charges of siRNA's phosphate groups; N_{PLR}/P, the molar ration of the positive charges of poly-L-arginine amine groups and the negative charges of siRNA's phosphate groups; HD, hydrodynamic diameter; PDI, polydispersity index; ZP, zeta potential; FBS, fetal bovine serum; SiGFP, siRNA anti-GFP; SiCtrl, non-targeted siRNA

* Corresponding author.
E-mail address: stephanie.david@univ-tours.fr (S. David).

https://doi.org/10.1016/j.ejpb.2018.07.024
Received 18 April 2018; Received in revised form 24 July 2018
Available online 29 July 2018
0939-6411/ © 2018 Elsevier B.V. All rights reserved.

circulation time, improve their bioavailability, allow their internalization by target cells and intracytoplasmic siRNA release.

One strategy is to associate siRNA with nanocarrier systems to effectively deliver the therapeutic siRNA towards their target [11,12]. In this context, superparamagnetic iron oxide nanoparticles (SPION) appear as a suitable candidate thanks to their safety for *in vivo* application. In fact, SPION are already used as contrast agents for magnetic resonance imaging (MRI) [13] and they are prevalently used in the development of nanocarriers for siRNA delivery [4,14–16]. In our team, we previously synthesized fluorescent SPION coated with polyethylene glycol (PEG) polymer and functionalized with the cell-penetrating-peptide (CPP) gH625 [17]. In the present paper, we will name these nanoparticles CS-FNP (as CPP-capped stealth fluorescent nanoparticles). The CS-FNP labeling with Cyanine 5.5 covalently attached to the SPION core allows to monitor them in cells and tissues using fluorescence. The PEG shell around SPION improves their colloidal stability and stealthiness [18,19]. The membranotropic gH625 peptide [20] conjugated to the PEG shell of the nanoparticles is intended to promote their uptake into cells. Due to their small size below 100 nm and their nearly neutral zeta potential, the CS-FNP appeared appropriate for intravenous (i.v) injection. CS-FNP showed a prolonged colloidal stability in biological medium and an efficient uptake by MDA-MB-231 cancer cells [17].

In this work, we used the CS-FNP nanoplatform to develop a magnetic siRNA nanovector called CS-MSN (as CPP-capped stealth magnetic siRNA nanovector) for triple negative breast cancer theranosis (Fig. 1).

Cationic polymers like chitosan carrying amino groups (NH_3^+, hereafter named N) are often formulated with poly-anionic siRNA carrying phosphate groups (PO_4^{3-}, hereafter named P), in order to protect the latter against degradation and promote internalization into cells [16,21,22]. Moreover, thanks to their buffering capacity and their action as “proton sponges”, cationic polymers escape from endosomes and thus can enhance the passage of siRNA to the cytosol [23]. Our CS-MSN included two cationic polymers: chitosan (hereafter called Cs) and poly-L-arginine (hereafter called PLR). Cs is known for its large use in siRNA delivery due to its safety, biocompatibility and biodegradability [24]. Several studies demonstrated the role of Cs in siRNA delivery and transfection efficiency [15,21,22]. The ability of polyarginine to bind anionic siRNA and to complex them with other components of nanovectors (such as other polymers and/or iron oxide nanoparticles) has been also reported and largely exploited in the development of siRNA delivery nanosystems [16,25].

First, the CS-MSN formulation was optimized by varying the N/P ratio of the different polymers. Then, the CS-MSN stability in biologically relevant conditions, their toxicity and the siRNA transfection efficiency were evaluated.

2. Materials and methods

2.1. Preparation of cell-penetrating peptide stealth magnetic siRNA nanovector

2.1.1. Synthesis of CPP-capped stealth-fluorescent nanoparticles (CS-FNP)

The synthesis of CS-FNP is based on a protocol previously published by our group [17]. Briefly, to obtain these nanoparticles, SPION were silanized, labeled with cyanine 5.5, PEGylated in their surface and then functionalized with gH625 peptide. After the functionalization we modified the purification protocol by performing a dialysis (MWCO 300KDa) against PBS at 4 °C and in the dark for around 6 h, while PBS in the acceptor volume was changed every 1 h. CS-FNP were finally concentrated by Vivaspin® (cut-off of 30 kDa, Fisher Scientific, Illkirch, France).

2.1.2. Formulation of CPP-capped stealth-magnetic siRNA nanovectors (CS-MSN)

The formulation of CS-MSN is based on a protocol developed by David *et al.* and previously published by our laboratory [26]. Briefly, CS-MSN were formulated by loading siRNA and cationic polymers, chitosan (Cs, MW 110–150 kDa; degree of acetylation: ≤ 40 mol.%) and poly-L-arginine (PLR, MW 15–70 kDa) (both from Sigma-Aldrich Chimie GmbH, St. Quentin Fallavier, France) into CS-FNP. On the one hand, siRNA were precomplexed with PLR, on the other hand CS-FNP were precomplexed with chitosan and then both precomplexes were mixed together to obtain CS-MSN. The siRNA loading was defined by the iron/siRNA w/w ratio (MR) of 10. The cationic polymers loading was defined as N/P ratio, i.e. the molar ratio of the positive charges of polymers and the negative charges of siRNA. In order to optimize the nanovectors, the Cs/siRNA relative content (hereafter called N_{CS}/P) was varied from 0 to 100. and the PLR/siRNA relative content (hereafter called N_{PLR}/P) was varied from 0 to 6.

2.2. Size and zeta potential analysis

The size, the polydispersity index (PDI) and the zeta potential (ZP) were determined using a Nanosizer apparatus (Zetasizer®, Malvern Instrument, UK). The measurements of hydrodynamic diameter (HD)

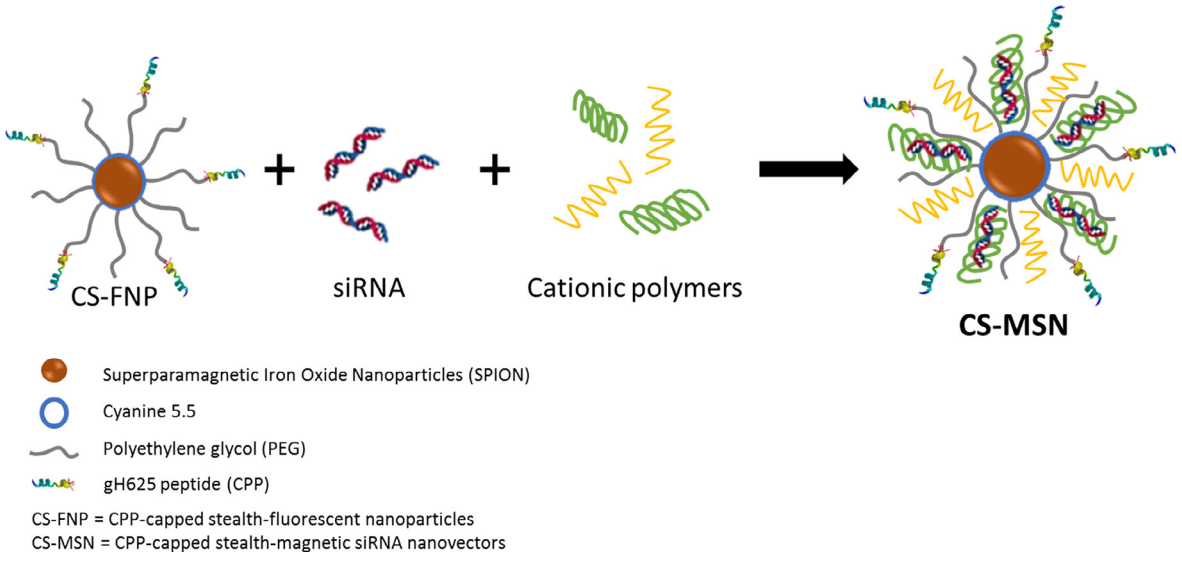

Fig. 1. Scheme of CS-MSN and its components, CS-FNP, siRNA and cationic polymers.

and zeta potential of CS-FNP (iron concentration of 50 mg/l) were performed in PBS 1X and $NaNO_3$ solution (0.01 M), respectively. For the CS-MSN, the HD and the ZP were obtained after dilution of CS-MSN in $NaNO_3$ 0.01 M (1:25 v/v) to fix the ionic strength. These measurements were achieved at 25 °C. The mean values of HD given were based on intensity. All measurements were made in triplicate and mean values ± SD were recorded.

2.3. Agarose gel electrophoresis and heparin decomplexation assay

Gel electrophoresis technique was used to verify the complexation of siRNA. Samples were prepared to deposit a content of 1.2 µM of siRNA per well. To release siRNA and control their integrity after formulation, heparin (Sigma-Aldrich Chemie GmbH, Steinheim, Germany) was added at a final concentration of 3 mg/ml. A loading buffer (Agarose gel loading dye 6X, Fisher, Bioreagents®, Illkirch, France) was added to all the samples before the deposit in wells. An agarose gel (1% m/v) was prepared containing 0.01% (v/v) ethidium bromide (EtBr) to visualize free siRNA. After deposition of the samples on the agarose gel, the migration was conducted in a Tris-acetate-EDTA (TAE) 1X buffer (Acros Organics, Geel, Belgium) for 15 min at 150 V. Free siRNA were visualized by UV-imaging using the EvolutionCapt software on a Fusion-Solo.65.WL imager (Vilbert Lourmat, Marne-la-Vallée, France). The fluorescence intensity of bands was quantified using Image J software.

2.4. Retention and protection in serum

To study the retention and the protection of siRNA in the presence of serum, CS-MSN or a solution of siRNA (2 µM) were added to an equal volume of a solution of Dulbecco's modified Eagle medium (DMEM) (Gibco®, Life Technologies, Paisley, UK) containing different percentages of fetal bovine serum (FBS) (Eurobio, Les Ulis, France) to obtain a final percentage of serum of 5%, 10% and 50%. After 4 h of incubation at 37 °C, gel retardation assay (as described in section 2.3) was performed.

2.5. Cell culture

Triple negative breast cancer cells MDA-MB-231 (a kind gift from the team MINT, UMR INSERM 1066 – CNRS 6021, University of Angers, France) and MDA-MB-231 stably expressing GFP (MDA-MB-231/GFP) (Euromedex, Souffelweyersheim, France) were maintained in DMEM supplemented with 10% fetal bovine serum, 1% non-essential amino acid (HyClone Laboratories, Logan, Utah) and 1% penicillin/streptomycin (Gibco®, Life Technologies, Paisley, UK) at 37 °C in an atmosphere containing 5% CO_2. Culture medium was changed every 48–72 h and the cells were harvested using trypsin/EDTA (0.05%) (Gibco®, Life Technologies, Paisley, UK) at 80% of confluency.

2.6. Transfection assay

One day before the transfection, MDA-MB-231/GFP cells were seeded at 3.10^4 cells/well in 12 well-plates. The day of transfection, CS-MSN and Oligofectamine™ (Invitrogen, Thermo Fisher Scientific, Paisley, UK) were prepared with anti-GFP siRNA at a final siRNA concentration of 50 nM according to the formulation protocol and the manufacture recommendation, respectively. Cells were treated with CS-MSN in equal parts of complete medium and Opti-MEM medium (Gibco®, Life Technologies, Paisley, UK) (1:1 v/v) and maintained in normal growth conditions for 30 min to 72 h or for 72 h with Oligofectamine™ (manufacture recommendation). Non-treated cells and cells transfected with CS-MSN loaded with a non-targeting siRNA sequence (siRNA Ctrl) were used as a negative control. Cells were removed using trypsin and then analyzed 24, 48 or 72 h after treatment using a FACSCalibur flow cytometer (BD Bioscience, Franklin Lakes, NJ). Data was analyzed using FlowJo v10 software. The percentage of gene silencing was calculated using the FL-1 median (median of the GFP fluorescence histogram).

2.7. Cytotoxicity

Cell viability was evaluated by a colorimetric assay based on the measurement of mitochondrial activity in viable cells using a stable tetrazolium salt WST-1 (Sigma Aldrich Chimie, St. Quentin Fallavier, France). MDA-MB-231 cells were seeded in 96 well-plate at 4.10^3 cells/well. After 24 h, cells were incubated with nanovectors prepared at different concentrations of siRNA (from 12.5 to 100 nM) for 4, 24 or 48 h. Then, the culture medium was replaced by a fresh complete medium containing 10% (v/v) WST-1 reagent for 3 h at 37 °C. Non-treated cells were used as a negative control while cells incubated with H_2O_2 at 20 mM were used as a positive control. The absorbance was measured at 450 nm using KC-junior V1.40 software on a BIO-TEK EL800 microplate reader. The number of viable cells is directly proportional to the absorbance value. The percentage of viable cells was calculated according to the followed equation:

$$Viability\,(\%) = \frac{As - Apc}{Anc - Apc} \times 100$$

As, Apc and Anc are, respectively, the absorbances of the sample, the positive control (H_2O_2) and the negative control (non-treated cells).

2.8. Internalization assay

Cellular internalization of CS-MSN by MDA-MB-231 cancer cells was evaluated by following the cyanine 5.5 fluorescence of CS-FNP using flow cytometry. MDA-MB-231 cells were seeded onto 6-well plates at 10^6 cells/well and were allowed to adhere for 24 h. CS-MSN were added to cells for 4 h after replacement of the complete cell culture medium by an equal part of complete medium and Opti-MEM medium (1:1 v/v). Non-treated cells were used as a negative control. Immediately after treatment, cells were washed and were removed using trypsin.

2.9. Statistics

Values were expressed as means ± standard deviations (SD). PRISM (GraphPad Prism 7) was used for statistical analysis. Data were compared among groups using Mann and Whitney test. The difference between groups was considered significant when p-value < 0.05 (*), < 0.01 (**) or < 0.001 (***).

3. Results and discussion

3.1. Development of an efficient CS-MSN formulation for siRNA delivery

3.1.1. Choice of poly-L-arginine for a complete siRNA complexation

The formulation of CS-MSN was based on the use of synthesized CS-FNP which had a size of 79 ± 8 nm and a zeta potential of −6 ± 1 mV. The first cationic polymer tested for CS-MSN development was chitosan. In order to obtain a CS-MSN formulation with a high transfection efficiency in cancer cells, we started by varying the molar ratio between the positive charges of chitosan amine groups and the negative charges of siRNA's phosphate groups (N_{CS}/P ratio). Fernandes and coworkers [27] used chitosan to siRNA weight ratio of 50:1 (the equivalent of N_{CS}/P ratio of 100:1) to completely complex siRNA with chitosan. In a study by Sun and colleagues [22], siRNA were complexed efficiently with PEG-chitosan at a weight ratio of PEG-CS to siRNA of 100:1. According to these results, the N_{CS}/P ratio was varied from 0 to 100. The second formulation parameter is the mass ratio (MR = iron mass of CS-FNP/siRNA mass) which was fixed at 10 for the following experiments, according to previously obtained results [26].

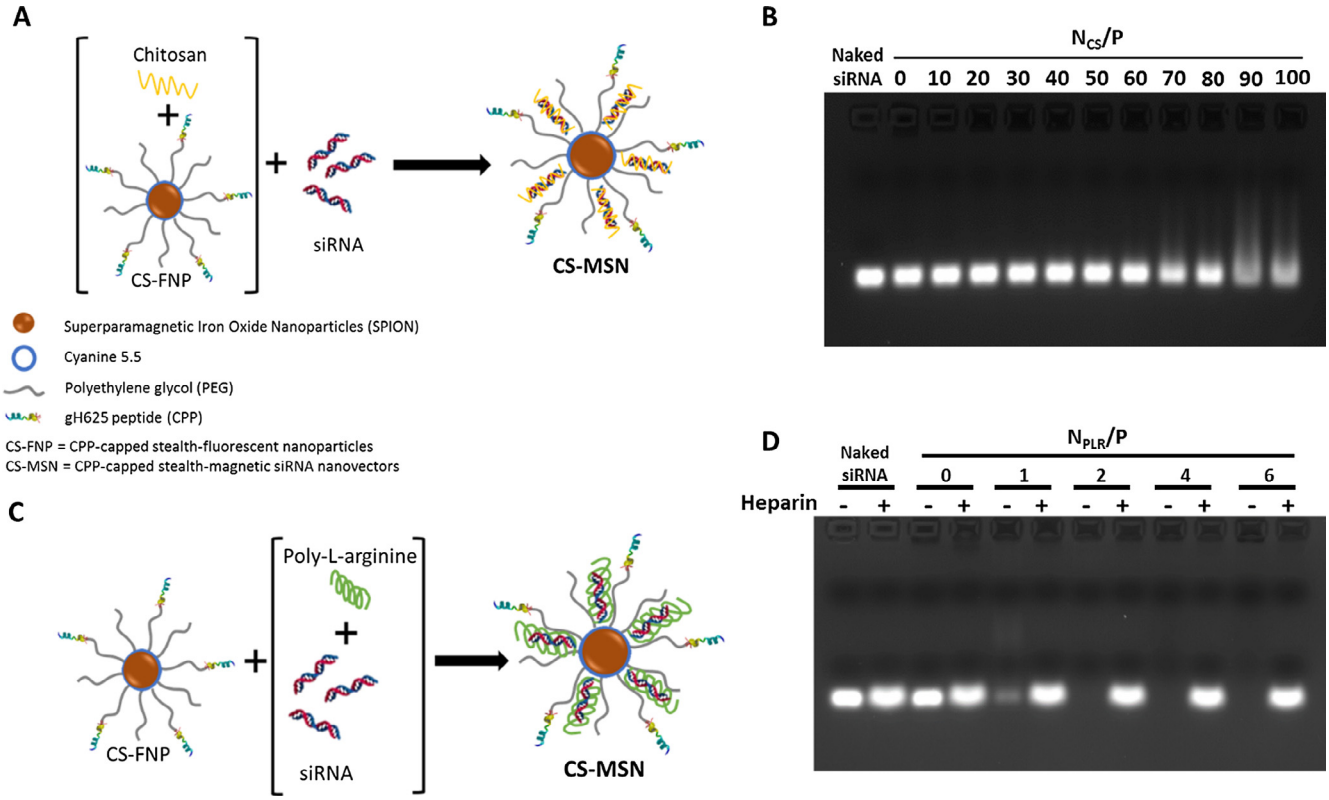

Fig. 2. Formulation of CS-MSN and detection of free siRNA in formulated CS-MSN. (A) Formulation scheme of CS-MSN prepared with CS-FNP, siRNA and chitosan. (B) Gel retardation assay to detect free siRNA in CS-MSN prepared with CS-FNP, siRNA and chitosan. (C) Formulation scheme of CS-MSN prepared with CS-FNP, siRNA and PLR. (D) Gel retardation assay to detect free siRNA in CS-MSN prepared with CS-FNP, siRNA and PLR, with (+) or without (−) heparin.

The formulation of CS-MSN was performed according to the following protocol: chitosan was firstly mixed with CS-FNP, then siRNA were added (Fig. 2. A). The siRNA retention in final complexes was evaluated using agarose gel retardation assay. After applying the electric field, free siRNA migrate and appear as fluorescent bands, while complexed siRNA remain in the loading wells. The fluorescence intensity is directly proportional to the quantity of free siRNA. As shown in Fig. 2B, the fluorescent bands, indicating free siRNA, were observed in all samples at different N_{CS}/P ratios. The fluorescence intensity seems to be reduced at a N_{CS}/P ratio higher than 80, but there is always more than 80% of free siRNA in the formulation. This result indicates that at these N_{CS}/P ratios chitosan was not able to promote complete siRNA complexation with CS-FNP.

In order to improve siRNA complexation, another highly cationic polymer, poly-L-arginine (PLR, pKa = 12) was investigated. PLR, similarly to chitosan, has a high capacity to complex negatively charged molecules like siRNA. The amount of PLR used in the formulation was defined, as for chitosan, using the N/P molar ration (N_{PLR}/P ratio). SiRNA were precomplexed with PLR at different N_{PLR}/P values from 0 to 6 and then added to CS-FNP (Fig. 2C). SiRNA retention was evaluated using agarose gel electrophoresis. To release siRNA and control their integrity after formulation, a heparin decomplexation assay was performed. As shown in Fig. 2D, the migration of siRNA was completely blocked from a N_{PLR}/P ratio of 2. In fact, without heparin, no fluorescent band was observed for samples prepared at N_{PLR}/P ≥ 2. However, when heparin was added, siRNA was released from the complexes, indicating that PLR can successfully complex the siRNA with the CS-FNP nanoparticles even at a low N_{PLR}/P ratio. In the literature, complexation efficiency of siRNA with polyarginine was already investigated. Zhao *et al.* demonstrated that polyarginine complexes siRNA from a N/P ratio of 10 in a study for the development of nanomicelles for siRNA delivery [16,25]. In another study, Veiseh *et al.* succeeded to completely condense siRNA with iron oxide nanoparticles coated with polyarginine at a weight ratio of 20 [16]. However, in our case, the N_{PLR}/P ratio for complete siRNA complexation are much lower than these reported.

The implication of CS-FNP in CS-MSN composed of CS-FNP, siRNA and PLR, was checked by performing a gel retardation assay of siRNA/PLR complexes (without CS-FNP), and it showed a total complexation of siRNA indicating that PLR is the major component which complex siRNA. The data for N_{PLR}/P = 2 are presented in Fig. S1. A, as at this N_{PLR}/P ratio all siRNA were complexed. Furthermore, the size and zeta potential of formulations prepared with siRNA and PLR with and without CS-FNP at N_{PLR}/P = 2 were measured (Fig. S1B and Table S1). Results indicated that CS-FNP improved the organization of siRNA and PLR and induced a more homogenous size distribution.

To choose the N_{PLR}/P ratio, the size and the surface charge of CS-MSN were measured as these parameters are two other important criteria to characterize when developing nanovector for siRNA delivery. As shown in Table 1, the addition of PLR increases the hydrodynamic diameter (HD) of the complexes to exceed 200 nm at N_{PLR}/P ratio of 6. The zeta potential remained lower than or equal to 0 mV up to N_{PLR}/P ratio of 6. It was previously reported that cellular uptake and biodistribution of nanoparticles is strongly affected by nanoparticles size. Indeed, large nanoparticles with diameters higher than 200 nm could stimulate immune system by activating the complement system [28]. As

Table 1
Hydrodynamic diameter (HD), polydispersity index (PDI) and zeta potential (ZP) of CS-MSN prepared with CS-FNP, siRNA and PLR.

	HD (nm)	PDI	ZP (mV)
N_{PLR}/P = 1	78 ± 7	0.34 ± 0.05	−7.3 ± 0.4
N_{PLR}/P = 2	143 ± 12	0.33 ± 0.04	−4.6 ± 0.3
N_{PLR}/P = 4	172 ± 9	0.26 ± 0.01	−2.1 ± 0.3
N_{PLR}/P = 6	255 ± 15	0.35 ± 0.01	0.3 ± 0.2

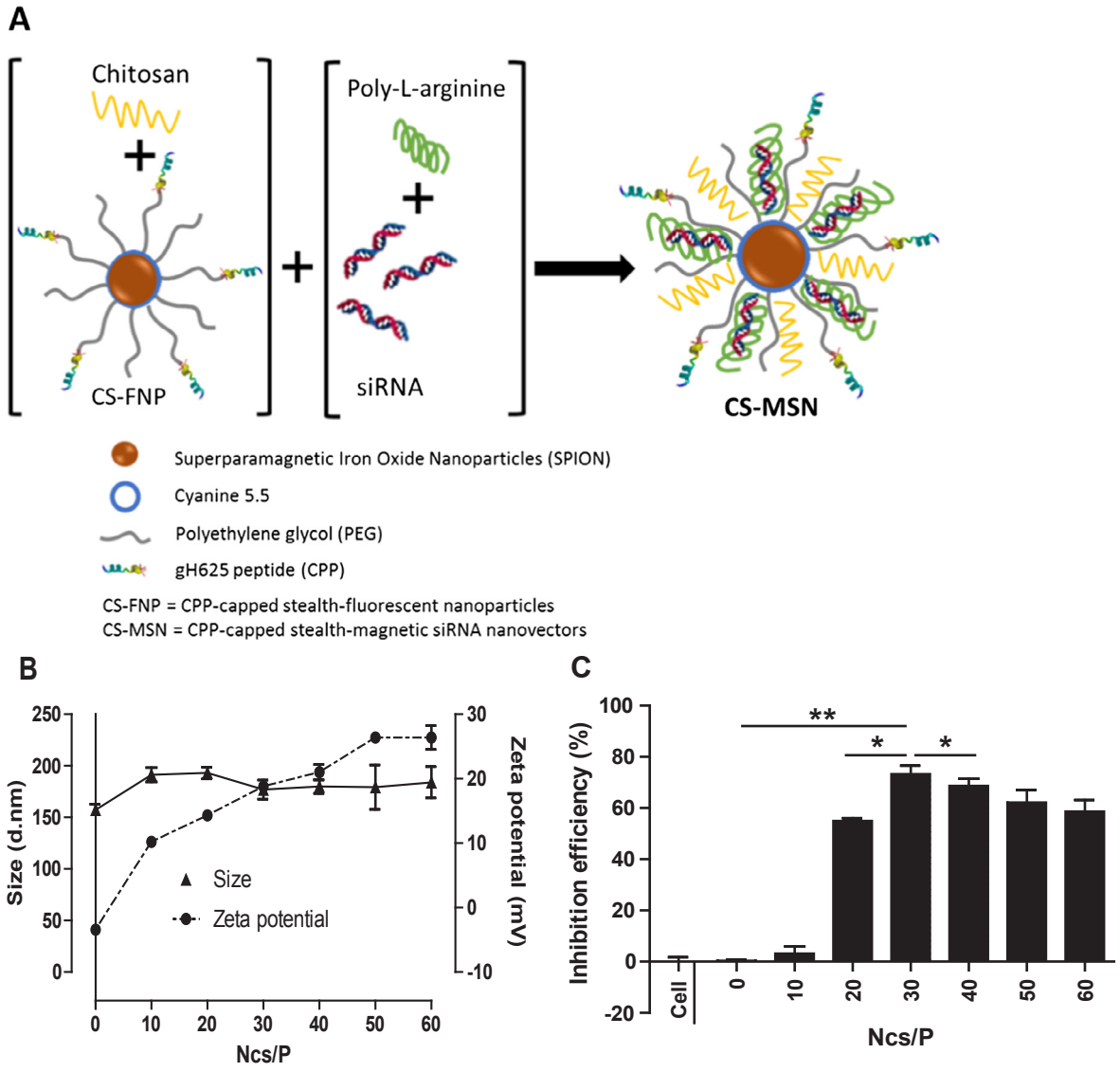

Fig. 3. Preparation and characterization of CS-MSN formulated with CS-FNP, siRNA, PLR and different amount of chitosan. (A) Formulation scheme of CS-MSN. (B) Hydrodynamic diameter and zeta potential. (C) Down regulation efficiency of GFP fluorescence in MDA-MB-231/GFP cells treated with CS-MSN prepared at MR = 10, $N_{PLR}/P = 2$ and at different N_{CS}/P ratio, siRNA/PLR ($N_{PLR}/P = 2$) and siRNA/PLR/CS ($N_{PLR}/P = 2$, $N_{CS}/P = 30$) complexes.

the size of complexes at $N_{PLR}/P = 6$ is higher than 200 nm, this N_{PLR}/P ratio was excluded from our choice. At $N_{PLR}/P = 1$, siRNA are not well complexed and to limit the quantity of PLR, we fixed the N_{PLR}/P at 2 for the following experiments. However, at this N_{PLR}/P ratio, the zeta potential of CS-MSN was rather negative, which could limit the internalization into cells. It was shown that positively charged nanoparticles are more internalized than negatively charged nanoparticles [29] and this could be explained by the increased electrostatic attraction between positive charges of nanoparticles and negative charged cell membrane.

3.1.2. Addition of chitosan for an efficient siRNA delivery

To add supplementary positive charges, which could promote the cellular entry of CS-MSN, we added chitosan (Fig. 3A), but we had to verify that it did not lead to an increase in the size beyond 200 nm. The size and the zeta potential of formulated CS-MSN formulated with N_{CS}/P ratios from 0 to 60 were measured (Fig. 3B) and the siRNA complexation was checked using gel electrophoresis (data not shown). Results indicate that the addition of chitosan to the formulation increased the hydrodynamic diameter of CS-MSN up to 170–190 nm. The polydispersity index (PDI) was around 0.3 for all formulations which is quite usual for formulations using electrostatic self-assembly. Moreover, the zeta potential increased gradually with the N_{CS}/P ratio up to 28 mV because of the increased amount of amino groups. Additionally, gel electrophoresis results show a total siRNA complexation at all tested N_{CS}/P ratios indicating that the addition of chitosan does not disturb the siRNA complexation with PLR and CS-FNP.

To select the N_{CS}/P ratio for an efficient siRNA delivery, a transfection assay was carried out. Therefore, MDA-MB-231/GFP cells were treated with CS-MSN containing anti-GFP siRNA (50 nM) and formulated at N_{CS}/P ratio from 0 to 60. Cells were analyzed using flow cytometry to measure the fluorescence intensity of GFP (Fig. 3C). Successful transfection of anti-GFP siRNA would result in reduced GFP fluorescence compared to non-transfected cells and would therefore indicate successful siRNA delivery. Without chitosan, no reduction in the GFP fluorescence intensity was observed compared to non-treated cells, indicating that CS-MSN failed to inhibit the GFP expression. When the N_{CS}/P ratio increased up to 30, the GFP fluorescence intensity decreased compared to non-treated cells indicating that the down regulation efficiency increased up to 73%. For higher N_{CS}/P ratios, the GFP fluorescence intensity seems to decrease less than for N_{CS}/P ratio of 30, indicating a decreased down regulation. Thus, the most efficient CS-

MSN were formulated at N_{CS}/P ratio of 30. These results indicate that even if chitosan is not involved in the complexation of siRNA into CS-MSN (Fig. 2B), it seems to be important to obtain a size less than 200 nm with a slightly positive zeta potential. Furthermore, flow cytometry result highlights the importance of chitosan for an efficient siRNA transfection. That suggest that chitosan plays a key role in the intracellular trafficking of the CS-MSN. Martens and coworkers demonstrated that chitosan has an important role in the endosomal escape [30] which is a crucial step for siRNA intracellular delivery. It was previously noted that the use of chitosan at a relatively high N/P ratio promote the compactness of the nanovector structure and led to smaller size compared to low N/P ratio [31]. Moreover, Liu et al. showed that a poor transfection efficiency is correlated to low N/P ratios. The greater knockdown efficiencies were observed with nanovectors formulated with chitosan at N/P ratios higher than 30, however cytotoxicity was recorded with formulations prepared at N/P ratios higher than 70 [32]. In this study, it appears that both polymers are complementary: PLR enables complete siRNA complexation (Fig. 2D) thanks to its high positive charge density, and chitosan improves the siRNA delivery and the transfection efficiency of CS-MSN (Fig. 3C). Taken these results together, we defined the optimal formulation parameters of CS-MSN with adequate characteristics and a high transfection efficiency in cancer cells at MR ratio of 10, N_{PLR}/P ratio of 2 and N_{CS}/P ratio of 30.

3.2. Characterization of the optimized CS-MSN formulation

3.2.1. Implication of CS-FNP in the CS-MSN formulation

To check if CS-FNP are included in final CS-MSN, the size of formulations prepared with siRNA, PLR and chitosan at $N_{PLR}/P = 2$ and $N_{CS}/P = 30$ were measured and compared with formulations including CS-FNP. Without CS-FNP, the complexes showed sizes higher than 200 nm, with a high standard deviation (36 nm). The addition of CS-FNP to the formulation reduced the size of the final complexes and their standard deviation to 175 ± 7 nm. Additionally, the polydispersity index, representing the size distribution within the sample, diminishes (Table 2) and the shape of the peak changed from a large peak to a well-defined peak with a maximum at 175 nm when CS-FNP are included (Fig. 4A and B). It seems that the presence of CS-FNP improved the organization of CS-MSN and induced a more homogenous size distribution. Moreover, the zeta potential decreased from +30.7 mV to +14.2 mV after the addition of CS-FNP, indicating also an implication of CS-FNP in the final CS-MSN. Furthermore, the implication of CS-FNP on the down regulation of GFP was checked by transfecting MDA-MB-231/GFP cells with these complexes (Fig. 4C). CS-MSN, including CS-FNP, appeared more efficient to transfect cells and to reduce the GFP expression, indicating the importance of CS-FNP in the formulation.

3.2.2. Retention and protection of siRNA in the presence of serum

The principal roles of the nanovector are the retention and the protection of siRNA in biological medium. Before moving to *in vitro* experiments, the ability of CS-MSN to provide these two needs, was studied in presence of cell culture medium containing different amount of serum (5–50%) and compared to non-formulated (naked) siRNA and CS-MSN or naked siRNA in water (Ctrl) (Fig. 5). Gel retardation assay shows that the fluorescence intensity of naked siRNA incubated with 5% and 10% of serum was reduced at 4 h compared to 0 h and Ctrl. Moreover, after 4 h of incubation in 50% of serum, the fluorescent band disappeared indicating that all siRNA are degraded (Fig. 5A). For CS-MSN, regardless of the serum amount and incubation time, no fluorescent band was observed in absence of heparin. In presence of heparin, fluorescent bands of CS-MSN incubated with serum were observed at a similar intensity to that of CS-MSN in water and to that of naked siRNA in water (Fig. 5B) demonstrating that siRNA were not degraded by enzymes in presence of serum. In the literature, the effect of chitosan and poly-L-arginine to protect siRNA loaded in nanocarriers has already been shown. For example, Sun and coworkers showed a good retention and protection of siRNA complexed with chitosan-PEG conjugate after incubation with 50% of serum for up to 12 h, even if there was a visible degradation between 8 h and 12 h [22]. Our results show a high serum-protection and siRNA retention in CS-MSN even after incubation for 4 h with a high concentration of serum (50%), which is largely superior to the one used in the following *in vitro* experiments (5%). Moreover, the complete release of siRNA by optimized CS-MSN observed immediately after the addition of heparin, reflects a good balance between serum-protection and siRNA release which present a desirable trait for siRNA transfection.

Table 2
Hydrodynamic diameter (HD), polydispersity index (PDI) and zeta potential (ZP) of complexes formed with siRNA, PLR and Cs and that of CS-MSN prepared with CS-FNP, siRNA, PLR and Cs.

	HD (nm)	PDI	ZP (mV)
SiRNA/PLR/Cs polyplex ($N_{PLR}/P = 2$, $N_{CS}/P = 30$)	213 ± 36	0.43 ± 0.05	30.7 ± 1.4
CS-MSN (MR = 10, $N_{PLR}/P = 2$, $N_{CS}/P = 30$)	175 ± 7	0.34 ± 0.04	14.2 ± 0.4

3.2.3. Absence of cytotoxicity in the presence of non-targeted siRNA

The low cytotoxicity of CS-MSN is another parameter to be considered for a future biological application. In fact, we should ensure the safety of CS-MSN and show that the cell death effect is only due to the target siRNA. For that, a WST-1 viability test was carried out on MDA-MB-231 cells treated for different time periods (4–48 h) with CS-MSN prepared with different concentrations (12.5–100 nM) of a non-targeted control siRNA (Fig. 6). Non-treated cells and cells treated with H_2O_2 were used as controls. After 4 h and 24 h of treatment, the cell viability remained higher than 90% for all tested concentrations. A slight decrease of cell viability was observed at high CS-MSN concentration (100 nM) after 48 h of treatment. However, cell viability remained above 80% for this condition indicating a limited cytotoxic effect. This result proves the safety of the use of CS-MSN (up to 100 nM). Moreover, it also confirms that the previously observed decrease of cell fluorescence after siRNA transfection using CS-MSN (Fig. 3C) was not due to cellular mortality but it was a siRNA specific down regulation of GFP expression. The slight cytotoxicity observed at high siRNA concentration can be explained by the high density of positive charge of PLR. Thus, many studies highlighted the toxic effect of strongly cationic polymers (poly-lysine, poly-ethylenimine, poly-arginine, …) and showed that it is dose-dependent and it can be reduced by the association with chitosan or polyethylene glycol [33,34]. Herein, PLR is used at low N/P ratio and is associated to chitosan and PEGylated nanoparticles which provide to CS-MSN a high safety.

3.3. Transfection efficiency of CS-MSN

3.3.1. Determination of treatment and analysis times for an efficient siRNA transfection

To obtain an efficient siRNA transfection, it is important to consider i) a sufficient contact duration of nanovectors with cells, for their internalization (treatment time) and ii) a time period between treatment and analysis, long enough for the inhibition of the target protein (analysis time). To define these optimal conditions, first, MDA-MB-231/GFP cells were treated with CS-MSN prepared with anti-GFP siRNA for different treatment times (30 min – 72 h) and then analyzed after 72 h by flow cytometry. The GFP down regulation efficiency increased up to 4 h of contact between CS-MSN and cells. After 72 h of treatment, the down regulation efficiency is similar to that of 4 h (Fig. 7A), demonstrating the quick internalization of CS-MSN into cells. This result was confirmed by the analysis of the cyanine 5.5 fluorescence of CS-FNP. Indeed, after 4 h of treatment with CS-MSN, all cells express cyanine 5.5 fluorescence, which indicates the internalization of CS-MSN by MDA-

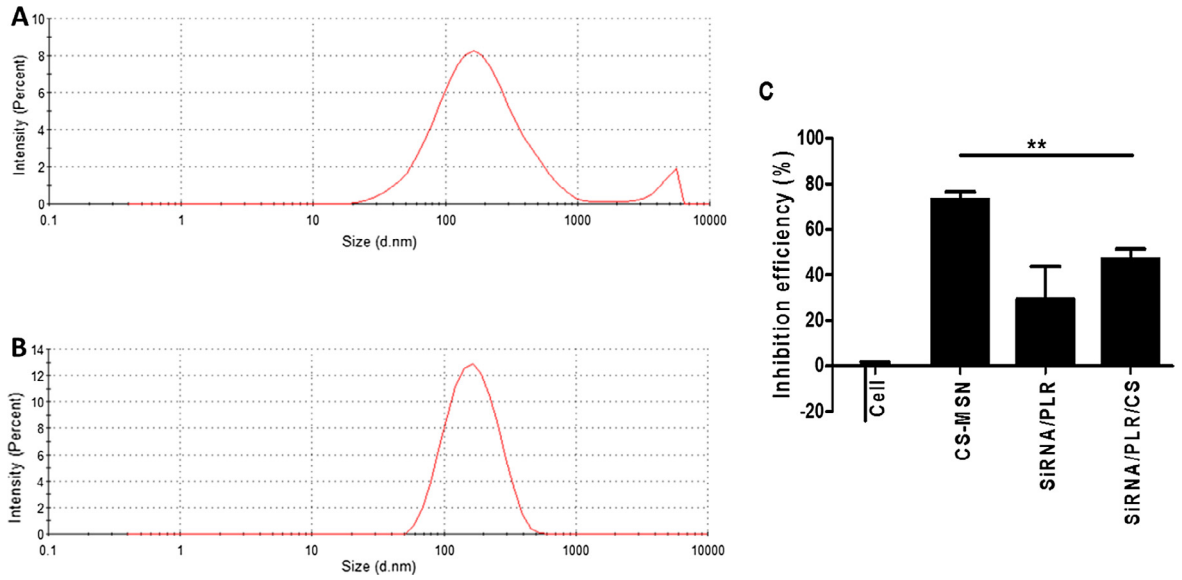

Fig. 4. Implication of CS-FNP in the CS-MSN formulation (A) Size distribution profile of complexes prepared with siRNA, PLR at $N_{PLR}/P = 2$ and Cs at $N_{CS}/P = 30$ measured by DLS. (B) Size distribution profile of CS-MSN prepared with CS-FNP (MR = 10), siRNA, PLR at $N_{PLR}/P = 2$ and Cs at $N_{CS}/P = 30$ measured by DLS. (C) Down regulation efficiency of GFP fluorescence in MDA-MB-231/GFP cells treated with CS-MSN (MR = 10, $N_{PLR}/P = 2$ and $N_{CS}/P = 30$), siRNA/PLR ($N_{PLR}/P = 2$) and siRNA/PLR/Cs complexes ($N_{PLR}/P = 2$, $N_{CS}/P = 30$).

MB-231 cancer cells (Fig. 7B). In a second stage, MDA-MB-231/GFP cells were treated for 4 h with CS-MSN and analyzed after different analysis time (24–72 h) using flow cytometry. The inhibition of the GFP expression in cells was more pronounced after 72 h than after 24 or 48 h (Fig. 7C). This indicates that even if the internalization of CS-MSN was fast, the inhibition of protein expression required more time (72 h). This relatively slow action of CS-MSN could be explained by the time needed to reach cytoplasm (intracellular trafficking and endosomal escape), for RNA interference mechanism and especially for the degradation of already produced GFP in target cells (half-life time of GFP). In fact, the GFP protein is known by its stability in cells which explain its large use as reporter in gene expression. It was reported that the stability of GFP depends highly on many factors like cell line and culturing conditions [35,36]. For the following experiments on MDA-MB-231 cells, the treatment time with CS-MSN and the analysis time by flow cytometry were fixed at 4 h and 72 h, respectively.

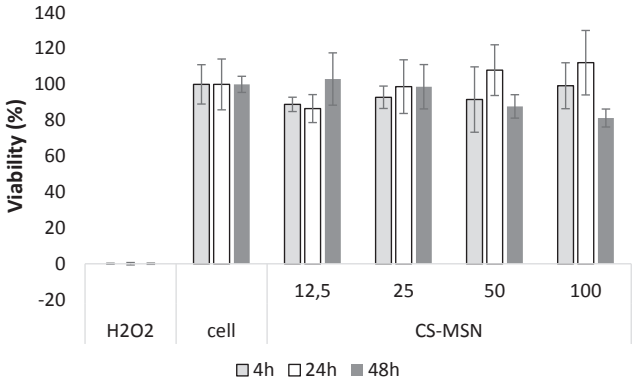

Fig. 6. Cellular viability of breast cancer cells treated for different time periods (4–48 h) with CS-MSN prepared with different concentrations (12.5–100 nM) of a non-targeted control siRNA.

3.3.2. Comparison of the transfection efficiency of CS-MSN with that of oligofectamine™

The last step of the proof-of-concept is to check that the transfection efficiency of CS-MSN is at least comparable to that of a commercial transfection agent, such as Oligofectamine™. Therefore, cells were treated with CS-MSN prepared with anti-GFP siRNA (siGFP) and the fluorescence intensity was measured using flow cytometry. Non-treated cells, Oligofectamine™-siRNA complexes and non-targeted vectorized siRNA (siCtrl) were used as controls (Fig. 8). With the non-targeted siRNA, transfection efficiency was comparable to non-treated cells independently of the nanovector (CS-MSN, Oligofectamine™-siRNA complexes). However, in presence of siGFP, the GFP down regulation efficiency of cells treated with CS-MSN (73 ± 3%) was significantly

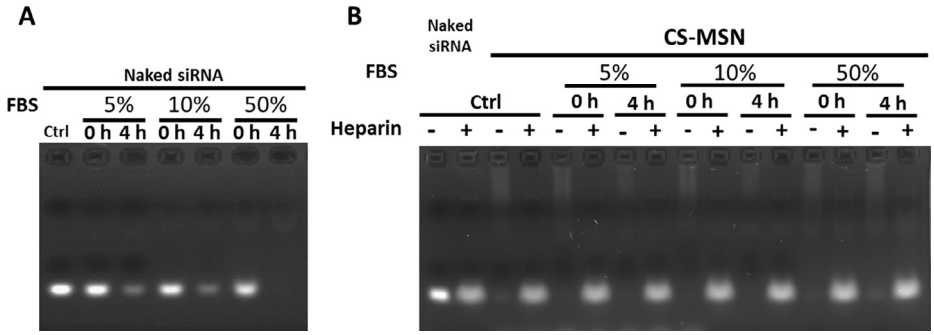

Fig. 5. Gel retardation assay to monitor siRNA degradation after incubation with serum. (A) Naked siRNA in water (Ctrl) or cell culture medium with FBS (5–50%). (B) Naked siRNA or CS-MSN in water (Ctrl) and CS-MSN in cell culture medium with FBS (5–50%), with (+) or without (−) heparin.

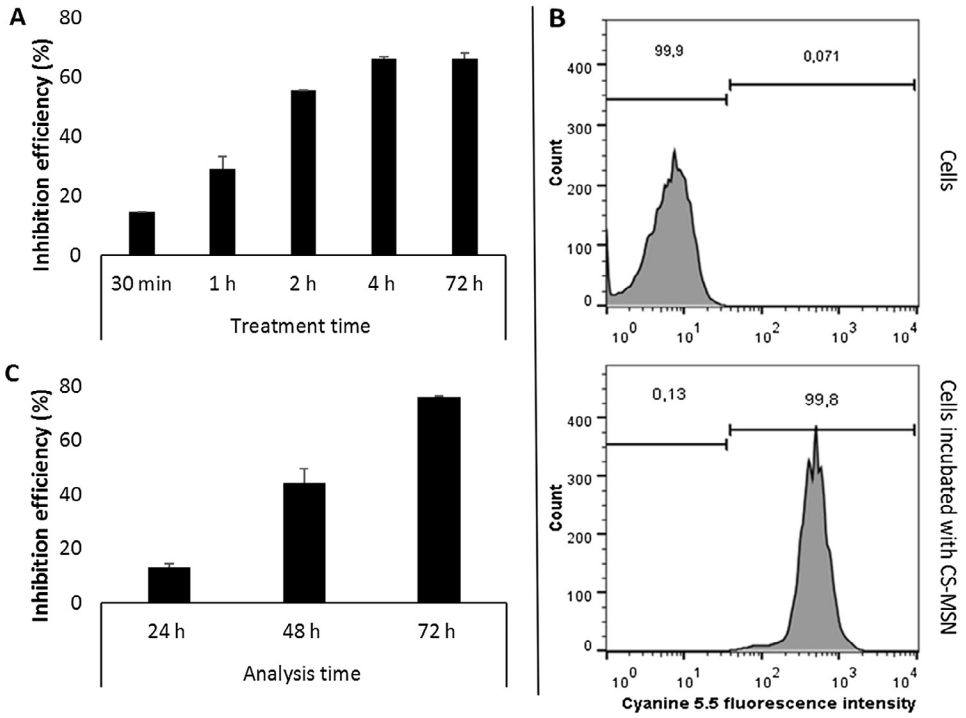

Fig. 7. Determination of treatment and analysis times for an efficient siRNA transfection in MDA-MB-231 cells. (A) Inhibition efficiency of GFP fluorescence with CS-MSN for different treatment times (30 min – 72 h). (B) Cyanine 5.5 fluorescence intensity of cells treated (lower figure) or not (upper figure) with CS-MSN for 4 h. (C) Inhibition efficiency of GFP fluorescence with CS-MSN for different analysis times (24–72 h).

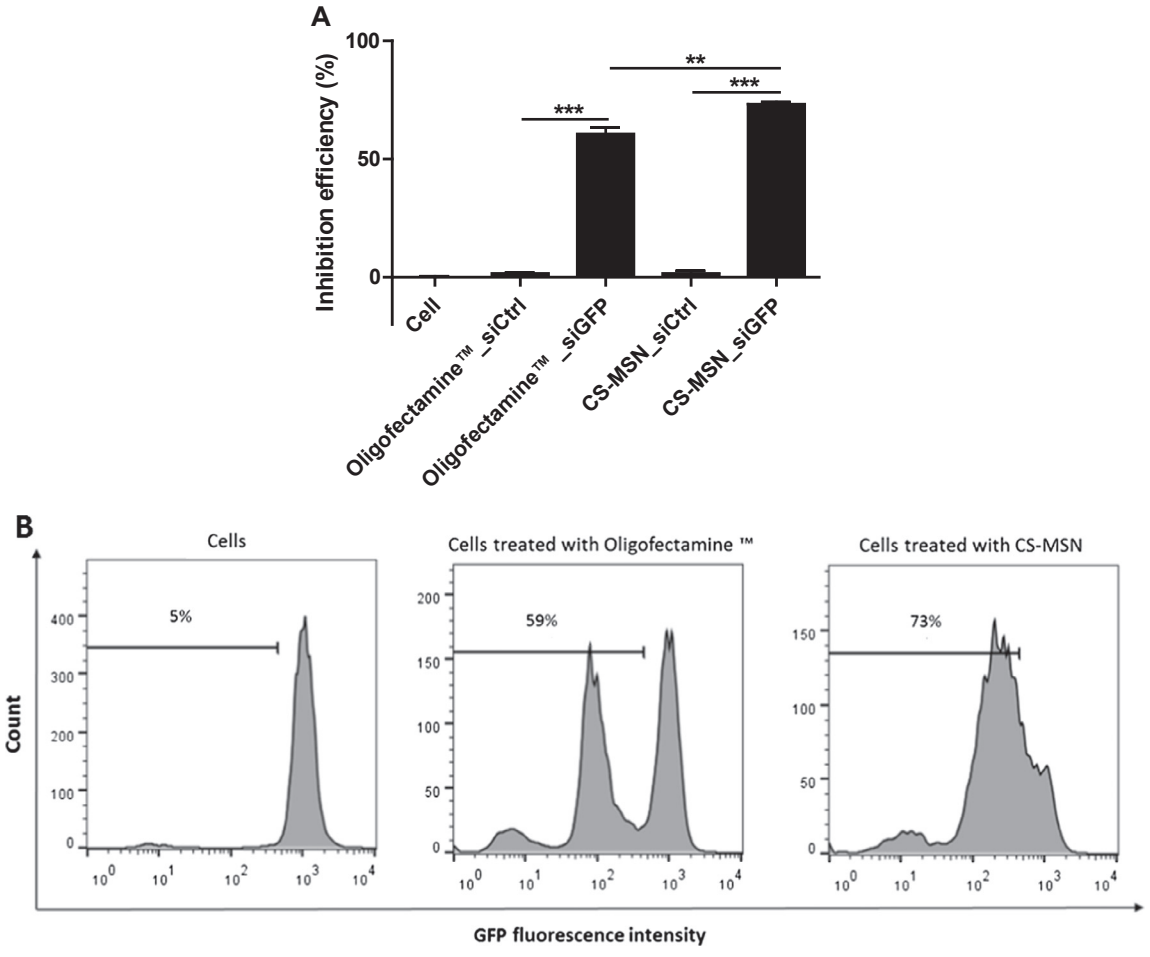

Fig. 8. Inhibition efficiency of GFP fluorescence with CS-MSN and Oligofectamine™-siRNA complexes. (A) Quantification of the down regulation efficiency of GFP fluorescent cells with Oligofectamine™-siRNA complexes and CS-MSN prepared with non-targeted siRNA (siCtrl) or anti-GFP siRNA (siGFP) (B) Fluorescence profiles obtained by Flow cytometer of untreated cells, cells treated with Oligofectamine™-siRNA complexes and cells treated with CS-MSN prepared with siGFP.

more pronounced than that of cells treated with Oligofectamine™ (59 ± 8%) ($p = 0.0026$) (Fig. 8A). That means, that the observed reduction in the GFP fluorescence intensity was due to the specific effect of the used siRNA. Fig. 8B shows differences in the fluorescence profile obtained by flow cytometry for cells treated with Oligofectamine™ and CS-MSN. Indeed, an efficient transfection is correlated either to a shift of the curve of the fluorescence to the left (CS-MSN) or to the appearance of a novel population of cells at lower fluorescence intensity (Oligofectamine™-siRNA complexes). The inhibition efficiencies of the transfected cell population were calculated and showed that Oligofectamine™ reduce the GFP expression by 91% in about 59% of cells without affecting the fluorescence of the other 41% of cells. For CS-MSN, the GFP expression was reduced by 82% in 73% of cells. These results indicate that even if our nanovector was a little bit less efficient in the transfected population than Oligofectamine™, it was able to affect more cells in an analogous manner. This explains the higher down regulation efficiency of GFP in treated cells with our nanovectors compared to Oligofectamine™. In the literature, the most effective siRNA nanovector have an efficiency between 60 and 88% [6,15,37] but, it is difficult to find the corresponding fluorescence profiles. These experiments prove the concept of CS-MSN as an efficient siRNA nanovector.

4. Conclusion

In view of a future application in theranosis of triple negative breast cancer, we successfully developed a novel siRNA delivery nanosystem, CS-MSN, which is based on PEGylated SPION functionalized with the cell-penetrating peptide gH625. The polymers poly-L-arginine and chitosan were added to the formulation to complex siRNA and to efficiently transfect breast cancer cells. CS-MSN exhibit a high ability to complex and protect siRNA against degradation in complete cell culture medium containing up to 50% of serum. In addition, CS-MSN showed a fast internalization (4 h) and a high siRNA transfection efficiency (73 ± 3%) in MDA-MB-231 cancer cells, while remaining non-toxic using a control siRNA at concentrations up to 100 nM. In contrast to Oligofectamine™, CS-MSN transfected almost all MDA-MB-231 cells with siRNA anti-GFP. Although CS-MSN were optimized using a model siRNA, they can be loaded with any siRNA sequence and thus are expected to allow a successful silencing of anti-apoptotic genes and oncogenes. The next step of this work will be the investigation of the role of the cell-penetrating peptide gH625 in the intracellular trafficking of CS-MSN and the *in vivo* application in a triple negative breast cancer mouse model.

Acknowledgments

This work was funded by the “Région Centre-Val de Loire” (MATURE Project) and supported by the “Cancéropôle Grand Ouest”. We thank Isabelle Dimier-Poisson, Nathalie Moire and Zineb Lakhrif (UMR INRA 1282, team of “Infectiologie et Santé Publique”, University of Tours) for their help with flow cytometry experiments.

Conflict of interest

The authors declare that they have no conflict of interest.

Appendix A. Supplementary material

Supplementary data associated with this article can be found, in the online version, at https://doi.org/10.1016/j.ejpb.2018.07.024.

References

[1] R. Venkitaraman, Triple-negative/basal-like breast cancer: clinical, pathologic and molecular features, Expert Rev. Anticancer Ther. 10 (2010) 199–207, https://doi.org/10.1586/era.09.189.
[2] E.A. Rakha, M.E. El-Sayed, A.R. Green, A.H.S. Lee, J.F. Robertson, I.O. Ellis, Prognostic markers in triple-negative breast cancer, Cancer 109 (2007) 25–32, https://doi.org/10.1002/cncr.22381.
[3] M. Kalimutho, K. Parsons, D. Mittal, J.A. López, S. Srihari, K.K. Khanna, Targeted therapies for triple-negative breast cancer: combating a stubborn disease, Trends Pharmacol. Sci. 36 (2015) 822–846, https://doi.org/10.1016/j.tips.2015.08.009.
[4] P. Guruprasath, J. Kim, G.R. Gunassekaran, L. Chi, S. Kim, R.-W. Park, S.-H. Kim, M.-C. Baek, S.M. Bae, S.-Y. Kim, D.-K. Kim, I.-K. Park, W.-J. Kim, B. Lee, Interleukin-4 receptor-targeted delivery of Bcl-xL siRNA sensitizes tumors to chemotherapy and inhibits tumor growth, Biomaterials 142 (2017) 101–111, https://doi.org/10.1016/j.biomaterials.2017.07.024.
[5] H. Jaganathan, S. Mitra, S. Srinivasan, B. Dave, B. Godin, Design and in vitro evaluation of layer by layer siRNA nanovectors targeting breast tumor initiating cells, PLOS One 9 (2014) e91986, https://doi.org/10.1371/journal.pone.0091986.
[6] T.A. Werfel, M.A. Jackson, T.E. Kavanaugh, K.C. Kirkbride, M. Miteva, T.D. Giorgio, C. Duvall, Combinatorial optimization of PEG architecture and hydrophobic content improves ternary siRNA polyplex stability, pharmacokinetics, and potency in vivo, J. Control. Release 255 (2017) 12–26, https://doi.org/10.1016/j.jconrel.2017.03.389.
[7] A. de Fougerolles, H.-P. Vornlocher, J. Maraganore, J. Lieberman, Interfering with disease: a progress report on siRNA-based therapeutics, Nat. Rev. Drug Discov. 6 (2007) 443–453, https://doi.org/10.1038/nrd2310.
[8] G. Meister, T. Tuschl, Mechanisms of gene silencing by double-stranded RNA, Nature (2004), https://doi.org/10.1038/nature02873.
[9] D. Haussecker, Current issues of RNAi therapeutics delivery and development, J. Control. Release 195 (2014) 49–54, https://doi.org/10.1016/j.jconrel.2014.07.056.
[10] M. Videira, A. Arranja, D. Rafael, R. Gaspar, Preclinical development of siRNA therapeutics: towards the match between fundamental science and engineered systems, Nanomed. Nanotechnol. Biol. Med. 10 (2014) 689–702, https://doi.org/10.1016/j.nano.2013.11.018.
[11] M. Ferrari, T. Sun, H. Shen, Nanovector delivery of siRNA for cancer therapy, Cancer Gene Ther. 19 (2012), https://doi.org/10.1038/cgt.2012.22.
[12] P. Resnier, T. Montier, V. Mathieu, J.-P. Benoit, C. Passirani, A review of the current status of siRNA nanomedicines in the treatment of cancer, Biomaterials 34 (2013) 6429–6443, https://doi.org/10.1016/j.biomaterials.2013.04.060.
[13] A. Carvalho, M.B.F. Martins, M.L. Corvo, G. Feio, Enhanced contrast efficiency in MRI by PEGylated magnetoliposomes loaded with PEGylated SPION: effect of SPION coating and micro-environment, Mater. Sci. Eng., C 43 (2014) 521–526, https://doi.org/10.1016/j.msec.2014.07.055.
[14] H. Mok, O. Veiseh, C. Fang, F.M. Kievit, F.Y. Wang, J.O. Park, M. Zhang, pH-sensitive siRNA nanovector for targeted gene silencing and cytotoxic effect in cancer cells, Mol. Pharm. 7 (2010) 1930–1939, https://doi.org/10.1021/mp100221h.
[15] O. Veiseh, F.M. Kievit, C. Fang, N. Mu, S. Jana, M.C. Leung, H. Mok, R.G. Ellenbogen, J.O. Park, M. Zhang, Chlorotoxin bound magnetic nanovector tailored for cancer cell targeting, imaging, and siRNA delivery, Biomaterials 31 (2010) 8032–8042, https://doi.org/10.1016/j.biomaterials.2010.07.016.
[16] O. Veiseh, F.M. Kievit, H. Mok, J. Ayesh, C. Clark, C. Fang, M. Leung, H. Arami, J.O. Park, M. Zhang, Cell transcytosing poly-arginine coated magnetic nanovector for safe and effective siRNA delivery, Biomaterials 32 (2011) 5717–5725, https://doi.org/10.1016/j.biomaterials.2011.04.039.
[17] E. Perillo, K. Hervé-Aubert, E. Allard-Vannier, A. Falanga, S. Galdiero, I. Chourpa, Synthesis and in vitro evaluation of fluorescent and magnetic nanoparticles functionalized with a cell penetrating peptide for cancer theranosis, J. Colloid Interf. Sci. 499 (2017) 209–217, https://doi.org/10.1016/j.jcis.2017.03.106.
[18] A.S. Hoffman, S.H. Pun, B.2 – Pegylation of drugs and nanocarriers, Biomater. Sci. third ed., Academic Press, 2013, p. 1028, , https://doi.org/10.1016/B978-0-08-087780-8.00090-5.
[19] D. Vllasaliu, R. Fowler, S. Stolnik, PEGylated nanomedicines: recent progress and remaining concerns, Expert Opin. Drug Deliv. 11 (2014) 139–154, https://doi.org/10.1517/17425247.2014.866651.
[20] S. Galdiero, A. Falanga, G. Morelli, M. Galdiero, gH625: a milestone in understanding the many roles of membranotropic peptides, Biochim. Biophys. Acta BBA – Biomembr. 2015 (1848) 16–25, https://doi.org/10.1016/j.bbamem.2014.10.006.
[21] M.S. Huh, S.-Y. Lee, S. Park, S. Lee, H. Chung, S. Lee, Y. Choi, Y.-K. Oh, J.H. Park, S.Y. Jeong, K. Choi, K. Kim, I.C. Kwon, Tumor-homing glycol chitosan/polyethylenimine nanoparticles for the systemic delivery of siRNA in tumor-bearing mice, J. Control. Release 144 (2010) 134–143, https://doi.org/10.1016/j.jconrel.2010.02.023.
[22] P. Sun, W. Huang, M. Jin, Q. Wang, B. Fan, L. Kang, Z. Gao, Chitosan-based nanoparticles for survivin targeted siRNA delivery in breast tumor therapy and preventing its metastasis, Int. J. Nanomed. 11 (2016) 4931–4945, https://doi.org/10.2147/IJN.S105427.
[23] M. Dominska, D.M. Dykxhoorn, Breaking down the barriers: siRNA delivery and endosome escape, J. Cell Sci. 123 (2010) 1183–1189, https://doi.org/10.1242/jcs.066399.
[24] J.J. Wang, Z.W. Zeng, R.Z. Xiao, T. Xie, G.L. Zhou, X.R. Zhan, S.L. Wang, Recent advances of chitosan nanoparticles as drug carriers, Int. J. Nanomed. 6 (2011) 765–774, https://doi.org/10.2147/IJN.S17296.
[25] Z.-X. Zhao, S.-Y. Gao, J.-C. Wang, C.-J. Chen, E.-Y. Zhao, W.-J. Hou, Q. Feng, L.-Y. Gao, X.-Y. Liu, L.-R. Zhang, Q. Zhang, Self-assembly nanomicelles based on cationic mPEG-PLA-b-Polyarginine(R15) triblock copolymer for siRNA delivery, Biomaterials 33 (2012) 6793–6807, https://doi.org/10.1016/j.biomaterials.2012.05.067.
[26] S. David, H. Marchais, D. Bedin, I. Chourpa, Modelling the response surface to

predict the hydrodynamic diameters of theranostic magnetic siRNA nanovectors, Int. J. Pharm. 478 (2015) 409–415, https://doi.org/10.1016/j.ijpharm.2014.11.061.
[27] J.C. Fernandes, X. Qiu, F.M. Winnik, M. Benderdour, X. Zhang, K. Dai, Q. Shi, Low molecular weight chitosan conjugated with folate for siRNA delivery in vitro: optimization studies, Int. J. Nanomed. 7 (2012) 5833–5845, https://doi.org/10.2147/IJN.S35567.
[28] N. Hoshyar, S. Gray, H. Han, G. Bao, The effect of nanoparticle size on in vivo pharmacokinetics and cellular interaction, Nanomedicine 11 (2016) 673–692, https://doi.org/10.2217/nnm.16.5.
[29] X. Liu, N. Huang, H. Li, Q. Jin, J. Ji, Surface and size effects on cell interaction of gold nanoparticles with both phagocytic and nonphagocytic cells, Langmuir 29 (2013) 9138–9148, https://doi.org/10.1021/la401556k.
[30] T.F. Martens, K. Remaut, J. Demeester, S.C. De Smedt, K. Braeckmans, Intracellular delivery of nanomaterials: how to catch endosomal escape in the act, Nano Today 9 (2014) 344–364, https://doi.org/10.1016/j.nantod.2014.04.011.
[31] S. Al-Qadi, A. Grenha, C. Remuñán-López, Chitosan and its derivatives as nanocarriers for siRNA delivery, J. Drug Deliv. Sci. Technol. 22 (2012) 29–42.
[32] X. Liu, K.A. Howard, M. Dong, M.Ø. Andersen, U.L. Rahbek, M.G. Johnsen, O.C. Hansen, F. Besenbacher, J. Kjems, The influence of polymeric properties on chitosan/siRNA nanoparticle formulation and gene silencing, Biomaterials 28 (2007) 1280–1288, https://doi.org/10.1016/j.biomaterials.2006.11.004.
[33] H. Lv, S. Zhang, B. Wang, S. Cui, J. Yan, Toxicity of cationic lipids and cationic polymers in gene delivery, J. Control. Release Off. J. Control. Release Soc. 114 (2006) 100–109, https://doi.org/10.1016/j.jconrel.2006.04.014.
[34] M.S. Shim, Y.J. Kwon, Efficient and targeted delivery of siRNA in vivo, FEBS J. 277 (2010) 4814–4827, https://doi.org/10.1111/j.1742-4658.2010.07904.x.
[35] P. Corish, C. Tyler-Smith, Attenuation of green fluorescent protein half-life in mammalian cells, Protein Eng. 12 (1999) 1035–1040.
[36] X. Li, X. Zhao, Y. Fang, X. Jiang, T. Duong, C. Fan, C.-C. Huang, S.R. Kain, Generation of destabilized green fluorescent protein as a transcription reporter, J. Biol. Chem. 273 (1998) 34970–34975, https://doi.org/10.1074/jbc.273.52.34970.
[37] Y. Ding, Y. Wang, J. Zhou, X. Gu, W. Wang, C. Liu, X. Bao, C. Wang, Y. Li, Q. Zhang, Direct cytosolic siRNA delivery by reconstituted high density lipoprotein for target-specific therapy of tumor angiogenesis, Biomaterials 35 (2014) 7214–7227, https://doi.org/10.1016/j.biomaterials.2014.05.009.

Supplementary material:

Formulation and in vitro evaluation of a siRNA delivery nanosystem decorated with gH625 peptide for triple negative breast cancer theranosis

Sanaa Ben Djemaa[a], Stephanie David[a]*, Katel Hervé-Aubert[a], Annarita Falanga[b], Stefania Galdiero[b], Emilie Allard-Vannier[a], Igor Chourpa[a] and Emilie Munnier[a]

[a] EA6295 Nanomédicaments et Nanosondes, Université de Tours – 31 avenue Monge, 37200 Tours, France
[b]Department of Pharmacy, CIRPEB - University of Naples "Federico II", Via Mezzocannone 16, 80134, Napoli, Italy

*: corresponding author: Stephanie David, EA6295 Nanomédicaments et Nanosondes, Université de Tours – 31 avenue Monge, 37200 Tours, France ; e-mail address: stephanie.david@univ-tours.fr

Implication of CS-FNP in CS-MSN composed of CS-FNP, siRNA and PLR (N_{PLR}/P = 2)

Gel electrophoresis of siRNA/PLR complexes (without CS-FNP) was performed, and it showed a total complexation of siRNA indicating that PLR is the major component which complex siRNA (Fig. S1. A). To check if CS-FNP are included in CS-MSN composed of CS-FNP, siRNA and PLR (N_{PLR}/P = 2), the size of formulations prepared with and without CS-FNP was measured. Without CS-FNP the complexes showed a big size, higher than 300 nm, with a high standard deviation (63 nm). The addition of CS-FNP to the formulation reduced the size of the final complexes and their standard deviation to 143 ± 12 nm (Table S1). Additionally, the polydispersity index, representing the size distribution within the sample, diminishes (Table S1) and the shape of the peak changed from a large peak with several maxima (Fig. S1. B and C) to a single well-defined peak with one maximum at 143 nm when CS-FNP are included (Fig. S1. B). Moreover, the zeta potential decreased from +28 mV to -4.6 mV after the addition of CS-FNP, indicating a neutralization with or hiding of the positive charges in CS-FNP (Table S1). It seems that the presence of CS-FNP improved the organization of siRNA and PLR and induced a more homogenous size distribution.

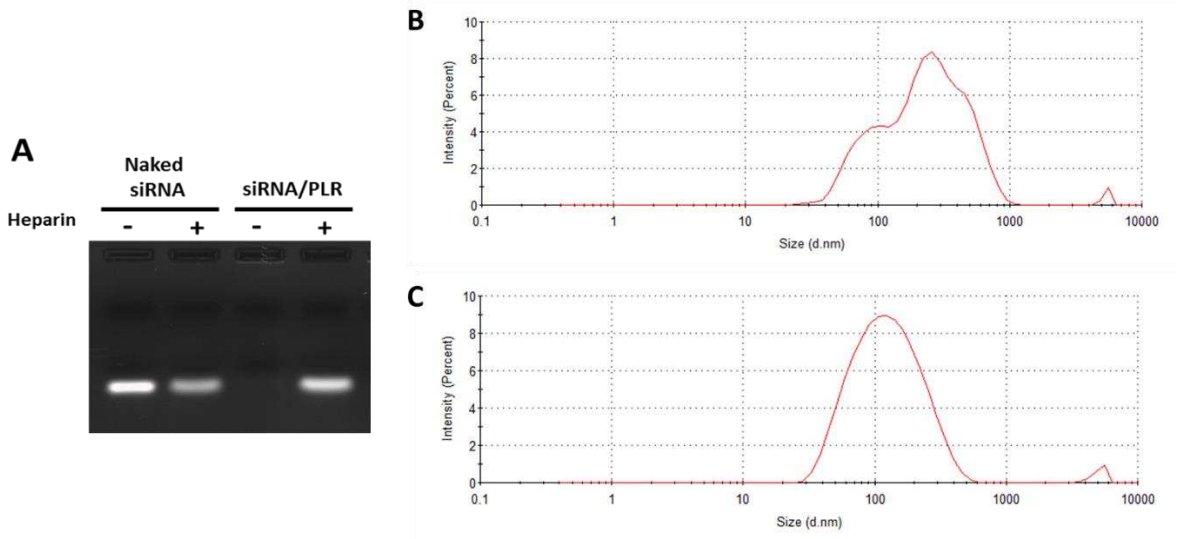

Fig. S1. A) Gel retardation assay to detect free siRNA in siRNA/PLR complexes prepared at N_{PLR}/P = 2. B) Size distribution of complexes prepared with CS-FNP, siRNA and PLR (N_{PLR}/P = 2), measured by DLS.

Table S1. Hydrodynamic diameter (HD), polydispersity index (PDI) and zeta potential (ZP) of complexes prepared with siRNA and PLR (N_{PLR}/P = 2) and that of CS-MSN prepared with CS-FNP, siRNA and PLR (N_{PLR}/P = 2).

		HD (nm)	PDI	ZP (mV)
SiRNA/PLR complex (N_{PLR}/P = 2)		322 ± 63	0.48 ± 0.05	28.2 ± 1.5
CS-MSN	N_{PLR}/P = 2	143 ± 12	0.33 ± 0.04	-4.6 ± 0.3

Troisième partie : Internalisation, trafic intracellulaire et devenir de nanovecteur de siRNA

Publication 3: gH625 cell-penetrating peptide promote the endosomal escape of nanovectorized siRNA in triple negative breast cancer cells

Publiée dans « Biomacromolecules », 2019

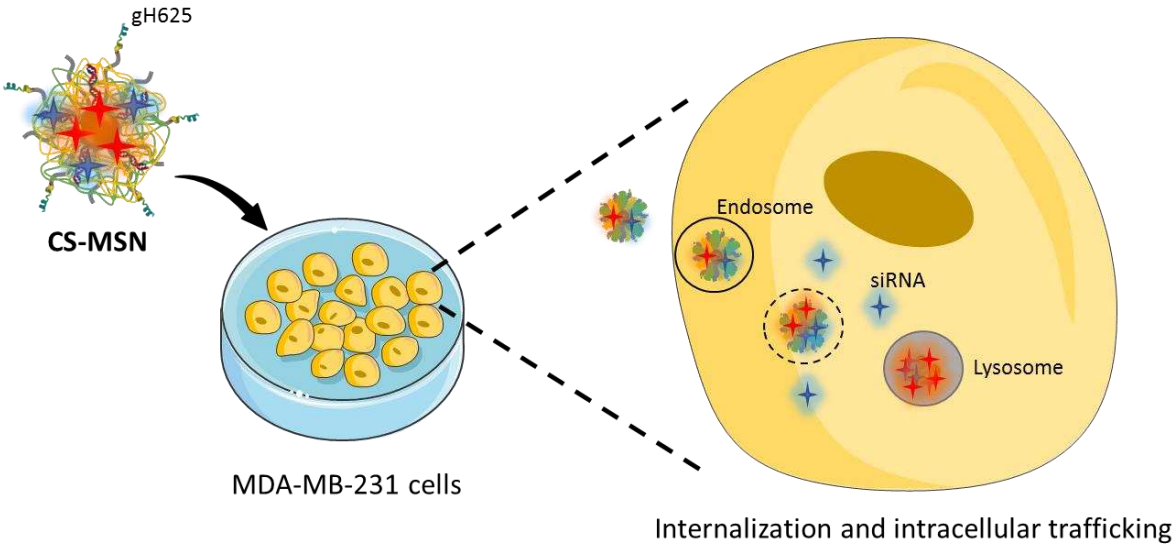

Préambule de la publication 3

Dans plusieurs types de cancers, tels que le cancer du sein triple négatif, le ciblage actif est difficilement envisageable et donc le choix s'oriente vers l'utilisation de l'effet EPR pour l'accumulation des nanovecteurs au niveau de la tumeur et des ligands biologiques pour augmenter l'entrée dans les cellules. Certaines études, telles que celle-ci, ont adopté cette stratégie en utilisant des séquences peptidiques capables de favoriser l'internalisation par les cellules, appelées peptides membranotropes. Ces peptides sont connus pour leur capacité à franchir la membrane cellulaire par un mécanisme indépendant de l'énergie et à gagner le compartiment cytoplasmique via la transcytose. Cependant, une fois conjugués à d'autres molécules ou structures telles que les nanovecteurs de siRNA, leur mécanisme d'internalisation est moins connu.

Cette étude se focalise sur l'investigation des mécanismes d'entrée, du trafic et du devenir des CS-MSN fonctionnalisés avec le peptide membranotrope gH625 dans une lignée cellulaire de cancer du sein triple négatif, la lignée MDA-MB-231. Ce travail souligne, aussi, le rôle du peptide gH625 à chacune de ces étapes en comparant les résultats obtenus à ceux d'un nanovecteur contrôle, sans peptide (S-MSN).

En raison de la complexité des études d'internalisation et de trafic intracellulaire des nanovecteurs, nous avons opté pour une stratégie basée sur l'utilisation de techniques complémentaires permettant de fournir des informations à différents niveaux pour pouvoir construire une image regroupant un maximum des données sur les évènements et les processus membranaires et intracellulaires qui se produisent au cours et après l'entrée du nanovecteurs dans la cellule. Afin de réaliser cette étude, plusieurs méthodes et techniques ont été mises en place en se basant sur l'utilisation des propriétés d'imagerie de notre nanovecteur. Nous avons utilisé 1) des inhibiteurs chimiques et la microscopie électronique en transmission (MET) pour révéler les voies d'internalisations, 2) la microscopie confocale et l'imagerie en flux en présence de marqueurs endosomaux et lysosomaux pour investiguer le trafic endo-lysosomal, et 3) l'imagerie à illumination structurée, l'imagerie en flux et un inhibiteur d'acidification des endosomes pour étudier l'échappement endosomal.

Les résultats obtenus montrent que l'entrée des nanovecteurs est augmentée 2,5 fois en présence de peptide gH625 et qu'elle se produit par endocytose médié par des clathrines et des cavéoles. Nous avons observé que le peptide gH625 favorise l'échappement endosomal, qui

implique, principalement, un mécanisme dépendant de l'acidification des endosomes. Cette internalisation et cet échappement endosomal facilités par le peptide gH625 résultent en une augmentation de l'efficacité délivrance de siRNA qui se traduit par une de transfection 1,7 fois plus importante que le nanovecteur non fonctionnalisé avec le peptide gH625.

Biomacromolecules

Article

Cite This: Biomacromolecules 2019, 20, 3076−3086

pubs.acs.org/Biomac

gH625 Cell-Penetrating Peptide Promotes the Endosomal Escape of Nanovectorized siRNA in a Triple-Negative Breast Cancer Cell Line

Sanaa Ben Djemaa,[†] Katel Hervé-Aubert,[†] Laurie Lajoie,[‡,§] Annarita Falanga,[∥] Stefania Galdiero,[⊥] Steven Nedellec,[#] Martin Soucé,[†] Emilie Munnier,[†] Igor Chourpa,[†] Stéphanie David,[†] and Emilie Allard-Vannier*[,†]

[†]EA6295 Nanomédicaments et Nanosondes, University of Tours, 37200 Tours, France

[‡]EA7501 Groupe Innovation et Ciblage Cellulaire, Equipe Fc Récepteurs, Anticorps et MicroEnvironnement, University of Tours, 37032 Tours, France

[§]Plateforme Scientifique et Technique, Analyse des systèmes biologiques département des cytométries, University of Tours, 37032 Tours, France

[∥]Department of Agricultural Sciences, University of Naples "Federico II", Via Università 100, 80055 Portici, Italy

[⊥]Department of Pharmacy, CIRPEB—University of Naples "Federico II", Via Mezzocannone 16, 80134 Napoli, Italy

[#]Plateforme microPICell, SFR santé François Bonamy-IRSUN, 8 quai Moncousu, BP 70721, 44007 Nantes Cedex, France

Supporting Information

ABSTRACT: The use of small interfering RNA (siRNA) to regulate oncogenes appears as a promising strategy in the context of cancer therapy, especially if they are vectorized by a smart delivery system. In this study, we investigated the cellular trafficking of a siRNA nanovector (called CS-MSN) functionalized with the cell-penetrating peptide gH625 in a triple-negative breast cancer model. With complementary techniques, we showed that siRNA nanovectors were internalized by both clathrin- and caveolae-mediated endocytosis. The presence of gH625 at the surface of the siRNA nanovector did not modify the entry pathway of CS-MSN, but it increased the amount of siRNA found inside the cells. Results suggested an escape of siRNA from endosomes, which is enhanced by the presence of the peptide gH625, whereas nanoparticles continued their trafficking into lysosomes. The efficiency of CS-MSN to inhibit the GFP in MDA-MB-231 cells was 1.7-fold higher than that of the nanovectors without gH625.

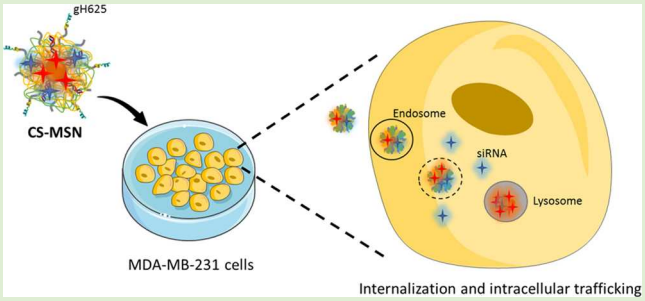

1. INTRODUCTION

The use of small interfering RNA (siRNA) for the treatment or the improvement of the treatment of serious diseases, such as cancer, has attracted great attention since the discovery of the RNA interference (RNAi) mechanism. This strategy is considered as a powerful alternative for noneffective therapies.[1] However, the use of these siRNA has some limitations related to their properties including the sensitivity to enzymatic degradation, difficulties to cross cell membranes, and accessibility to the cytoplasm.[2,3] Therefore, to overcome these difficulties, the development of an effective siRNA delivery tool is essential. One promising approach is the nanovectorization of siRNA, which consists of the complexation of siRNA with other components, leading to the formulation of nanosized complexes. Nanovectorization of siRNA is associated with some benefits such as (i) the protection of loaded siRNA from degradation in the biological environments, (ii) the gain of access and the accumulation in cells, and (iii) the increase of siRNA activity resulting from the siRNA half-life extension.[3]

To improve the siRNA nanovector efficacy, many research groups are interested to enhance cell internalization through the addition of surface ligands. The use of cell-penetrating peptides (CPP), also called membranotropic peptides, in siRNA nanovector development has recently received considerable attention, and it has shown promising results.[4−6] Indeed, CPP are a group of short positively charged peptides, able to cross the cell membrane bilayer both in an energy-dependent or -independent manner.[7] This property is well suitable for siRNA delivery systems to facilitate the passage of biological barriers. The CPP gH625 is a membrane-interacting domain of Herpes simplex virus type 1,[8] which has been shown to have a great ability to cross the cell membrane and

Received: May 8, 2019
Revised: July 10, 2019
Published: July 15, 2019

Downloaded via UNIV FRANCOIS-RABELAIS DE TOURS on August 19, 2019 at 11:22:03 (UTC).
See https://pubs.acs.org/sharingguidelines for options on how to legitimately share published articles.

© 2019 American Chemical Society

DOI: 10.1021/acs.biomac.9b00637
Biomacromolecules 2019, 20, 3076−3086

biological barriers and to successfully deliver different cargoes.[9−12] Associated with siRNA nanovectors, this peptide could be an addition or an alternative to targeting ligands, to enhance the efficiency in the treatment of some diseases when targeted cells do not overexpress any specific receptor or marker at their surface. A well-known model for such diseases is triple-negative breast cancer (TNBC). This cancer is defined by a lack of expression of the estrogen receptor, progesterone receptor, and human epidermal growth factor receptor 2 (HER2) by cancer cells,[13] which prevents the active targeting and favors the passive targeting by the enhanced permeability and retention (EPR) effect. The synergy between the EPR effect and the use of the CPP could offer an effective treatment for TNBC.

During the last decade, the siRNA nanovectors have made considerable progress in terms of developing formulation strategies and *in vitro* and *in vivo* assays. Numerous promising siRNA nanovectors have appeared with high downregulation efficiency of targeted genes.[14−16] Nevertheless, the internalization mechanisms and the intracellular trafficking of these siRNA nanovectors are poorly studied. Answering questions about the entry route of the nanovector, the release of siRNA inside the cells, the mechanisms of siRNA endosomal escape, and the monitoring of the components of the nanovector could provide more information about the improvement of the nanovector formulation and may explain the obtained efficiency of gene silencing.

We recently developed a siRNA nanovector based on fluorescent PEGylated superparamagnetic iron oxide nanoparticles (SPION) functionalized with the CPP gH625.[17] This nanoplatform was loaded, by electrostatic assembly, with siRNA and cationic polymers (chitosan and poly-L-arginine) to obtain CPP-capped stealth magnetic siRNA nanovectors called CS-MSN.[18] In the present study, we investigate the internalization and the intracellular trafficking of CS-MSN in the MDA-MB-231 TNBC cell line using their imaging properties thanks to their fluorescent labeling or their iron oxide core. In parallel, we highlighted the role of the peptide gH625 by comparing the trafficking and the monitoring of siRNA nanovectors with and without this CPP.

2. MATERIALS AND METHODS

2.1. Synthesis of gH625. The peptide gH625 with a cysteine at the C-terminal was synthesized by the standard Fmoc solid-phase method on a Rink amide resin. The amino acids were attached to the resin support; the first coupling was conducted in the presence of 4 equiv Fmoc-protected amino acid, 4 equiv DIC, and 4 equiv OxymaPure, whereas the second coupling was conducted in the presence of 4 equiv amino acid, 4 equiv HATU, and 8 equiv DIPEA. The crude peptide was cleaved with an acid solution of trifluoroacetic acid (TFA), precipitated with ice-cold diethyl ether, and purified by HPLC. The linear gradient used was 20−80% of acetonitrile in water (both containing 0.1%TFA) on a Phenomenex Jupiter 4 μm Proteo 90 Å 250 × 21.20 mm^2 column with UV detection at 210 nm. The pure peptide was analyzed by LC-MS.

2.2. Nanoparticle Preparation. The preparation of labeled and PEGylated superparamagnetic iron oxide nanoparticles (SPION) functionalized with the gH625 peptide is based on a previously published protocol,[17] with some modifications. Amino-silanized SPION were successively functionalized with sulfocyanine 5-NHS ester, NHS-PEG-maleimide, and the cell-penetrating peptide gH625. We substituted the hydrophobic cyanine 5,5-NHS by the hydrophilic sulfocyanine 5-NHS to facilitate purification. The resulting functionalized nanoparticles, further called CS-FNP (as CPP-capped stealth fluorescent nanoparticles), were purified by size-exclusion chromatography (SEC, detailed in Section 2.3.4). CS-FNP suspension was then concentrated by a Vivaspin concentrator with a cutoff of 30 kDa. A control batch of nanoparticles without gH625 peptide, further called S-FNP (as stealth fluorescent nanoparticles), was synthesized by replacing the CPP solution by PBS buffer.

2.3. Physicochemical Characterization of Nanoparticles and siRNA Nanovectors. *2.3.1. Size and ζ-Potential Analysis.* The hydrodynamic diameter (HD) and ζ-potential (ZP) of (C)S-FNP were measured in PBS 1× and $NaNO_3$ solution (0.01 M), respectively, at an iron concentration of 50 mg/L. For "CPP-capped" stealth magnetic siRNA nanovector [(C)S-MSN], the HD, the polydispersity index (PDI), and the ZP were obtained after dilution in $NaNO_3$ (0.01 M) to obtain a constant ionic strength. These measurements were performed using a Nanosizer apparatus (Zetasizer, Malvern Instrument) at 25 °C. The mean values of HD given were based on intensity. Measurements are presented as mean values ± SD.

2.3.2. Atomic Absorption Spectroscopy. Atomic absorption spectroscopy (AAS) was used to determine iron concentration on nanoparticle suspension. For that, (C)S-FNPs were digested by adding concentrated hydrochloric acid (6 M) for at least 2 h and then diluted with hydrochloric acid (0.12 M). Measurements were performed at 248 nm, and the concentrations of the samples were determined using a calibration curve (iron concentrations of 0.25, 0.5, 1, 2, and 5 mg/L).

2.3.3. High-Performance Liquid Chromatography (HPLC). Th Ultimate 3000 HPLC apparatus (Dionex, Voisins le Bretonneux, France) using a mixture of acetonitrile (HPLC gradient grade, Fisher Chemical, Loughborough, U.K.) with 0.1% TFA (Sigma-Aldrich Chemie GmbH, Steinheim, Germany) and an aqueous solution of TFA at 0.1% as a mobile phase at a flow rate of 1 mL/min. The gradient elution program was set up from 20 to 80% of acetonitrile in 20 min. The injected volume of peptide solutions or nanoparticle suspensions was fixed at 5 μL. A Kromasil C18 reversed-phase column (150 × 4.6 mm^2) was used for the analysis, and the temperature of the column was fixed at 25 °C. The peptide was detected with a fluorescence detector (RF-10AXL Shimadzu) after excitation of the tryptophan residue (excitation at 280 nm, emission at 350 nm). Results were acquired and analyzed using the software Chromeleon 7. The calibration curve was obtained from peak areas of gH625 peptide solutions in Milli-Q water at concentrations of 0.05, 0.1, 0.2, 0.3, and 0.5 g/L, using the chromatographic conditions described above.

2.3.4. Size-Exclusion Chromatography (SEC). The purification of nanoparticles by eliminating the free gH625 peptide was performed by size-exclusion chromatography using an ÄKTApurifier FPLC system equipped with a prepacked Superdex 200 pg column (600 × 16 mm^2) (GE Healthcare Bio-Science AB, Uppsala, Sweden) and a PBS 1× solution as the mobile phase (flow rate of 1 mL/min). The injected volume was 5 mL at an iron concentration of 0.4 g/L. The different components of the suspension were detected using a UV/vis detector at 280 nm. Purified fractions containing either nanoparticles or the free peptide were collected.

2.3.5. Fluorescence Spectroscopy. The presence of gH625 in CS-FNP suspension was checked at an iron concentration of 10 mg/L in DMSO/PBS (3:1, v/v) using an FS5 spectrofluorometer (Edinburgh Instruments, Livingston, U.K.). Fluorescence emission spectra were recorded in the range of 300−450 nm with excitation of the tryptophan residue of the peptide at 280 nm.

2.4. Formulation of siRNA Nanovectors. Cell-penetrating-peptide (CPP)-capped stealth magnetic siRNA nanovectors (CS-MSN) and stealth magnetic siRNA nanovectors (S-MSN) were prepared as described in our previous publication.[18] Briefly, CS-MSN and S-MSN were formulated by the electrostatic assembly of siRNA and cationic polymers with CS-FNP and with S-FNP, respectively. Cationic polymers were chitosan (Cs, MW 110−150 kDa; degree of acetylation: ≤40 mol %) and poly-L-arginine (PLR, MW 15−70 kDa) (Sigma-Aldrich Chimie GmbH, St. Quentin Fallavier, France). The content of (C)S-FNP was related to that of iron and was defined by the iron/siRNA w/w ratio (mass ratio, MR), and that of cationic polymers was defined by the molar ratio of the positive charges of

DOI: 10.1021/acs.biomac.9b00637
Biomacromolecules 2019, 20, 3076−3086

amine groups (NH_3^+, hereafter named N) of each polymer and the negative charges of siRNA's phosphate groups (PO_4^{3-}, hereafter named P) (N/P ratio). siRNA were first precomplexed with PLR at an N_{PLR}/P ratio of 2 and then added to the mix of CS-FNP_chitosan or S-FNP_chitosan prepared at an MR of 10 and an N_{CS}/P ratio of 30 to obtain CS-MSN or S-MSN, respectively.

2.5. Gel Retardation Assay and Heparin Decomplexation Assay. Agarose gel electrophoresis was used to verify the loading of siRNA in nanovectors. S-MSN and CS-MSN were prepared to deposit a siRNA concentration of 1.2 μM per well. Heparin solution (Sigma-Aldrich Chemie GmbH, Steinheim, Germany) was added at a final concentration of 3 mg/mL to release siRNA and control their integrity after formulation. Before the deposition of samples, a loading buffer (Agarose gel loading dye 6×, Fisher, Bioreagents, Illkirch, France) was added. An agarose gel (1% w/v) was prepared containing 0.01% (v/v) ethidium bromide to visualize free siRNA. The migration was conducted in a Tris−acetate−EDTA 1× buffer (Acros Organics, Geel, Belgium) for 15 min at 150 V. UV imaging was used to visualize free siRNA using the EvolutionCapt software on a Fusion-Solo.65.WL imager (Vilbert Lourmat, Marne-la-Vallée, France).

2.6. Cell Culture. Triple-negative breast cancer cells MDA-MB-231 (ECACC, Salisbury, U.K.) and MDA-MB-231 stably expressing GFP (MDA-MB-231/GFP) (Euromedex, Souffelweyersheim, France) were maintained in Dulbecco's modified Eagle's medium (Gibco, Life Technologies, Paisley, U.K.) supplemented with 10% fetal bovine serum (Eurobio, Les Ulis, France), nonessential amino acid 1× (HyClone Laboratories, Logan, Utah), and 1% penicillin/streptomycin (Gibco, Life Technologies, Paisley, U.K.) at 37 °C in a humid atmosphere containing 5% CO_2. The culture medium was changed every 48−72 h, and the cells were removed using trypsin/EDTA (0.05%) (Gibco, Life Technologies, Paisley, U.K.) at 80% confluency.

2.7. Nanovector Uptake. *2.7.1. Imaging Flow Cytometry (Amnis ImageStream^X Mark II).* MDA-MB-231 cells were seeded at 2×10^6 cells per well in a 6-well plate for 24 h. After cellular adhesion, cells were incubated with CS-MSN or S-MSN prepared with a nontargeted siRNA-Atto390 conjugate (Sigma-Aldrich, St. Quentin Fallavier, France) (50 nM siRNA) in an equal part of complete medium and Opti-MEM medium (Gibco, Life Technologies, Paisley, U.K.) (1:1 v/v), further named transfection medium, and maintained in normal cell culture conditions for 15 min, 30 min, 1 h, 2 h, 4 h, or 24 h. Next, cells were detached using trypsin−EDTA 0.05%, washed using HBSS 1× solution (HyClone Laboratories, Logan, Utah), and fixed using 4% paraformaldehyde solution (Electron Microscopy Sciences, Hatfield, U.K.) for 15 min at room temperature. In each experiment, 10 000 events for each sample were acquired using a 12-channel Amnis ImageStream^X Mark II (Amnis Corp., part of EMD Millipore, Seattle, WA) imaging flow cytometer equipped with the 405, 488, and 642 nm lasers. MDA-MB-231 images were captured with the Inspire imaging flow cytometry software at 60× magnification and extended depth-of-field (EDF) function. Single-stained samples of 500 cells were also illuminated by the 405 and 642 nm lasers with the brightfield (BF) and darkfield inactivated to perform color compensation controls. The spectral compensation matrix was applied to each of the files. Cells in the best focus were identified using Gradient RMS of the BF image. Single cells were then separated from debris and doublets using a plot of the aspect ratio vs the area of the BF image. The intracellular fluorescence intensity of siRNA-Atto390 (channel 7) and that of sulfocyanine 5 (channel 11) conjugated to CS-FNP or S-FNP were analyzed among double-positive cells using "erode mask" (Erode (M04, 3)) with IDEAS v6.2 software (Amnis-Merck).

2.7.2. Confocal Microscopy. MDA-MB-231 cells were seeded at 15 $\times 10^3$ cells per well in a poly-D-lysine-coated Ibidi 8-well plate and were allowed to adhere for 48 h. The cell culture medium was replaced by the transfection medium, and then CS-MSN or S-MSN prepared with the siRNA-Atto390 conjugate (50 nM siRNA) was added for 4 h. After that, cells were washed, incubated or not for additional 20 h, and then stained with Wheat germ agglutinin-Alexa Fluor 488 (WGA-AF488) (Invitrogen by Thermo Fisher Scientific, Life Technologies Corporation, Eugene). For the staining of the cell membrane with WGA-AF488 conjugate, the transfection medium was replaced with WGA-AF488 solution (1.25 μg/mL) for 10 min. Next, cells were washed with DPBS 1× (HyClone Laboratories, Logan, Utah) and fixed with 4% paraformaldehyde solution for 15 min. Finally, cells were washed and mounted with Fluoromount-G (Invitrogen by Thermo Fisher Scientific, San Diego, CA). Cells were visualized and imaged with a confocal microscope Nikon A1R using ×60/1.4 objective and NIS elements software. Images were acquired with a resolution of 0.21 μm/px and were constructed using ImageJ software.

2.8. CS-MSN Internalization Pathway Determination. *2.8.1. Chemical Inhibitors of Internalization Pathways.* MDA-MB-231 cells were seeded at 85×10^3 cells per well in a 12-well plate for 24 h. After cellular adhesion, cells were incubated with chemical inhibitors of known endocytic pathways for 1 h in serum free medium, then CS-MSN or S-MSN (50 nM siRNA) were added for 4 h. Dynasore (100 μM, EMD, Millipore Corp) was used to inhibit dynamin, which is implicated in the formation of vesicles of many endocytosis processes. The combination between sodium azide (Sigma-Aldrich, Steinheim, Germany) and 2-deoxy-D-glucose (Alfa Aesar, Thermo Fisher GmbH, Erlenbachweg, Germany) (50 mM for both) was used to inhibit the energy-dependent internalization. Chlorpromazine (10 μg/mL, Sigma Life Science, Sigma-Aldrich, St Louis) and pitstop 2 (30 μM, Sigma Life Science, Sigma-Aldrich, St Louis), were used to disrupt clathrin-mediated endocytosis. Methyl-β-cyclodextrin (MβCD) (2.5 mM, Sigma Life Science, Sigma-Aldrich, St Louis) and nystatin (50 μg/mL, Sigma Life Science, Sigma-Aldrich, St Louis) were used to block caveolae-mediated endocytosis. Dimethyl amiloride (DMA) (200 mM, Sigma Life Science, Sigma-Aldrich, St Louis) was used to inhibit the internalization of nanovectors mediated by macropinocytosis. After incubation, cells were detached and fixed with 4% paraformaldehyde solution for 15 min. Finally, intracellular sulfocyanine 5 fluorescence was measured using a flow cytometer (Gallios flow cytometer, Beckman Coulter) equipped with a 642 nm laser and acquired by Gallios software. Data were analyzed by FlowJo v10 software.

2.8.2. Transmission Electron Microscopy Imaging. MDA-MB-231 cells were cultured in cell culture tubes at a concentration of 2×10^6 cells per tube. Thereafter, cells were incubated with S-MSN or CS-MSN (750 nM siRNA, equivalent of 100 mg/L of iron) for 4 h in a humidified atmosphere with 5% CO_2 at 37 °C and under constant agitation using a Stuart SB2 tube rotator (Bibby Scientific Ltd, U.K.). Nontreated cells were used as a negative control. After incubation, cells were washed three times with DBPS 1×, then fixed with Trump's solution consisting of 0.1 M phosphate buffer and 4% paraformaldehyde (Sigma, Steinheim, Germany) and 1% glutaraldehyde (EMS, Hatfield, PA). Cells were postfixed with 2% osmium tetroxide (EMS, Hatfield, PA), dehydrated with a series of increasing ethanol solutions, and embedded in Epon resin (Sigma, Steinheim, Germany). Ultrathin sections (90 nm) were stained with 2% aqueous uranyl acetate and 1% lead citrate (Merck, Darmstadt, Germany). Images were acquired using a JEOL 1011 transmission electron microscope operating at 100 kV.

2.9. Intracellular Trafficking of S-MSN and CS-MSN. *2.9.1. Confocal Microscopy.* MDA-MB-231 cells were seeded at 15 $\times 10^3$ cells per well in a poly-D-lysine-coated Ibidi 8-well plate and were allowed to adhere for 48 h. The cell culture medium was replaced by the transfection medium, and then S-MSN or CS-MSN prepared with the siRNA-Atto390 conjugate (50 nM) siRNA were added for 4 h. After that, cells were washed, incubated or not for additional 20 h, and then stained with WGA-AF488, anti-EEA-1-Alexa Fluor 488 (Abcam, Cambridge, U.K.) or anti-Lamp1-Alexa Fluor 488 (eBiosciences, Thermo Fisher Scientific, San Diego, CA) antibodies. For the staining with antibodies, cells were fixed using 4% paraformaldehyde solution for 15 min. A solution of Triton X-100 at 0.1% was added for 15 min to permeabilize cells. A solution of 5% BSA was used for 30 min to block unspecific interaction sites. Then, cells were incubated with antibody solutions of anti-EEA-1-AF488 (10 μg/mL) or anti-Lamp1-AF488 (1.25 μg/mL) antibodies in 1% BSA for 30 min and then washed with DPBS 1×. The staining of the cell

DOI: 10.1021/acs.biomac.9b00637
Biomacromolecules 2019, 20, 3076−3086

membrane with WGA-AF488 was done as described in Section 2.7.2. After the staining, cells were mounted with Fluoromount-G. Cells were visualized and imaged with a confocal microscope Nikon A1R using ×60/1.4 objective and NIS elements software. Images were acquired with a resolution of 0.21 μm/px and were constructed using Fiji software (ImageJ).

2.9.2. Imaging Flow Cytometry (Amnis ImageStream^X Mark II). MDA-MB-231 cells were seeded at 2 × 10^6 cells per well in a 6-well plate for 24 h. After cellular adhesion, cells were incubated with CS-MSN or S-MSN prepared with the siRNA-Atto390 conjugate (50 nM siRNA). The fluorescence of the siRNA-Atto390 conjugate and sulfocyanine 5 conjugated to CS-FNP or S-FNP was monitored in early endosomes and lysosomes after incubation with CS-MSN or S-MSN, respectively. MDA-MB-231 cells were incubated with CS-MSN or S-MSN prepared with the siRNA-Atto390 conjugate for 4 h, then the cell culture medium was changed, and cells were incubated or not for additional 20 h. After that, cells were stained with anti-EEA-1-AF488 (channel 2) or anti-Lamp1-AF488 (channel 2) antibodies as described in Section 2.8.1. In each experiment, 10 000 events for each sample were acquired with Inspire imaging flow cytometry software using Amnis ImageStream^X Mark II. MDA-MB-231 images were captured at 60× magnification and EDF. Single-stained samples of 500 cells were also illuminated by the 405 nm (70 mW), 488 nm (100 mW), and 642 nm (150 mW) lasers with the brightfield (BF) and darkfield inactivated to perform color compensation controls. The spectral compensation matrix was applied to each of the files. Cells in the best focus were identified using Gradient RMS of the BF image. Single cells were then separated from debris and doublets using a plot of the aspect ratio vs the area of the BF image. The internalization scores (IS) of siRNA-Atto390 (channel 7) and that of sulfocyanine 5 (channel 11) conjugated to CS-FNP or S-FNP were analyzed in early endosome and lysosomes using "fluorescent intracellular compartment mask" [Erode (M02, 4)] and calculated using the internalization feature provided by IDEAS V6.2 software.

*2.9.3. Structured Illumination Microscopy (**SIM**).* Cells were prepared and stained with anti-EEA-1-Alexa Fluor 488 antibody as described in Section 2.8.1. After that, cells were analyzed and imaged with a structured illumination microscope Nikon N-SIM using ×100/1.49 objective and NIS elements software. Images were acquired with a resolution of 0.03 μm/px and were constructed by Fiji software.

2.9.4. Downregulation of GFP Protein and Inhibition of Endosomal Acidification. After 24 h of the seeding of MDA-MB-231/GFP (Euromedex, Souffelweyersheim, France) at 30 × 10^3 cells per well in a 12-well plate, cells were pretreated or not for 1 h with an inhibitor of endosomal acidification, bafilomycin A1 (5 μM, Enzo Life Science, Villeurbanne, France), then a transfection assay was carried out as described in our previous publication.[18] Briefly, S-MSN and CS-MSN were prepared according to the formulation protocol with anti-GFP siRNA. S-MSN or CS-MSN formulation (50 nM siRNA) was added to cells after replacement of the complete cell culture medium by the transfection medium. After 4 h, the transfection medium was replaced with the complete cell culture medium and then cells were incubated in normal growth conditions until 72 h. Nontreated cells were used as a negative control, and cells treated with the commercial transfection agent Oligofectamine (Invitrogen, Thermo Fisher Scientific, Paisley, U.K.) were used as a positive control (cells were transfected with Oligofectamine according to the manufacturer's recommendations). Cells were removed using 0.05% trypsin−EDTA, gene silencing was evaluated using Gallios flow cytometry, and data were analyzed by FlowJo v10 software.

2.10. Statistics. PRISM (GraphPad Prism 7) was used for statistical analysis. Data were compared among groups using the Mann−Whitney test. The difference between groups was considered significant when p-value <0.05 (*) or <0.01 (**). # is the reference value for statistics.

3. RESULTS AND DISCUSSION

3.1. Nanoparticle Characterizations. To eliminate the nongrafted gH625 peptide, suspensions of CS-FNP and the control S-FNP were purified by size-exclusion chromatography (SEC). The SEC chromatogram of S-FNP showed only one peak, which corresponds to the absorbance of SPION (Figure 1A). However, the SEC chromatogram of CS-FNP showed

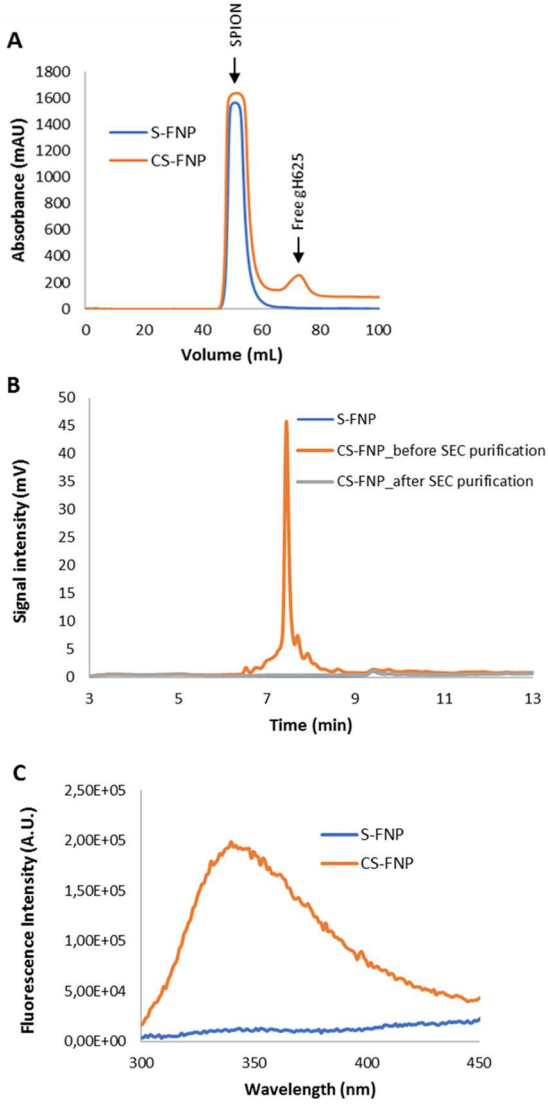

Figure 1. (A) Chromatograms of the purification of S-FNP and CS-FNP by SEC. (B) HPLC chromatograms of S-FNP and CS-FNP before and after SEC purification for the detection of free gH625. (C) Fluorescence profiles of the tryptophan-based gH625 peptide in S-FNP and CS-FNP after excitation at 280 nm.

two peaks. According to their respective sizes, the first one corresponds to SPION (at 50 mL) and the second one corresponds to the free gH625 peptide (at 75 mL). Thereafter, high-performance liquid chromatography (HPLC) was used to check and quantify the presence of the free peptide in purified CS-FNP suspensions and to determine the grafting efficiency on nanoparticles. Only free gH625 is detected with this technique as an identifiable peak (Figure S1). Therefore, HPLC was used to check and quantify the fractions of the free gH625 peptide collected from SEC purification. The chromatograms show that no gH625 peak was observed in purified CS-FNP contrary to nonpurified CS-FNP (Figure 1B). This indicates that SEC is an efficient method to eliminate nongrafted peptides. The amount of the free peptide collected

DOI: 10.1021/acs.biomac.9b00637
Biomacromolecules 2019, 20, 3076−3086

from SEC purification represented 9.75 ± 1.38% of the total amount of peptides used for the grafting. Subsequently, the presence of the gH625 peptide grafted on nanoparticles was assessed by detecting the fluorescence of its tryptophan residue. The presence of gH625 on the surface of CS-FNP was confirmed by the strong fluorescence signal of tryptophan under excitation at 280 nm and with a maximum emission at 340 nm (Figure 1C). Control nanoparticles (S-FNP) showed no fluorescence at 340 nm because of the absence of peptides.

The physicochemical properties of synthesized nanoparticles with or without gH625 were then determined. The hydrodynamic diameters (HD) were 73 ± 6 and 86 ± 6 nm, respectively, for S-FNP and CS-FNP with a polydispersity index below 0.2 (Table 1 and Figure S2). No significant

Table 1. Hydrodynamic Diameter (HD), Polydispersity Index (PDI), and ζ-Potential (ZP) of S-FNP and CS-FNP

	HD (nm)	PDI	ZP (mV)
S-FNP	73 ± 6	0.19 ± 0.05	−6 ± 1
CS-FNP	86 ± 6	0.18 ± 0.02	−7 ± 2

difference between the ζ-potential of S-FNP and CS-FNP was observed. Therefore, the presence of gH625 at the surface of our nanoparticles did not perturb their physicochemical properties, no significant increase of the HD was observed, and the surface of SPION remained almost neutral. Taking all of these results together, we successfully grafted the gH625 peptide at the surface of PEGylated SPION at a grafting efficiency of almost 90% and with suitable colloidal properties for injectable nanoformulations.

3.2. Formulation and Characterization of siRNA Nanovectors. Subsequently, S-FNP and CS-FNP were used as a nanoplatform for the formulation of siRNA delivery nanovectors called S-MSN and CS-MSN denoting stealth magnetic siRNA nanovector and CPP-capped stealth magnetic siRNA nanovector, respectively (Figure 2). The formulation of

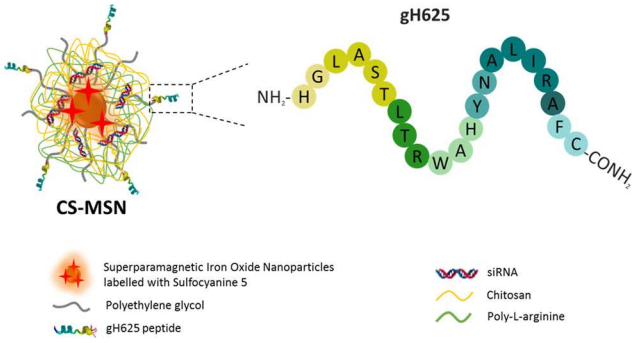

Figure 2. Schematic illustration of CS-MSN with the gH625 peptide sequence.

S-MSN and CS-MSN was performed according to our previously optimized protocol.[18] The size values of S-MSN and CS-MSN were 155 and 150 nm, respectively, with a polydispersity index of almost 0.3. The ζ-potentials of S-MSN (+16 mV) and CS-MSN (+13 mV) were slightly positive thanks to the presence of cationic polymers (Table 2 and Figure S3). These results showed that no significant differences were observed in the physicochemical characteristics of the nanovectors formulated with S-FNP and CS-FNP. Moreover, the loading of siRNA in S-MSN and CS-MSN was checked

Table 2. Hydrodynamic Diameter (HD), Polydispersity Index (PDI), and ζ-Potential (ZP) of S-MSN and CS-MSN

	HD (nm)	PDI	ZP (mV)
S-MSN	155 ± 15	0.30 ± 0.05	+16 ± 2
CS-MSN	150 ± 13	0.29 ± 0.04	+13 ± 1

using a gel retardation assay. As shown in Figure 3, no fluorescence was detected in the case of S-MSN and CS-MSN.

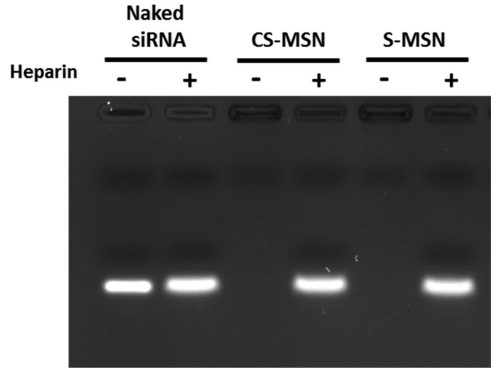

Figure 3. Gel retardation assay to detect free siRNA in S-MSN and CS-MSN.

However, in the presence of heparin, fluorescent bands appear at the same fluorescence intensity as the control free siRNA. This result showed that siRNA are completely complexed in both nanovectors, as it was shown for CS-MSN in our previously published results.[18] Therefore, the presence of the peptide gH625 did not affect the complexation of siRNA with cationic polymers and with the nanoplatforms (S-FNP and CS-FNP).

3.3. Internalization Mechanisms and Intracellular Trafficking of siRNA Nanovectors. *3.3.1. Cell Uptake.* The internalization of CS-MSN and S-MSN in cells was investigated using confocal microscopy by detecting the fluorescence of the sulfocyanine 5-labeled (C)S-FNP or siRNA-Atto390 conjugate at a concentration of 50 nM (siRNA equivalent). The labeling of the cell membrane appears in green in images. The fluorescence related to nanovectors [pink or red spots corresponding to (C)S-MSN or (C)S-FNP] was found inside the cell, showing that nanovectors were internalized by the cells and were more abundant in the condition CS-MSN, i.e., when the siRNA nanovectors were functionalized with the CPP gH625 (Figure 4).

The uptake kinetics of siRNA nanovectors (S-MSN and CS-MSN) in triple-negative breast cancer cells was performed up to 4 h by monitoring the fluorescence of the sulfocyanine 5-labeled (C)S-FNP or siRNA-Atto390 conjugate. As shown in Figure 5A, the fluorescence intensity of sulfocyanine increased up to 4 h for both nanovectors, CS-MSN and S-MSN (Figure 5B). The presence of the peptide gH625 enhances the entry of CS-MSN in cells starting from 2 h compared to S-MSN, and this entry is approximately 2.5-fold higher for CS-MSN after 4 h of incubation. The same kind of results was found when monitoring the fluorescence of Atto390 conjugated to siRNA (Figure S4).

The potential of CPP to enhance the internalization of conjugated nanovectors has already been demonstrated,[19−21] as well as that of gH625 peptide.[10,11] In a previous study, we demonstrated an increase of the cell uptake of doxorubicin-

DOI: 10.1021/acs.biomac.9b00637
Biomacromolecules 2019, 20, 3076−3086

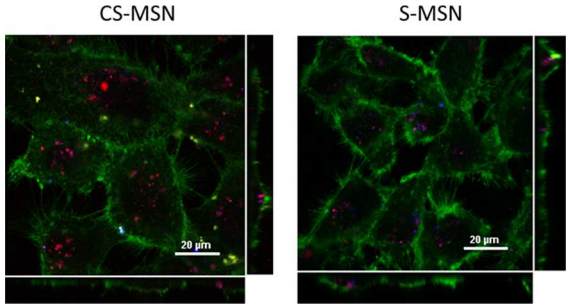

Figure 4. Confocal images of MDA-MB-231 cells treated with CS-MSN (left image) or S-MSN (right image) for 4 h and stained with wheat germ agglutinin-Alexa Fluor 488 as a membrane stain (green). Red fluorescence: Sulfocyanine 5 conjugated to CS-FNP or S-FNP; blue fluorescence: Atto390 conjugated to siRNA. The scale bar is 20 μm.

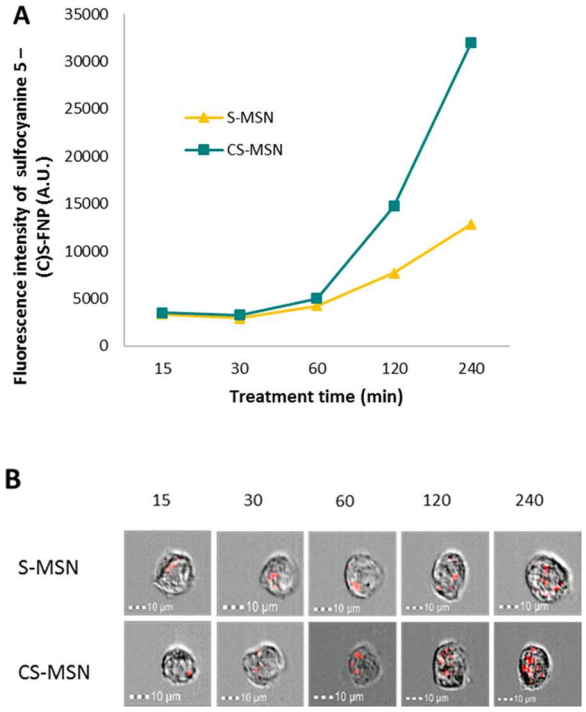

Figure 5. Uptake kinetics of CS-MSN and S-MSN in MDA-MB-231 cells. Intracellular fluorescence intensity of sulfocyanine 5 conjugated to CS-FNP or S-FNP was monitored by imaging flow cytometry after the incubation of nanovectors for 15, 30, 60, 120, and 240 min: (A) intracellular fluorescence intensity and (B) representative brightfield images of cells containing intracellular fluorescent nanovectors (red spots) derived from the imaging flow cytometry data collection.

loaded liposomes by conjugating the peptide gH625 on the surface of the liposomes.[10] In another study, Valiante and co-workers showed the success of the peptide gH625 to cross an *in vitro* model of the blood–brain barrier and the ability to deliver a conjugated cargo into neuron and astrocyte cells.[11] The enhanced internalization of the nanovectors in the presence of gH625 can be supported by the presence of both hydrophobic and hydrophilic amino acids in the sequence of this CPP.[22] The correct balance of this characteristic enables the local and temporary destabilization of the membrane bilayer favoring a direct crossing of the membrane. Apart from the presence of both hydrophobic and hydrophilic residues, several other structural features are responsible for the gH625 cell internalization mechanism such as the ability to change from a random to an amphipathic α-helical structure when in contact with membrane bilayers, the ability to oligomerize in membrane bilayers, and the presence of a histidine residue at the N-terminus.[23] In the present study, the increase of the cell internalization of CS-MSN by gH625 shows that this nanovector may be an efficient system for the delivery of siRNA in cancer cells.

3.3.2. Internalization Pathway. The pathway used to enter cells could determine the intracellular trafficking of nanovectors and affects their efficiency to deliver their contents. To determine the internalization pathway of S-MSN and CS-MSN, the fluorescence intensity of sulfocyanine 5 conjugated to S-FNP or CS-FNP was measured after incubation with chemical inhibitors. As shown in Figure 6A, the incubation of cells with the combination of sodium azide and 2-deoxy-D-glucose (energy inhibitors) or with dynasore (dynamin inhibitor) resulted in an evident reduction of the sulfocyanine 5 fluorescence intensity in treated cells. Indeed, in the cells pretreated with energy inhibitors, the fluorescence intensity decreased from 100 to 26 ± 11 and 24 ± 16% for S-MSN and CS-MSN, respectively, and to 30 ± 7 and 33 ± 7% in cells incubated with dynasore. These decreases in fluorescence intensity indicate a reduction of S-MSN and CS-MSN cell uptake and therefore an inhibition of nanovector internalization by the cells. Nevertheless, there is no significant difference between the two kinds of nanovectors. This result implies that the entry of S-MSN and CS-MSN was energy- and dynamin-dependent; thus, the internalization process may be an endocytosis phenomenon. Moreover, the analysis of MDA-MB-231 cells treated with the nanovectors and stained with the membrane marker (WGA-AF488), by confocal microscopy, shows highly fluorescent intracellular spots (Figure 6B) representing the colocalization of fluorophores conjugated to nanovectors (sulfocyanine 5 and Atto390) and fluorophore conjugated to the membrane marker (AF488). These bright spots look like vesicles formed from the cell membrane, as they were stained with Alexa Fluor 488 conjugated to WGA, containing nanovectors (Figure 6B, white arrows), such as endosomes. This result confirms the hypothesis of an endocytic pathway for the internalization route of (C)S-MSN into MDA-MB-231 cells. In addition, to specify the used endocytic pathway, we evaluated the internalization of nanovectors in the presence of some chemical inhibitors of endocytic pathways. Figure 6B shows a significant reduction of the intracellular fluorescence intensity of both nanovectors after incubation for cells with caveolae-mediated endocytosis inhibitors, methyl-β-cyclodextrin (MβCD) and nystatin. The effect of pitstop 2, a clathrin inhibitor, in the internalization of S-MSN and CS-MSN was investigated, and results show a significant decrease of cell uptake. In contrast, no effect was observed after the cell incubation with chlorpromazine, a clathrin inhibitor, and dimethyl amiloride (DMA), an inhibitor of macropinocytosis. Thus, one concludes that the internalization occurs via endocytosis mediated by clathrin and caveolae.

Furthermore, MDA-MB-231 cells were analyzed by transmission electron microscopy (TEM) after their incubation with S-MSN or CS-MSN to visualize their localization in the cells. TEM images showed the presence of nanovectors in clathrin-coated and caveolae vesicles (Figure 6D). Thus, these images confirmed the endocytic mechanism and the internalization of S-MSN and CS-MSN via both clathrin- and

DOI: 10.1021/acs.biomac.9b00637
Biomacromolecules 2019, 20, 3076–3086

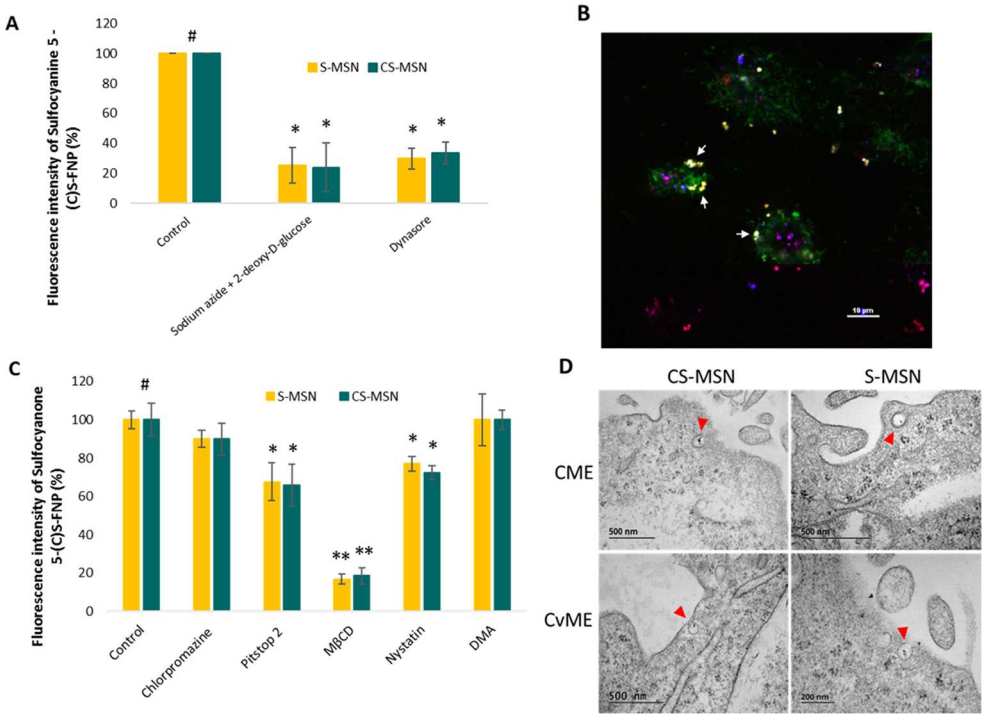

Figure 6. Mechanism and pathway of entry of the siRNA nanovectors: (A) Fluorescence intensity of sulfocyanine 5 conjugated to S-FNP or CS-FNP measured by flow cytometry in MDA-MB-231 cells incubated with nanovectors with or without sodium azide and 2-deoxy-D-glucose or dynasore. (B) Confocal microscopy image of MDA-MB-231 cells treated with CS-MSN for 4 h and stained with WGA-AF488. (C) Fluorescence intensity of sulfocyanine 5 conjugated to S-FNP or CS-FNP measured by flow cytometry in MDA-MB-231 cells incubated with nanovectors with or without chlorpromazine, methyl-β-cyclodextrin (MβCD), pitstop 2, nystatin, or dimethyl amiloride (DMA). (D) Transmission electron microscopy images of MDA-MB-231 cells incubated with S-MSN or CS-MSN for 4 h. The scale bar is 500 nm.

caveolae-dependent endocytosis pathways. From these results, we showed that the presence of gH625 was able to enhance the internalization (Figure 5) but did not affect the entry route of our siRNA nanovectors. We can, therefore, conclude that even if gH625 is known for its ability to translocate directly into the cytosol, the CPP-conjugated nanovectors follow an endocytic pathway. Without polyplex loading, nanoparticles CS-FNP have been shown to be endocytosed by MDA-MB-231 cells.[17] In their study, Carberry et al. showed that the functionalization of a dendrimer with the peptide gH625 leads to cell internalization involving both direct translocation and endocytosis.[9] In the same context, Madani et al. reported, in their review, that the conjugated cargo could modify the internalization pathway of the CPP.[24] In the present study, we demonstrated that the presence of gH625 at the surface of the nanovector did not modify the entry pathway of CS-MSN and that siRNA nanovectors were internalized by both clathrin- and caveolae-mediated endocytosis.

3.3.3. Intracellular Trafficking of siRNA Nanovectors. The intracellular trafficking of siRNA nanovectors was investigated using intracellular compartments markers. Therefore, cells were incubated with S-MSN or CS-MSN, then stained with an anti-EEA-1 antibody as an early endosome marker (Figure 7A) or an anti-Lamp1 antibody to label the lysosomes of the cells (Figure 7B). Images of cells treated with the siRNA nanovectors after endosomal staining show both nanovector fluorophores [sulfocyanine 5 conjugated to (C)S-FNP (red) and Atto390 conjugated to siRNA (blue)] inside green vesicles (AF488 conjugated to the endosomal marker) at 4 h (Figure 7A). Therefore, these images indicate the presence of S-MSN and CS-MSN in early endosomes after 4 h of incubation. However, after 24 h of incubation, the colocalization of nanovector dyes and fluorophore conjugated to EEA-1 antibody seems to be reduced as we can observe more red spots alone (Figure 7A). That indicates either a progression toward lysosomes or the escape of nanovectors from endosomes. Moreover, images of cells treated with nanovectors after lysosomal staining show at 4 h a low colocalization of sulfocyanine 5 (red) and Atto390 (blue) nanovector fluorophores with AF488 conjugated to the lysosomal marker (green) (Figure 7B). This colocalization increased after 24 h mainly with sulfocyanine 5 (red) conjugated to nanoparticles (S-FNP and CS-FNP). That indicates that the accumulation of nanoparticles in lysosomes was higher than that of siRNA.

To confirm this tendency, treated cells were also analyzed by imaging flow cytometry and the internalization scores (IS) of sulfocyanine 5 and Atto390 in endosomes or lysosomes were determined (Table 3). The IS measure the relative amount of a signal inside versus outside endosomes or lysosomes. The higher the score, the greater the quantity of nanovectors found in the organelle. In this study, we especially investigated the variation of the IS between 4 and 24 h in early endosomes and lysosomes for the nanovectors with or without gH625. For S-MSN, the internalization scores of siRNA and S-FNP in early endosomes largely increased after 24 h compared to 4 h, which indicates an accumulation of S-MSN in early endosomes (0.4 vs 1.3 and 0.5 vs 1.6, respectively). On the contrary, the internalization scores of siRNA and CS-FNP of CS-MSN in early endosomes did not change so much (0.6 vs 0.5 and 0.4 vs 0.7, respectively). This result suggests that the presence of the gH625 peptide in the nanovector promotes the endosomal escape. In lysosomes, the internalization score of nanovector

DOI: 10.1021/acs.biomac.9b00637
Biomacromolecules 2019, 20, 3076−3086

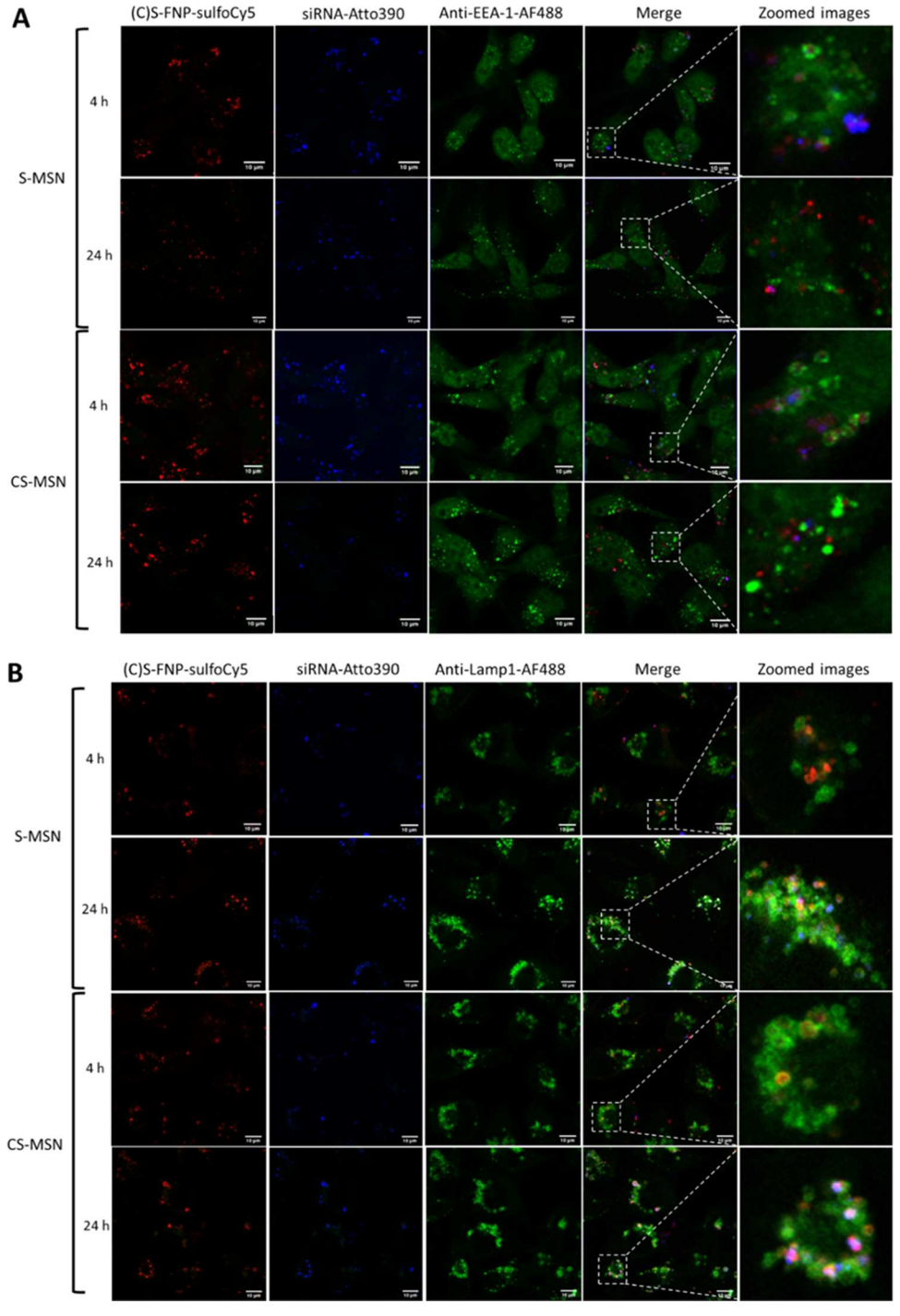

Figure 7. Intracellular trafficking of S-MSN and CS-MSN in MDA-MB-231 cells. Colocalization of siRNA-Atto390 (blue) and CS-FNP or S-FNP conjugated with sulfocyanine 5 (red) with (A) anti-EEA-1-AF480 antibody and (B) anti-Lamp1-AF488 antibody (green) after 4 h of contact. The staining and cell fixation were made immediately (4 h) or 20 h later (24 h), followed by confocal imaging.

Table 3. Variation of the Internalization Score (IS) between 4 and 24 h of siRNA or (C)S-FNP of S-MSN or CS-MSN in Early Endosomes and in Lysosomes

	early endosomes (anti-EEA-1 antibody)				lysosomes (anti-Lamp1 antibody)			
	siRNA		(C)S-FNP		siRNA		(C)S-FNP	
incubation time	4 h	24 h	4 h	24 h	4 h	24 h	4 h	24 h
S-MSN	0.4	1.3	0.5	1.6	1.1	1.3	0.6	1.7
CS-MSN	0.6	0.5	0.4	0.7	1.2	1.5	0.7	1.7

DOI: 10.1021/acs.biomac.9b00637
Biomacromolecules 2019, 20, 3076−3086

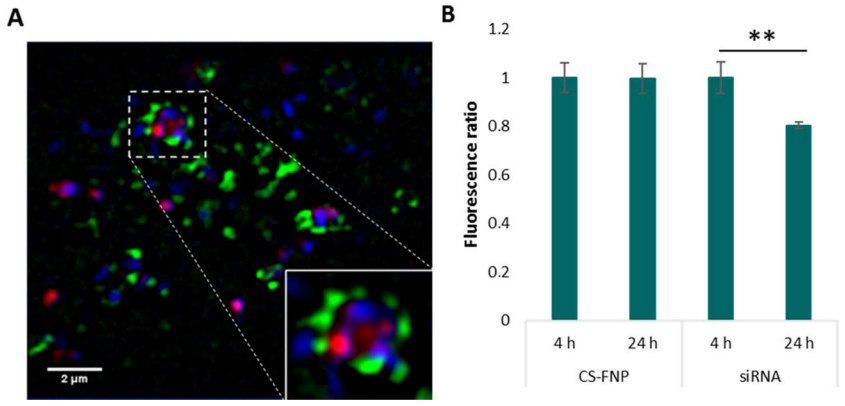

Figure 8. Endosomal escape of nanovectorized siRNA with CS-MSN. (A) Structured illumination microscopy (SIM) image of MDA-MB-231 cells incubated with CS-MSN prepared with siRNA-Atto390 and anti-EEA-1-AF488 antibody. The scale bar is 2 μm. (B) Ratio of the fluorescence intensity of sulfocyanine 5 and Atto390 conjugated to CS-FNP and siRNA, respectively, in cells treated with CS-MSN for 4 h or 24 h measured by flow cytometry.

cores (S-FNP and CS-FNP) increased strongly, showing progressive accumulation in lysosomes. However, the internalization score of siRNA of both nanovectors (S-MSN and CS-MSN) did not increase significantly. This could suggest that siRNA were freed before reaching the lysosomes.

In this part of the study, some discrepancies between confocal microscopy and imaging flow cytometry results were observed. For example, in the case of S-MSN, the increase of the internalization score of siRNA or S-FNP in early endosomes after 24 h was not detected in confocal microscopy. On the contrary, a reduction of the colocalization of the fluorescence of Atto390 or sulfocyanine 5 conjugated to siRNA or S-FNP, respectively, and that of AF488 conjugated to the endosomal marker was observed. This discrepancy could be explained by a hypothesis reported by Selby and co-workers in their review. With the presence of endosomal and lysosomal markers in the vesicular membrane, an enclosed part of the nanovectors can be missed.[25] Indeed, the analysis of the cells with confocal microscopy can illustrate this limitation as it is based on the fluorescence colocalization. However, the calculation of the IS in intracellular compartments considers even enclosed nanovectors. Therefore, the analysis of the colocalization in images and the internalization score were complementary.

Results of the intracellular trafficking suggest an escape of siRNA from endosomes, which is enhanced by the presence of the peptide gH625, whereas nanoparticles (S-FNP and CS-FNP) continue their trafficking into lysosomes. However, this traffic is possible only if endosomes are not destroyed. Previous studies reported that, in the presence of cationic polymers, the complete rupture of the endosomal membrane is highly unlikely.[26−28] One hypothesis is that the endosomal escape occurs by local endosomal membrane destabilization provoked by the increase of the positive charge density of the cationic polymers. This destabilization results in the permeabilization of the membrane and the formation of transient "nanoscale holes".[29] Thus, to complete this study and to verify this hypothesis, the investigation of the endosomal escape of CS-MSN is needed.

3.3.4. Endosomal Escape of siRNA and Down-regulation Efficiency of CS-MSN. To achieve their mission, nanovectorized siRNA need to be released from the nanovectors and must be found in the cytosol. For that, the endosomal escape represents a major step for siRNA delivery. To investigate the capability of siRNA loaded in CS-MSN to escape endosomes, MDA-MB-231 cells incubated with nanovectors prepared with fluorescent siRNA (siRNA-Atto390) and stained with conjugated anti-EEA-1 antibody were imaged using structured illumination microscopy (SIM) and the intensity of CS-MSN's fluorophores, conjugated to siRNA and CS-FNP, was measured by imaging flow cytometry.

SIM images show the breaking of endosomes (green) and the escape of siRNA (blue) in the cytosol (Figure 8A). The measurement of the fluorescence intensity of the fluorophores conjugated to siRNA (Atto390) and CS-FNP (sulfocyanine 5) in cells treated with CS-MSN for 4 and 24 h shows a significant decrease of the fluorescence intensity of Atto390 conjugated to siRNA after 24 h compared to 4 h, whereas that of sulfocyanine 5 conjugated to CS-FNP remained constant (Figure 8B). The reduction of the siRNA fluorescence intensity could be explained by the dispersion of siRNA in the cytosol, which suggests (1) the endosomal escape of siRNA or (2) their degradation. To invalidate the second hypothesis, a downregulation experiment was performed on MDA-MB-231/GFP cells.

Cells were alternatively treated with the commercial transfection agent Oligofectamine, with S-MSN or CS-MSN formulated with an anti-GFP siRNA for 4 h, and the fluorescence intensity of GFP was measured using flow cytometry after 72 h of the treatment. As shown in Figure 9, the cell GFP expression was reduced using both siRNA nanovectors. This could be explained by the ability of cationic polymers (chitosan and poly-L-arginine) to deliver siRNA in cells.[30,31] Furthermore, the efficiency of CS-MSN to inhibit the GFP in cells was 1.7-fold higher than that of S-MSN. This difference of transfection efficiency for the nanovectors with and without the CPP gH625 could be explained by the increased internalization of CS-MSN and by the enhanced endosomal escape in the presence of gH625. In the literature, many virus-derived peptides are known for their ability to escape endosomes and were used as endosomal escape agents or to enhance the endosomal escape of some molecules. These peptides use various mechanisms to pass through the endosomal membrane such as membrane fusion, pore formation, and proton sponge mechanisms. Oliveira and colleagues used a lipid-based nanovector with influenza-derived peptide diINF-7 for siRNA delivery to silence the epidermal growth factor receptor and the K-ras oncogenes.

DOI: 10.1021/acs.biomac.9b00637
Biomacromolecules 2019, 20, 3076−3086

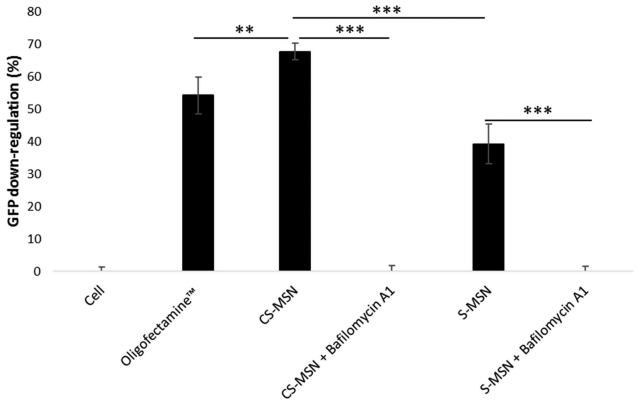

Figure 9. Quantification of GFP downregulation efficiency in MDA-MB-231/GFP cells pretreated or not with bafilomycin A1 and treated with Oligofectamine, CS-MSN, or S-MSN for 4 h and analyzed after 72 h of the treatment using flow cytometry.

The presence of this peptide efficiently enhances the endosomal escape of this complex.[32] This peptide is known to be able to fuse with the membrane of endosomes to facilitate the passage of associated cargo toward the cytosol.[33] For gH625, the mechanism of endosomal escape is not well understood, but based on our SIM results (Figure 8A), the hypothesis of transient pore formation in the endosomal membrane is highly likely. This hypothesis was supported by results presented by Guarnieri et al. where they showed that nanoparticles decorated on their surface with gH625 were able to escape the endo/lysosomal compartment by local and temporary destabilization of the membrane.[34] This ability of the gH625 peptide to escape endosomes results in improving the delivery of therapeutics, which was confirmed in the literature by Galdiero's team using different delivery systems.[22] For example, the conjugation of this peptide to liposomes enhanced the delivery of loaded doxorubicin in doxorubicin-resistant A549 cells and results in an induction of cell death, significantly more pronounced than liposomes without gH625 or free doxorubicin.[10]

Moreover, the pretreatment of cells with an inhibitor of endosomal acidification, bafilomycin A1, blocked the inhibition of the GFP fluorescence and reduced the transfection efficiency of both nanovectors with and without gH625. This result could be explained by the dependence of the endosomal escape mechanism on the acidification of this compartment. In fact, the inhibition of the acidification of endosomes affects the mechanisms of the proton sponge effect and the umbrella effect and blocks the transfer of siRNA to the cytosol. Furthermore, in a previous study, we proved that in a solution of trifluoroethanol, that mimics the environment of cellular membranes, the CPP gH625 changes its conformation to α-helix, which favors the membranotropic properties of this peptide.[17] However, by blocking the umbrella effect of polymers, the contact between the peptide gH625 and the cell membrane can be reduced. Thus, the inhibition of the acidification of endosomes preserved the integrity of the endosomal membrane and prevented the endosomal escape.

4. CONCLUSIONS

In this study, we highlighted the role of a cell-penetrating peptide gH625 in the internalization and the intracellular trafficking of siRNA magnetic nanovectors (CS-MSN). We showed that the cellular uptake of CS-MSN was increased 2.5-fold in the presence of gH625 in a triple-negative breast cancer cell line. Moreover, this peptide appears to play a major role in the endosomal escape. In fact, the functionalization of our siRNA nanovectors with this peptide enhances their passage into the cytosol. In addition to the induction of the endosomal escape with cationic polymers, we suggested that the peptide gH625 may interact with the endosomal membrane and probably promotes transient pore formation, which enhances the escape of siRNA from endosomes. The enhanced entry and the endosomal escape offered by CS-MSN result in high transfection efficiency, 1.7-fold higher than the same nanovector without gH625 peptide.

■ ASSOCIATED CONTENT

Supporting Information

The Supporting Information is available free of charge on the ACS Publications website at DOI: 10.1021/acs.biomac.9b00637.

HPLC chromatograms and a calibration curve of gH625 solutions (Figure S1); size distribution profiles of S-FNP and CS-FNP (Figure S2); size distribution profiles of S-MSN and CS-MSN (Figure S3); uptake kinetics of nanovectorized siRNA obtained by flow imaging (Figure S4) (PDF)

■ AUTHOR INFORMATION

Corresponding Author

*E-mail: emilie.allard@univ-tours.fr.

ORCID

Katel Hervé-Aubert: 0000-0002-3315-903X
Martin Soucé: 0000-0002-6627-9660
Emilie Allard-Vannier: 0000-0002-6973-6812

Funding

We are grateful to the "Ligue Nationale Contre le Cancer" for their financial support and especially to the local committees of the departments 17, 37, 49, 53, and 56 (EVASION project and INTERACTION project). We also thank the "Région Centre-Val de Loire", the "Cancéropole Grand Ouest" (MATURE project), and Campus France (PHC GALILEE 2017, project No 39635TB) for the funding.

Notes

The authors declare no competing financial interest.

■ ACKNOWLEDGMENTS

We thank Nicolas Aubrey (UMR INRA 1282, team of "Infectiologie et Santé Publique", University of Tours) for his help in SEC experiments. We are grateful to Julien Burlaud-Gaillard (Département des Microscopies, Université de Tours, France) for TEM images. Our data were obtained with the assistance of the IBiSA Electron Microscopy Facility of Tours University. The authors would like to thank Thibaut Blondy (CRCINA, Inserm U1232, team 4, University of Nantes) for his help with confocal microscopy experiments.

■ REFERENCES

(1) Tokatlian, T.; Segura, T. siRNA Applications in Nanomedicine. *Wiley Interdiscip. Rev.: Nanomed. Nanobiotechnol.* **2010**, 305−315.
(2) Videira, M.; Arranja, A.; Rafael, D.; Gaspar, R. Preclinical Development of SiRNA Therapeutics: Towards the Match between Fundamental Science and Engineered Systems. *Nanomedicine* **2014**, *10*, 689−702.

(3) Wang, J.; Lu, Z.; Wientjes, M. G.; Au, J. L.-S. Delivery of SiRNA Therapeutics: Barriers and Carriers. *AAPS J.* **2010**, *12*, 492−503.
(4) Steinbach, J. M.; Seo, Y.-E.; Saltzman, W. M. Cell Penetrating Peptide-Modified Poly(Lactic-Co-Glycolic Acid) Nanoparticles with Enhanced Cell Internalization. *Acta Biomater.* **2016**, *30*, 49−61.
(5) Guan, X.; Hu, X.; Cui, F.; Li, Y.; Jing, X.; Xie, Z. EGFP-Based Protein Nanoparticles with Cell-Penetrating Peptide for Efficient SiRNA Delivery. *Macromol. Biosci.* **2015**, *15*, 1484−1489.
(6) Malhotra, M.; Tomaro-Duchesneau, C.; Prakash, S. Synthesis of TAT Peptide-Tagged PEGylated Chitosan Nanoparticles for SiRNA Delivery Targeting Neurodegenerative Diseases. *Biomaterials* **2013**, *34*, 1270−1280.
(7) Gräslund, A.; Madani, F.; Lindberg, S.; Langel, Ü.; Futaki, S.; Gräslund, A.; Madani, F.; Lindberg, S.; Langel, Ü.; Futaki, S. Mechanisms of Cellular Uptake of Cell-Penetrating Peptides. *J. Biophys.* **2011**, *2011*, No. 414729.
(8) Galdiero, S.; Falanga, A.; Morelli, G.; Galdiero, M. GH625: A Milestone in Understanding the Many Roles of Membranotropic Peptides. *Biochim. Biophys. Acta, Biomembr.* **2015**, *1848*, 16−25.
(9) Carberry, T. P.; Tarallo, R.; Falanga, A.; Finamore, E.; Galdiero, M.; Weck, M.; Galdiero, S. Dendrimer Functionalization with a Membrane-Interacting Domain of Herpes Simplex Virus Type 1: Towards Intracellular Delivery. *Chem. - Eur. J.* **2012**, *18*, 13678−13685.
(10) Perillo, E.; Porto, S.; Falanga, A.; Zappavigna, S.; Stiuso, P.; Tirino, V.; Desiderio, V.; Papaccio, G.; Galdiero, M.; Giordano, A.; Galdiero, S.; Caraglia, M. Liposome Armed with Herpes Virus-Derived GH625 Peptide to Overcome Doxorubicin Resistance in Lung Adenocarcinoma Cell Lines. *Oncotarget* **2016**, *7*, 4077−4092.
(11) Valiante, S.; Falanga, A.; Cigliano, L.; Iachetta, G.; Busiello, R. A.; La Marca, V.; Galdiero, M.; Lombardi, A.; Galdiero, S. Peptide GH625 Enters into Neuron and Astrocyte Cell Lines and Crosses the Blood−Brain Barrier in Rats. *Int. J. Nanomed.* **2015**, *10*, 1885−1898.
(12) Falanga, A.; Lombardi, L.; Tarallo, R.; Franci, G.; Perillo, E.; Palomba, L.; Galdiero, M.; Pontoni, D.; Fragneto, G.; Weck, M.; Galdiero, S. The Intriguing Journey of GH625-Dendrimers. *RSC Adv.* **2017**, *7*, 9106−9114.
(13) Venkitaraman, R. Triple-Negative/Basal-like Breast Cancer: Clinical, Pathologic and Molecular Features. *Expert Rev. Anticancer Ther.* **2010**, *10*, 199−207.
(14) Hatakeyama, H.; Akita, H.; Kogure, K.; Oishi, M.; Nagasaki, Y.; Kihira, Y.; Ueno, M.; Kobayashi, H.; Kikuchi, H.; Harashima, H. Development of a Novel Systemic Gene Delivery System for Cancer Therapy with a Tumor-Specific Cleavable PEG-Lipid. *Gene Ther.* **2007**, *14*, 68−77.
(15) Love, K. T.; Mahon, K. P.; Levins, C. G.; Whitehead, K. A.; Querbes, W.; Dorkin, J. R.; Qin, J.; Cantley, W.; Qin, L. L.; Racie, T.; et al. Lipid-like Materials for Low-Dose, in Vivo Gene Silencing. *Proc. Natl. Acad. Sci. U.S.A.* **2010**, *107*, 1864−1869.
(16) Müller, L. K.; Kaps, L.; Schuppan, D.; Brose, A.; Chai, W.; Fischer, K.; Müller, S.; Frey, H.; Schmidt, M.; Mohr, K. Physicochemical and Preclinical Evaluation of Spermine-Derived Surfactant Liposomes for in Vitro and in Vivo SiRNA-Delivery to Liver Macrophages. *Mol. Pharmaceutics* **2016**, *13*, 3636−3647.
(17) Perillo, E.; Hervé-Aubert, K.; Allard-Vannier, E.; Falanga, A.; Galdiero, S.; Chourpa, I. Synthesis and in Vitro Evaluation of Fluorescent and Magnetic Nanoparticles Functionalized with a Cell Penetrating Peptide for Cancer Theranosis. *J. Colloid Interface Sci.* **2017**, *499*, 209−217.
(18) Ben Djemaa, S.; David, S.; Hervé-Aubert, K.; Falanga, A.; Galdiero, S.; Allard-Vannier, E.; Chourpa, I.; Munnier, E. Formulation and in Vitro Evaluation of a SiRNA Delivery Nanosystem Decorated with GH625 Peptide for Triple Negative Breast Cancer Theranosis. *Eur. J. Pharm. Biopharm.* **2018**, *131*, 99−108.
(19) Muratovska, A.; Eccles, M. R. Conjugate for Efficient Delivery of Short Interfering RNA (SiRNA) into Mammalian Cells. *FEBS Lett.* **2004**, *558*, 63−68.
(20) Oh, B.; Lee, M. Combined Delivery of HMGB-1 Box A Peptide and S1PLyase SiRNA in Animal Models of Acute Lung Injury. *J. Controlled Release* **2014**, *175*, 25−35.
(21) Sakurai, Y.; Hatakeyama, H.; Akita, H.; Oishi, M.; Nagasaki, Y.; Futaki, S.; Harashima, H. Efficient Short Interference RNA Delivery to Tumor Cells Using a Combination of Octaarginine, GALA and Tumor-Specific, Cleavable Polyethylene Glycol System. *Biol. Pharm. Bull.* **2009**, *32*, 928−932.
(22) Falanga, A.; Galdiero, M.; Galdiero, S. Membranotropic Cell Penetrating Peptides: The Outstanding Journey. *Int. J. Mol. Sci.* **2015**, *16*, 25323−25337.
(23) Galdiero, S.; Falanga, A.; Vitiello, M.; Raiola, L.; Russo, L.; Pedone, C.; Isernia, C.; Galdiero, M. The Presence of a Single N-Terminal Histidine Residue Enhances the Fusogenic Properties of a Membranotropic Peptide Derived from Herpes Simplex Virus Type 1 Glycoprotein H. *J. Biol. Chem.* **2010**, *285*, 17123−17136.
(24) Tünnemann, G.; Martin, R. M.; Haupt, S.; Patsch, C.; Edenhofer, F.; Cardoso, M. C. Cargo-Dependent Mode of Uptake and Bioavailability of TAT-Containing Proteins and Peptides in Living Cells. *FASEB J.* **2006**, *20*, 1775−1784.
(25) Selby, L. I.; Cortez-Jugo, C. M.; Such, G. K.; Johnston, A. P. R. Nanoescapology: Progress toward Understanding the Endosomal Escape of Polymeric Nanoparticles. *Wiley Interdiscip. Rev.: Nanomed. Nanobiotechnol.* **2017**, *9*, No. e1452.
(26) Trützschler, A. K.; Bus, T.; Reifarth, M.; Brendel, J. C.; Hoeppener, S.; Traeger, A.; Schubert, U. S. Beyond Gene Transfection with Methacrylate-Based Polyplexes - The Influence of the Amino Substitution Pattern. *Bioconjugate Chem.* **2018**, *29*, 2181−2194.
(27) Mishra, S.; Webster, P.; Davis, M. E. PEGylation Significantly Affects Cellular Uptake and Intracellular Trafficking of Non-Viral Gene Delivery Particles. *Eur. J. Cell Biol.* **2004**, *83*, 97−111.
(28) Jonker, C.; de Heus, C.; Faber, L.; ten Brink, C.; Potze, L.; Fermie, J.; Liv, N.; Klumperman, J. An Adapted Protocol to Overcome Endosomal Damage Caused by Polyethylenimine (PEI) Mediated Transfections. *Matters* **2017**, *3*, No. e201711000012.
(29) Schubert, U. S.; Traeger, A.; Bus, T. The Great Escape: How Cationic Polyplexes Overcome the Endosomal Barrier. *J. Mater. Chem. B* **2018**, *6*, 6904−6918.
(30) Xie, Y.; Qiao, H.; Su, Z.; Chen, M.; Ping, Q.; Sun, M. PEGylated Carboxymethyl Chitosan/Calcium Phosphate Hybrid Anionic Nanoparticles Mediated HTERT SiRNA Delivery for Anticancer Therapy. *Biomaterials* **2014**, *35*, 7978−7991.
(31) Veiseh, O.; Kievit, F. M.; Mok, H.; Ayesh, J.; Clark, C.; Fang, C.; Leung, M.; Arami, H.; Park, J. O.; Zhang, M. Cell Transcytosing Poly-Arginine Coated Magnetic Nanovector for Safe and Effective SiRNA Delivery. *Biomaterials* **2011**, *32*, 5717−5725.
(32) Oliveira, S.; van Rooy, I.; Kranenburg, O.; Storm, G.; Schiffelers, R. M. Fusogenic Peptides Enhance Endosomal Escape Improving SiRNA-Induced Silencing of Oncogenes. *Int. J. Pharm.* **2007**, *331*, 211−214.
(33) Varkouhi, A. K.; Scholte, M.; Storm, G.; Haisma, H. J. Endosomal Escape Pathways for Delivery of Biologicals. *J. Controlled Release* **2011**, *151*, 220−228.
(34) Guarnieri, D.; Muscetti, O.; Falanga, A.; Fusco, S.; Belli, V.; Perillo, E.; Battista, E.; Panzetta, V.; Galdiero, S.; Netti, P. A. Surface Decoration with GH625-Membranotropic Peptides as a Method to Escape the Endo-Lysosomal Compartment and Reduce Nanoparticle Toxicity. *Nanotechnology* **2015**, *26*, No. 415101.

DOI: 10.1021/acs.biomac.9b00637
Biomacromolecules 2019, 20, 3076−3086

Supporting Information

gH625 cell-penetrating peptide promotes the endosomal escape of nanovectorized siRNA in a triple negative breast cancer cell line

*Sanaa Ben Djemaa[1], Katel Hervé-Aubert[1], Laurie Lajoie[2,3], Annarita Falanga[4], Stefania Galdiero[5], Steven Nedellec[6], Martin Soucé[1], Emilie Munnier[1], Igor Chourpa[1], Stéphanie David[1], Emilie Allard-Vannier[1]**

[1] EA6295 Nanomédicaments et Nanosondes, University of Tours – Tours, France
[2] EA7501 Groupe Innovation et Ciblage Cellulaire, Equipe Fc Récepteurs, Anticorps et MicroEnvironnement, University of Tours – Tours, France
[3] Plateforme Scientifique et Technique, Analyse des systèmes biologiques département des cytométries, University of Tours – Tours, France
[4] Department of Agricultural Sciences- University of Naples "Federico II", Via Università 100, 80055, Portici, Italy
[5] Department of Pharmacy, CIRPEB - University of Naples "Federico II", Via Mezzocannone 16, 80134, Napoli, Italy
[6] Plateforme microPICell, SFR santé François Bonamy-IRSUN, 8 quai Moncousu, BP 70721, 44007 Nantes Cedex

* Corresponding author. E-mail address: emilie.allard@univ-tours.fr (E. Allard-Vannier)

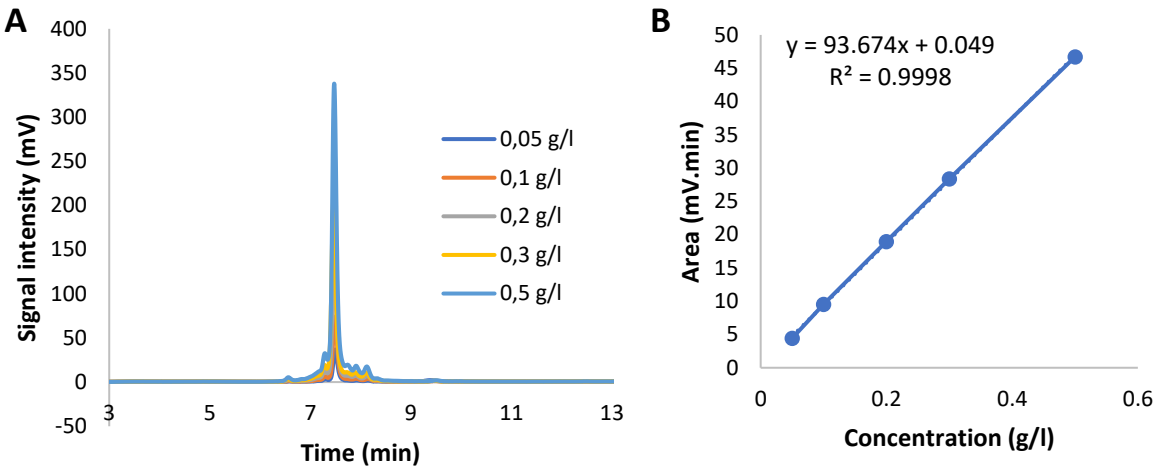

Figure S1. A) HPLC chromatograms of gH625 solutions at different concentrations (from 0.05 g/l to 0.5 g/l). B) Calibration curve for the quantification of free peptide obtained from the analysis of gH625 solutions.

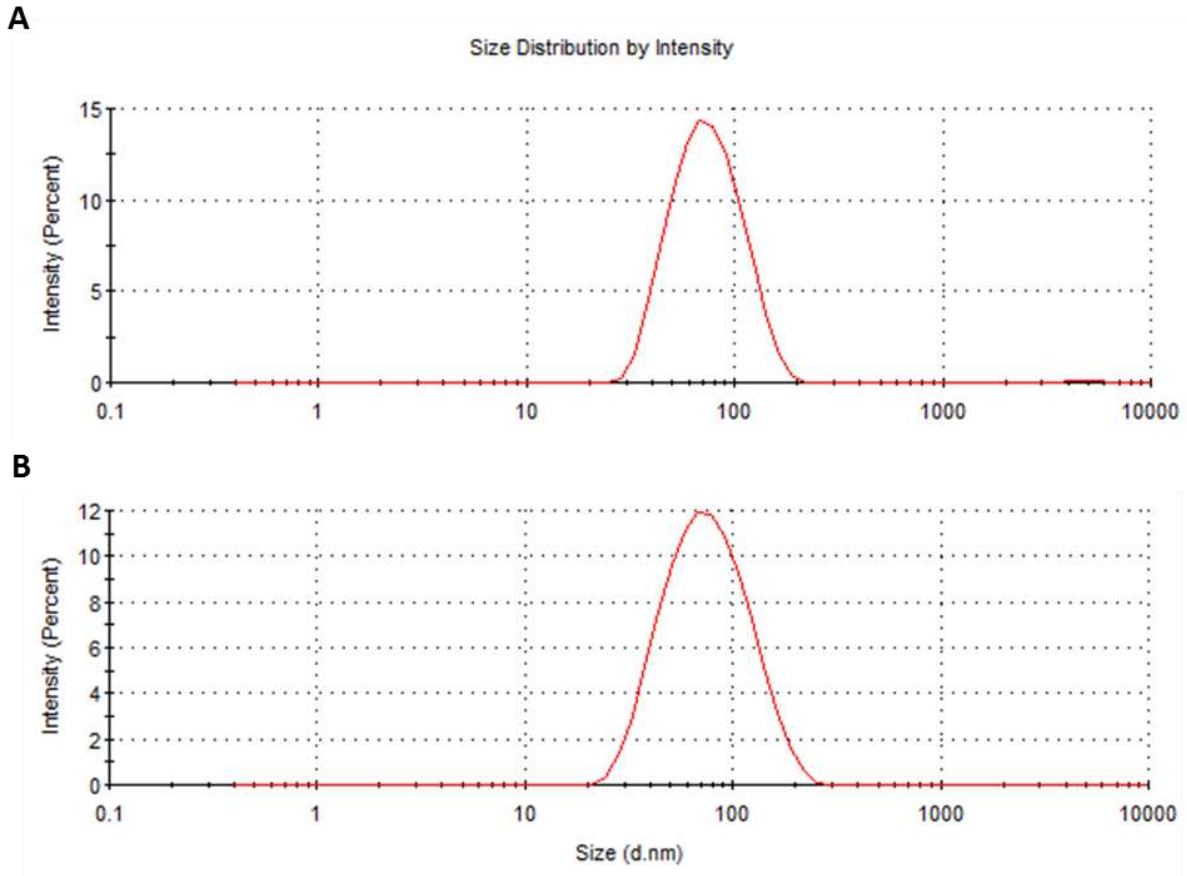

Figure S2. Size distribution profile of A) S-FNP and B) CS-FNP

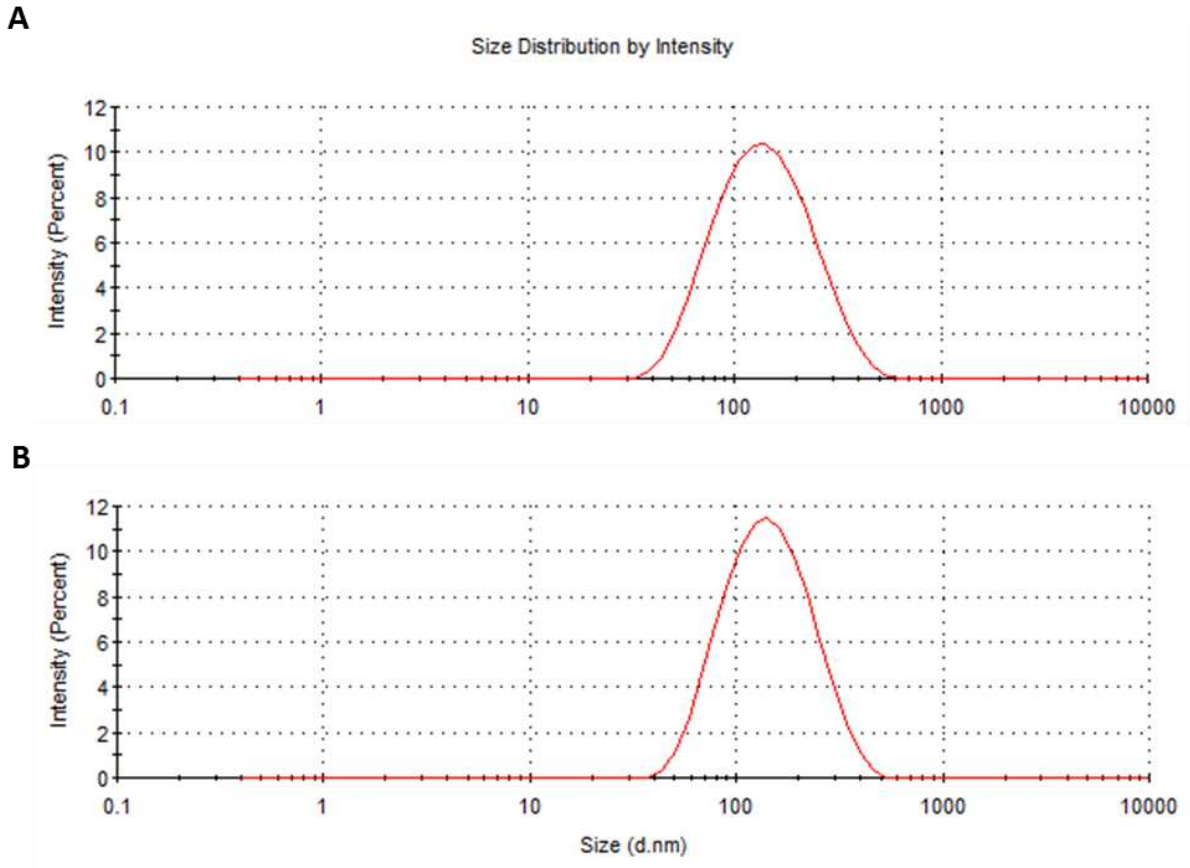

Figure S3. Size distribution profile of A) S-MSN and B) CS-MSN

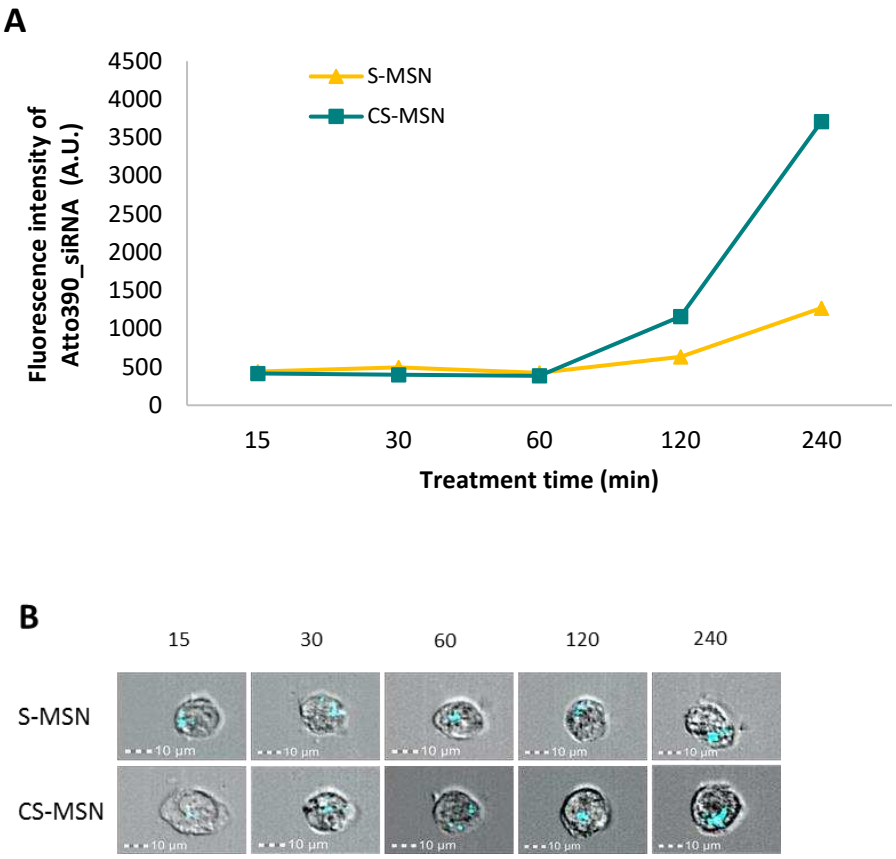

Figure S4. Uptake kinetics of CS-MSN and S-MSN in MDA-MB-231 cells. Intracellular fluorescence intensity of Atto390 conjugated to siRNA loaded in S-MSN or CS-MSN was monitored by flow imaging after the incubation of nanovectors for 15, 30, 60, 120 and 240 min: A) fluorescence intensity, B) images of intracellular fluorescence in cells.

Quatrième partie : Efficacité du nanovecteur de siRNA sur le gène cible codant pour la protéine Bcl-xL

1. Introduction

Durant les premières étapes de développement d'un nanovecteur de siRNA pour le traitement du cancer, il est très commun d'utiliser un siRNA modèle qui cible un gène rapporteur. L'utilisation de ce siRNA modèle apporte souvent de la facilité pour l'optimisation de la formulation du nanovecteur et sert en même temps à fournir une preuve de concept pour les étapes suivantes. Dans ces travaux de thèse, nous avons sélectionné le gène GFP (green fluorescent protein) en tant que gène rapporteur et les siRNA anti-GFP en tant que siRNA modèle pour optimiser la formulation des CS-MSN et évaluer l'efficacité de ce nanovecteur *in vitro*. Cependant, il est important de confirmer ces résultats et de vérifier l'efficacité des CS-MSN sur une protéine cible, impliquée dans le processus tumoral.

Dans le contexte du cancer, généralement, le choix idéal se tourne vers les oncoprotéines ou les mutants responsables du développement du cancer en question. Cependant, dans certains cas, la croissance tumorale est due à une dérégulation de l'expression de protéines physiologiques non mutées, impliquées dans la survie de la cellule ou dans la régulation du cycle cellulaire (45–47). Par exemple, une dérégulation de l'apoptose, qui joue un rôle indispensable dans le développement et le maintien de l'homéostasie dans tous les organismes multicellulaires, peut être à l'origine d'un cancer (107). En effet, la surexpression d'une protéine anti-apoptotique bloque la mort cellulaire et favorise l'amplification des cellules cancéreuses et la croissance de la tumeur. En se basant sur la littérature, nous avons orienté nos recherches vers une protéine surexprimée dans les cellules de cancer du sein triple négatif, la protéine Bcl-xL (pour B-cell lymphoma-extra large).

Cette protéine, appelée aussi Bcl2-like1 ou BCL2L1, est une protéine anti-apoptotique appartenant à la famille Bcl-2. Le gène codant pour cette protéine est localisé sur le chromosome 20 (au niveau de la bande q11.21). Cette protéine est de 26 kDa et est constituée de 233 acides aminés répartis sur quatre domaines BH (Bcl-2 homology domaine) et un segment transmembranaire (TM) (108). La protéine Bcl-xL est localisée principalement au niveau de la membrane mitochondriale. Elle joue un rôle majeur dans la répression de l'apoptose. En effet, elle bloque la signalisation cellulaire qui active l'apoptose en bloquant les protéines pro-apoptotiques Bax et Bak, en empêchant la libération du cytochrome c et l'activation des caspases responsables de l'induction de la mort cellulaire (109). De plus, plusieurs études ont démontré l'implication de la surexpression de cette protéine dans la résistance à la

chimiothérapie (110,111). Ainsi, le ciblage de cette protéine pourrait être avantageux pour le traitement ou l'amélioration du traitement du cancer du sein triple négatif.

Dans la première partie de cette étude, les caractéristiques des CS-MSN préparés avec les siRNA anti-Bcl-xL pour une utilisation *in vitro* sont vérifiées. De plus, la formulation des nanovecteurs a été adaptée pour une future application *in vivo*. En se basant sur la littérature et sur des études antérieures effectuées au sein de notre laboratoire, nous avons choisi d'utiliser une dose en siRNA de 12,5 µg/ souris. Pour une injection par voie intraveineuse, l'osmolarité de la formulation doit être de 300 ± 20 mosm/l. Les caractéristiques physico-chimiques des nanovecteurs sont vérifiées après préparation dans ces nouvelles conditions.

L'évaluation *in vitro* de l'efficacité de la transfection des siRNA ciblant un gène non rapporteur, ici Bcl-xL, et de leur action se fait par l'étude à l'échelle moléculaire et/ ou à l'échelle cellulaire des effets induits par l'inhibition de l'expression de ce gène cible. Nous avons évalué l'effet des siRNA à l'échelle cellulaire en mesurant la viabilité des cellules MDA-MB-231 après traitement avec les CS-MSN ciblant Bcl-xL pour déterminer l'efficacité de ces nanovecteurs à induire la mort cellulaire en réponse à l'inhibition de la protéine anti-apoptotique Bcl-xL. Pour réaliser l'évaluation à l'échelle moléculaire, nous avons choisi de regarder l'effet des CS-MSN préparés avec les siRNA anti-Bcl-xL sur l'expression i) de l'ARNm et ii) de la protéine Bcl-xL en utilisant les techniques RT-qPCR (reverse transcription quantitative polymerase chain reaction) et Western Blot, respectivement.

La RT-qPCR représente une technique robuste et sensible pour quantifier l'expression d'un ARNm. La réalisation d'une RT-qPCR nécessite plusieurs étapes préparatives et expérimentales dans lesquelles plusieurs paramètres sont à considérer. Ces étapes peuvent être groupées en deux parties : 1) la rétrotranscription : il s'agit de la production de l'ADN complémentaire (ADNc) à partir d'une séquence d'ARN. 2) la qPCR qui consiste à amplifier le nombre de séquences d'ADNc produit et à quantifier cette amplification au cours du temps (en temps réel). Pour la mise en place de cette technique, quelques paramètres doivent être optimisés tels que la quantité d'ARN à rétrotranscrire, l'efficacité de chaque étape (extraction, RT, qPCR, …), l'efficacité des amorces. Une fois la RT-qPCR mise en place et le protocole expérimental validé, cette technique sera utilisée pour l'évaluation de l'expression de l'ARNm Bcl-xL après traitement des cellules avec les CS-MSN véhiculant les siRNA anti-Bcl-xL.

L'étape suivante après les études *in vitro* est l'évaluation de l'efficacité des CS-MSN *in vivo*. Elle nécessite la mise en place d'un modèle de cancer du sein triple négatif chez la souris.

2. Matériels et méthodes

2.1. Formulation et caractérisation des CS-MSN

2.1.1. Formulation des CS-MSN

Les CS-MSN sont préparés selon le protocole optimisé et décrit dans la publication 2 (112). La quantité des composants utilisés dans la formulation est définie par des rapports qui lient chaque composant aux siRNA. Le rapport de masse (m/m ; MR) fer/siRNA qui définit la quantité de CS-FNP est fixé à 10. Le contenu en chitosan (Cs, MW 110-150 kDa ; dégrée d'acétylation : ≤ 40 mol.%) et en poly-L-arginine (PLR, MW 15-70 kDa) (Sigma-Aldrich Chimie GmbH, St. Quentin Fallavier, France) est défini par le rapport N/P. D'abord, les siRNA anti-Bcl-xL (Sigma-Aldrich, St. Quentin Fallavier, France) (TableauII) sont pré-complexés avec la poly-L-arginine à un rapport N_{PLR}/P de 2 et sont rajoutés au mélange de chitosan (N_{CS}/P = 30) et de CS-FNP pour formuler les CS-MSN.

Tableau II. Séquences des siRNA utilisées

Séquence N°	Séquence des siRNA utilisées
Séquence 1	5'-CUGAUUGGUGCAACCCUUA/UAAGGGUUGCACCAAUCAG-3'
Séquence 2	5'-GGAUACAGCUGGAGUCAGU/ACUGACUCCAGCUGUAUCC-3'
Séquence 3	5'-GACUGUGGCCGGCGUGGUU/AACCACGCCGGCCACAGUC-3'

Pour une future application *in vivo*, la dose à injecter est fixée à 12,5 µg de siRNA par souris dans un volume de 150 µl (concentration en siRNA de 84 µg/ml, soit 6,265 µM). Le protocole de préparation des nanovecteurs est le même que celui décrit pour l'application *in vitro*. La formulation est préparée à une concentration finale en mannitol de 4,5 % (Sigma-Aldrich, St Louis, Etats-Unis) pour être isotonique au sang.

2.1.2. Mesure de la taille et du potentiel zêta

Le diamètre hydrodynamique (HD), l'indice de polydispersité (PDI) et le potentiel zêta (ZP) des nanovecteurs sont déterminés à l'aide d'un Nanosizer ZS (Zetasizer®, malvern Instruments, Malvern, Royaume-Uni). Les mesures sont effectuées à 25°C après dilution dans une solution de $NaNO_3$ à 0,01 M. Les valeurs moyennes de HD présentées sont basées sur l'intensité.

2.1.3. Evaluation de la complexation : électrophorèse sur gel d'agarose

L'électrophorèse sur gel d'agarose est utilisée pour vérifier la complexation des siRNA dans les nanovecteurs. Une solution d'héparine à une concentration finale de 3 mg/ml est utilisée pour libérer les siRNA et contrôler leur intégrité. Avant le dépôt sur le gel, un tampon de charge (Agarose gel loading dye 6X, Fisher, Bioreagents®, Illkirch, France) est ajouté aux échantillons. Un gel d'agarose (1 % m/v) est préparé contenant 0,01 % (v/v) de bromure d'éthidium pour visualiser les siRNA libres. La migration des échantillons est réalisée dans un tampon Tris-acetate-EDTA (TAE) 1X (Acros Organics, Geel, Belgique) pendant 15 min à 150V. L'imagerie UV est utilisée pour révéler le gel à l'aide d'un imageur Fusion-Solo.65.WL (Vilbert Lourmat, Marne-la-Vallée, France) et du logiciel Evolutioncapt.

2.1.4. Mesure de l'osmolarité

L'osmolarité des formulations de nanovecteurs est mesurée après préparation, sur un volume de 100 µl à une concentration en siRNA de 6,265 µM, à l'aide d'un micro-osmomètre (Löser Messtechnik, Berlin, Germany) après calibration avec de l'eau distillée et une solution de NaCl de 0,9 %.

2.2. Evaluation de l'efficacité des CS-MSN à transfecter les siRNA Bcl-xL *in vitro*

2.2.1. Culture cellulaire

Des cellules de cancer du sein triple négatif de la lignée MDA-MB-231 (ECACC, Salisbury, Royaume-Uni) sont cultivées dans le milieu DMEM (Dulbecco's modified Eagle medium) (Gibco®, Life Technologies, Paisley, Royaume-Uni) supplémenté avec 10 % de sérum de veau fœtal (Eurobio, Les Ulis, France), des acides aminés non-essentiels 1X (HyClone Laboratories, Logan, Utah) et 1 % d'antibiotiques (peniciline/streptomycin) (Gibco®, Life Technologies, Paisley, Royaume-Uni) à 37°C dans une atmosphère humide enrichie de 5 % de CO_2.

2.2.2. Transfection

Des cellules MDA-MB-231 sont ensemencées 24 h avant la transfection à une densité de $2x10^5$ cellules par puits dans une plaque 6 puits. Les S-MSN et les CS-MSN sont préparés avec des siRNA anti-Bcl-xL selon le protocole de formulation. Les nanovecteurs sont ajoutés aux cellules à une concentration en siRNA de 50 nM, 100 nM ou 200 nM pendant 4 h. Le milieu

de culture est changé et les cellules sont réincubées jusqu'à 72 h. Des cellules non traitées sont utilisées comme un contrôle négatif et des cellules traitées avec l'agent de transfection commerciale l'Oligofectamine™ (50 nM de siRNA) (Invitrogen, Thermo Fisher Scientific, Paisley, Royaume-Uni) sont utilisées comme un contrôle positif.

2.2.3. Mise au point de la rétrotranscription- PCR quantitative (RT-qPCR)

2.2.3.1. Rétrotranscription

La quantification de l'expression de l'ARNm Bcl-xL par RT-qPCR nécessite trois étapes. La première consiste à l'extraction des ARN totaux des cellules en utilisant le kit « NucleoSpin® RNA » (Macherey-Nagel) et en suivant le protocole détaillé dans le guide de l'utilisation. Après l'extraction, les ARN sont quantifiés à l'aide d'un spectrophotomètre de type Nanodrop 2000c (ThermoFisher scientific, Wilmington, Etats-Unis). La deuxième étape est la rétrotranscription de l'ARN en ADN complémentaire (ADNc). Cette étape est réalisée en utilisant le kit « RevertAid First Strand cDNA Synthesis » (ThermoFisher scientific) et en suivant le protocole du TableauIII :

Tableau III. Protocole de la rétrotranscription

Quantité d'ARN		1µg
Amorce Oligo(dT)$_{18}$		1 µl
Volume d'eau		**QSP 12 µl**
Mix	Tampon de Réaction 5X	4 µl
	RiboLock RNase inhibitor (20 U/µl)	1 µl
	dNTP mix 10 mM	2 µl
	RevertAid (200 U/µl)	1µl
Volume final		**20 µl**

Avant de rajouter le « Mix », les ARN sont incubés avec les amorces Oligo(dT)$_{18}$ à 65 °C pendant 5 min puis mises sur glace. Ensuite, le mix est rajouté et les échantillons sont incubés pendant 60 min à 42°C. Enfin, la réaction est arrêtée par une incubation à 65°C pendant 5 min.

L'étape de la rétrotranscription est contrôlée par une amplification par PCR en utilisant les amorces des gènes Bcl-xL et GAPDH selon le protocole détaillé dans le TableauIV et le programme du TableauV.

Tableau IV. Protocole de la PCR

ADNc de la RT		0,5 µl
Tampon Dream Taq10X		5 µl
dNTP mix 10 mM		1 µl
Amorces	Forward (10 µM)	1,5 µl
	Reverse (10 µM)	1,5 µl
Dream Taq		0,2 µl
Eau « nuclease free »		20,3 µl
Volume total		**25 µl**

Tableau V. Programme de la PCR

Etapes	**Température (°C)**	**Durée**	**Nombre des cycles**
Dénaturation initiale	95	2 min	1
Dénaturation	95	20 s	40
Hybridation des amorces	60	20 s	
Elongation	72	20 s	

L'amplification d'ADN par PCR est vérifiée par électrophorèse sur gel d'agarose. Un volume de 15 µl de produit de PCR de chaque échantillon est déposé sur un gel d'agarose à 1 %. La migration est faite dans un tampon TAE 1X pendant 25 min à 120 V.

2.2.3.2. Courbes de calibration

L'établissement des courbes de calibration nécessite trois étapes principales :

- La purification des ADN en utilisant le kit « Nucleospin™ gel and PCR clean-up » (Machery-Nagel) selon le protocole détaillé dans le manuel d'utilisation.
- La préparation d'une gamme d'ADN purifié des dilutions de 1 log : une dilution en cascade de l'ADN est réalisée pour obtenir 10^3, 10^4, 10^5, 10^6 ou 10^7 molécules d'ADN par échantillon.
- La réalisation de la qPCR : à partir des ADNc obtenus, une PCR quantitative (qPCR) est réalisée en utilisant le « 2X Takyon for SYBR Assay - No ROX » (Takyon™, Eurogentec, Seraing, Belgique) et des amorces pour les gènes Bcl-xL et GAPDH (TableauVI, N°1 : Sigma-Aldrich, St. Quentin Fallavier, France ; N°2 : Eurogentec, Seraing, Belgique). La réaction de la polymérisation est faite dans un thermocycleur CFX96™ Real-Time PCR Detection Systems (C1000 Touch™, Bio-Rad) selon le protocole du TableauVII et le programme du TableauVIII.

L'efficacité des amorces est calculée en utilisant l'équation suivante :

$$Efficacité = (10^{-\left(\frac{1}{a}\right)} - 1) * 100$$

a = la pente de la courbe

Tableau VI. Séquences des amorces de gènes Bcl-xL et GAPDH utilisées

Gène	N°	Séquences des amorces
Bcl-xL	1	5'-ATCTCTTTCTCTCCCTTCAG/CTTTCTGGGAAAGCTTGTAG-3'
	2	5'- TTCAGTGACCTGACATCCCA/ TCCACAAAAGTATCCCAGCC-3'
GAPDH	1	5'-CTTTTGCGTCGCCAG/TTGATGGCAACAATATCCAC-3'
	2	5'- CAAAAGGGTCATCATCTCTGC/ AGTTGTCATGGATGACCTTGG-3'

Tableau VII. Protocole de la qPCR

		Pour 1 puits
Takyon		3,75 µl
Amorces 10 µM, concentration finale à 150 nM dans les 15 µl	Forward	0,225 µl
	Reverse	0,225 µl
Eau		4,8 µl
Total mix		**9 µl**
Echantillon		**6 µl**

Tableau VIII. Programme de la qPCR

Etapes	**Température (°C)**	**Durée**	**Nombre de cycle**
Activation de Takyon	95	3 min	1
Dénaturation	95	10 s	X 40
Hybridation et élongation	60	40 s	

L'efficacité des CS-MSN à inhiber l'expression de l'ARNm Bcl-xL est évaluée par le calcul du taux d'expression relative de ce dernier par rapport à l'ARNm GAPDH.

$\Delta Ct\ (X) = Ct\ (X_{Bcl\text{-}xL}) - Ct\ (X_{GAPDH})$

$\Delta\Delta Ct\ (X) = \Delta Ct\ (X) - \Delta Ct\ (Ctrl)$

Quantification relative (RQ) = $2^{-\Delta\Delta Ct}$

Avec : X : échantillon ; Ctrl : les cellules non traitées

La RQ de Ctrl (Cellules) = 1

2.2.4. Western Blot

La détection de la protéine Bcl-xL est réalisée en utilisant une technique semi-quantitative, la technique de Western Blot. Cette expérience nécessite une extraction protéique, suivi d'une séparation des protéines selon leurs poids moléculaires par migration sur un gel de

polyacrylamide dans des conditions dénaturantes (SDS-PAGE), puis un transfert des protéines séparées sur une membrane de nitrocellulose et leur détection en utilisant une réaction immune spécifique de type anticorps-antigène.

Pour extraire les protéines, les cellules sont lavées avec de l'HBSS (sans Ca^{2+} et Mg^{2+}) et lysées pendant 30 minutes à 4°C avec un tampon de lyse (Tampon RIPA, Protease Inhibitor Cocktail (PIC)) (Thermo Fisher Scientific, Meridian Rd, Rockford, Etats-Unis). La concentration des protéines est déterminée par un dosage colorimétrique avec le kit Bicinchoninic Acid Kit for Protein Determination (BCA, Sigma-Aldrich Chimie GmbH, St. Quentin Fallavier, France). Afin de déterminer la concentration, une gamme d'étalonnage de BSA (Bovine Serum Albumine) est utilisée. La mesure de l'absorbance de la gamme et des échantillons est faite à l'aide d'un lecteur de microplaques BIO-TEK EL800® et du logiciel KC-junior V1.4.0.

Pour la séparation par SDS-PAGE, 20 µg de protéines de chaque échantillon sont déposés sur un gel de polyacrylamide 4 – 12 % (Life Technologies Corporation, Carlsbad, CA) en présence d'un réducteur (Sample Reducing Agent (10X), novex by life technologies, Carlsbad, CA) et d'un tampon de charge (LDS Sample Buffer (4X), novex by life technologies, Carlsbad, CA). La migration des échantillons se fait dans un tampon MES-SDS 1X pendant 45 min à 120 V. Le transfert des bandes protéiques sur une membrane en nitrocellulose (Life Technologies Corporation, Carlsbad, CA) est réalisé dans un iBlot® 2 (life technologies, Carlsbad, CA). Ensuite, la membrane est incubée dans une solution de lait écrémé TBS-Tween 20 1X à 5 % pendant 1 h à température ambiante et sous agitation constante pour la saturation des sites non spécifiques. Après la saturation, la membrane est incubée avec l'anticorps primaire anti-Bcl-xL (Abcam, Cambridge, Royaume-Uni) ou anti-GAPDH (ThermoFisher scientific, Rockford, Etats-Unis) dilué au 1/1000 dans une solution de lait_TBS-Tween 20 1X (5 %) pendant 2 h à température ambiante sous agitation constante. Après lavage, la membrane est incubée avec un anticorps secondaire IgG anti-lapin couplé à l'HRP (ThermoFisher scientific, Rockford, Etats-Unis) dilué au 1/1000 dans une solution de lait_TBS-Tween 20 1X (5 %) pendant 1 h sous agitation constante. Après lavage, une solution d'ECL (Enhanced ChemiLuminescence) est déposée sur la membrane pendant 5 min. Les bandes obtenues sont visualisées grâce à un système d'imagerie par chimioluminescence (imageur Fusion-Solo.65.WL, Vilbert Lourmat, Marne-la-Vallée, France). L'abondance de la protéine Bcl-xL dans chaque condition est normalisée à l'expression de la GAPDH et est comparée à celle des cellules contrôles non traitées.

2.2.5. Test de cytotoxicité

Les cellules MDA-MB-231 sont ensemencées dans des plaques 96 puits à une densité de $3x10^3$ cellules par puits dans le milieu de culture. 24 heures plus tard, les cellules sont traitées avec les CS-MSN ou l'Oligofectamine™ formulés avec les siRNA anti-Bcl-xL ou avec les siRNA anti-Bcl-xL non nanovectorisés à une concentration de 50 nM. Des cellules non traitées ou traitées avec une solution de H_2O_2 sont utilisées comme contrôles négatif et positif, respectivement. Les cellules sont incubées pendant 24 h, 48 h, 72 h ou 96 h à 37°C. Après traitement, le réactif WST-1® (Sigma Aldrich CHIMIE, Saint-Quentin Fallavier, France) est rajouté dans chaque puits, et la mesure de l'absorbance à 450 nm est effectuée après 2 h d'incubation à 37°C à l'aide d'un micro-spectrophotomètre (BIO-TEK) et du logiciel KC-junior v1.40. Le pourcentage de viabilité cellulaire est calculé selon l'équation indiquée dans la publication 2 (112).

2.3. Mise en place d'un modèle orthotopique de cancer du sein triple négatif chez la souris

2.3.1. Tumorisation des souris

Des souris femelles Balb/c nude âgées de 6 à 7 semaines (janvier Labs, Saint Berthevin, France) sont anesthésiées par inhalation d'un mélange isoflurane/dioxygène. $2x10^6$ cellules MDA-MB-231 préparées dans une matrice de Matrigel® (Corning GmbH HQ, Wiesbaden, Allemagne) (v/v = 1/1, volume final à injecter par souris = 100 µl) sont injectées en sous-cutané au niveau du tissu graisseux de la glande mammaire. Les souris sont placées dans une cage de réveil et se réveillent spontanément.

Les souris sont surveillées pendant la période de la croissance tumorale et leur poids est mesuré régulièrement.

2.3.2. Echographie de contraste

Après 4 semaines de tumorisation, la vascularisation des tumeurs est évaluée en utilisant l'échographie. Un agent de contraste à base de microbulles (Vevo Micromarkers, VIsualsonics Fujifilm, Amsterdam, Pays-Bas) permettant de visualiser le flux sanguin est injecté (70 µl) par voie intraveineuse. La distribution de cet agent de contraste est détectée par un échographe (Vevo 2100, Visualsonics Fujifilm, Amsterdam, Pays-Bas) et en utilisant le logiciel VevoCQ (Visualsonics Fujifilm, Amsterdam, Pays-Bas).

2.3.3. Mesure des masses et des volumes des tumeurs

Après 6 semaines de croissance tumorale, les souris sont sacrifiées est les tumeurs sont récupérées. La longueur et la largeur de chaque tumeur sont mesurées à l'aide d'un pied à coulisse et sont utilisées pour le calcul du volume de la tumeur. La masse de la tumeur est déterminée à l'aide d'une balance de précision (Denver Instrument GmbH, Goettingen, Germany).

3. Résultats

3.1. Formulation et caractérisation des nanovecteurs de siRNA anti-Bcl-xL

La formulation des CS-MSN avec les siRNA anti-Bcl-xL est effectuée selon le protocole optimisé dans la première partie de ces travaux de thèse (112). Pour les formulations destinées aux analyses *in vitro*, la taille des CS-MSN est d'environ 154 nm avec un indice de polydispersité inférieur à 0,3. La charge de surface des CS-MSN est légèrement positive et est de 12 mV (Tableau). L'évaluation de la complexation des siRNA par électrophorèse sur gel d'agarose ne montre aucune bande fluorescente dans le cas des CS-MSN. Cependant, en présence d'héparine, une bande fluorescente est détectée et elle apparait à la même intensité que la bande contrôle des siRNA libres (Figure10 A). Ces résultats montrent que l'utilisation des siRNA anti-Bcl-xL ne modifie pas la taille des CS-MSN comparé aux siRNA contrôles utilisés dans les premières parties de ces travaux de thèse. De plus, la complexation de ces siRNA anti-Bcl-xL est parfaite avec une bonne balance entre la rétention et la libération.

Pour une future administration *in vivo*, des CS-MSN sont préparés à une concentration en siRNA de 6,265 µM. Les caractéristiques physico-chimiques des nanovecteurs ainsi que la complexation des siRNA sont vérifiés dans les nouvelles conditions. La mesure de la taille des CS-MSN montre une valeur de 165 nm avec un PDI d'environ 0,3 et un potentiel zêta de 17 mV (TableauIX). La vérification de la complexation des siRNA dans les CS-MSN par électrophorèse sur gel d'agarose ne montre aucune bande fluorescente. Cependant, en présence d'héparine, une bande fluorescente, à la même intensité que la bande contrôle des siRNA libres, est détectée (Figure10 B). Ainsi, la formulation des CS-MSN à une concentration plus élevée et l'utilisation d'une solution de mannitol n'affectent ni la taille ni le potentiel zêta des CS-MSN ni la complexation des siRNA.

Tableau IX. Taille, indice de polydispersité (PDI), potentiel zêta (ZP) et osmolarité des CS-MSN préparés pour une application *in vitro* ou *in vivo*.

Application	Concentration en siRNA	Taille (nm)	PDI	Potentiel zêta (mV)	Osmolarité (mosm/l)
In vitro	50 nM	154 ± 19	0,28 ± 0,05	12 ± 2	-
In vivo	6,265 µM	165 ± 23	0,31 ± 0,05	17,5 ± 1,6	296 ± 10

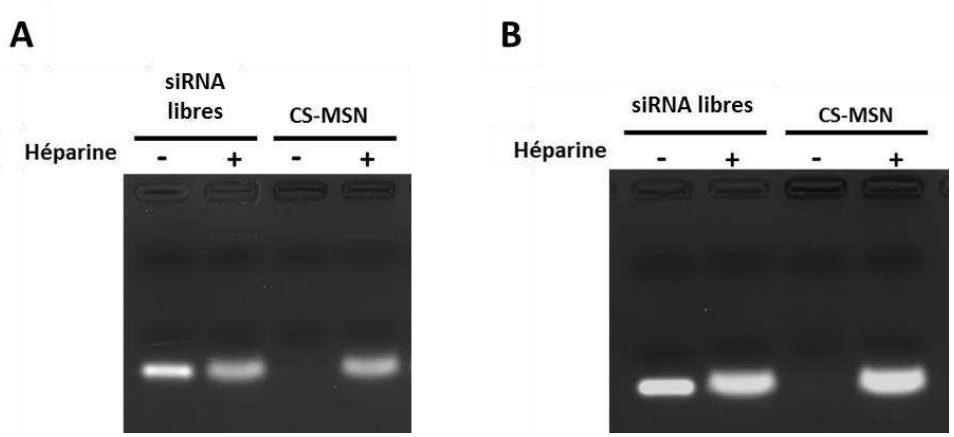

Figure 10. Gel d'agarose pour évaluer la complexation des siRNA dans les CS-MSN et la libération des siRNA en présence de la solution d'héparine (A) pour une application *in vitro* ou (B) *in vivo*.

3.2. Mise au point de la technique de RT-qPCR pour évaluer l'efficacité de la transfection

Pour utiliser la RT-qPCR dans l'évaluation de l'efficacité des CS-MSN, il est nécessaire de mettre en place la technique et le protocole expérimental.

3.2.1. La rétrotranscription

Après l'extraction d'ARN des cellules MDA-MB-231 non-traitées, trois quantités d'ARN sont testées pour la rétrotranscription : 500 ng, 1 µg et 2 µg. A la fin de cette réaction, une PCR est réalisée pour vérifier l'efficacité de la rétrotranscription des ARN en ADNc et l'amplification en utilisant des amorces pour le gène cible Bcl-xL et le gène contrôle GAPDH. Le produit obtenu par PCR est analysé en utilisant l'électrophorèse sur gel d'agarose. La Figure11 montre la présence de bandes fluorescentes à des intensités comparables pour toutes les quantités d'ARN utilisées. Cela indique que les quantités d'ARN utilisées sont suffisantes pour être détectées, que la rétrotranscription des ARN en ADNc est efficace et que les amorces utilisées permettent l'amplification de l'ADNc obtenu par PCR.

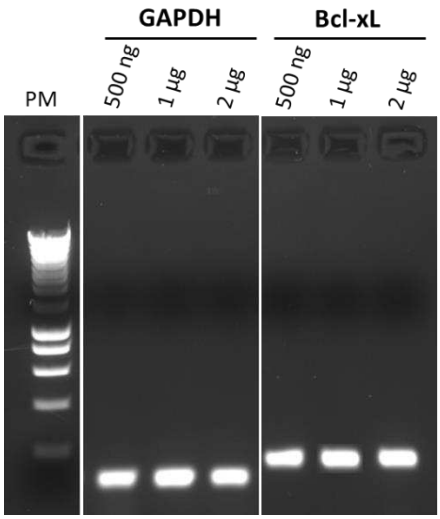

Figure 11. Gel d'agarose pour vérifier la rétrotranscription des ARN en ADNc et l'amplification par PCR.

3.2.2. Courbes de calibration

Une courbe de calibration est établie pour chaque gène (Bcl-xL et GAPDH) pour vérifier l'efficacité des amorces et pour permettre la quantification des ARN par qPCR. Après l'amplification par PCR, la purification de l'ADN obtenu et sa quantification, une électrophorèse sur gel d'agarose est réalisée pour vérifier l'amplification (Figure12). A partir des résultats de la qPCR de la gamme de calibration obtenue, les courbes de calibration sont tracées (Figure13) et l'efficacité de chaque amorce est calculée. L'amplification des ADNc des gènes Bcl-xL et GAPDH en utilisant les amorces N°1 est confirmée. Cependant, la qPCR montre des résultats non reproductibles avec des courbes de calibration présentant un coefficient de détermination R^2 de 0,9015 et 0,4244 pour Bcl-xL et GAPDH, respectivement (Figure13 A et B). Ces résultats indiquent que les amorces utilisées ne sont pas efficaces.

L'utilisation des amorces N°2, montre des résultats assez reproductibles avec une efficacité calculée de 99 % pour les amorces de gène Bcl-xL et de 107 % pour le gène GAPDH. Généralement, pour les amorces PCR une efficacité entre 90 % et 110 % est considérée comme étant acceptable (113). Donc, les amorces N°2 pour Bcl-xL et GAPDH sont choisies pour les expériences de qPCR.

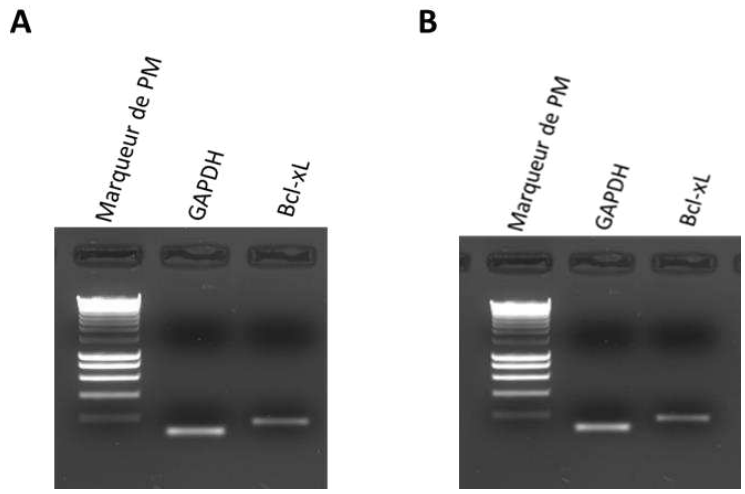

Figure 12. Gel d'agarose pour vérifier l'amplification de l'ADN par PCR en utilisant les amorces A) N°1 et B) N°2.

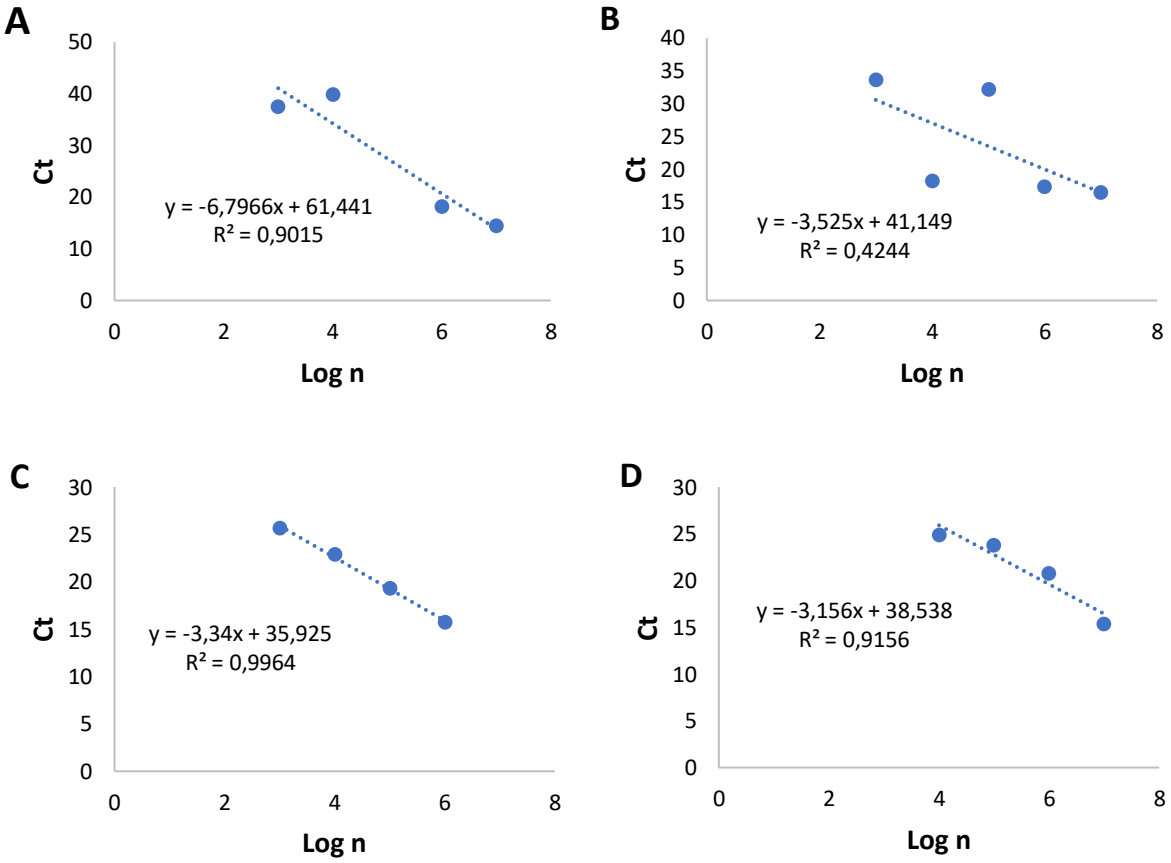

Figure 13. Courbes de calibration des amorces N°1 des gènes A) Bcl-xL et B) GAPDH et des amorces N°2 des gènes C) Bcl-xL et D) GAPDH

3.3. Choix de la séquence de siRNA

Pour avoir une efficacité de transfection élevée, le choix de la séquence de siRNA est important. Pour cela, dans un premier temps, nous avons commencé par évaluer, à l'aide de la technique Western Blot, l'efficacité de trois séquences de siRNA séparément et le mélange de ces trois séquences à inhiber l'expression de la protéine Bcl-xL en utilisant un agent de transfection commercial, l'Oligofectamine™. Comme présenté dans la Figure14, l'expression de la protéine Bcl-xL est inhibée de 30 à 50 % avec toutes les séquences de siRNA. Il semble que la séquence N°3 de siRNA est un peu plus efficace à inhiber la protéine Bcl-xL.

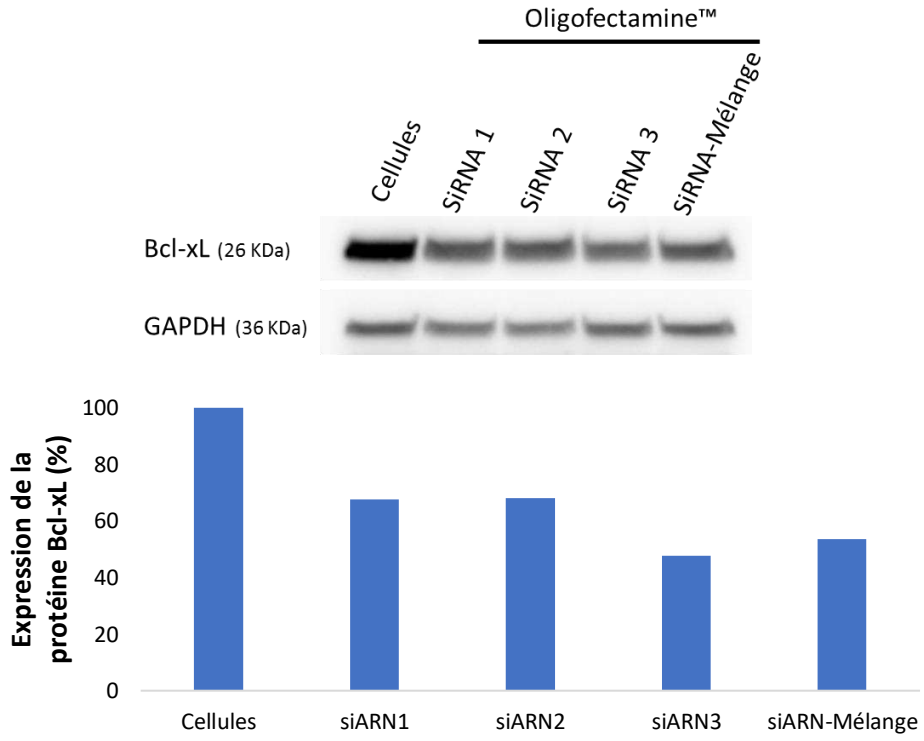

Figure 14. Expression de la protéine Bcl-xL normalisée par rapport à l'expression de la protéine GAPDH dans des cellules MDA-MB-231 traitées ou non avec l'Oligofectamine™ préparé avec les différentes séquences des siRNA (1, 2 ou 3) ou le mélange de trois séquences, à une concentration en siRNA de 50 nM

Pour valider les résultats obtenus par Western Blot, les mêmes conditions sont testées par RT-qPCR. Comme présenté dans la Figure15, l'expression de l'ARNm Bcl-xL est inhibée d'environ 60 % (de 1 à 0,4) avec toutes les séquences de siRNA. Aucune différence significative entre l'efficacité des séquences n'est mise en évidence. Cela montre que les trois séquences de siRNA ont la même efficacité à inhiber l'ARNm Bcl-xL et que le mélange de ces séquences

n'améliore pas cette efficacité. Ces résultats de RT-qPCR, ne mettent en avant aucune séquence de siRNA.

En se basant sur les résultats obtenus, aucune séquence préférentielle n'a été mise en évidence. Cependant, le résultat de Western Blot suggère que la séquence N°3 pourrait être un peu plus efficace. Donc, cette dernière est choisie pour évaluer l'efficacité des nanovecteurs.

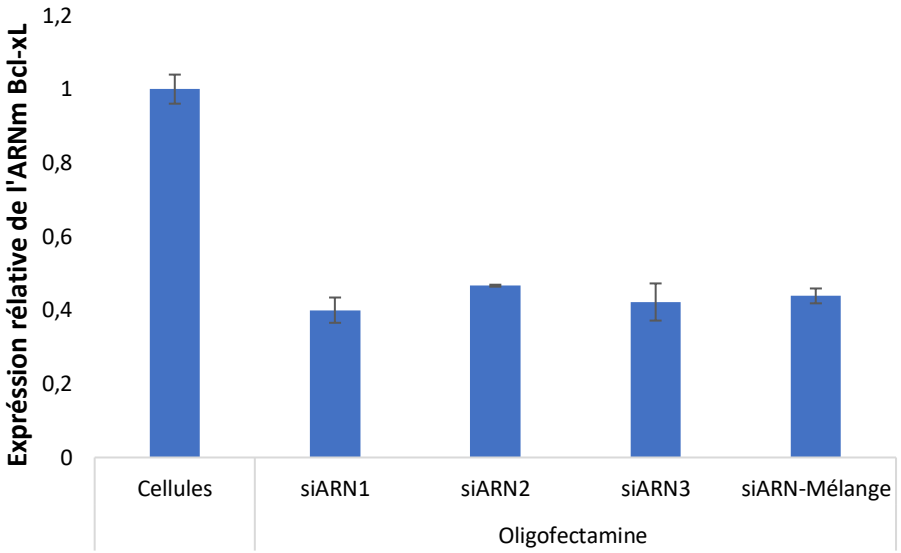

Figure 15. Expression de l'ARNm Bcl-xL relative à l'expression de l'ARNm GAPDH dans des cellules MDA-MB-231 traitées ou non avec l'Oligofectamine™ préparé avec les différentes séquences des siRNA (1, 2 ou 3) ou le mélange de trois séquences, à une concentration en siRNA de 50 nM.

3.4. Evaluation de l'efficacité des CS-MSN *in vitro*

3.4.1. Viabilité cellulaire

En conséquence de l'utilisation des siRNA anti-Bcl-xL, des effets à l'échelle cellulaire peuvent être observés. Cependant, ces effets peuvent se manifester assez tardivement. Pour cela, un test de viabilité cellulaire sur des cellules traitées avec des siRNA anti-Bcl-xL libres ou vectorisés avec l'Oligofectamine™ ou les CS-MSN est effectué sur différents temps jusqu'à 96h. Comme le montre la Figure 16, l'utilisation des siRNA libres ou d'Oligofectamine™ n'a pas affecté la viabilité des cellules au cours du temps. De la même façon, aucun effet n'est observé après traitement des cellules avec les CS-MSN pendant 24 h et 48 h. Cependant, une réduction de la viabilité des cellules est notée pour le temps 72 h et 96 h avec une valeur d'environ 55 %. Cela montre que les CS-MSN préparés avec les siRNA anti-Bcl-xL sont

capables de transfecter les cellules et d'induire la mort cellulaire à partir de 72 h de traitement en réponse à l'action intracellulaire des siRNA. Aucune différence significative n'est observée entre le temps 72 h et 96 h. Le temps 72 h est donc choisi pour l'évaluation de l'effet moléculaire.

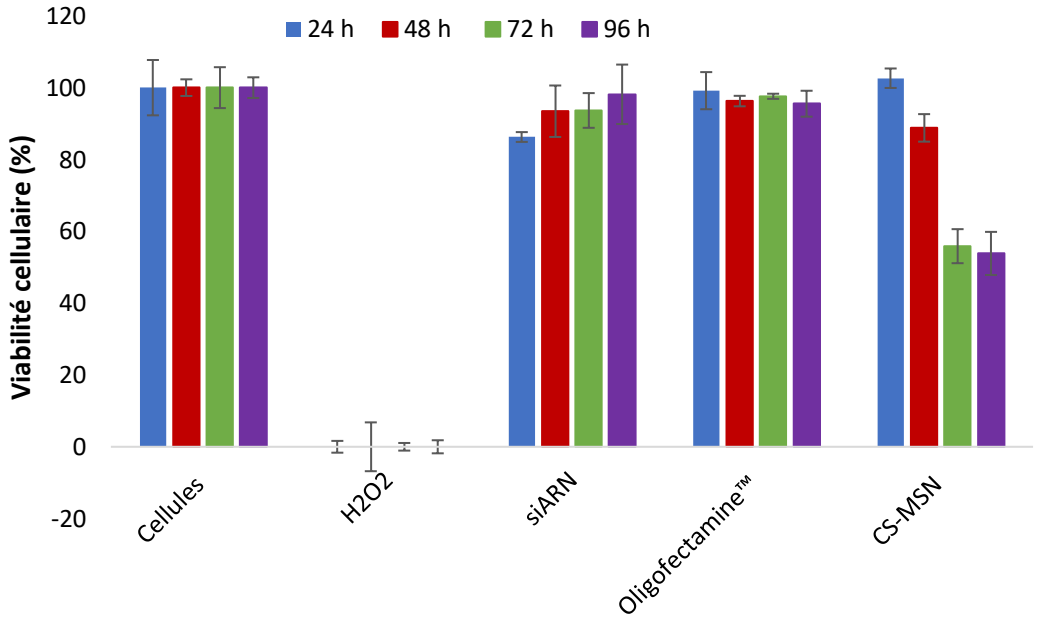

Figure 16. Viabilité cellulaire des cellules MDA-MB-231 traitées ou non avec H_2O_2, siRNA anti-Bcl-xL libres, Oligofectamine™ ou CS-MSN (50nM) pendant 24 h, 48 h, 72 h ou 96 h.

3.4.2. Immuno-détection de la protéine par Western Blot

L'expression de la protéine Bcl-xL a été évaluée par Western Blot, dans des cellules traitées avec les CS-MSN ou l'Oligofectamine™. Le résultat de la Figure 17 montre une inhibition de l'expression de la protéine Bcl-xL avec l'Oligofectamine™ et les CS-MSN avec une efficacité d'environ 55 % et 20 %, respectivement. Ce résultat indique que les CS-MSN sont capables de délivrer les siRNA anti-Bcl-xL dans les cellules MDA-MB-231 et d'induire l'inhibition de l'expression de la protéine correspondante. Cependant, cette efficacité à inhiber la protéine Bcl-xL est faible dans ces conditions.

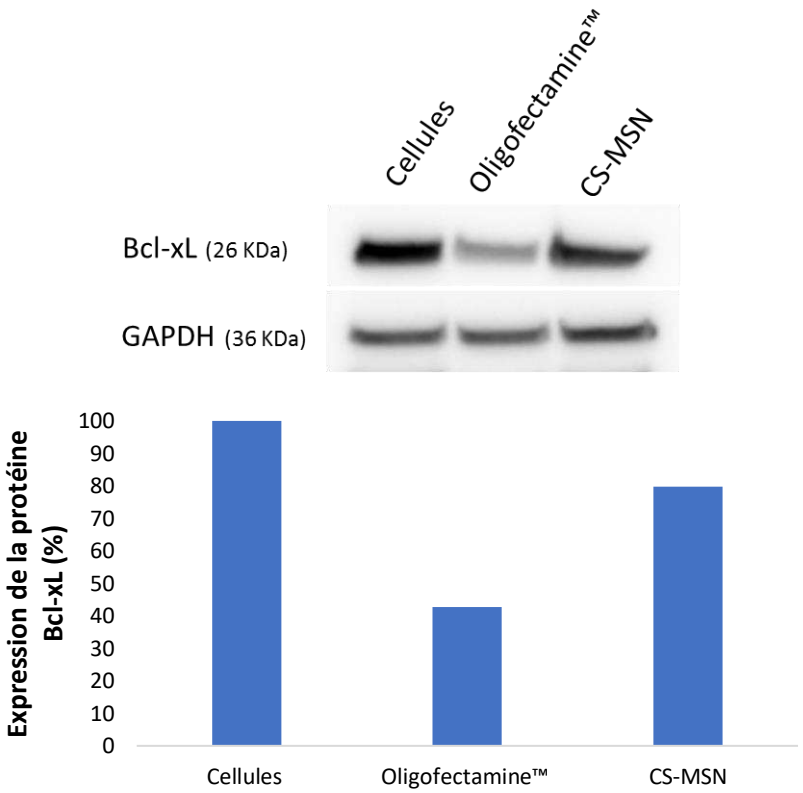

Figure 17. Evaluation de l'expression de la protéine Bcl-xL dans des cellules MDA-MB-231 traitées ou non avec l'Oligofectamine™ ou les CS-MSN à une concentration de 50 nM en siRNA.

Dans un deuxième temps, pour augmenter l'efficacité des nanovecteurs, nous avons testé des concentrations en siRNA plus élevées allant de 50 à 200 nM. La membrane de Western Blot obtenue montre une diminution de l'intensité des bandes des échantillons des cellules traitées avec les CS-MSN comparé aux cellules contrôles non traitées (Figure 18). A une concentration en siRNA de 50 et 100 nM, une inhibition d'environ 30 % est observée. En augmentant la concentration en siRNA jusqu'à 200 nM, l'efficacité d'inhibition de la protéine Bcl-xL atteint 70 %. Cela montre que l'efficacité d'inhibition de la protéine Bcl-xL est dose dépendante.

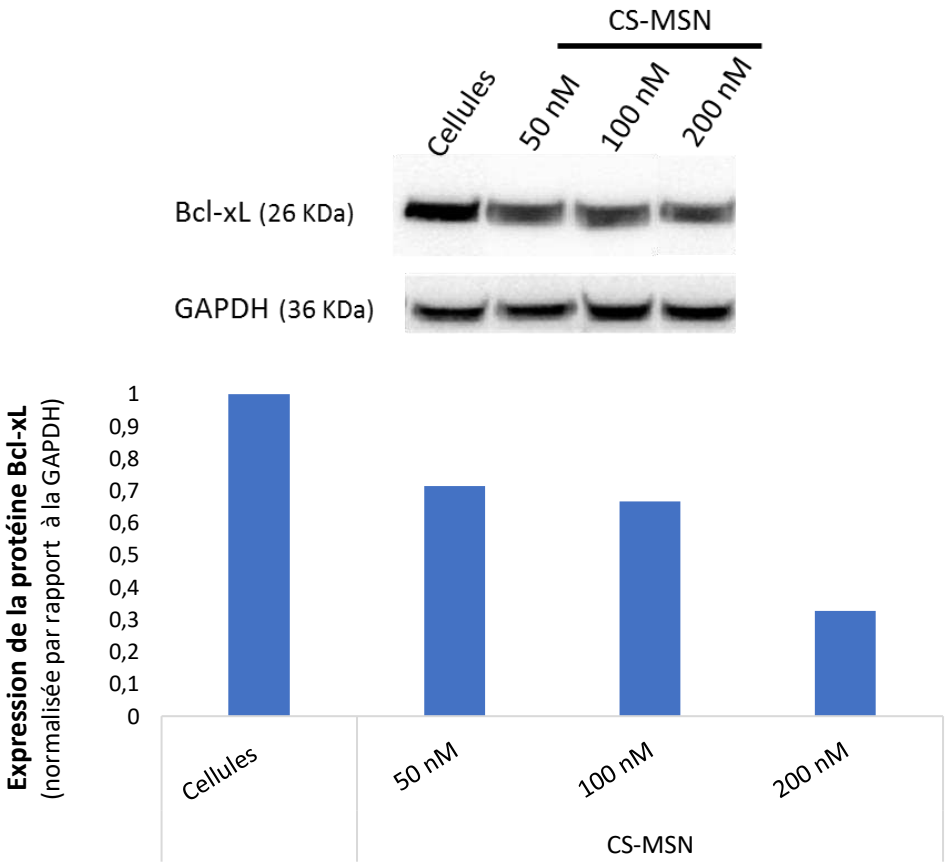

Figure 18. Evaluation de l'expression de la protéine Bcl-xL dans des cellules MDA-MB-231 traitées ou non avec des CS-MSN à différentes concentrations (50, 100 ou 200 nM).

3.4.3. Evaluation du taux d'expression des ARNm Bcl-xL

Après sa mise en place et l'optimisation de son protocole, la RT-qPCR est utilisée pour quantifier l'expression de l'ARNm Bcl-xL dans des cellules traitées avec des CS-MSN à différentes concentrations en siRNA ou avec l'Oligofectamine™ préparés avec les siRNA anti-Bcl-xL. La Figure19 montre une réduction de l'expression de l'ARNm Bcl-xL dans les cellules traitées avec l'Oligofectamine™ ou les CS-MSN. Cependant, l'inhibition avec les CS-MSN est significativement plus prononcée qu'avec l'Oligofectamine™. De plus, aucune différence significative n'est mise en évidence avec les trois concentrations en siRNA véhiculés par les CS-MSN.

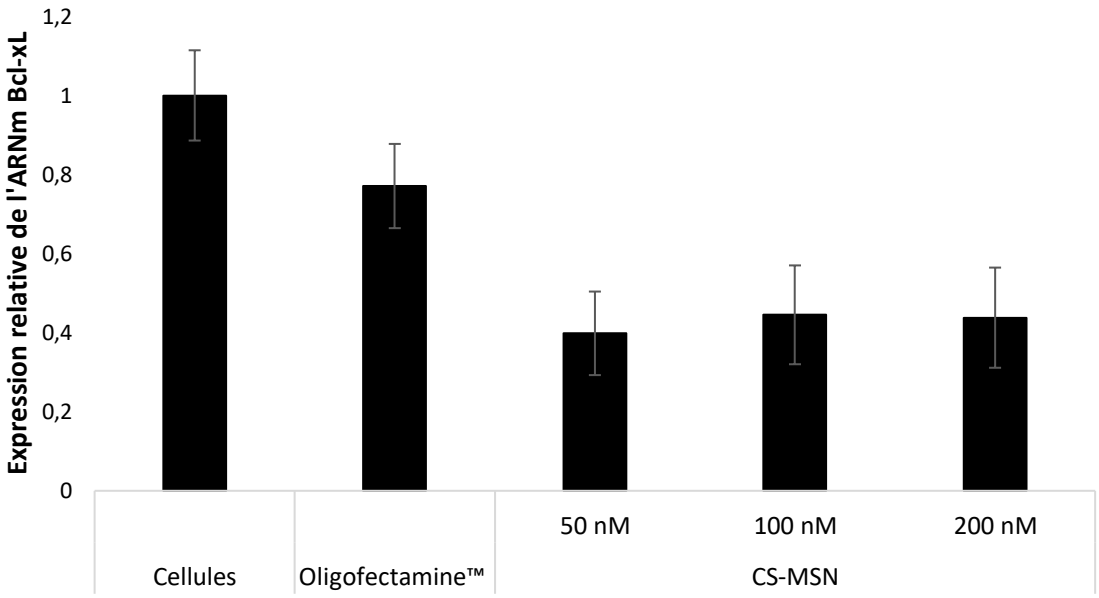

Figure 19. Expression de l'ARNm Bcl-xL relative à l'expression de l'ARNm GAPDH dans des cellules MDA-MB-231 traitées on non avec l'Oligofectamine™ ou des CS-MSN à différentes concentrations (50, 100 ou 200 nM en siRNA).

3.5. Préparation du passage vers l'*in vivo* : induction d'une tumeur de cancer du sein triple négatif chez la souris

Pour une future application des CS-MSN *in vivo*, un modèle de cancer du sein orthotopique chez la souris est induit en utilisant des cellules MDA-MB-231. Le taux de prise tumorale est évalué par un calcul du pourcentage de souris qui ont développé la tumeur par rapport au nombre total de souris. Ce calcul montre un pourcentage de prise tumorale élevé, d'environ 90 %. L'observation régulière des tumeurs montre une croissance tumorale rapide. Ce suivi de la vitesse de la croissance tumorale nous a permis d'estimer la date du traitement, qu'on a fixée à 4 semaines après l'injection des cellules cancéreuses.

La vascularisation des tumeurs est évaluée par échographie en suivant la distribution intra-tumorale d'un agent de contraste ultrasonore injecté par voie intraveineuse. Ce dernier permet de changer le contraste des tissus et d'évaluer la densité de la vascularisation sanguine au niveau de ces tissus. Au cours de cette étude, nous nous sommes focalisés sur la vascularisation au niveau des tumeurs induites chez les souris. La Figure 20 montre un changement de contraste au niveau de la tumeur après l'injection de cet agent. Ce changement de contraste est détecté principalement en périphérie et est très faible, voire absent, au centre de la tumeur. Cela indique que ce modèle de tumeur est vascularisé en périphérie et peu ou pas

vascularisé au centre. L'absence de la vascularisation au centre résulte, souvent, en un cœur nécrotique.

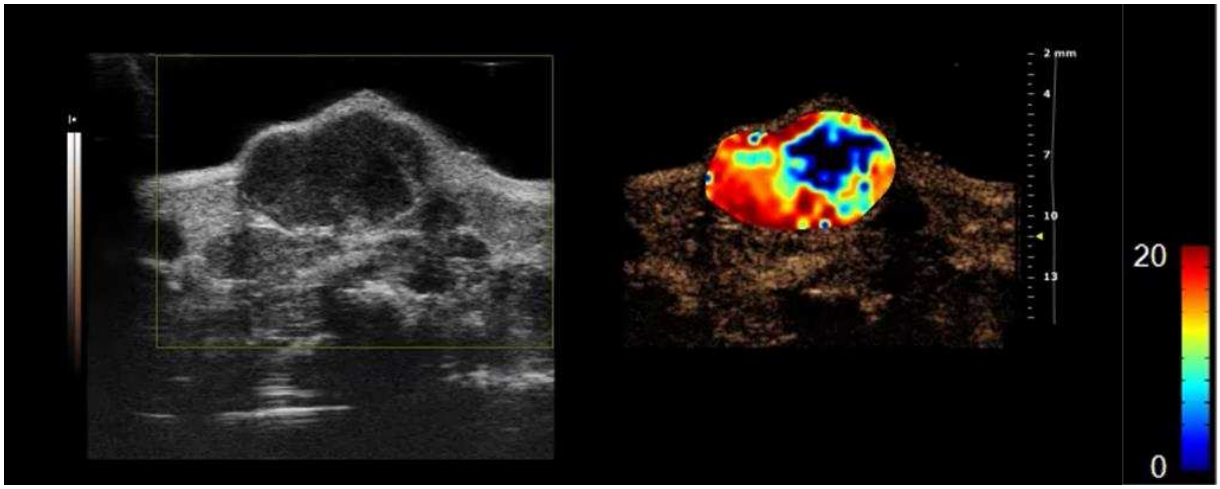

Figure 20. Image en échographie d'une tumeur orthotopique de cancer du sein triple négatif chez la souris après injection intraveineuse d'un agent de contraste.

Lors de la dissection, de nombreux vaisseaux sanguins sont observés autour des tumeurs. Cela confirme une vascularisation développée au niveau des tissus tumoraux. La dissection de la tumeur montre la présence d'un milieu visqueux au centre de celle-ci. Cette observation témoigne de la présence d'une nécrose de liquéfaction.

Après la dissection, le volume et la masse des tumeurs extraites sont mesurés. Un rapport entre la masse et le volume est calculé pour renseigner la densité du tissu tumoral et la reproductibilité du modèle. Ce rapport masse /volume est de 0,95 ± 0,17 g/cm^3. Cette valeur montre que le tissu tumoral est d'une densité très proche de la densité moyenne des tissus du corps humain (0,98 g/ cm^3) (114), une densité proche de la densité de l'eau. La valeur faible de l'écart-type indique une homogénéité et une reproductibilité de ce modèle tumoral.

De plus, avant l'injection sous-cutanée des cellules cancéreuses (MDA-MB-231) (jour 0), les souris sont pesées afin d'en déterminer leurs masses. Ensuite, ce paramètre est contrôlé régulièrement pour renseigner de l'état général des animaux. L'évolution de la masse est présentée dans la Figure 21 en se basant sur la valeur du jour 0. Ce résultat montre une augmentation de la masse des souris au cours de temps, indiquant, ainsi, une croissance normale des souris sans dégradation de l'état général.

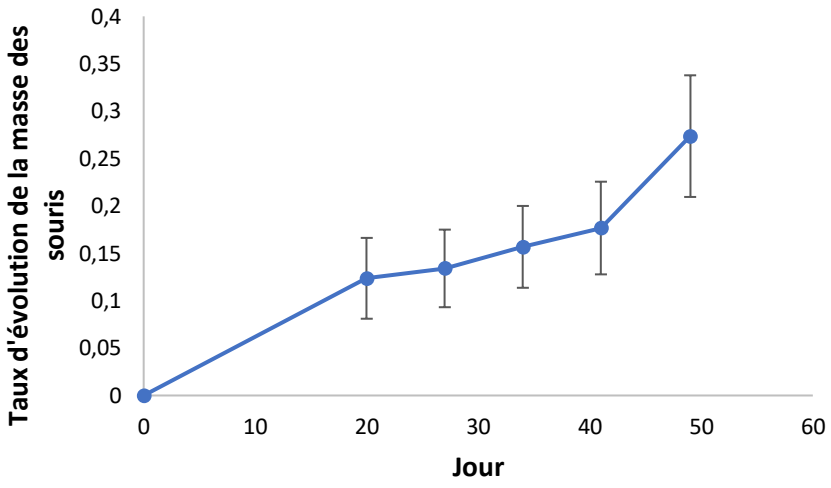

Figure 21. Taux d'évolution de la masse des souris comparé au jour 0.

4. Discussion

Pendant les étapes de développement d'un nanovecteur de siRNA pour le traitement de cancer et après la preuve de concept, il est important d'appliquer ce nanovecteur à une protéine qui pourrait être ciblée pour améliorer le traitement de ce cancer. Dans cette optique, nous avons utilisé les CS-MSN pour inhiber l'expression du gène Bcl-xL. Ce gène code pour une protéine anti-apoptotique, dont l'inhibition pourrait induire la mort des cellules cancéreuses. Nous avons commencé par la vérification des paramètres physico-chimiques et de la complexation des siRNA anti-Bcl-xL dans les CS-MSN. Les résultats obtenus montrent des caractéristiques comparables à ceux obtenus auparavant avec les séquences de siRNA modèles (112,115). Cela montre que le changement de la séquence des siRNA n'influence pas les caractéristiques des nanovecteurs et la complexation des siRNA.

La future application des CS-MSN *in vivo* demande une vérification des caractéristiques physico-chimiques et de l'isotonie de la formulation lorsque celle-ci est plus concentrée (formulation à une concentration de 6,265 µM en siRNA) et préparée dans une solution aqueuse de mannitol. Les résultats obtenus montrent des caractéristiques comparables à celles obtenues auparavant dans les conditions de l'utilisation *in vitro*. Cela montre que l'augmentation de la concentration et la formulation dans du mannitol n'influencent pas les caractéristiques des nanovecteurs et la complexation des siRNA.

Après sa mise en place et l'optimisation de son protocole expérimental, la technique de RT-qPCR est complétée par la technique de Western Blot pour sélectionner la séquence de siRNA anti-Bcl-xL la plus efficace. D'après les résultats obtenus par Western Blot et RT-qPCR

aucune différence significative d'efficacité entre les séquences n'a pu être mise en évidence. Bien que les techniques utilisées n'aient ni le même niveau de sensibilité ni la même cible (le Western Blot est une technique semi-quantitative permettant la détection de la protéine et la RT-qPCR permet la quantification précise de l'ARNm), les résultats sont cohérents avec une efficacité de 50 à 60 %. Cette observation implique que ces trois séquences peuvent être utilisées pour l'évaluation de l'efficacité des CS-MSN.

Ensuite, nous avons évalué l'efficacité des CS-MSN à deux niveaux : le niveau cellulaire (la viabilité des cellules) et le niveau moléculaire (l'expression de l'ARNm et de la protéine). Pour évaluer l'effet cellulaire de l'inhibition de la protéine Bcl-xL, un test de viabilité cellulaire est réalisé. Les résultats obtenus montrent une réduction de la viabilité des cellules traitées avec les CS-MSN à partir de 72 h. Ces résultats sont cohérents avec les observations précédentes. Cet effet cellulaire est la conséquence de l'effet moléculaire (inhibition de la protéine anti-apoptotique) et ne peut être détecté qu'après l'installation de ce dernier. Dans le cas des CS-MSN, le maximum d'inhibition de l'expression de la protéine cible (GFP) n'est observé qu'après 72 h de traitement (112). Ce qui fait que l'induction de la mort cellulaire est attendue à partir de 72 h de traitement. Dans cette partie, l'effet cellulaire est évalué avec une seule concentration en siRNA. Il est possible que l'augmentation de la dose en siRNA améliore le résultat obtenu et induise un pourcentage de mort cellulaire plus élevé. Au niveau moléculaire, le résultat de Western Blot montre une réduction de la quantité de la protéine Bcl-xL dans les cellules traitées avec les CS-MSN ciblant Bcl-xL. De même, le résultat obtenu par RT-qPCR montre une diminution du taux d'expression d'ARNm Bcl-xL comparé aux cellules contrôles jusqu'à une valeur d'environ 0,4, ce qui indique une efficacité d'inhibition d'environ 60 %. Cependant, des divergences sont observées entre l'efficacité d'inhibition de l'ARNm et celle de la protéine Bcl-xL. En effet, un effet dose-réponse est mis en évidence, où l'inhibition de la protéine parait être dépendante de la dose des siRNA délivrée par les CS-MSN. Néanmoins, le taux d'inhibition d'ARNm est constant avec les trois concentrations testées.

La différence de taux d'inhibition entre l'ARNm et la protéine Bcl-xL pourrait être expliquée par un décalage médié par les mécanismes intermédiaires qui permettent le passage de l'ARNm à la protéine correspondante. De plus, parfois, la détection d'une inhibition de la protéine prend plus de temps, le temps nécessaire pour la dégradation de la quantité de la protéine déjà produite (temps de demi-vie de la protéine). Il a été rapporté que Bcl-xL est une protéine stable avec une demi-vie moyenne relativement longue, d'environ 20 h. Cette stabilité de Bcl-xl participe, aussi, à la contribution de cette protéine à la résistance à des thérapies

anticancéreuses (116). Donc, il serait intéressant d'évaluer l'inhibition de la protéine Bcl-xL sur des temps encore plus longs.

Par ailleurs, des incohérences sont détectées entre les résultats obtenus à l'échelle cellulaire et moléculaire. En inhibant une protéine anti-apoptotique avec les siRNA, on s'attend à ce que l'effet sur la protéine soit plus prononcé que celui sur la cellule, c'est-à-dire le taux d'inhibition de la protéine soit plus élevé que celui de la mortalité cellulaire. Cette hypothèse est supportée par les résultats obtenus par Guruprasath *et al.* en évaluant l'efficacité d'un nanovecteur de siRNA hybride fonctionnalisé avec un peptide de ciblage pour transfecter des cellules MDA-MB-231. La délivrance des siRNA Bcl-xL a montré des résultats significatifs au niveau de l'inhibition de la protéine correspondante et l'induction de la mort cellulaire. Toutefois, l'effet moléculaire observé est plus prononcé que l'effet cellulaire (117). Une telle différence est expliquée par le fait que l'effet cellulaire est la conséquence de l'effet moléculaire. Or, ici ce n'est pas le cas. Avec une concentration en siRNA de 50 nM, la viabilité cellulaire est réduite de 45 %, alors que l'expression de la protéine n'est inhibée que de 20 à 30%. Cette divergence nécessite plus d'investigation pour la résoudre ou l'expliquer.

Au vu des résultats présentés dans cette partie, des manipulations supplémentaires sont nécessaires afin de confirmer ces résultats préliminaires.

5. Conclusion

Dans l'objectif d'une future application dans le traitement du cancer du sein triple négatif (CSTN), nous avons utilisé les CS-MSN pour inhiber l'expression du gène Bcl-xL codant pour une protéine anti-apoptotique surexprimée dans les cellules de CSTN et impliquée dans la résistance à la chimiothérapie. La substitution de la séquence de siRNA modèle avec une séquence de siRNA anti-Bcl-xL n'a pas affecté les paramètres physico-chimiques et la complexation du nanovecteur. De plus, les caractéristiques physico-chimiques des CS-MSN préparés pour une future administration *in vivo* ont montré des valeurs comparables à celles obtenues pour les nanovecteurs utilisés *in vitro*. Bien que l'évaluation du traitement des cellules MDA-MB-231 avec les CS-MSN présente quelques divergences, elle montre des résultats encourageants au niveau de l'inhibition de l'ARNm et la protéine Bcl-xL ainsi que sur l'induction de la mort cellulaire. De plus, à la fin de cette étude, un modèle orthotopique de cancer du sein triple négatif a été mis en place avec succès chez la souris. Cela représente un pas supplémentaire sur le chemin vers une application *in vivo*.

Observations complémentaires et discussion

Le cancer du sein triple négatif (CSTN) est une pathologie agressive qui représente environ 20 % des cancers du sein. Ce cancer est souvent associé à un mauvais pronostic et est responsable d'une mortalité importante. A cause des caractéristiques des cellules tumorales, le choix de traitement disponible est très restreint et tourne autour de la chimiothérapie, la radiothérapie et la chirurgie, qui n'est pas toujours possible. Ces traitements manquent de spécificité et de sélectivité pour les cellules cancéreuses et touchent aussi les cellules et les tissus sains, ce qui induit des effets indésirables importants. Cela rend nécessaires la recherche de nouvelles thérapies et le développement de nouvelles approches plus spécifiques et sélectives dans le contexte du traitement des CSTN.

Les objectifs de cette thèse sont : le développement d'un nanovecteur capable de délivrer les siRNA dans des cellules de cancer du sein triple négatif ; l'investigation des mécanismes et des voies d'entrée de ce nanovecteur et de son trafic et devenir intracellulaire ; l'évaluation de son efficacité de transfection et son action au niveau des cibles.

Développement d'un nanovecteur capable de délivrer les siRNA dans des cellules du cancer du sein triple négatif

Toutes les recherches sur les nanovecteurs théragnostiques de siRNA pour le traitement des cancers ont l'objectif de développer un nanosystème qui s'approche le plus possible du nanovecteur idéal capable de : 1) protéger les siRNA de la dégradation et de l'élimination précoce par l'organisme, 2) éviter le déclenchement d'une réponse immunitaire, 3) franchir les barrières biologiques extracellulaires, 4) faciliter l'accumulation et la pénétration au niveau de la tumeur, 5) cibler spécifiquement les cellules cancéreuses, 6) délivrer les siRNA dans les cellules, 7) échapper à la dégradation endosomale, 8) induire la dégradation de l'ARNm cible et 9) permettre la visualisation de la tumeur et le suivi de sa distribution dans l'organisme (58).

En se basant sur la littérature, il semble que la notion d'un nanovecteur efficace n'est pas liée à un composant ou un groupe de composants précis. Différents nanovecteurs de siRNA de compositions différentes et de types différents ont montré des résultats prometteurs *in vitro* et *in vivo* et sont allés jusqu'aux essais cliniques (33,75,118–120), voire même sont mis sur le marché tels que l'exemple du patisiran (ONPATTRO®) qui représente le premier nanovecteur de siRNA injectable approuvé par la FDA et l'EMA. Cependant ce médicament est indiqué dans le cadre de l'amyloïdose héréditaire à transthyrétine qui est lié à une mutation du gène

transthyrétine (76,121). La cible est donc bien connue, contrairement aux cancers qui sont, généralement, multifactoriels.

Il est généralement admis que chaque composant a des avantages et des inconvénients pour la nanovectorisation des siRNA. Par exemple, les composants cationiques (lipides, polymères, peptides …) se montrent très efficaces pour la complexation des siRNA par une condensation avec ces acides nucléiques chargés négativement. Par ailleurs, l'efficacité de transfection des siRNA avec ces composants cationiques se montre assez élevée, notamment grâce à un échappement endosomal facilité (32,52,58,78). En revanche, la toxicité cellulaire induite par leur charge positive limite leur utilisation (55). Ainsi, une alternative, par association avec d'autres composants (neutres ou naturels), est nécessaire pour le développement de nanovecteurs (122). À l'inverse, les composants non-cationiques (tels que les lipides et les polymères anioniques ou neutres) semblent globalement être moins cytotoxiques, mais possèdent un pouvoir tampon faible par rapport à celui demandé pour la fuite de l'endosome. Sans cet échappement endosomal, la majorité des siRNA se dégradent avant d'atteindre leur cible intracellulaire et avant d'exercer leur action. Les composants inorganiques apportent une multifonctionnalité avec la possibilité de suivre la distribution des nanovecteurs qu'ils composent (123). Cependant, ils nécessitent une association avec des polymères, peptides et/ou lipides, favorisant la transfection des siRNA (124–126). En outre, l'utilisation de métaux lourds peut engendrer une certaine toxicité, voire des problèmes de métabolisation lors d'applications *in vivo* (127,128).

Ainsi, il est important de bien choisir les composants des nanovecteurs en fonction des rôles attendus. Dans cette étude, nous avons opté pour une construction rationnelle basée sur la connaissance et la compréhension des avantages et des limites de chaque composant pour formuler les CS-MSN. Dans ce manuscrit, le rôle de chaque composant et son implication dans la formulation, en particulier les polymères cationiques et le peptide gH625, sont discutés dans les différentes parties. Néanmoins, la préparation de la nanoplateforme (CS-FNP) qui représente le cœur du nanovecteur est moins évoquée et sera discutée ici en se focalisant, en particulier, sur les difficultés rencontrées et les améliorations apportées.

Comme décrit dans le début de ces travaux, la formulation des CS-MSN est basée sur l'utilisation d'une nanoplateforme (CS-FNP) développée dans notre équipe (102). Cette nanoplateforme est composée d'un cœur de SPION marqué avec un fluorochrome proche infra-rouge (cyanine 5.5 ou sulfocyanine 5), revêtu avec du PEG_{5000} et fonctionnalisé avec le peptide

gH625. Selon ce protocole, la purification des composants non greffés se fait par dialyse contre de l'eau ou du PBS. Le choix de cette méthode de purification est basé sur les propriétés de solubilité des composants des CS-FNP. Cependant, l'efficacité de cette purification n'avait pas encore été vérifiée. Pour quantifier le peptide greffé, nous avions besoin d'évaluer l'efficacité de cette étape de purification. Pour cela, nous avons analysé les CS-FNP par chromatographie en phase liquide à haute performance (HPLC) avant et après dialyse, qui permet la détection et la quantification du peptide libre. Le chromatogramme obtenu montre que la quantité de gH625 libre diminue après dialyse. Cependant, une partie du peptide libre persiste dans la suspension des CS-FNP (Figure 22). Cela montre que la dialyse n'est pas assez efficace pour éliminer le peptide libre. Nous avons donc testé la méthode de purification par chromatographie d'exclusion stérique (SEC). Après purification, l'efficacité de la SEC à éliminer le peptide libre est confirmée par HPLC (Partie 3 : publication 3). Suite à cette purification efficace, les analyses en HPLC ont permis d'estimer le pourcentage de peptide greffé qui est d'environ 90%.

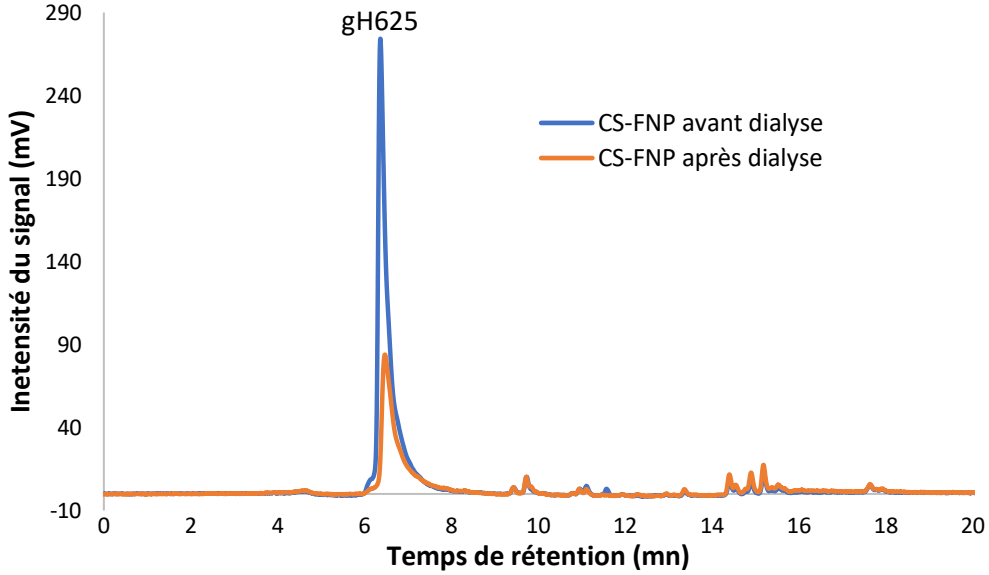

Figure 22. Chromatogramme HPLC des CS-FNP avant et après dialyse pour la détection du peptide gH625 libre.

Le deuxième aspect décisif est le choix du fluorochrome qui servira pour l'investigation des mécanismes d'entrée et du trafic intracellulaire des CS-MSN. Une étude préliminaire a permis d'identifier une difficulté quant à l'utilisation de la cyanine 5.5 comme un fluorochrome pour le suivi des CS-MSN dans les cellules. En effet, après incubation des cellules avec les CS-MSN-cyanine 5.5 (CS-MSN avec un cœur marqué avec la cyanine 5.5) nous avons observé une fluorescence diffuse dans tout le cytoplasme (bleu) avec des points fluorescents (jaune) représentant la fluorescence du fluorochrome conjugué aux siRNA (Alexa Fluor 488) et celle

de la cyanine 5.5 (Figure 23, haut). Ce résultat suggère que les siRNA internalisés sont dans des vésicules et qu'une partie de la cyanine 5.5 suit le même trafic que les siRNA. Probablement, cette partie est celle conjuguée aux CS-FNP. Alors que le trafic d'une autre partie de la cyanine 5.5 se montre différent avec une localisation cytoplasmique diffuse. Il semble que cette partie de la cyanine 5.5 ne suive pas la même distribution que les CS-FNP et elle représente une forme libre, même présente après l'étape de la purification, et ayant son propre trafic. Pour vérifier cette hypothèse, nous avons synthétisé des CS-FNP marqués avec la sulfocyanine 5. Contrairement à la cyanine 5.5, la sulfocyanine 5 est un fluorochrome hydrophile, donc son élimination est facilitée par les deux méthodes de purification utilisées dans ces travaux de thèse : la dialyse contre de l'eau ou du PBS et la chromatographie d'exclusion stérique avec une phase mobile composée de PBS. L'imagerie des cellules après incubation avec les CS-MSN-sulfocyanine 5 (CS-MSN avec un cœur marqué avec la sulfocyanine 5) montre une fluorescence localisée dans des structures vésiculaires avec absence de marquage cellulaire diffus observé en présence de la cyanine 5.5 (Figure 23, bas). Ce résultat indique que la sulfocyanine 5 suit une distribution intracellulaire comparable à celle des siRNA et, probablement, la même que celle des CS-FNP. Cela montre que la fluorescence observée est celle de la sulfocyanine 5 conjuguée aux CS-FNP et confirme que la fluorescence diffuse de la cyanine 5.5 résulte d'une partie du fluorochrome libre.

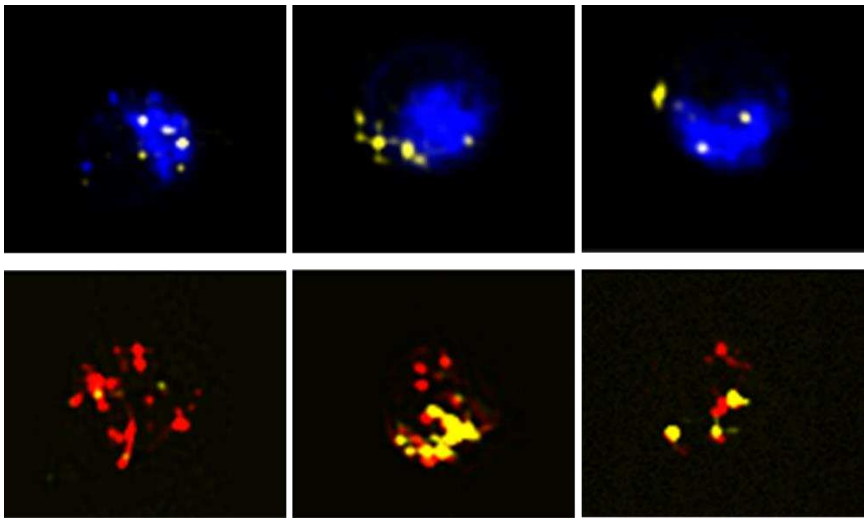

Figure 23. Images des cellules MDA-MB-231 incubées avec des CS-MSN marqués avec la cyanine 5.5 (bleu, ligne de haut) ou la sulfocyanine 5 (rouge, ligne de bas) et préparés avec des siRNA conjugués à l'Alexa Fluor 488, et obtenues par imagerie en flux AMNIS®.

Nous avons, ensuite, confirmé que le changement du fluorochrome et de la méthode de purification n'affecte pas les caractéristiques des nanovecteurs. Nous avons choisi d'utiliser la

sulfocyanine 5 pour investiguer les mécanismes d'internalisation et le trafic intracellulaire des nanovecteurs.

Le choix de la composition du nanovecteur de siRNA est important, mais pas suffisant pour avoir une efficacité élevée. La stratégie de formulation influence aussi l'efficacité. Dans cette étude, nous avons combiné l'assemblage covalent et l'assemblage électrostatique pour obtenir les CS-MSN (Figure *24*24). Les SPION, le fluorochrome, le PEG ainsi que le peptide gH625 sont associés avec des liaisons covalentes pour avoir une base stable pour le nanovecteur (les CS-FNP). En effet, ce greffage résulte en une structure assez organisée et contrôlée. Nous avons également utilisé un assemblage électrostatique pour complexer cette nanoplateforme (CS-FNP), les polymères cationiques (le chitosan et la poly-L-arginine) et les siRNA. Les liaisons électrostatiques donnent une structure moins solide que celle obtenue par les liaisons covalentes, mais elles permettent une libération plus aisée des siRNA dans les cellules.

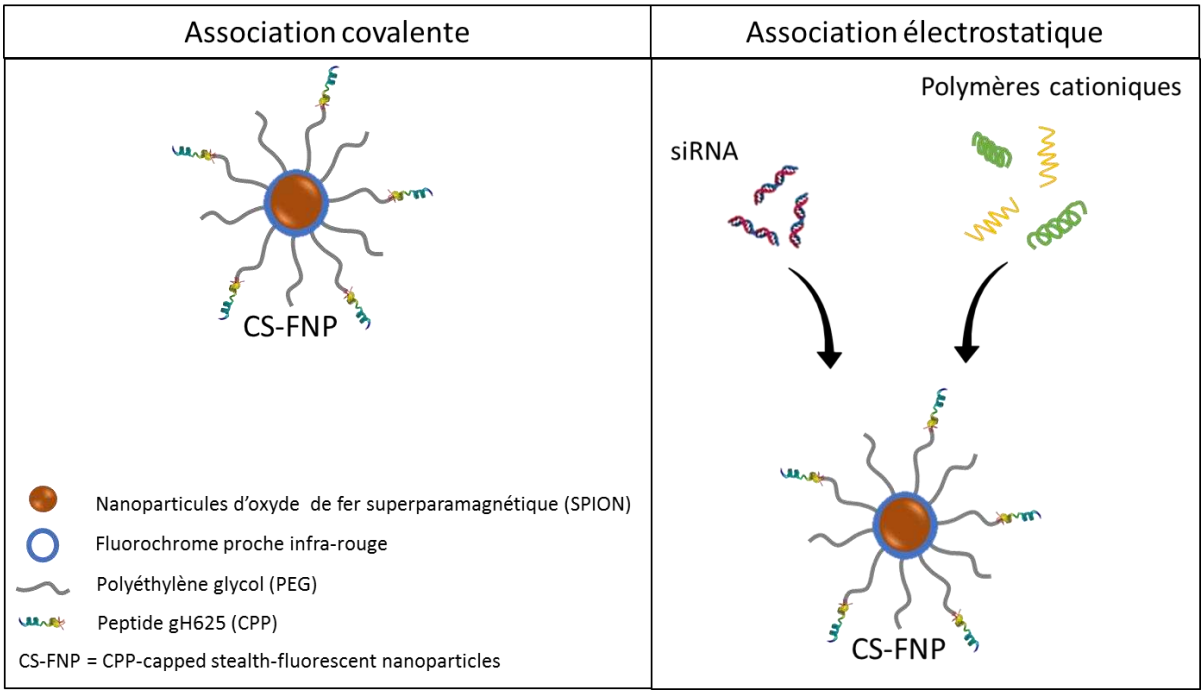

Figure 24. Illustration schématique des types d'interactions entre les différents composants du nanovecteur.

Le deuxième point de discussion de cette partie concerne l'influence du protocole de formulation sur les caractéristiques physico-chimiques du nanovecteur. L'établissement du protocole de formulation des nanovecteurs nécessite une optimisation des paramètres qui peuvent influencer la complexation des siRNA et l'efficacité de transfection. Parmi ces paramètres, nous citons les rapports qui définissent la quantité de chaque composant à utiliser.

Dans ces travaux de thèse, nous avons utilisé deux types de rapports qui lient la quantité de chaque composant à la quantité de siRNA pour formuler les CS-MSN. La quantité de CS-FNP est représentée par leur teneur en fer et est déterminée selon le rapport de masse entre le fer et les siRNA. La quantité de polymères est définie par le rapport molaire entre les charges positives et les charges négatives de chaque polymère et des siRNA, respectivement. L'objectif de cette optimisation est d'obtenir des caractéristiques physico-chimiques compatibles avec les exigences de la voie intraveineuse pour une future administration *in vivo* tout en maîtrisant la complexation des siRNA. Cette complexation se traduit par une balance équilibrée entre la rétention dans le milieu extracellulaire et la libération en intracellulaire pour une efficacité élevée. Par ailleurs, dans le cas du cancer du sein triple négatif, l'absence de cibles cellulaires spécifiques complique le ciblage actif de ces tumeurs. Le ciblage passif par effet EPR s'avère être une alternative intéressante pour accumuler les nanovecteurs au niveau du site tumoral. Cet effet est dû à l'hyperperméabilité des vaisseaux sanguins au niveau de la tumeur due à des ouvertures anormalement larges entre les cellules endothéliales. Contrairement aux vaisseaux sanguins normaux, où l'ouverture est inférieure à 10 nm, ces ouvertures pourraient être d'une centaine de nanomètres de large au niveau des vaisseaux sanguins tumoraux. Par conséquent, l'utilisation de l'effet EPR pour traiter le cancer est justifiée par le fait que les particules thérapeutiques d'une taille supérieure à 10 nm ne peuvent pas extravaser des tissus normaux, réduisant ainsi les effets indésirables, et passent d'une manière sélective à travers les ouvertures des vaisseaux tumoraux (129,130). Une raison additionnelle pour l'utilisation d'une taille supérieure à 10 nm est d'éviter l'élimination précoce par filtration rénale pour augmenter l'accumulation au niveau de la tumeur (131). De plus, la capacité des nanovecteurs à traverser efficacement les vaisseaux sanguins tumoraux ainsi que l'espace interstitiel dépend du rapport entre la taille du nanovecteur et la largeur de l'ouverture. Plus le rapport est faible, plus le transport à travers les vaisseaux est facile (129,132). Malgré la difficulté de définir une taille idéale précise à cause de l'hétérogénéité élevée de la nature et du type à la fois des tumeurs et des nanovecteurs, il est généralement admis qu'une taille comprise entre 20 et 200 nm est un bon compromis pour profiter de l'effet EPR après une administration intraveineuse (130,131,133). Cet effet EPR reste actuellement la voie principale dans les mesures où le ciblage actif n'est pas possible même si son utilisation est largement remise en question chez l'Homme surtout dans le cas des tumeurs faiblement irriguées telles que celles du sein.

Pour être compatible avec les exigences de la voie intraveineuse, pour profiter de l'effet EPR et pour une efficacité de transfection élevée, une optimisation de la formulation des CS-

MSN est réalisée. En se basant sur des études antérieures réalisées dans notre laboratoire (134,135), le rapport de masse (MR) entre le fer et les siRNA est fixé à 10. La complexation des siRNA avec les CS-FNP et le chitosan se montre non efficace avec différents rapports de chitosan (N_{CS}/P de 0 à 100). Contrairement à ce qui est observé ici, des études de développement de nanovecteurs de siRNA, en utilisant le chitosan, ont montré une complexation parfaite avec des rapports N/P inférieurs à 100. Chen *et al.* ont conçu un nanovecteur pour la délivrance des siRNA en complexant, dans un premier temps, par assemblage électrostatique les siRNA avec le chitosan et en encapsulant, dans un deuxième temps, ces complexes avec des nanofibres de PLGA (pour poly(D,L-lactic-co-glycolic acid)). La première étape montre une complexation élevée des siRNA par le chitosan à un rapport N/P de 10 (136). De même, Köping-Höggård *et al.* ont investigué la capacité de complexation de 5 chitosans de degré d'acétylation et de masse moléculaire différents. Les résultats obtenus ont montré une complexation optimale avec des rapports N/P qui varient entre 3 et 4 (137). Dans ces études, les siRNA n'étaient complexés qu'avec les polymères. Donc, cette incohérence entre les résultats obtenus dans notre étude et celles de la littérature pourrait être expliquée par la présence de CS-FNP qui résulte en une organisation et des interactions différentes entre les siRNA et le chitosan.

Dans notre étude, après son échec à complexer les siRNA, le chitosan est remplacé par un autre polymère cationique avec une densité de charge positive plus élevée (pKa = 12), la poly-L-arginine. En présence de ce polymère, les siRNA sont complètement complexés à partir d'un rapport N_{PLR}/P de 2. Ce rapport est faible comparé aux rapports utilisés dans la littérature qui sont généralement supérieurs à 10 (138–140). L'utilisation d'une faible quantité de poly-L-arginine pourrait limiter l'effet cytotoxique de ce polymère dû à sa densité élevée de charge positive (122). A un rapport N_{PLR}/P de 2, la taille des complexes est d'environ 143 nm, une valeur compatible avec l'administration intraveineuse et l'utilisation de l'effet EPR. Cependant, l'efficacité des siRNA délivrés par ces complexes dans les cellules est très faible. L'ajout du chitosan à la formulation augmente considérablement l'efficacité de transfection en inhibant la protéine GFP dans des cellules MDA-MB-231 exprimant la GFP jusqu'à un rapport N_{CS}/P de 30. La taille des complexes (à un MR de 10, N_{PLR}/P de 2 et N_{CS}/P de 30) est d'environ 170 nm (< 200 nm) avec un PDI de 0,3 et une charge de surface légèrement positive. Ces caractéristiques sont compatibles avec les exigences de la voie d'administration intraveineuse et sont adaptés pour profiter de l'effet EPR. Dans la littérature, les nanovecteurs hybrides avec

une composition assez complexe et fonctionnalisés avec un ligand biologique ont une taille généralement supérieure à 100 nm (117,138,141).

De plus, la complexation des siRNA et leur protection contre la dégradation en présence de sérum sont évaluées en utilisant la technique d'électrophorèse sur gel d'agarose. Ce test a montré une bonne rétention et protection des siRNA complexés dans les CS-MSN même en présence de 50 % de sérum après une incubation de 4 h. Des résultats similaires ont été observés par Plianwong *et al.* durant le développement d'un nanovecteur de siRNA basé sur l'utilisation de chitosan et de poly-L-arginine. Ils ont montré une bonne protection des siRNA par ces deux polymères en présence de sérum et même en présence de RNases pendant 6 h (142).

La cytotoxicité représente une des barrières pour l'utilisation de certains nanovecteurs *in vivo*. Ainsi, l'évaluation de la cytotoxicité est une étape essentielle dans le développement de nanovecteurs. Le test de viabilité cellulaire réalisé sur des cellules MDA-MB-231, en utilisant un siRNA contrôle, montre une viabilité supérieure ou égale à 80 % avec toutes les concentrations et tous les temps d'incubation. Donc, la formulation des CS-MSN n'est pas (ou peu) cytotoxique jusqu'à une concentration en siRNA de 100 nM (dans ces conditions). Malgré que la poly-L-arginine soit classée parmi les polymères cationiques avec une densité de charge positive élevée responsable d'une toxicité importante au niveau de la membrane cellulaire, il a été démontré que cette toxicité est dose-dépendante (143) et que l'association de la poly-L-arginine à des polymères naturels tels que le chitosan réduit cette toxicité (142).

Investigation des mécanismes et des voies d'entrée de ce nanovecteur et de son trafic et devenir intracellulaire

Pour l'étude des mécanismes d'internalisation et du trafic intracellulaire des CS-MSN, nous avons exploité leurs propriétés d'agents d'imagerie. Cette étude est basée sur le suivi de la fluorescence des fluorochromes des nanovecteurs (conjugués aux siRNA et aux CS-FNP) avec des techniques d'imagerie telles que la microscopie confocale, la cytométrie en flux et l'imagerie en flux AMNIS®.

En raison de la complexité des mécanismes d'internalisation et du trafic intracellulaire des nanovecteurs, il est compliqué de construire une image complète qui représente tous les processus et les mécanismes produits dès l'entrée du nanovecteur dans la cellule jusqu'à

l'arrivée des siRNA au niveau de leur cible intracellulaire (les ARNm cibles). Pour obtenir un schéma le plus proche possible de la réalité, plusieurs techniques sont utilisées. Pour chaque étape de cette étude, nous avons choisi d'utiliser au moins deux techniques différentes pour avoir un maximum d'informations.

Dans un premier temps, nous avons comparé l'efficacité d'entrée des nanovecteurs sans (S-MSN) et fonctionnalisés par le peptide gH625 (CS-MSN) dans les cellules MDA-MB-231. Les résultats obtenus montrent une entrée rapide avec un signal élevé pour les deux nanovecteurs. Cependant, après 4 h d'internalisation, la présence du peptide gH625 sur les CS-MSN a augmenté 2,5 fois leur entrée par rapport aux S-MSN, ce qui indique que ce peptide favorise l'entrée du nanovecteur dans les cellules. Dans un deuxième temps, l'utilisation des inhibiteurs chimiques pour déterminer la voie d'entrée nous a permis de souligner l'implication de l'endocytose médiée par clathrines et cavéoles. De plus, les résultats obtenus nous ont permis de mettre en évidence quelques limites de l'utilisation de ces inhibiteurs chimiques comme le cas de la chlorpromazine qui n'a pas montré une inhibition significative de l'entrée des CS-MSN et de la méthyl-β-cyclodextrine (MβCD) qui a induit une inhibition de 80 %. En effet, la chlorpromazine est un inhibiteur de Rho GTPase qui agit sur la distribution de la clathrine à la surface des cellules (144). Cependant, il n'est pas efficace sur toutes les cellules (145). La MβCD, elle, agit par déplétion du cholestérol de la membrane cellulaire. En plus de l'inhibition de la voie des cavéoles, elle agit sur d'autres voies d'internalisation telles que la voie dépendante de la clathrine et la macropinocytose (145). L'inhibition simultanée de plusieurs voies d'entrée pourrait expliquée l'efficacité élevée de la MβCD dans notre cas.

Les inhibiteurs chimiques sont très utilisés pour déterminer le mécanisme endocytaire responsable de l'entrée des nanovecteurs. Cette approche est souvent basée sur l'hypothèse que ces inhibiteurs ont des effets spécifiques sur les voies d'entrée. Cependant, plusieurs études ont montré que, généralement, ce n'est pas le cas (146). Pour surmonter ces limites, d'autres approches sont de plus en plus utilisées telles que l'utilisation de cellules « knock-down » ou exprimant des protéines mutées (Arf6, cavéoline, dynamine, …) ou des marqueurs de compartiments intracellulaires (cavéoline, EEA-1, Lamp-1, LysoTracker, Rab7, …) (145). Malgré la spécificité de ces approches, leur utilisation reste plus lourde que celle des inhibiteurs chimiques.

Pour compléter cette étude de la voie d'entrée des nanovecteurs, des cellules incubées avec les nanovecteurs sont analysées par microscopie électronique en transmission (MET). Des

SPION (seul composant détectable par MET) sont observées dans des vésicules à clathrine et à cavéole. Cela confirme qu'il s'agit d'une internalisation via l'endocytose dépendante des clathrines et des cavéoles et indique que les résultats des deux techniques utilisées sont cohérents. Dans la littérature, différentes voies d'entrée sont utilisées par les nanovecteurs de siRNA pour gagner les compartiments intracellulaires (84). Les voies d'endocytose sont les plus impliquées dans ce passage telles que la voie de macropinocytose (141,147), l'endocytose médiée par les clathrines (148), l'endocytose cavéole dépendante (149) et l'endocytose dépendante de récepteur (117,150,151). Comme observé dans cette étude, plus d'une voie peut être impliquée simultanément. Dans ce sens, Du *et al.* ont mis en évidence l'implication de la voie d'endocytose médiée par les clathrines et celle médiée par les cavéoles dans l'entrée d'un nanovecteur polymère de siRNA dans des cellules MDA-MB-231 (152).

Pour investiguer le trafic endo-lysosomal des nanovecteurs, nous avons commencé par une technique qualitative, la microscopie confocale avec le marquage des endosomes et des lysosomes, qui pourrait nous donner une vision globale sur ce qui se passe dans les endosomes et les lysosomes après 4 h ou 24 h de séjour des nanovecteurs dans les cellules. Pour les deux temps d'analyse, l'incubation des cellules avec les nanovecteurs est stoppée après 4 h. Donc la quantité de nanovecteurs internalisée dans les cellules est la même pour toutes les conditions. Le temps 4 h nous renseigne sur ce qui se passe dans les cellules au cours de l'internalisation et le trafic pendant ces 4 premières heures. Le temps 24 h nous renseigne sur le devenir de ces nanovecteurs et leur trafic au cours des 20 h suivantes. La colocalisation de la fluorescence des fluorochromes des nanovecteurs (Atto390 et sulfocyanine 5) avec les marqueurs des compartiments intracellulaires indique la localisation et l'évolution du trafic des nanovecteurs dans les cellules. Cependant, la colocalisation des fluorochromes peut donner des faux négatifs. En effet, les marqueurs utilisés sont localisés au niveau de la membrane des compartiments et donc la colocalisation implique que des nanovecteurs soient dans le même plan que les marqueurs compartimentaux alors que la partie enfermée dans les endosomes ou les lysosomes n'est pas prise en compte (153). Pour cela, la même expérience est réalisée et analysée avec une technique quantitative, l'imagerie en flux AMNIS® qui combine la cytométrie en flux et l'imagerie de fluorescence. Le temps de contact pour les deux conditions 4 h et 24 h étant le même (4 h), les variations observées sont liées au trafic des nanovecteurs. En utilisant cette technique, le score d'internalisation des siRNA ou des (C)S-FNP dans les endosomes ou les lysosomes est calculé. Ce score prend en compte les siRNA et les (C)S-FNP qui sont colocalisés avec les marqueurs utilisés et ceux qui sont à l'intérieur des compartiments, qui ne montrent

pas de colocalisation avec les marqueurs de ces compartiments. La combinaison des résultats obtenus par les deux techniques permet de donner une vision plus précise de ce qui se passe dans ces vésicules.

Quand l'entrée des nanovecteurs se produit par une voie d'endocytose, l'échappement endosomal représente une étape décisive pour la suite du trafic des siRNA et pour leur efficacité d'inhibition de l'expression du gène cible. En effet, pour que les siRNA atteignent leur site d'action, ils ont besoin de quitter les endosomes pour échapper à la dégradation et accéder au cytosol pour rencontrer les ARNm. Selon le type de composants utilisés dans la formulation des nanovecteurs, il existe différents mécanismes d'échappement endosomal. Pour évaluer la capacité des CS-MSN à sortir des endosomes et pour identifier le(s) mécanisme(s) impliqué(s), différentes techniques sont utilisées : l'analyse des cellules par microscopie à illumination structurée (SIM), la mesure de l'intensité de fluorescence intracellulaire par cytométrie en flux et la transfection en présence d'un inhibiteur de l'acidification des endosomes. L'imagerie SIM montre la rupture des endosomes et le passage des siRNA vers le cytosol. La fluorescence intracellulaire des fluorochromes des CS-MSN (Atto390 et sulfocyanine 5 conjugués aux siRNA et aux CS-FNP, respectivement) est mesurée après 4 h et 24 h d'incubation des cellules avec les CS-MSN. Le résultat obtenu montre une réduction de la fluorescence des siRNA alors que celle de la nanoplateforme (marquée à la sulfocyanine 5) reste constante. Cela suggère que cette réduction est due à une dispersion des siRNA dans le cytosol, ce qui réduit la détectabilité de leur fluorescence. Les mécanismes les plus probablement utilisés par les CS-MSN pour échapper les endosomes sont ceux de la pompe à proton et l'effet parapluie, médiés par les polymères cationiques. Ces mécanismes dépendent fortement de l'acidification du compartiment endosomal. Un test de transfection des cellules avec les nanovecteurs est réalisé en présence d'un inhibiteur de l'acidification des endosomes, la bafilomycine A1. Les résultats obtenus montrent qu'en présence de cet inhibiteur, aucune réduction de l'expression de la GFP n'est observée. Ce résultat suggère une incapacité des nanovecteurs à échapper les endosomes et une absence d'efficacité. Dans la première partie de ces travaux de thèse, nous avons montré le rôle majeur du chitosan dans la formulation pour l'efficacité des CS-MSN. A ce niveau, notre hypothèse est que ce polymère facilite l'échappement endosomal. Cependant, dans la littérature, le chitosan est connu pour son inefficacité à échapper les endosomes à cause de ses propriétés tampon très limitées (137,154,155).

De plus, une variation au niveau du trafic intracellulaire et une différence significative de l'efficacité est observée entre les CS-MSN et les S-MSN (avec et sans peptide,

respectivement). Cette observation est liée au peptide gH625. Il semble que, en plus de son rôle de faciliter l'internalisation des CS-MSN, ce peptide favorise l'échappement endosomal en interagissant, probablement, avec la membrane interne des endosomes. Bien que les mécanismes utilisés par le peptide gH625 pour faciliter l'échappement endosomal des nanovecteurs ne soient pas encore bien déterminés, son rôle à ce niveau est confirmé (156). D'après les résultats présentés dans la troisième partie de cette étude (résultats SIM) et les résultats obtenus par Guarnieri *et al.* (156), il semble qu'il s'agisse d'une induction de la formation de pores transitionnels permettant la sortie des siRNA vers le cytosol. Pour résumer, il semble que l'échappement endosomal des CS-MSN est médié par les mécanismes de pompe à proton, dans un premier temps, suivi par l'effet parapluie et la formation des pores transitionnels.

Le mécanisme utilisé pour l'internalisation et celui de l'échappement endosomal peuvent être liés ou non. En effet, dans le cas où ils sont liés, les composants de surface du nanovecteur qui facilitent l'entrée dans les cellules sont les mêmes à assurer la sortie des siRNA ou des siRNA nanovectorisés de l'endosome et leur passage dans le cytosol, et ces mécanismes sont, généralement, assez similaires. Dans le cas contraire, ce ne sont pas les mêmes composants du nanovecteur qui sont impliqués dans les deux processus et les mécanismes utilisés peuvent être complètement différents. Par exemple, dans leur étude, Akita *et al*. ont montré que l'internalisation de leur nanovecteur, contenant plusieurs couches lipidiques, se fait par macropinocytose alors que l'échappement endosomal se produit par fusion. Ce nanovecteur a été conçu d'une manière à permettre l'intervention de chaque composant à une étape bien précise (99).

Notre étude a permis de tracer le trafic des CS-MSN, dans les cellules MDA-MB-231, dès l'entrée en déterminant les voies impliquées jusqu'au passage des siRNA dans le cytosol et leur action sur le gène cible, en passant par les endosomes et les lysosomes. Cependant, il a été démontré que les mécanismes d'internalisation et le trafic intracellulaire d'un nanovecteur peuvent changer d'un type cellulaire à un autre. En ce sens, Capel *et al.* ont investigué les voies d'entrée d'un nanovecteur polymère dans trois lignées cellulaires. Les résultats obtenus montrent que le mécanisme d'internalisation dominant dans les cellules Calu-3 est l'endocytose clathrine-dépendante, alors que l'endocytose clathrine-indépendante domine dans les cellules H1299. Dans les cellules A549, une endocytose médiée par les cavéoles et les clathrines est mise en évidence. De plus, ils ont montré que la voie d'entrée empruntée par le nanovecteur influence l'efficacité de transfection (157). Cela implique que le devenir intracellulaire ainsi

que l'efficacité peuvent aussi varier en fonction du type cellulaire. Il serait donc intéressant d'élargir l'étude sur d'autres lignées cellulaires de CSTN pour mieux comprendre les interactions cellulaires et subcellulaires des CS-MSN et pour expliquer les effets biologiques observés.

D'une manière générale, le trafic d'un nanovecteur ne s'arrête pas au niveau de l'action des siRNA sur les ARNm. A ce niveau, des questions restent en suspens sur le devenir des autres composants des nanovecteurs. A côté des mécanismes utilisés pour l'internalisation des nanovecteurs, il a été démontré que d'autres voies et mécanismes de trafic intracellulaires sont impliqués tels que l'exocytose et l'autophagie (158–160). L'exocytose est un mécanisme physiologique impliqué dans la régulation de l'homéostasie cellulaire et regroupe trois voies. L'une de ces voies implique les lysosomes et permet de transporter leur contenu de l'intérieur de la cellule vers la membrane pour être expulsé (161,162). Après l'endocytose, les nanoparticules qui restent dans les lysosomes pourraient être expulsées à l'extérieur de la cellule par exocytose (163). L'autophagie est un mécanisme qui désigne la dégradation d'une partie du cytoplasme d'une cellule par ses propres lysosomes. Certaines études ont mis en évidence une augmentation de l'autophagie dans des cellules traitées avec des nanovecteurs (160,164,165). Song *et al.* ont montré que l'efficacité de transfection des siRNA varie en fonction du type d'autophagie induit (160). Par conséquent, pour mieux comprendre l'ensemble du trafic intracellulaire et le devenir des nanovecteurs de siRNA, il serait important d'étudier l'exocytose et l'autophagie.

Evaluation de l'efficacité de transfection des siRNA par les CS-MSN et de leur action au niveau des cibles

Au niveau cellulaire, un nanovecteur de siRNA doit traverser plusieurs barrières avant de permettre l'inhibition de la protéine cible en commençant par l'internalisation cellulaire et l'échappement endosomal. Ces deux étapes influencent largement l'efficacité du nanovecteur et sont elles-mêmes influencées par la composition et les caractéristiques de surface des nanovecteurs. L'entrée dépend, en plus, du temps de contact avec les cellules et il est propre à chaque nanovecteur. Généralement, ces étapes ne durent que quelques heures. En revanche, l'observation d'une extinction de la protéine cible nécessite plus de temps (166). Une fois dans le cytosol, les siRNA activent le complexe RISC chargé de dégrader spécifiquement les ARNm

dont la séquence est ciblée par les siRNA. Le processus de dégradation des ARNm prend un certain temps, mais c'est la demi-vie des protéines qui permet de déterminer leur cinétique d'extinction. En effet, les protéines traduites avant la dégradation de l'ARNm ont une durée de vie plus ou moins longue, ce qui détermine le moment où leur diminution est visualisable. Généralement, l'extinction d'une protéine est évaluée à partir de 48 heures après transfection. Toutefois, l'efficacité d'extinction d'une protéine peut être analysée jusqu'à 96 heures ou plus dans certains cas où la protéine est très stable et possède une demi-vie longue (167).

En ce sens, le temps d'incubation avec les cellules (nécessaire pour l'entrée des nanovecteurs) et le temps d'analyse des cellules (nécessaire pour observer l'extinction de la protéine) influencent très fortement les résultats d'efficacité du nanovecteur. Une optimisation du protocole de transfection est réalisée pour déterminer les paramètres optimaux permettant d'obtenir une efficacité de transfection élevée. Dans un premier temps, la variation du temps d'incubation des CS-MSN préparés avec des siRNA anti-GFP avec des cellules exprimant la GFP montre une augmentation de l'efficacité de transfection des nanovecteurs jusqu'à 4 h, avec une valeur constante au-delà de ce temps. Cela montre que le maximum des CS-MSN internalisés par les cellules est atteint à 4 h. Cette internalisation assez rapide est facilitée par la présence du peptide gH625 à la surface des CS-MSN. Dans la littérature, généralement, le temps de traitement nécessaire pour l'entrée des nanovecteurs avec une quantité suffisante pour une transfection élevée est inférieur à 24 h (117,138,168–170). Ensuite, la variation du temps d'analyse des cellules montre une augmentation de l'efficacité jusqu'à 72 h. Ce temps est justifié par la demi-vie assez longue de la protéine GFP (171). Généralement, le maximum d'extinction de la protéine GFP est détecté à partir de 48 h de traitement (138,151,168). L'optimisation de la formulation des CS-MSN et du protocole de transfection a abouti à une efficacité d'inhibition de la protéine GFP dans des cellules MDA-MB-231/GFP par les siRNA anti-GFP délivrés par les CS-MSN d'environ 73 %.

Pour la validation de l'effet des CS-MSN, l'évaluation de leur efficacité sur une protéine impliquée dans le processus tumoral, la protéine Bcl-xL, est nécessaire. Bien que l'inhibition de l'ARNm et de la protéine Bcl-xL soit significative par rapport aux cellules non traitées, l'efficacité reste inférieure à celle observée sur la GFP (112). Cette différence d'efficacité pourrait être expliquée par la localisation et la distribution de la cible. En effet, une fois les CS-MSN entrés dans les cellules et les siRNA échappés des endosomes, ces derniers se trouvent dispersés dans le cytoplasme. La localisation des ARNm au sein de la cellule fait que la probabilité que les siRNA rencontrent l'ARNm d'une protéine cytoplasmique telle que la GFP

est plus élevée que celle d'une protéine à localisation compartimentale telle que la protéine Bcl-xL qui se situe au niveau de la membrane mitochondriale. Il a été rapporté que la répartition des ARNm dans le cytoplasme et leur traduction suivent une cartographie précise. La localisation des ARNm est influencée par différents paramètres et selon la destinée de la protéine correspondante, le complexe de la traduction de cet ARNm peut être associé à des organelles (172). Cela fait que certains ARNm sont plus accessibles aux siRNA que d'autres. Pour concentrer les nanovecteurs (ou les siRNA) dans un compartiment intracellulaire précis, plusieurs études se dirigent, actuellement, vers un ciblage actif de ce compartiment. Cette stratégie permet de localiser la distribution intracellulaire et d'améliorer l'efficacité des thérapeutiques (173,174). Par exemple, Wang *et al.* ont développé une nanoplateforme à base de poly-L-lysine décorée à la surface avec un ligand pour cibler les mitochondries, le triphenylphosphonium (TPP). La conjugaison de TPP à ces nanoparticules a montré un ciblage sélectif des mitochondries avec une concentration des nanoparticules dans la région péri-mitochondriale. Cette nanoplateforme se montre prometteuse pour la délivrance des thérapies anticancéreuses avec un ciblage des mitochondries (175). Dans le cadre de projet Galileo, nous souhaitons améliorer les CS-MSN en les fonctionnalisant, en plus du gH625, avec un peptide de ciblage mitochondrial, le peptide MS. Dans ce cas, après l'internalisation et l'échappement des CS-MSN facilités par le peptide gH625, le peptide MS qui cible la mitochondrie favoriserait l'accumulation du nanovecteur aux alentours de ce compartiment. Cela pourrait augmenter l'efficacité des CS-MSN à inhiber l'expression de Bcl-xL.

De plus, il a été rapporté que l'efficacité des nanovecteurs de siRNA est étroitement dépendante du type cellulaire et de la protéine cible. En effet, un nanovecteur de siRNA polymère testé sur deux lignées cellulaires exprimant la luciférase (MDA-MB-231 et NIH3T3) a montré une efficacité de transfection différente entre ces deux lignées avec une internalisation environ 1,5 fois plus importante dans les cellules MDA-MB-231(176). De même, Veiseh *et al.* ont développé des nanovecteurs hybrides composés d'un cœur inorganique de SPION avec un revêtement polymère. L'efficacité de ces nanovecteurs de siRNA est évaluée sur trois lignées cancéreuses exprimant la GFP (MCF-7, C6 et TC2). Les résultats obtenus montrent une inhibition de la GFP qui varie entre 70 % et 30 % (138). Corbet *et al.* ont ciblé deux protéines d'intérêts (ASCT2 et MCT1) avec des nanovecteurs formulés avec les siRNA correspondants dans des cellules cancéreuses du col utérin, la lignée siHa. Les résultats obtenus montrent une différence d'efficacité des nanovecteurs à inhiber ces deux protéines, observée par Western Blot (151). Cependant, ici, l'effet des CS-MSN est étudié sur une seule lignée cellulaire de

cancer du sein triple négatif, MDA-MB-231, et une seule protéine d'intérêt (la protéine Bcl-xL) est ciblée. Pour élargir cette étude et mieux évaluer l'efficacité des CS-MSN, il serait intéressant de les tester sur d'autres lignées cellulaires de cancer du sein triple négatif ou sur des cellules en cultures primaires, et de cibler d'autres protéines impliquées dans le processus tumoral (survivine (177,178), PD-L1 (179), BET (180), PIM1 (181,182), …), voir tester l'inhibition de plusieurs protéines en même temps.

Conclusion

L'application de la nanomédecine pour le traitement des cancers est en croissance exponentielle. Bien qu'un certain nombre de nanoformulations pour l'imagerie ou la délivrance de molécules anticancéreuses soient déjà disponibles sur le marché, les nanovecteurs pour la délivrance de siRNA pour le traitement des cancers en sont encore au stade du développement ou des essais cliniques.

Dans ces travaux de thèse, plusieurs choix, études et techniques sont réalisés pour la première fois dans notre laboratoire. Ces nouveautés ont formé des difficultés et des défis pour l'avancement du travail et pour la réalisation de nos objectifs.

La première décision ambitieuse fut de faire le choix du cancer du sein triple négatif comme maladie cible, à cause de l'absence des cibles cellulaires spécifiques et/ou surexprimées dans les cellules tumorales. Cette difficulté nous a incité à chercher des alternatives au ciblage de récepteurs surexprimés pour améliorer la délivrance des nanovecteurs de siRNA. Notre choix s'est orienté vers l'utilisation de l'effet EPR qui permet l'accumulation des nanovecteurs au niveau du site tumoral et vers l'utilisation de peptide gH625 qui a montré une capacité élevée à faciliter l'entrée des nanovecteurs dans les cellules cancéreuses.

Le second objectif était de développer au laboratoire ou à chercher à l'extérieur via des collaborations les techniques nécessaires à l'étude des mécanismes d'internalisation, du trafic et du devenir intracellulaire des nanovecteurs des siRNA. Cette investigation a fait appel à des techniques très variées qui nécessitent une certaine polyvalence et une maîtrise de plusieurs aspects. A l'issue de cette étude, nous avons conclu que le choix du peptide gH625 n'a pas influencé uniquement l'entrée des nanovecteurs dans les cellules, mais aussi leur trafic intracellulaire et, par conséquent, leur efficacité de transfection.

La troisième difficulté de ce travail se résume dans le choix du gène cible et l'évaluation de l'inhibition de son expression. En effet, le choix du gène cible est d'une importance majeure et il demande des connaissances sur la maladie et de l'implication des gènes dans son développement et son évolution. De plus, cette partie de thèse contient des mises en place et des optimisations de certaines techniques de biologie moléculaire (RT-qPCR et Western Blot). Ces techniques sont connues pour la multitude de leurs étapes qui complique leur utilisation en tant que débutants.

Malgré ces difficultés, nous avons réussi à développer un nanovecteur pour la délivrance des siRNA dans des cellules de cancer du sein triple négatif avec des caractéristiques

compatibles avec l'administration par voie systémique. Les premières applications *in vitro* ont montré des résultats prometteurs en termes d'efficacité de délivrance des siRNA par les CS-MSN. Cette étude a permis, également, de construire un schéma du devenir intracellulaire du nanovecteur qui regroupe les voies d'internalisations impliquées, son séjour dans les compartiments intracellulaires et les mécanismes mis en place pour passer dans le cytosol afin d'exercer l'action thérapeutique.

A la fin de cette étude, la formulation des CS-MSN est adaptée pour une future application *in vivo*. De plus, un modèle orthotopique de cancer du sein triple négatif a été mis en place avec succès chez la souris. Donc, il serait intéressant d'utiliser ce modèle pour investiguer la bio-distribution des nanovecteurs, évaluer leur accumulation au niveau tumoral et étudier leur efficacité à inhiber la croissance tumorale, en association ou non à une chimiothérapie.

Bibliographie

1. The International Agency for Research on Cancer (IARC). Latest global cancer data [Internet]. 2018 [cited 2019 Jan 15]. Available from: https://www.iarc.fr/wp-content/uploads/2018/09/pr263_E.pdf

2. The International Agency for Research on Cancer (IARC). Latest world cancer statistics [Internet]. 2012 [cited 2019 Jan 15]. Available from: https://www.iarc.fr/wp-content/uploads/2018/07/pr223_E.pdf

3. Wild CP, Ferlay J, Soerjomataram I, Bray F. The Global Cancer Burden 2018: implications for cancer prevention and control [Internet]. Lyon; 2018 [cited 2019 Feb 26]. Available from: https://www.worldcancercongress.org/sites/congress/files/atoms/files/Plenary 1_presentations.pdf

4. Luengo-Fernandez R, Leal J, Gray A, Sullivan R. Economic burden of cancer across the European Union: a population-based cost analysis. Lancet Oncol [Internet]. 2013 Nov 1 [cited 2019 Feb 27];14(12):1165–74. Available from: https://www.sciencedirect.com/science/article/pii/S147020451370442X

5. Bloom, D.E., Cafiero, E.T., Jané-Llopis, E., Abrahams-Gessel, S., Bloom, L.R., Fathima, S. F, A.B., Gaziano, T., Mowafi, M., Pandya, A., Prettner, K., Rosenberg, L., Seligman, B., Stein, A., & Weinstein C. The Global Economic Burden of Non-communicable Diseases [Internet]. Geneva: World Economic Forum; 2011 [cited 2019 Jan 11]. Available from: www.weforum.org/EconomicsOfNCD

6. Bray F, Ferlay J, Soerjomataram I, Siegel RL, Torre LA, Jemal A. Global cancer statistics 2018: GLOBOCAN estimates of incidence and mortality worldwide for 36 cancers in 185 countries. CA Cancer J Clin [Internet]. 2018 Nov 1 [cited 2019 Feb 27];68(6):394–424. Available from: http://doi.wiley.com/10.3322/caac.21492

7. Lacey J V, Kreimer AR, Buys SS, Marcus PM, Chang S-C, Leitzmann MF, et al. Breast cancer epidemiology according to recognized breast cancer risk factors in the Prostate, Lung, Colorectal and Ovarian (PLCO) Cancer Screening Trial Cohort. BMC Cancer [Internet]. 2009 Mar 17 [cited 2019 Feb 28];9:84. Available from: http://www.ncbi.nlm.nih.gov/pubmed/19292893

8. Carey LA, Perou CM, Livasy CA, Dressler LG, Cowan D, Conway K, et al. Race, Breast Cancer Subtypes, and Survival in the Carolina Breast Cancer Study. JAMA [Internet]. 2006 Jun 7 [cited 2019 Mar 20];295(21):2492. Available from: http://jama.jamanetwork.com/article.aspx?doi=10.1001/jama.295.21.2492

9. Sporikova Z, Koudelakova V, Trojanec R, Hajduch M. Genetic Markers in Triple-Negative Breast Cancer. Clin Breast Cancer [Internet]. 2018 Oct 1 [cited 2019 Mar 20];18(5):e841–50. Available from: https://www.sciencedirect.com/science/article/pii/S1526820918300934

10. Baselga J, Campone M, Piccart M, Burris HA, Rugo HS, Sahmoud T, et al. Everolimus in Postmenopausal Hormone-Receptor–Positive Advanced Breast Cancer. N Engl J Med [Internet]. 2012 Feb 9 [cited 2019 Aug 21];366(6):520–9. Available from: http://www.nejm.org/doi/10.1056/NEJMoa1109653

11. Aromatase inhibitors versus tamoxifen in early breast cancer: patient-level meta-analysis of the randomised trials. Lancet [Internet]. 2015 Oct 3 [cited 2019 Aug 21];386(10001):1341–52. Available from: https://www.sciencedirect.com/science/article/pii/S0140673615610741

12. Slamon DJ, Leyland-Jones B, Shak S, Fuchs H, Paton V, Bajamonde A, et al. Use of Chemotherapy plus a Monoclonal Antibody against HER2 for Metastatic Breast Cancer That Overexpresses HER2. N Engl J Med [Internet]. 2001 Mar 15 [cited 2019 Aug 21];344(11):783–92. Available from: http://www.nejm.org/doi/abs/10.1056/NEJM200103153441101

13. Romond EH, Perez EA, Bryant J, Suman VJ, Geyer CE, Davidson NE, et al. Trastuzumab plus Adjuvant Chemotherapy for Operable HER2-Positive Breast Cancer. N Engl J Med [Internet]. 2005 Oct 20 [cited 2019 Aug 21];353(16):1673–84. Available from: http://www.nejm.org/doi/abs/10.1056/NEJMoa052122

14. Nahta R, Hung M-C, Esteva FJ. The HER-2-Targeting Antibodies Trastuzumab and Pertuzumab Synergistically Inhibit the Survival of Breast Cancer Cells. Cancer Res [Internet]. 2004 Apr 1 [cited 2019 Aug 21];64(7):2343–6. Available from: http://www.ncbi.nlm.nih.gov/pubmed/15059883

15. Amiri-Kordestani L, Blumenthal GM, Xu QC, Zhang L, Tang SW, Ha L, et al. FDA Approval: Ado-Trastuzumab Emtansine for the Treatment of Patients with HER2-Positive Metastatic Breast Cancer. Clin Cancer Res [Internet]. 2014 Sep 1 [cited 2019

Aug 21];20(17):4436–41. Available from: http://www.ncbi.nlm.nih.gov/pubmed/24879797

16. Burstein HJ, Sun Y, Dirix LY, Jiang Z, Paridaens R, Tan AR, et al. Neratinib, an Irreversible ErbB Receptor Tyrosine Kinase Inhibitor, in Patients With Advanced ErbB2-Positive Breast Cancer. J Clin Oncol [Internet]. 2010 [cited 2019 Aug 21];28:1301–7. Available from: www.jco.orgon

17. Geyer CE, Forster J, Lindquist D, Chan S, Romieu CG, Pienkowski T, et al. Lapatinib plus Capecitabine for HER2-Positive Advanced Breast Cancer. N Engl J Med [Internet]. 2006 Dec 28 [cited 2019 Aug 21];355(26):2733–43. Available from: http://www.nejm.org/doi/abs/10.1056/NEJMoa064320

18. Wang C, Kar S, Lai X, Cai W, Arfuso F, Sethi G, et al. Triple negative breast cancer in Asia: An insider's view. Cancer Treat Rev [Internet]. 2018 Jan 1 [cited 2019 Mar 20];62:29–38. Available from: https://www.sciencedirect.com/science/article/pii/S0305737217301846#f0010

19. Lebert JM, Lester R, Powell E, Seal M, McCarthy J. Advances in the systemic treatment of triple-negative breast cancer. Curr Oncol [Internet]. 2018 [cited 2019 Aug 21];25(Suppl 1):S142–50. Available from: http://www.ncbi.nlm.nih.gov/pubmed/29910657

20. Park JH, Ahn J-H, Kim S-B. How shall we treat early triple-negative breast cancer (TNBC): from the current standard to upcoming immuno-molecular strategies. ESMO open [Internet]. 2018 [cited 2019 Aug 21];3(Suppl 1):e000357. Available from: http://www.ncbi.nlm.nih.gov/pubmed/29765774

21. Clancy S, Brown W. Translation: DNA to mRNA to Protein. Nat Educ [Internet]. 2008;1(1):101. Available from: https://www.nature.com/scitable/topicpage/translation-dna-to-mrna-to-protein-393

22. Matoulkova E, Michalova E, Vojtesek B, Hrstka R. The role of the 3' untranslated region in post-transcriptional regulation of protein expression in mammalian cells. RNA Biol [Internet]. 2012 May 27 [cited 2019 Apr 5];9(5):563–76. Available from: http://www.tandfonline.com/doi/abs/10.4161/rna.20231

23. Filipowicz W, Bhattacharyya SN, Sonenberg N. Mechanisms of post-transcriptional regulation by microRNAs: are the answers in sight? Nat Rev Genet [Internet]. 2008 Feb

1 [cited 2019 Apr 5];9(2):102–14. Available from: http://www.nature.com/articles/nrg2290

24. Schwanhäusser B, Busse D, Li N, Dittmar G, Schuchhardt J, Wolf J, et al. Global quantification of mammalian gene expression control. Nature [Internet]. 2011 May 19 [cited 2019 Apr 5];473(7347):337–42. Available from: http://www.nature.com/articles/nature10098

25. Napoli C, Lemieux C, Jorgensen R. lntroduction of a Chimeric Chalcone Synthase Gene into Petunia Results in Reversible Co-Suppression of Homologous Genes Ín trans [Internet]. Vol. 2, The Plant Cell. American Society of Plant Physiologists; 1990 [cited 2019 Apr 24]. Available from: http://www.plantcell.org/content/plantcell/2/4/279.full.pdf

26. Fire A, Xu S, Montgomery MK, Kostas SA, Driver SE, Mello CC. Potent and specific genetic interference by double-stranded RNA in Caenorhabditis elegans. Nature [Internet]. 1998 Feb 19 [cited 2019 Mar 21];391(6669):806–11. Available from: http://www.nature.com/articles/35888

27. Elbashir SM, Harborth J, Lendeckel W, Yalcin A, Weber K, Tuschl T. Duplexes of 21-nucleotide RNAs mediate RNA interference in cultured mammalian cells. Nature [Internet]. 2001 May 24 [cited 2019 Mar 21];411(6836):494–8. Available from: http://www.ncbi.nlm.nih.gov/pubmed/11373684

28. Lam JKW, Chow MYT, Zhang Y, Leung SWS. siRNA Versus miRNA as Therapeutics for Gene Silencing. Mol Ther - Nucleic Acids [Internet]. 2015 [cited 2019 Mar 21];4:e252. Available from: https://linkinghub.elsevier.com/retrieve/pii/S2162253116300373

29. Golden DE, Gerbasi VR, Sontheimer EJ. An inside job for siRNAs. Mol Cell [Internet]. 2008 Aug 8 [cited 2019 Apr 19];31(3):309–12. Available from: http://www.ncbi.nlm.nih.gov/pubmed/18691963

30. Carthew RW, Sontheimer EJ. Origins and Mechanisms of miRNAs and siRNAs. Cell [Internet]. 2009 Feb 20 [cited 2019 Apr 19];136(4):642–55. Available from: http://www.ncbi.nlm.nih.gov/pubmed/19239886

31. Carthew, Richard W. and Sontheimer EJ, Carthew RW, Sontheimer EJ. Origins and Mechanisms of miRNAs and siRNAs. Cell [Internet]. 2009;136(4):642–55. Available

from: http://www.ncbi.nlm.nih.gov/pmc/articles/PMC2675692/

32. Gavrilov K, Saltzman WM. Therapeutic siRNA: principles, challenges, and strategies. Yale J Biol Med [Internet]. 2012 Jun [cited 2019 Feb 14];85(2):187–200. Available from: http://www.ncbi.nlm.nih.gov/pubmed/22737048

33. Tatiparti K, Sau S, Kashaw S, Iyer A. siRNA Delivery Strategies: A Comprehensive Review of Recent Developments. Nanomaterials [Internet]. 2017 Apr 5 [cited 2019 Mar 11];7(4):77. Available from: http://www.ncbi.nlm.nih.gov/pubmed/28379201

34. Scherr M, Battmer K, Winkler T, Heidenreich O, Ganser A, Eder M. Specific inhibition of bcr-abl gene expression by small interfering RNA. Blood [Internet]. 2003 Feb 15 [cited 2019 Apr 23];101(4):1566–9. Available from: http://www.ncbi.nlm.nih.gov/pubmed/12393533

35. Martinez LA, Naguibneva I, Lehrmann H, Vervisch A, Tchénio T, Lozano G, et al. Synthetic small inhibiting RNAs: efficient tools to inactivate oncogenic mutations and restore p53 pathways. Proc Natl Acad Sci U S A [Internet]. 2002 Nov 12 [cited 2019 Apr 23];99(23):14849–54. Available from: http://www.ncbi.nlm.nih.gov/pubmed/12403821

36. Yoshinouchi M, Yamada T, Kizaki M, Fen J, Koseki T, Ikeda Y, et al. In vitro and in vivo growth suppression of human papillomavirus 16-positive cervical cancer cells by e6 siRNA. Mol Ther [Internet]. 2003 Nov 1 [cited 2019 Apr 23];8(5):762–8. Available from: https://www.sciencedirect.com/science/article/pii/S1525001603002831

37. Choudhury A, Charo J, Parapuram SK, Hunt RC, Hunt DM, Seliger B, et al. Small interfering RNA (siRNA) inhibits the expression of the Her2/neu gene, upregulates HLA class I and induces apoptosis of Her2/neu positive tumor cell lines. Int J Cancer [Internet]. 2004 Jan 1 [cited 2019 Apr 23];108(1):71–7. Available from: http://doi.wiley.com/10.1002/ijc.11497

38. Hammond SM, Bernstein E, Beach D, Hannon GJ. An RNA-directed nuclease mediates post-transcriptional gene silencing in Drosophila cells. Nature [Internet]. 2000 Mar [cited 2019 Apr 23];404(6775):293–6. Available from: http://www.nature.com/articles/35005107

39. Rivas F V, Tolia NH, Song J-J, Aragon JP, Liu J, Hannon GJ, et al. Purified Argonaute2 and an siRNA form recombinant human RISC. Nat Struct Mol Biol [Internet]. 2005 Apr

30 [cited 2019 Apr 23];12(4):340–9. Available from: http://www.nature.com/articles/nsmb918

40. Murchison EP, Partridge JF, Tam OH, Cheloufi S, Hannon GJ. Characterization of Dicer-deficient murine embryonic stem cells. Proc Natl Acad Sci U S A [Internet]. 2005 Aug 23 [cited 2019 Apr 23];102(34):12135–40. Available from: http://www.ncbi.nlm.nih.gov/pubmed/16099834

41. Gredell JA, Dittmer MJ, Wu M, Chan C, Walton SP. Recognition of siRNA asymmetry by TAR RNA binding protein (TRBP). Biochemistry [Internet]. 2010 Apr 13 [cited 2019 Apr 23];49(14):3148. Available from: http://www.ncbi.nlm.nih.gov/pubmed/20184375

42. Peng J, Li X, Zhang D, Chen J-K, Su Y, Smith SB, et al. Hyperglycemia, p53, and mitochondrial pathway of apoptosis are involved in the susceptibility of diabetic models to ischemic acute kidney injury. Kidney Int [Internet]. 2015 Jan [cited 2019 Apr 25];87(1):137–50. Available from: http://www.ncbi.nlm.nih.gov/pubmed/24963915

43. Zuber J, Shi J, Wang E, Rappaport AR, Herrmann H, Sison EA, et al. RNAi screen identifies Brd4 as a therapeutic target in acute myeloid leukaemia. Nature [Internet]. 2011 Aug 3 [cited 2019 Apr 25];478(7370):524–8. Available from: http://www.ncbi.nlm.nih.gov/pubmed/21814200

44. Magalhães M, Alvarez-Lorenzo C, Concheiro A, Figueiras A, Santos AC, Veiga F. RNAi-based therapeutics for lung cancer: biomarkers, microRNAs, and nanocarriers. Expert Opin Drug Deliv [Internet]. 2018 Oct 3 [cited 2019 Apr 25];15(10):965–82. Available from: https://www.tandfonline.com/doi/full/10.1080/17425247.2018.1517744

45. Ponder BAJ. Cancer genetics. Nature [Internet]. 2001 May [cited 2019 Apr 25];411(6835):336–41. Available from: http://www.nature.com/articles/35077207

46. Marone M, Scambia G, Giannitelli C, Ferrandina G, Masciullo V, Bellacosa A, et al. Analysis of cyclin E and CDK2 in ovarian cancer: Gene amplification and RNA overexpression. Int J Cancer [Internet]. 1998 Jan 5 [cited 2019 Apr 25];75(1):34–9. Available from: http://doi.wiley.com/10.1002/%28SICI%291097-0215%2819980105%2975%3A1%3C34%3A%3AAID-IJC6%3E3.0.CO%3B2-2

47. Bell SM, Scott N, Cross D, Sagar P, Lewis FA, Blair GE, et al. Prognostic value of p53 overexpression and c-Ki-ras gene mutations in colorectal cancer. Gastroenterology

[Internet]. 1993 Jan 1 [cited 2019 Apr 25];104(1):57–64. Available from: https://www.sciencedirect.com/science/article/pii/001650859390835Z

48. Aagaard L, Rossi JJ. RNAi therapeutics: principles, prospects and challenges. Adv Drug Deliv Rev [Internet]. 2007 Mar 30 [cited 2019 Feb 13];59(2–3):75–86. Available from: http://www.ncbi.nlm.nih.gov/pubmed/17449137

49. Ozcan G, Ozpolat B, Coleman RL, Sood AK, Lopez-Berestein G, Medicine R. Preclinical and clinical development of siRNA-based therapeutics. Adv Drug Deliv Rev [Internet]. 2015 Jun 29 [cited 2018 Nov 26];87:108–19. Available from: http://www.ncbi.nlm.nih.gov/pubmed/25666164

50. Schroeder A, Levins CG, Cortez C, Langer R, Anderson DG. Lipid-based nanotherapeutics for siRNA delivery. J Intern Med [Internet]. 2010 Jan [cited 2019 Jun 7];267(1):9–21. Available from: http://www.ncbi.nlm.nih.gov/pubmed/20059641

51. Xia Y, Tian J, Chen X. Effect of surface properties on liposomal siRNA delivery. Biomaterials [Internet]. 2016 Feb [cited 2019 Jun 7];79:56–68. Available from: http://www.ncbi.nlm.nih.gov/pubmed/26695117

52. Tseng Y, Mozumdar S, Huang L. Lipid-based systemic delivery of siRNA. Adv Drug Deliv Rev. 2009;61(9):721–31.

53. Granot Y, Peer D. Delivering the right message: Challenges and opportunities in lipid nanoparticles-mediated modified mRNA therapeutics—An innate immune system standpoint. Semin Immunol [Internet]. 2017 Dec 1 [cited 2019 Jun 7];34:68–77. Available from: https://www.sciencedirect.com/science/article/pii/S1044532317300398?via%3Dihub#fig0015

54. Kong WH, Park K, Lee M-Y, Lee H, Sung DK, Hahn SK. Cationic solid lipid nanoparticles derived from apolipoprotein-free LDLs for target specific systemic treatment of liver fibrosis. Biomaterials [Internet]. 2013 Jan 1 [cited 2019 Aug 28];34(2):542–51. Available from: https://www.sciencedirect.com/science/article/pii/S0142961212010903#fig1

55. Arnold AE, Czupiel P, Shoichet M. Engineered polymeric nanoparticles to guide the cellular internalization and trafficking of small interfering ribonucleic acids. J Control Release [Internet]. 2017;259:3–15. Available from:

http://dx.doi.org/10.1016/j.jconrel.2017.02.019

56. Shrestha R, Elsabahy M, Florez-Malaver S, Samarajeewa S, Wooley KL. Endosomal escape and siRNA delivery with cationic shell crosslinked knedel-like nanoparticles with tunable buffering capacities. Biomaterials [Internet]. 2012 Nov 1 [cited 2018 Nov 13];33(33):8557–68. Available from: https://www.sciencedirect.com/science/article/pii/S0142961212008496#sch2

57. Videira M, Arranja A, Rafael D, Gaspar R. Preclinical development of siRNA therapeutics: Towards the match between fundamental science and engineered systems. Nanomedicine Nanotechnology, Biol Med [Internet]. 2014;10(4):689–702. Available from: http://www.sciencedirect.com/science/article/pii/S1549963413006837

58. Cavallaro G, Sardo C, Craparo EF, Porsio B, Giammona G. Polymeric nanoparticles for siRNA delivery: Production and applications. Int J Pharm [Internet]. 2017 Jun 20 [cited 2019 Feb 15];525(2):313–33. Available from: https://www.sciencedirect.com/science/article/pii/S0378517317302880?via%3Dihub

59. Endoh T, Ohtsuki T. Cellular siRNA delivery using cell-penetrating peptides modified for endosomal escape. Adv Drug Deliv Rev [Internet]. 2009 Jul 25 [cited 2019 May 29];61(9):704–9. Available from: https://www.sciencedirect.com/science/article/pii/S0169409X09000970

60. Meade BR, Dowdy SF. Exogenous siRNA delivery using peptide transduction domains/cell penetrating peptides. Adv Drug Deliv Rev [Internet]. 2007 Mar 30 [cited 2019 May 29];59(2–3):134–40. Available from: https://www.sciencedirect.com/science/article/pii/S0169409X0700021X

61. Thapa RK, Sullivan MO. Gene delivery by peptide-assisted transport. Curr Opin Biomed Eng [Internet]. 2018 Sep 1 [cited 2019 Jun 5];7:71–82. Available from: https://www.sciencedirect.com/science/article/pii/S246845111830014X

62. Tai W, Gao X. Functional peptides for siRNA delivery. Adv Drug Deliv Rev [Internet]. 2017 Feb 1 [cited 2019 Jun 4];110–111:157–68. Available from: https://www.sciencedirect.com/science/article/pii/S0169409X16302368

63. Conde J, Ambrosone A, Hernandez Y, Tian F, McCully M, Berry CC, et al. 15 years on siRNA delivery: Beyond the State-of-the-Art on inorganic nanoparticles for RNAi therapeutics. Nano Today [Internet]. 2015 Aug 1 [cited 2019 May 29];10(4):421–50.

Available from: https://www.sciencedirect.com/science/article/pii/S174801321500078X#fig0015

64. Malmsten M. Inorganic nanomaterials as delivery systems for proteins, peptides, DNA, and siRNA. Curr Opin Colloid Interface Sci [Internet]. 2013 Oct 1 [cited 2019 May 29];18(5):468–80. Available from: https://www.sciencedirect.com/science/article/pii/S1359029413000897

65. Pan X, Thompson R, Meng X, Wu D, Xu L. Tumor-targeted RNA-interference: functional non-viral nanovectors. Am J Cancer Res [Internet]. 2010;1(1):25–42. Available from: http://www.ncbi.nlm.nih.gov/pmc/articles/PMC3092671/

66. Sosnovik DE, Nahrendorf M, Weissleder R. Magnetic nanoparticles for MR imaging: agents, techniques and cardiovascular applications. Basic Res Cardiol [Internet]. 2008;103(2):122–30. Available from: http://www.ncbi.nlm.nih.gov/pmc/articles/PMC2597271/

67. Derfus AM, Chen AA, Min D-H, Ruoslahti E, Bhatia SN. Targeted Quantum Dot Conjugates for siRNA Delivery. Bioconjug Chem [Internet]. 2007;18(5):1391–6. Available from: http://dx.doi.org/10.1021/bc060367e

68. Fan C, Wang S, Hong JW, Bazan GC, Plaxco KW, Heeger AJ. Beyond superquenching: Hyper-efficient energy transfer from conjugated polymers to gold nanoparticles. Proc Natl Acad Sci U S A [Internet]. 2003;100(11):6297–301. Available from: http://www.ncbi.nlm.nih.gov/pmc/articles/PMC164440/

69. Bañobre-López M, Teijeiro A, Rivas J. Magnetic nanoparticle-based hyperthermia for cancer treatment [Internet]. Vol. 18, Reports of Practical Oncology and Radiotherapy. Elsevier; 2013 [cited 2018 Nov 26]. p. 397–400. Available from: https://www.sciencedirect.com/science/article/pii/S1507136713010614

70. Giustini AJ, Petryk AA, Cassim SM, Tate JA, Baker I, Hoopes PJ. Magnetic nanoparticle hyperthermia in cancer treatment. Nano Life [Internet]. 2010;1(01n02). Available from: http://www.ncbi.nlm.nih.gov/pmc/articles/PMC3859910/

71. Wahajuddin, Arora S. Superparamagnetic iron oxide nanoparticles: Magnetic nanoplatforms as drug carriers [Internet]. Vol. 7, International Journal of Nanomedicine. Dove Press; 2012 [cited 2018 Nov 27]. p. 3445–71. Available from: http://www.ncbi.nlm.nih.gov/pubmed/22848170

72. Ehlerding EB, Chen F, Cai W. Biodegradable and Renal Clearable Inorganic Nanoparticles. Adv Sci [Internet]. 2016 Feb 1 [cited 2019 May 29];3(2):1500223. Available from: http://doi.wiley.com/10.1002/advs.201500223

73. Davis ME, Zuckerman JE, Choi CHJ, Seligson D, Tolcher A, Alabi C a, et al. Evidence of RNAi in humans from systemically administered siRNA via targeted nanoparticles. October. 2010;464(7291):1067–70.

74. Zuckerman JE, Gritli I, Tolcher A, Heidel JD, Lim D, Morgan R, et al. Correlating animal and human phase Ia/Ib clinical data with CALAA-01, a targeted, polymer-based nanoparticle containing siRNA. Proc Natl Acad Sci U S A [Internet]. 2014 Aug 5 [cited 2019 Mar 18];111(31):11449–54. Available from: http://www.ncbi.nlm.nih.gov/pubmed/25049380

75. Tabernero J, Shapiro GI, LoRusso PM, Cervantes A, Schwartz GK, Weiss GJ, et al. First-in-humans trial of an RNA interference therapeutic targeting VEGF and KSP in cancer patients with liver involvement. Cancer Discov [Internet]. 2013 Apr 1 [cited 2019 Apr 26];3(4):406–17. Available from: http://www.ncbi.nlm.nih.gov/pubmed/23358650

76. Al Shaer D, Al Musaimi O, Albericio F, de la Torre B, Al Shaer D, Al Musaimi O, et al. 2018 FDA Tides Harvest. Pharmaceuticals [Internet]. 2019 Apr 5 [cited 2019 May 12];12(2):52. Available from: https://www.mdpi.com/1424-8247/12/2/52

77. Search of: siRNA | Cancer - List Results - ClinicalTrials.gov [Internet]. [cited 2019 Aug 21]. Available from: https://clinicaltrials.gov/ct2/results?cond=Cancer&term=siRNA&cntry=&state=&city=&dist=

78. Lee J-M, Yoon T-J, Cho Y-S. Recent Developments in Nanoparticle-Based siRNA Delivery for Cancer Therapy. Biomed Res Int [Internet]. 2013 Jun 17 [cited 2019 Apr 30];2013. Available from: https://www.hindawi.com/journals/bmri/2013/782041/

79. Li Y, Humphries B, Yang C, Wang Z. Nanoparticle-Mediated Therapeutic Agent Delivery for Treating Metastatic Breast Cancer-Challenges and Opportunities. Nanomater (Basel, Switzerland) [Internet]. 2018 May 24 [cited 2019 Apr 30];8(6). Available from: http://www.ncbi.nlm.nih.gov/pubmed/29794968

80. Donahue ND, Acar H, Wilhelm S. Concepts of nanoparticle cellular uptake, intracellular trafficking, and kinetics in nanomedicine. Adv Drug Deliv Rev [Internet]. 2019 Apr 22

[cited 2019 May 2]; Available from: https://www.sciencedirect.com/science/article/pii/S0169409X1930050X?via%3Dihub#bb0165

81. Chen X, Irani NG, Friml J. Clathrin-mediated endocytosis: the gateway into plant cells. Curr Opin Plant Biol [Internet]. 2011;14(6):674–82. Available from: http://www.ncbi.nlm.nih.gov/pubmed/21945181

82. Conner SD, Schmid SL. Regulated portals of entry into the cell. Nature [Internet]. 2003 [cited 2016 Dec 28];422(6927):37–44. Available from: http://www.nature.com/nature/journal/v422/n6927/full/nature01451.html

83. Bareford LM, Swaan PW, Swaan LMB and PW. Endocytic mechanisms for targeted drug delivery. Adv Drug Deliv Rev [Internet]. 2007 Aug 10 [cited 2018 Nov 27];59(8):748–58. Available from: http://www.ncbi.nlm.nih.gov/pubmed/17659804

84. Hillaireau H, Couvreur P. Nanocarriers' entry into the cell: relevance to drug delivery. Cell Mol Life Sci [Internet]. 2009 Sep 5 [cited 2019 Aug 20];66(17):2873–96. Available from: http://link.springer.com/10.1007/s00018-009-0053-z

85. Vercauteren D, Rejman J, Martens TF, Demeester J, De Smedt SC, Braeckmans K. On the cellular processing of non-viral nanomedicines for nucleic acid delivery: Mechanisms and methods. J Control Release [Internet]. 2012 [cited 2017 Jan 20];161(2):566–81. Available from: http://dx.doi.org/10.1016/j.jconrel.2012.05.020

86. Prokop A, Davidson JMJ. Nanovehicular Intracellular Delivery Systems. J Pharm Sci [Internet]. 2008;97(9):3518–90. Available from: http://www.ncbi.nlm.nih.gov/pmc/articles/PMC3747665/

87. Sahay G, Alakhova DY, Kabanov A V. Endocytosis of Nanomedicine. J Control Release. 2010;145(3):182–95.

88. Gao X, Gu X, Chen H. The Distribution and Elimination of Nanomaterials in Brain. Neurotox Nanomater Nanomedicine [Internet]. 2017 Jan 1 [cited 2019 May 27];59–74. Available from: https://www.sciencedirect.com/science/article/pii/B9780128045985000039

89. Lee H, Kim I-K, Park TG. Intracellular Trafficking and Unpacking of siRNA/Quantum Dot-PEI Complexes Modified with and without Cell Penetrating Peptide: Confocal and Flow Cytometric FRET Analysis. Bioconjug Chem [Internet]. 2010 Feb 17 [cited 2019

Jun 10];21(2):289–95. Available from: https://pubs.acs.org/doi/10.1021/bc900342p

90. Valiante S, Falanga A, Cigliano L, Iachetta G, Busiello RA, La Marca V, et al. Peptide gH625 enters into neuron and astrocyte cell lines and crosses the blood–brain barrier in rats. Int J Nanomedicine. 2015;10:1885–98.

91. Mauroy C, Castagnos P, Orio J, Blache MC, Rico-Lattes I, Teissié J, et al. Versatile cellular uptake mediated by catanionic vesicles: Simultaneous spontaneous membrane fusion and endocytosis. Mol Pharm [Internet]. 2015 [cited 2018 Nov 27];12(1):103–10. Available from: https://pubs.acs.org/sharingguidelines

92. Kunisawa J, Masuda T, Katayama K, Yoshikawa T, Tsutsumi Y, Akashi M, et al. Fusogenic liposome delivers encapsulated nanoparticles for cytosolic controlled gene release. J Control Release. 2005;105(3):344–53.

93. Deeba F, Tahseen HN, Sharad KS, Ahmad N, Akhtar S, Saleemuddin M, et al. Phospholipid diversity: Correlation with membrane–membrane fusion events. Biochim Biophys Acta - Biomembr [Internet]. 2005 May 20 [cited 2019 Aug 23];1669(2):170–81. Available from: https://www.sciencedirect.com/science/article/pii/S0005273605000465

94. Ma D. Enhancing endosomal escape for nanoparticle mediated siRNA delivery. Nanoscale [Internet]. 2014 May 29 [cited 2019 Jun 11];6(12):6415. Available from: http://xlink.rsc.org/?DOI=c4nr00018h

95. Varkouhi AK, Scholte M, Storm G, Haisma HJ. Endosomal escape pathways for delivery of biologicals. J Control Release [Internet]. 2011 May 10 [cited 2019 Apr 11];151(3):220–8. Available from: https://www.sciencedirect.com/science/article/pii/S0168365910009053#bb0340

96. Schubert US, Traeger A, Bus T. The great escape: How cationic polyplexes overcome the endosomal barrier. J Mater Chem B [Internet]. 2018 Nov 7 [cited 2018 Nov 20];6(43):6904–18. Available from: http://xlink.rsc.org/?DOI=C8TB00967H

97. Nguyen J, Szoka FC. Nucleic acid delivery: The missing pieces of the puzzle? Acc Chem Res [Internet]. 2012 Jul 17 [cited 2018 Nov 27];45(7):1153–62. Available from: http://www.ncbi.nlm.nih.gov/pubmed/22428908

98. Varkouhi AK, Scholte M, Storm G, Haisma HJ. Endosomal escape pathways for delivery of biologicals. J Control Release Off J Control Release Soc [Internet]. 2011;151(3):220–

8. Available from: file://www.sciencedirect.com/science/article/pii/S0168365910009053

99. Akita H, Kudo A, Minoura A, Yamaguti M, Khalil IA, Moriguchi R, et al. Multi-layered nanoparticles for penetrating the endosome and nuclear membrane via a step-wise membrane fusion process. Biomaterials [Internet]. 2009 May 1 [cited 2019 Jun 11];30(15):2940–9. Available from: https://www.sciencedirect.com/science/article/pii/S0142961209001574

100. El-Sayed A, Khalil IA, Kogure K, Futaki S, Harashima H. Octaarginine- and octalysine-modified nanoparticles have different modes of endosomal escape. J Biol Chem [Internet]. 2008 Aug 22 [cited 2019 Jun 12];283(34):23450–61. Available from: http://www.ncbi.nlm.nih.gov/pubmed/18550548

101. Martens TF, Remaut K, Demeester J, De Smedt SC, Braeckmans K. Intracellular delivery of nanomaterials: How to catch endosomal escape in the act. Nano Today [Internet]. 2014;9(3):344–64. Available from: http://www.sciencedirect.com/science/article/pii/S1748013214000565

102. Perillo E, Hervé-Aubert K, Allard-Vannier E, Falanga A, Galdiero S, Chourpa I. Synthesis and in vitro evaluation of fluorescent and magnetic nanoparticles functionalized with a cell penetrating peptide for cancer theranosis. J Colloid Interface Sci [Internet]. 2017 Aug 1 [cited 2018 Nov 26];499:209–17. Available from: https://www.sciencedirect.com/science/article/pii/S0021979717303740?via%3Dihub

103. Galdiero S, Falanga A, Morelli G, Galdiero M. gH625: A milestone in understanding the many roles of membranotropic peptides. Biochim Biophys Acta - Biomembr [Internet]. 2015 Jan 1 [cited 2018 Nov 26];1848(1, Part A):16–25. Available from: https://www.sciencedirect.com/science/article/pii/S0005273614003411?via%3Dihub

104. Carberry TP, Tarallo R, Falanga A, Finamore E, Galdiero M, Weck M, et al. Dendrimer functionalization with a membrane-interacting domain of herpes simplex virus type 1: Towards intracellular delivery. Chem - A Eur J. 2012;18(43):13678–85.

105. Perillo E, Porto S, Falanga A, Zappavigna S, Stiuso P, Tirino V, et al. Liposome armed with herpes virus-derived gH625 peptide to overcome doxorubicin resistance in lung adenocarcinoma cell lines. Oncotarget [Internet]. 2016 Jan 26 [cited 2019 Jun 14];7(4):4077–92. Available from: http://www.ncbi.nlm.nih.gov/pubmed/26554306

106. Falanga A, Lombardi L, Tarallo R, Franci G, Perillo E, Palomba L, et al. The intriguing journey of gH625-dendrimers. RSC Adv [Internet]. 2017 Jan 27 [cited 2019 Jun 14];7(15):9106–14. Available from: http://xlink.rsc.org/?DOI=C6RA28405A

107. Oltvai Z, Korsmeyer SJ. Checkpoints of dueling dimers foil death wishes. Cell [Internet]. 1994 Oct 21 [cited 2019 Jul 11];79(2):189–92. Available from: http://www.ncbi.nlm.nih.gov/pubmed/7954787

108. Varna M, Ratajczak P, Bertheau P, Janin A. Atlas of Genetics and Cytogenetics in Oncology and Haematology [Internet]. BCL2L1 (BCL2-like 1). 2009 [cited 2019 Jul 12]. Available from: http://atlasgeneticsoncology.org/Genes/GC_BCL2L1.html

109. Vander Heiden MG, Chandel NS, Williamson EK, Schumacker PT, Thompson CB. Bcl-xL Regulates the Membrane Potential and Volume Homeostasis of Mitochondria. Cell [Internet]. 1997 Nov 28 [cited 2019 Jul 11];91(5):627–37. Available from: https://www.sciencedirect.com/science/article/pii/S009286740080450X

110. Reed JC. Bcl-2 family proteins: regulators of apoptosis and chemoresistance in hematologic malignancies. Semin Hematol [Internet]. 1997 Oct [cited 2019 Jul 11];34(4 Suppl 5):9–19. Available from: http://www.ncbi.nlm.nih.gov/pubmed/9408956

111. Reed JC. Bcl-2 Family Proteins: Strategies for Overcoming Chemoresistance in Cancer. Adv Pharmacol [Internet]. 1997 Jan 1 [cited 2019 Jul 11];41:501–32. Available from: https://www.sciencedirect.com/science/article/abs/pii/S1054358908610704

112. Ben Djemaa S, David S, Hervé-Aubert K, Falanga A, Galdiero S, Allard-Vannier E, et al. Formulation and in vitro evaluation of a siRNA delivery nanosystem decorated with gH625 peptide for triple negative breast cancer theranosis. Eur J Pharm Biopharm [Internet]. 2018;131(July):99–108. Available from: https://doi.org/10.1016/j.ejpb.2018.07.024

113. Taylor S, Wakem M, Dijkman G, Alsarraj M, Nguyen M. A practical approach to RT-qPCR—Publishing data that conform to the MIQE guidelines. Methods [Internet]. 2010 Apr 1 [cited 2019 Aug 30];50(4):S1–5. Available from: https://www.sciencedirect.com/science/article/pii/S1046202310000204

114. Katch F, Michael ED, Horvath SM. Estimation of body volume by underwater weighing: description of a simple method. J Appl Physiol [Internet]. 1967 Nov [cited 2019 Jul 9];23(5):811–3. Available from: http://www.ncbi.nlm.nih.gov/pubmed/6061401

115. Ben Djemaa S, Hervé-Aubert K, Lajoie L, Falanga A, Galdiero S, Nedellec S, et al. gH625 Cell-Penetrating Peptide Promotes the Endosomal Escape of Nanovectorized siRNA in a Triple-Negative Breast Cancer Cell Line. Biomacromolecules [Internet]. 2019 Jul 30 [cited 2019 Aug 4];acs.biomac.9b00637. Available from: http://www.ncbi.nlm.nih.gov/pubmed/31305991

116. Rooswinkel RW, van de Kooij B, de Vries E, Paauwe M, Braster R, Verheij M, et al. Antiapoptotic potency of Bcl-2 proteins primarily relies on their stability, not binding selectivity. Blood [Internet]. 2014 May 1 [cited 2019 Jul 12];123(18):2806–15. Available from: http://www.ncbi.nlm.nih.gov/pubmed/24622325

117. Guruprasath P, Kim J, Gunassekaran GR, Chi L, Kim SYSS-YHS-H, Park R-WW, et al. Interleukin-4 receptor-targeted delivery of Bcl-xL siRNA sensitizes tumors to chemotherapy and inhibits tumor growth. Biomaterials [Internet]. 2017;142(Supplement C):101–11. Available from: http://dx.doi.org/10.1016/j.biomaterials.2017.07.024

118. Nikam RR, Gore KR. Journey of siRNA: Clinical Developments and Targeted Delivery. Nucleic Acid Ther [Internet]. 2018 Aug 1 [cited 2019 Mar 11];28(4):209–24. Available from: http://www.liebertpub.com/doi/10.1089/nat.2017.0715

119. Judge AD, Robbins M, Tavakoli I, Levi J, Hu L, Fronda A, et al. Confirming the RNAi-mediated mechanism of action of siRNA-based cancer therapeutics in mice. J Clin Invest [Internet]. 2009 Mar 2 [cited 2019 May 9];119(3):661–73. Available from: http://www.ncbi.nlm.nih.gov/pubmed/19229107

120. Kaczmarek JC, Kowalski PS, Anderson DG. Advances in the delivery of RNA therapeutics: From concept to clinical reality [Internet]. Vol. 9, Genome Medicine. BioMed Central; 2017 [cited 2019 Mar 29]. p. 60. Available from: http://genomemedicine.biomedcentral.com/articles/10.1186/s13073-017-0450-0

121. Rizk M, Tüzmen Ş. Update on the clinical utility of an RNA interference-based treatment: Focus on Patisiran [Internet]. Vol. 10, Pharmacogenomics and Personalized Medicine. Dove Press; 2017 [cited 2019 Jun 3]. p. 267–78. Available from: http://www.ncbi.nlm.nih.gov/pubmed/29184431

122. Lv H, Zhang S, Wang B, Cui S, Yan J. Toxicity of cationic lipids and cationic polymers in gene delivery. J Control Release Off J Control Release Soc [Internet]. 2006;114(1):100–9. Available from: http://www.ncbi.nlm.nih.gov/pubmed/16831482

123. Lee J-H, Lee K, Moon SH, Lee Y, Park TG, Cheon J. All-in-one target-cell-specific magnetic nanoparticles for simultaneous molecular imaging and siRNA delivery. Angew Chem Int Ed Engl [Internet]. 2009;48(23):4174–9. Available from: http://www.ncbi.nlm.nih.gov/pubmed/19408274

124. Yezhelyev M V, Qi L, O'Regan RM, Nie S, Gao X. Proton-Sponge-Coated Quantum Dots for siRNA Delivery and Intracellular Imaging. J Am Chem Soc [Internet]. 2008;130(28):9006–12. Available from: http://www.ncbi.nlm.nih.gov/pmc/articles/PMC2621273/

125. Plassat V, Martina MS, Barratt G, Ménager C, Lesieur S. Sterically stabilized superparamagnetic liposomes for MR imaging and cancer therapy: Pharmacokinetics and biodistribution. Int J Pharm [Internet]. 2007;344(1–2):118–27. Available from: http://www.sciencedirect.com/science/article/pii/S0378517307003766

126. Song W-J, Du J-Z, Sun T-M, Zhang P-Z, Wang J. Gold Nanoparticles Capped with Polyethyleneimine for Enhanced siRNA Delivery. Small [Internet]. 2010;6(2):239–46. Available from: http://onlinelibrary.wiley.com/doi/10.1002/smll.200901513/abstract

127. Soenen SJ, Rivera-Gil P, Montenegro J-M, Parak WJ, De Smedt SC, Braeckmans K. Cellular toxicity of inorganic nanoparticles: Common aspects and guidelines for improved nanotoxicity evaluation. Nano Today [Internet]. 2011 Oct 1 [cited 2019 Aug 19];6(5):446–65. Available from: https://www.sciencedirect.com/science/article/pii/S1748013211000909

128. Choi S-J, Lee JK, Jeong J, Choy J-H. Toxicity evaluation of inorganic nanoparticles: considerations and challenges. Mol Cell Toxicol [Internet]. 2013 Sep 3 [cited 2019 Aug 19];9(3):205–10. Available from: http://link.springer.com/10.1007/s13273-013-0026-z

129. Stylianopoulos T. EPR-effect: Utilizing size-dependent nanoparticle delivery to solid tumors [Internet]. Vol. 4, Therapeutic Delivery. Future Science Ltd London, UK; 2013 [cited 2019 Aug 19]. p. 421–3. Available from: http://www.future-science.com/doi/10.4155/tde.13.8

130. Nel A, Ruoslahti E, Meng H. New Insights into "Permeability" as in the Enhanced Permeability and Retention Effect of Cancer Nanotherapeutics. ACS Nano [Internet]. 2017 Oct 24 [cited 2019 Aug 20];11(10):9567–9. Available from: http://pubs.acs.org/doi/10.1021/acsnano.7b07214

131. Resnier P, Montier T, Mathieu V, Benoit J-PP, Passirani C. A review of the current status of siRNA nanomedicines in the treatment of cancer. Biomaterials [Internet]. 2013 Sep 1 [cited 2018 Nov 26];34(27):6429–43. Available from: https://www.sciencedirect.com/science/article/pii/S0142961213005346?via%3Dihub

132. Perry JL, Reuter KG, Luft JC, Pecot C V, Zamboni W, DeSimone JM. Mediating Passive Tumor Accumulation through Particle Size, Tumor Type, and Location. Nano Lett [Internet]. 2017 [cited 2019 Aug 20];17(5):2879–86. Available from: http://www.ncbi.nlm.nih.gov/pubmed/28287740

133. Acharya S, Sahoo SK. PLGA nanoparticles containing various anticancer agents and tumour delivery by EPR effect. Adv Drug Deliv Rev [Internet]. 2011 Mar 18 [cited 2019 Aug 20];63(3):170–83. Available from: https://www.sciencedirect.com/science/article/pii/S0169409X10002024

134. Bruniaux J, Djemaa S Ben, Hervé-Aubert K, Marchais H, Chourpa I, David S, et al. Stealth magnetic nanocarriers of siRNA as platform for breast cancer theranostics. Int J Pharm [Internet]. 2017;532(2):660–8. Available from: http://www.sciencedirect.com/science/article/pii/S0378517317304325

135. David S, Marchais H, Bedin D, Chourpa I. Modelling the response surface to predict the hydrodynamic diameters of theranostic magnetic siRNA nanovectors. Int J Pharm [Internet]. 2014 Jan 15 [cited 2018 Nov 27];478(1):409–15. Available from: https://www.sciencedirect.com/science/article/pii/S037851731400876X?via%3Dihub

136. Chen M, Gao S, Dong M, Song J, Yang C, Howard KA, et al. Chitosan / siRNA Nanoparticles Encapsulated in PLGA Nanofibers for siRNA Delivery. ACS Nano. 2012;(6):4835–44.

137. Köping-Höggård M, Tubulekas I, Guan H, Edwards K, Nilsson M, Vårum K, et al. Chitosan as a nonviral gene delivery system. Structure–property relationships and characteristics compared with polyethylenimine in vitro and after lung administration in vivo. Gene Ther [Internet]. 2001 Jul 13 [cited 2019 Jul 24];8(14):1108–21. Available from: http://www.nature.com/articles/3301492

138. Veiseh O, Kievit FM, Mok H, Ayesh J, Clark C, Fang C, et al. Cell transcytosing poly-arginine coated magnetic nanovector for safe and effective siRNA delivery. Biomaterials [Internet]. 2011 Aug [cited 2016 Oct 28];32(24):5717–25. Available from: http://www.ncbi.nlm.nih.gov/pubmed/21570721

139. Zhao ZX, Gao SY, Wang JC, Chen CJ, Zhao EY, Hou WJ, et al. Self-assembly nanomicelles based on cationic mPEG-PLA-b-Polyarginine(R15) triblock copolymer for siRNA delivery. Biomaterials [Internet]. 2012 Oct 1 [cited 2018 Apr 17];33(28):6793–807. Available from: https://www.sciencedirect.com/science/article/pii/S0142961212006217?via%3Dihub

140. Huang Y, Wang X, Huang W, Cheng Q, Zheng S, Guo S, et al. Systemic Administration of siRNA via cRGD-containing Peptide. Sci Rep [Internet]. 2015 Aug 24 [cited 2019 Sep 4];5:12458. Available from: http://www.ncbi.nlm.nih.gov/pubmed/26300278

141. Xie Y, Qiao H, Su Z, Chen M, Ping Q, Sun M. PEGylated carboxymethyl chitosan/calcium phosphate hybrid anionic nanoparticles mediated hTERT siRNA delivery for anticancer therapy. Biomaterials [Internet]. 2014;35(27):7978–91. Available from: http://www.sciencedirect.com/science/article/pii/S0142961214006255

142. Plianwong S, Opanasopit P, Ngawhirunpat T, Rojanarata T. Chitosan combined with poly-l-arginine as efficient, safe, and serum-insensitive vehicle with RNase protection ability for siRNA delivery. Biomed Res Int [Internet]. 2013 Jun 23 [cited 2018 Nov 27];2013:574136. Available from: http://www.ncbi.nlm.nih.gov/pubmed/23865058

143. Shim MS, Kwon YJ. Efficient and targeted delivery of siRNA in vivo. FEBS J [Internet]. 2010;277(23):4814–27. Available from: http://www.ncbi.nlm.nih.gov/pubmed/21078116

144. Wang LH, Rothberg KG, Anderson RG. Mis-assembly of clathrin lattices on endosomes reveals a regulatory switch for coated pit formation. J Cell Biol [Internet]. 1993 Dec [cited 2019 Jul 24];123(5):1107–17. Available from: http://www.ncbi.nlm.nih.gov/pubmed/8245121

145. Iversen T-G, Skotland T, Sandvig K. Endocytosis and intracellular transport of nanoparticles: Present knowledge and need for future studies. Nano Today [Internet]. 2011 Apr 1 [cited 2019 Jul 24];6(2):176–85. Available from: https://www.sciencedirect.com/science/article/pii/S1748013211000181#bib0445

146. Kou L, Sun J, Zhai Y, He Z. The endocytosis and intracellular fate of nanomedicines: Implication for rational design. Asian J Pharm Sci [Internet]. 2013 Feb 1 [cited 2019 Jul 24];8(1):1–10. Available from: https://www.sciencedirect.com/science/article/pii/S1818087613000020?via%3Dihub

147. Liu X, Zhou J, Yu T, Chen C, Cheng Q, Sengupta K, et al. Adaptive Amphiphilic Dendrimer-Based Nanoassemblies as Robust and Versatile siRNA Delivery Systems. Angew Chemie Int Ed [Internet]. 2014 Oct 27 [cited 2019 Aug 20];53(44):11822–7. Available from: http://doi.wiley.com/10.1002/anie.201406764

148. Park D-H, Cho J, Kwon O-J, Yun C-O, Choy J-H. Biodegradable Inorganic Nanovector: Passive versus Active Tumor Targeting in siRNA Transportation. Angew Chemie Int Ed [Internet]. 2016 Mar 24 [cited 2019 Aug 20];55(14):4582–6. Available from: http://doi.wiley.com/10.1002/anie.201510844

149. Dauty E, Remy J-S, Zuber G, Behr J-P. Intracellular delivery of nanometric DNA particles via the folate receptor. Bioconjug Chem [Internet]. 2002;13(4):831–9. Available from: http://www.ncbi.nlm.nih.gov/pubmed/12121139

150. Zhu H, Zhang S, Ling Y, Meng G, Yang Y, Zhang W. PH-responsive hybrid quantum dots for targeting hypoxic tumor siRNA delivery. J Control Release [Internet]. 2015;220:529–44. Available from: http://dx.doi.org/10.1016/j.jconrel.2015.11.017

151. Corbet C, Ragelle H, Pourcelle V, Vanvarenberg K, Marchand-Brynaert J, Préat V, et al. Delivery of siRNA targeting tumor metabolism using non-covalent PEGylated chitosan nanoparticles: Identification of an optimal combination of ligand structure, linker and grafting method. J Control Release [Internet]. 2016;223:53–63. Available from: http://dx.doi.org/10.1016/j.jconrel.2015.12.020

152. Du L, Zhou J, Meng L, Wang X, Wang C, Huang Y, et al. The pH-Triggered Triblock Nanocarrier Enabled Highly Efficient siRNA Delivery for Cancer Therapy. Theranostics [Internet]. 2017 [cited 2019 Aug 20];7(14):3432–45. Available from: http://www.ncbi.nlm.nih.gov/pubmed/28912886

153. Selby LI, Cortez-Jugo CM, Such GK, Johnston APR. Nanoescapology: progress toward understanding the endosomal escape of polymeric nanoparticles. Wiley Interdiscip Rev Nanomedicine Nanobiotechnology [Internet]. 2017 Sep 1 [cited 2018 Nov 20];9(5):e1452. Available from: http://doi.wiley.com/10.1002/wnan.1452

154. Chang K-L, Higuchi Y, Kawakami S, Yamashita F, Hashida M. Efficient Gene Transfection by Histidine-Modified Chitosan through Enhancement of Endosomal Escape. Bioconjug Chem [Internet]. 2010 Jun 16 [cited 2019 Jul 24];21(6):1087–95. Available from: https://pubs.acs.org/doi/10.1021/bc1000609

155. Liang W, Lam JKW. Endosomal Escape Pathways for Non-Viral Nucleic Acid Delivery Systems. 2012 [cited 2019 Jul 24]; Available from: http://dx.doi.org/10.5772/46006

156. Guarnieri D, Muscetti O, Falanga A, Fusco S, Belli V, Perillo E, et al. Surface decoration with gH625-membranotropic peptides as a method to escape the endo-lysosomal compartment and reduce nanoparticle toxicity. Nanotechnology [Internet]. 2015 Oct 16 [cited 2019 Jul 5];26(41):415101. Available from: http://stacks.iop.org/0957-4484/26/i=41/a=415101?key=crossref.1c79a228878381f42de67eb905ce5e0e

157. Capel V, Vllasaliu D, Watts P, Stolnik S. Insight into the relationship between the cell culture model, cell trafficking and siRNA silencing efficiency. Biochem Biophys Res Commun [Internet]. 2016 [cited 2018 Nov 27];477(2):260–5. Available from: http://www.ncbi.nlm.nih.gov/pubmed/27349867

158. Shukla RS, Jain A, Zhao Z, Cheng K. Intracellular trafficking and exocytosis of a multi-component siRNA nanocomplex. Nanomedicine Nanotechnology, Biol Med [Internet]. 2016;12(5):1323–34. Available from: http://dx.doi.org/10.1016/j.nano.2016.02.003

159. Sakai-Kato K, Un K, Nanjo K, Nishiyama N, Kusuhara H, Kataoka K, et al. Elucidating the molecular mechanism for the intracellular trafficking and fate of block copolymer micelles and their components. Biomaterials [Internet]. 2014;35(5):1347–58. Available from: http://dx.doi.org/10.1016/j.biomaterials.2013.11.027

160. Song W, Ma Z, Zhang Y, Yang C. Autophagy plays a dual role during intracellular siRNA delivery by lipoplex and polyplex nanoparticles. Acta Biomater [Internet]. 2017;58:196–204. Available from: http://dx.doi.org/10.1016/j.actbio.2017.05.038

161. Behzadi S, Serpooshan V, Tao W, Hamaly MA, Alkawareek MY, Dreaden EC, et al. Cellular uptake of nanoparticles: journey inside the cell. Chem Soc Rev [Internet]. 2017 Jul 17 [cited 2018 Dec 13];46(14):4218–44. Available from: http://xlink.rsc.org/?DOI=C6CS00636A

162. Bruce A, Alexander J, Julian L, Martin R, Keith R, Peter W. Transport from the Trans Golgi Network to the Cell Exterior: Exocytosis. In: Science G, editor. Molecular Biology of the Cell [Internet]. 4 th. New York; 2002. Available from: https://www.ncbi.nlm.nih.gov/books/NBK26892/

163. Sakhtianchi R, Minchin RF, Lee K-B, Alkilany AM, Serpooshan V, Mahmoudi M. Exocytosis of nanoparticles from cells: Role in cellular retention and toxicity. Adv

Colloid Interface Sci [Internet]. 2013 Dec 1 [cited 2019 Jan 29];201–202:18–29. Available from: https://www.sciencedirect.com/science/article/pii/S0001868613001280

164. Becker AL, Orlotti NI, Folini M, Cavalieri F, Zelikin AN, Johnston APR, et al. Redox-Active Polymer Microcapsules for the Delivery of a Survivin-Specific siRNA in Prostate Cancer Cells. ACS Nano [Internet]. 2011 Feb 22 [cited 2019 Jul 25];5(2):1335–44. Available from: http://pubs.acs.org/doi/10.1021/nn103044z

165. Beretta GL, Folini M, Cavalieri F, Yan Y, Fresch E, Kaliappan S, et al. Unravelling "off-target" effects of redox-active polymers and polymer multilayered capsules in prostate cancer cells. Nanoscale [Internet]. 2015 Mar 26 [cited 2019 Jul 25];7(14):6261–70. Available from: http://xlink.rsc.org/?DOI=C4NR07240E

166. Ribet C. Analyse cinétique de l'interférence par l'ARN dans les compartiments nucléaire et cytoplasmique des cellules de mammifères. 2008 Dec 15 [cited 2019 Jul 18];1–334. Available from: https://tel.archives-ouvertes.fr/tel-00084397

167. Bruniaux J. Développement de nanoparticules lipidiques pour la délivrance de courtes séquences d'ARN interférents [Internet]. 2014 [cited 2019 Jul 18]. Available from: https://tel.archives-ouvertes.fr/tel-01553465

168. Veiseh O, Kievit FM, Fang C, Mu N, Jana S, Leung MC, et al. Chlorotoxin bound magnetic nanovector tailored for cancer cell targeting, imaging, and siRNA delivery. Biomaterials [Internet]. 2010 [cited 2016 Oct 28];31(31):8032–42. Available from: http://www.ncbi.nlm.nih.gov/pmc/articles/PMC2930137/

169. Ragelle H, Colombo S, Pourcelle V, Vanvarenberg K, Vandermeulen G, Bouzin C, et al. Intracellular siRNA delivery dynamics of integrin-targeted, PEGylated chitosan-poly(ethylene imine) hybrid nanoparticles: A mechanistic insight. J Control Release [Internet]. 2015;211(1):1–9. Available from: http://dx.doi.org/10.1016/j.jconrel.2015.05.274

170. Miteva M, Kirkbride KC, Kilchrist K V., Werfel TA, Li H, Nelson CE, et al. Tuning PEGylation of mixed micelles to overcome intracellular and systemic siRNA delivery barriers. Biomaterials [Internet]. 2015;38:97–107. Available from: http://dx.doi.org/10.1016/j.biomaterials.2014.10.036

171. Corish P, Tyler-Smith C. Attenuation of green fluorescent protein half-life in mammalian cells. Protein Eng [Internet]. 1999;12(12):1035–40. Available from:

http://www.ncbi.nlm.nih.gov/pubmed/10611396

172. Katz ZB, English BP, Lionnet T, Yoon YJ, Monnier N, Ovryn B, et al. Mapping translation “hot-spots” in live cells by tracking single molecules of mRNA and ribosomes. Elife [Internet]. 2016 Jan 13 [cited 2019 Jul 12];5. Available from: http://www.ncbi.nlm.nih.gov/pubmed/26760529

173. Nurunnabi M, Khatun Z, Badruddoza AZM, McCarthy JR, Lee Y, Huh KM. Biomaterials and Bioengineering Approaches for Mitochondria and Nuclear Targeting Drug Delivery. ACS Biomater Sci Eng [Internet]. 2019 Apr 8 [cited 2019 Jul 12];5(4):1645–60. Available from: http://pubs.acs.org/doi/10.1021/acsbiomaterials.8b01615

174. Jhaveri A, Torchilin V. Intracellular delivery of nanocarriers and targeting to subcellular organelles. Expert Opin Drug Deliv [Internet]. 2016 Jan 2 [cited 2019 Aug 20];13(1):49–70. Available from: http://www.tandfonline.com/doi/full/10.1517/17425247.2015.1086745

175. Wang X-H, Peng H-S, Yang L, You F-T, Teng F, Tang A-W, et al. Poly-l-lysine assisted synthesis of core–shell nanoparticles and conjugation with triphenylphosphonium to target mitochondria. J Mater Chem B [Internet]. 2013 Sep 11 [cited 2019 Jul 12];1(38):5143. Available from: http://xlink.rsc.org/?DOI=c3tb20884b

176. Werfel TA, Jackson MA, Kavanaugh TE, Kirkbride KC, Miteva M, Giorgio TD, et al. Combinatorial optimization of PEG architecture and hydrophobic content improves ternary siRNA polyplex stability, pharmacokinetics, and potency in vivo. J Control Release [Internet]. 2017 [cited 2018 Nov 27];255(Supplement C):12–26. Available from: http://www.sciencedirect.com/science/article/pii/S0168365917304935

177. Ding Y, Su S, Zhang R, Shao L, Zhang Y, Wang B, et al. Precision combination therapy for triple negative breast cancer via biomimetic polydopamine polymer core-shell nanostructures. Biomaterials [Internet]. 2017 Jan 1 [cited 2019 Aug 20];113:243–52. Available from: https://www.sciencedirect.com/science/article/pii/S0142961216306032

178. Hu Y, Xu K, Yagüe E. miR-218 targets survivin and regulates resistance to chemotherapeutics in breast cancer. Breast Cancer Res Treat [Internet]. 2015 Jun 22 [cited 2019 Aug 20];151(2):269–80. Available from: http://link.springer.com/10.1007/s10549-015-3372-9

179. Li C-W, Lim S-O, Chung EM, Kim Y-S, Park AH, Yao J, et al. Eradication of Triple-Negative Breast Cancer Cells by Targeting Glycosylated PD-L1. Cancer Cell [Internet]. 2018 Feb 12 [cited 2019 Aug 20];33(2):187-201.e10. Available from: https://www.sciencedirect.com/science/article/pii/S1535610818300096

180. Bai L, Zhou B, Yang C-Y, Ji J, McEachern D, Przybranowski S, et al. Targeted Degradation of BET Proteins in Triple-Negative Breast Cancer. Cancer Res [Internet]. 2017 May 1 [cited 2019 Aug 20];77(9):2476–87. Available from: http://www.ncbi.nlm.nih.gov/pubmed/28209615

181. Brasó-Maristany F, Filosto S, Catchpole S, Marlow R, Quist J, Francesch-Domenech E, et al. PIM1 kinase regulates cell death, tumor growth and chemotherapy response in triple-negative breast cancer. Nat Med [Internet]. 2016 Nov 24 [cited 2019 Aug 20];22(11):1303–13. Available from: http://www.nature.com/articles/nm.4198

182. Horiuchi D, Camarda R, Zhou AY, Yau C, Momcilovic O, Balakrishnan S, et al. PIM1 kinase inhibition as a targeted therapy against triple-negative breast tumors with elevated MYC expression. Nat Med [Internet]. 2016 Nov 24 [cited 2019 Aug 20];22(11):1321–9. Available from: http://www.nature.com/articles/nm.4213

Annexes

Annexe 1 : Fluorescence Microscopy as a Tool for Nanomedicine-Cell Interactions Study: Input of Particle Design and of Analytical Strategy

Publié dans Microscopy and Microanalysis, 2018

1316
doi:10.1017/S1431927618007067
Microsc. Microanal. 24 (Suppl 1), 2018
© Microscopy Society of America 2018

Fluorescence Microscopy as a Tool for Nanomedicine-Cell Interactions Study: Input of Particle Design and of Analytical Strategy

Sanaa Ben Djemaa[1], Mathias Pacaud[1,2], Katel Hervé-Aubert[1], Stéphanie David[1], Emilie Allard-Vannier[1], Emilie Munnier[1], Anastasia Ignatova[3], Amir Fahmi[2], Alexey Feofanov[3,4] and Igor Chourpa[1]

[1.] EA6295 Nanomedicine & Nanoprobes, University of Tours, Tours, France.
[2.] Faculty Technology&Bionics, Rhein-Waal University of Applied Sciences, Kleve, Germany.
[3.] Shemyakin and Ovchinnikov Institute of Bioorganic Chemistry, Russian Academy of Sciences, Moscow, Russia.
[4.] Biological Faculty, Lomonosov Moscow State University, Moscow, Russia.

Various nanomedicine platforms are developed in perspective of disease diagnosis, therapy or theragnosis, namely those based on superparamagnetic iron oxide nanoparticles (SPIONs) and/or gold nanoparticles (AuNPs) [1]. For each nanomedicine platform, one of critical parameters to evaluate is its interaction with target cells, namely its adhesion to cell surface, its internalization, subcellular distribution and action mechanism(s) [2-4]. For this kind of studies, optical microscopy is often used, as it provides physiological and complete view of cells. Some of AuNPs and AgNPs can be detected by dark field microscopy, due to plasmon-enhanced scattering of light. For more specific and spatially resolved optical microscopy of a wide range of metal NPs (MNPs), usual strategy consists in labelling them with fluorescent dyes and detecting them with laser scanning confocal microscopy (LSCM). However, in order to take benefit of the fluorescence microscopy and make relevant conclusions from it, choice of an appropriate particle design and analytical strategy are critical.

Based on our recent studies of fluorescent MNPs coated with various organic shells, we have established several rules [2-4]. First of all, they concern the MNPs fluorescent labelling: (i) covalent binding of the dye can be not enough to ensure its chemical stability – it can be degraded and/or detached from the MNP inside cells; (ii) the dye covalently bound to the MNP core should be hidden under the organic shell (typically under the polymer like polyethylene glycol, PEG), otherwise it can be cleaved from the particle and/or quenched, as well as it may affect the colloidal stability of the particle and its interactions with biological targets. Secondly, relevant assessment of nanoparticle behavior within cells is also dependent on the ability to distinguish the fluorophore attached to the nanoparticles from that one detached from them. The latter is also very important to follow delivery of fluorescent active molecules.

We describe here two analytical strategies helpful in understanding of the fluorescence originating from cells treated with nanomedicine platforms. The first one consisted in using

confocal spectral imaging (CSI, made with a LabRam microscope, Horiba SA, France) of the fluorescence (Fig 1): recording full spectra of AlexaFluor488-labelled siRNA from each point of the cell scanned with excitation laser beam (491 nm line of a Calypso 75 laser, Cobolt, France) allowed us to map separately the siRNA loaded into SPION-PEG and the siRNA released to the cytosol (em max at 521 and 527 nm, respectively, Fig 1 C).

The second strategy consisted in adjusting non-spectral LSCM microscope (Model SP2, Leica, Germany) for complementary spatially-resolved analysis of the elastic scattering from AuNPs (633 nm) together with the fluorescence from the Nile Blue dye (exc/em 633/(670-676) nm). This allowed us to establish that MNPs remain attached on the cellular membranes while the released dye enters the cells and accumulated in cytoplasmic vesicles (Fig 2).

To conclude, rational particle design together with innovative analytical approaches based on laser-scanning confocal microscopy (spectral and non-spectral detection of fluorescence and of light scattering) contribute into a reliable understanding of nanomedicine-cell interactions [5].

References:

[1] J Gautier et al. J Control Release **169**(1-2) 2013, p. 48.

[2] J Bruniaux et al. Int J Pharm. **S0378-5173**(17) (2017), p. 30432.

[3] E Allard-Vannier et al. Biochim Biophys Acta **1861**(6) (2017), p. 1578.

[4] E Perillo et al. J Colloid Interface Sci. **499** (2017), p. 209.

[5] The authors acknowledge funding from the following grants in the frames of MINERVA project (ERA-NET RUS PLUS program): RFBR 16-54-76013 (Russia), 01DJ16019 (Germany) and MENESR N°321 (France). We acknowledge also the support from Institut National du Cancer (INCa), Fondation ARC and Ligue Nationale Contre le Cancer (LNCC) (grant ARC_INCa_LNCC_7636).

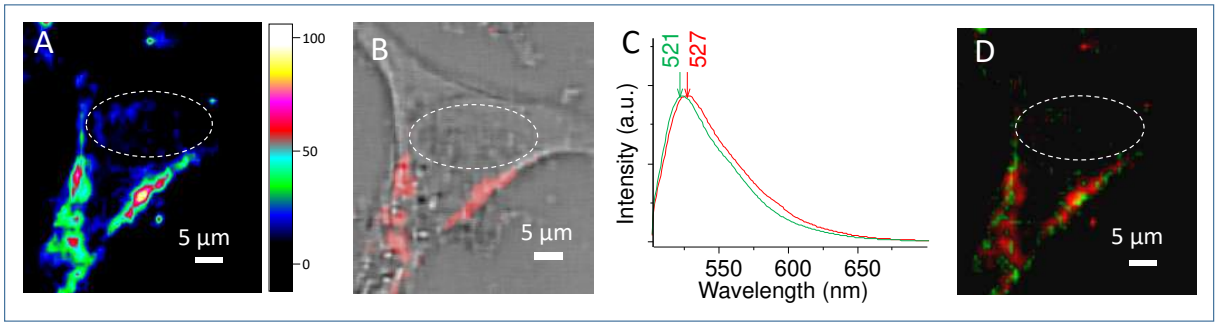

Figure 1. Delivery of siRNA to a live BT474 cancer cell by SPION-PEG nanovectors as studied by CSI: A - map of the total fluorescence intensity distribution over the cell (dashed line indicates nucleus); B – merge of the map A (red zones) with a white-light image of the cell; C – typical fluorescence emission spectra from Alexa 488-labelled siRNA loaded to the nanovectors suspended in PBS (green line) and once delivered to cytosol (red line); D: merge of two spectral maps: siRNA still carried by the nanovectors (green zones seen on the cell membrane) and siRNA released to cytosol (red zones).

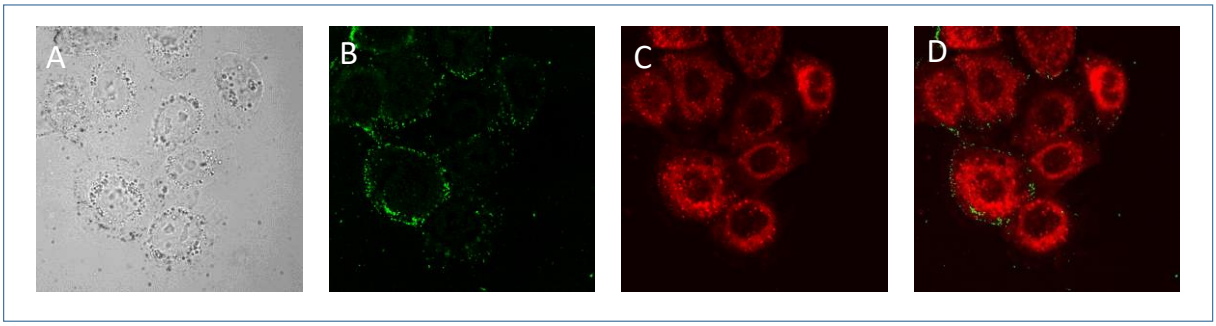

Figure 2. Delivery of fluorescent dye Nile Blue (NB) to SKBR3 cancer cells by plasmonic gold nanoparticles (AuNPs) as studied by LSCM: A – white-light image of cells; B – plasmon-enhanced elastic scattering image shows that AuNPs are mainly accumulated on cell membrane; C – far red fluorescence of NB shows that the dye is internalized and accumulated in vesicular cytoplasmic structures. D – merge of the B and C images.

Annexe 2 : siRNA delivery system based on magnetic nanovectors: Characterization and stability evaluation

Publié dans European Journal of Pharmaceutical Sciences, 2017

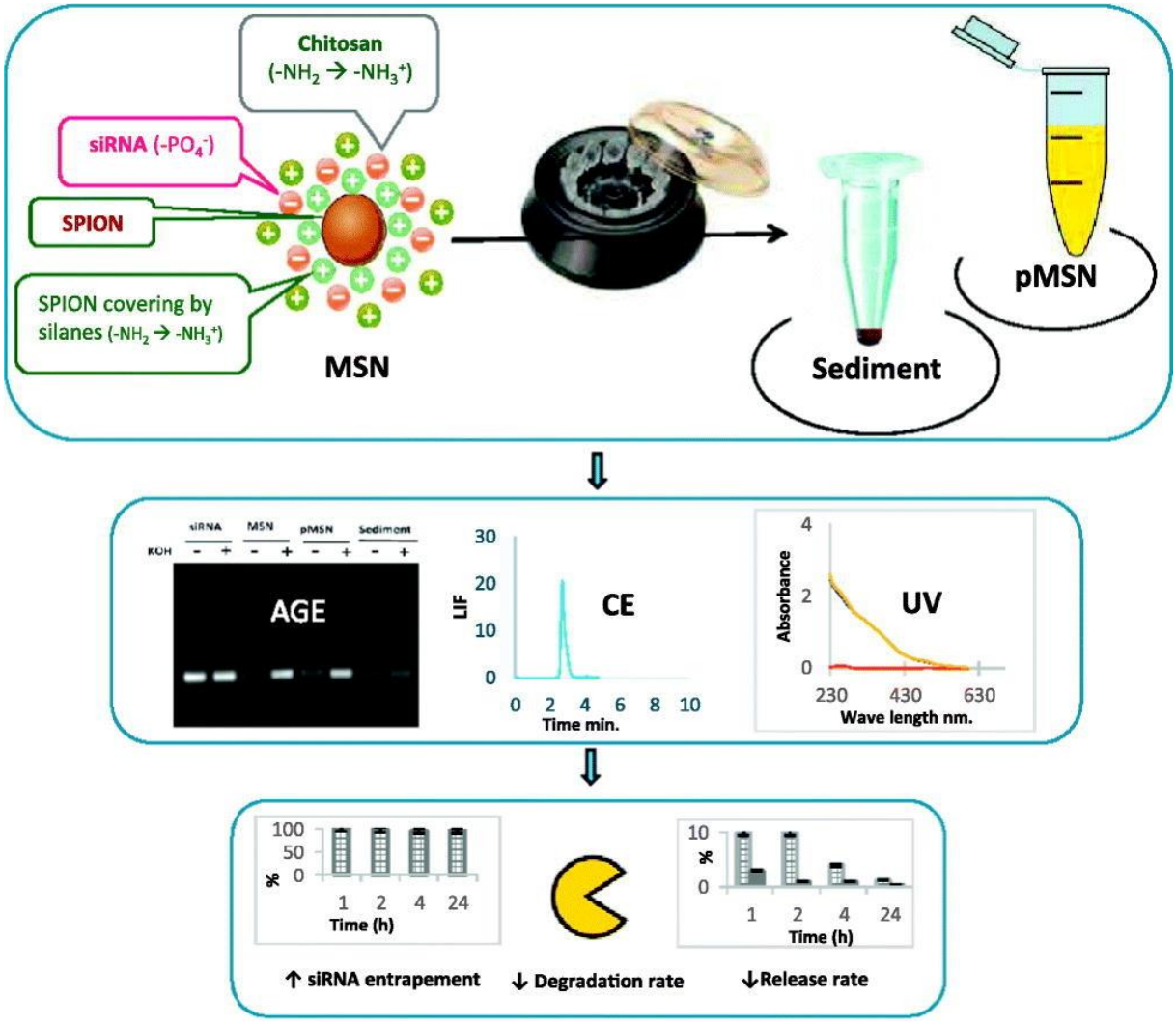

European Journal of Pharmaceutical Sciences 106 (2017) 287–293

Contents lists available at ScienceDirect

European Journal of Pharmaceutical Sciences

journal homepage: www.elsevier.com/locate/ejps

siRNA delivery system based on magnetic nanovectors: Characterization and stability evaluation

Mohammed Abdelrahman[a,b], Laurence Douziech Eyrolles[a,*], Suad Y. Alkarib[c], Katel Hervé-Aubert[a], Sanaa Ben Djemaa[a], Hervé Marchais[a], Igor Chourpa[a], Stephanie David[a]

[a] Université François-Rabelais de Tours, EA 6295 Nanomédicaments et Nanosondes, 31 Avenue Monge, 37200 Tours, France
[b] Department of Pharmaceutics, Faculty of Pharmacy, University of Gezira, P.O. Box 20, Wad Medani, Sudan
[c] Department of Pharmaceutics, College of Pharmacy, Karary University, Khartoum, Sudan

ARTICLE INFO

Keywords:
Small interfering RNA
Magnetic siRNA nanovectors (MSN)
Superparamagnetic iron oxide nanoparticles (SPION)
Capillary electrophoresis (CE)
Purification

ABSTRACT

Gene therapy and particularly small interfering RNA (siRNA) is a promising therapeutic method for treatment of various human diseases, especially cancer. However the lack of an ideal delivery system limits its clinical applications. Effective anticancer drug development represents the key for translation of research advances into medicines. Previously we reported, the optimization of magnetic siRNA nanovectors (MSN) formulation based on superparamagnetic iron oxide nanoparticles (SPION) and chitosan for systemic administration.

This work aimed at using rational design to further optimize and develop MSN. Therefore, formulated MSN were first purified, then their physical and chemical properties were studied mainly through capillary electrophoresis. 95% of siRNA was found enclosed within the purified MSN (pMSN). pMSN showed colloidal stability at pH 7.4, effective protection of siRNA against ribonuclease degradation up to 24 hours and few siRNA release (less than 10%) at pH 7.4. These findings push toward further evaluation studies *in vitro* and/or *in vivo*, indicating the appropriateness of pMSN for cancer theranostics.

1. Introduction

Current challenges to develop innovative and effective systemic delivery systems aiming to improve gene therapy include a significant time and cost involvement with very low success rates. These have led to increasing efforts toward enhancing the effectiveness of the development process and to minimize failure of candidates at later stages of development to achieve the translation of research advances into medicines. These efforts include particularly the rational design of new formulations, *i.e.* the strategy of creating a new delivery system by adding components with known properties and the characterization and stability evaluation of this delivery system in different conditions permitting to predict how the delivery system's structure will affect its behavior after administration *in vivo*. Thus, to predict the behavior of the delivery system, it is essential to well characterize the delivery system and to evaluate its stability. Therefore, increasing emphasis has been placed on developing a mechanistic understanding of the physicochemical and biological phenomena involved in gene therapy delivery system development such as chemical, physical and biological stability (Haussecker, 2014).

Gene therapy and particularly small interfering RNA (siRNA) is a promising tool for treatment of various diseases, especially cancer. siRNA can cause specific down regulation of proteins through RNA interference (RNAi) inducing either degradation of mRNA or inhibition of the translation (Buschmann et al., 2013; Meister and Tuschl, 2004). In theory, siRNA has great advantages, such as high degree of safety, high efficacy, unrestricted choice of targets and specificity (Xu and Wang, 2015). However, siRNA applications are limited by its intrinsic properties such as short plasma half-life, lack of specific biodistribution and poor membrane permeability. In consideration of these limitations, and for realizing the broad potential of siRNA-based therapeutics, suitable, safe and effective siRNA delivery methods are desired.

Nonviral Nanometer-scaled Drug Delivery Systems (Nano DDSs) represent a flexible and growing technology that is expected to become of high importance in cancer therapy and diagnosis (theranosis) in the near future. Regarding cancer theranosis, Bennett et al. classified Nano DDSs according to the component carrier materials into metal particles, polymeric particles, vesicles, nanomicelles, *etc.*... (Bennett et al., 2014). Among them, siRNA nanocarriers based on functionalized Superparamagnetic Iron Oxide Nanoparticles (SPION) have attracted increasing attention because of their magnetic properties, low cost and easy synthesis and well-defined functionalization protocols (Devarasu

* Corresponding author at: EA 6295 Nanomédicaments et Nanosondes, 31 Avenue Monge, Université François-Rabelais de Tours, 37200 Tours, France.
E-mail address: douziech.eyrolles@univ-tours.fr (L. Douziech Eyrolles).

http://dx.doi.org/10.1016/j.ejps.2017.05.062
Received 31 January 2017; Received in revised form 18 May 2017; Accepted 29 May 2017
Available online 01 June 2017
0928-0987/ © 2017 Elsevier B.V. All rights reserved.

et al., 2013). SPION are highly magnetized in magnetic field, allowing magnetic tumor targeting and biomedical magnetic resonance imaging (MRI) (Estelrich et al., 2015).

For treatment of most cancers, systemic routes of siRNA delivery are needed. The design criteria of an *in vivo* systemic siRNA delivery system should include biocompatibility, biodegradability, and non-immunogenicity. Additionally, the system should protect siRNA from serum nucleases and deliver it into target cells efficiently. Finally, the delivery system should provide siRNA an endosome escape ability to enter the RNAi machinery and activate RNAi pathways (Juliano et al., 2008). To solve the delivery problems of siRNA, many delivery systems have been developed. These delivery systems are quite different in terms of structure, size and chemistry, but there are still some deficiencies regarding the characteristics of optimal delivery systems.

Magnetic siRNA nanovectors (MSN) composed of silanised SPION, chitosan and siRNA were recently developed in our laboratory (David et al., 2013). MSN were formulated *via* electrostatic deposition of siRNA and chitosan layers on the surface of the magnetic core made of aminosilane-coated SPION (SPION-NH_3^+). The formulation parameters used were those determined in our previous study to obtain MSN with a hydrodynamic diameter (D_H, *i.e.* the apparent size of hypothetical spherical hydrated/solvated MSN) around 100 nm, suitable for systemic administration (David et al., 2014). For some experiments, in order to improve the sensitivity of analytical methods, we replaced native siRNA by siRNA labeled with a fluorochrome Alexa 488, hereafter called Fl.siRNA.

The present paper aimed at optimizing systemic siRNA magnetic nanovector using rational formulation design. Therefore, formulated MSN were purified and their physical, chemical and biological stability was determined. Many nanoparticles purification methods are described in the literature such as dialysis, ultrafiltration, ultracentrifugation and size exclusion chromatography (SEC). Among these methods, we have used centrifugation which represents a good compromise between easiness and efficiency (Limayem et al., 2004; Pedro et al., 2008).

The detailed MSN characterization has been achieved using a spectrum of biochemical and analytical techniques, including capillary electrophoresis (CE), agarose gel electrophoresis (AGE) and UV–visible spectrophotometry. Due to its specificity, short detection time and small volume of samples used (Li et al., 2014), CE has become a universal technique applied for identification and separation of many molecules from small to macromoleculars (Ban et al., 2001; Chen and Bartlett, 2012; Chen and Evangelista, 1998; Wang et al., 2006; Yu et al., 2004). Laser-induced fluorescence (LIF) detection has been used routinely in CE systems for detection of nucleotides and their applications due to its high sensitivity and selectivity compared to the UV detector (Li et al., 2014; Song et al., 2001). One challenge of CE consists in the selection of the separation buffer. This is particularly important for nanoparticles which exhibit a great tendency to aggregate into large superstructures. Such formations can occur during the CE analysis, resulting in an instable electrophoretic behavior. Another challenge, is the possible adsorption of analytes onto the inner surface of the fused silica capillary (Matczuk et al., 2015), accordingly we optimized the CE analytical conditions for MSN detection and quantification of siRNA loaded in and released from MSN.

2. Materials and methods

2.1. Chemicals

Two siRNA models targeted against PCSK9, sense sequence: GGAAGAUCAUAAUGGACAGdTdT, (Eurogenetec, Seraing, Belgium) were used. One without modification while the other was modified with Alexa 488, and referred to as Fl.siRNA (Sigma-Aldrich, St. Quentin Fallavier, France). Ferric chloride, ferric nitrate nonhydrate, chitosan high purity, MW 110,000–150,000, ammonium persulphate (APS), acrylamide, ribonuclease A, 3-(trimethoxysilyl)propyl methacrylate, ethidium bromide (Ethidium bromide solution 1%) and *N,N,N′,N′*-tetramethyl ethylene diamine (TEMED) were obtained from Sigma–Aldrich GmbH (Schnelldorf, Germany). Dulbecco's Modified Eagle Medium (DMEM) (ThermoFisher Scientific, Illkirch, France). Agarose (Invitrogen, Carlsbad, USA). Ammonia, sodium nitrate and sodium hydroxide were obtained from PROLABO Chemicals (Paris XI, France). Potassium hydroxide (LABOSI Chemicals, Paris, France), Ferrous chloride tetrahydrate, acetic acid, citric acid and Tris/acetate/EDTA buffer (TAE 1 ×, 40 mM Trisacetate, EDTA 1 mM, pH 7.6) were obtained from Acros Organics (Geel, Belgium). Nitric acid, acetone, methanol and disodium hydrogen phosphate dihydrate were obtained from CARLO ERBA Reagents S.A.S (Paris, France). All reagents were of analytical grades. Water was obtained from a Milli-Q system, Millipore, (Paris, France).

2.2. MSN preparation

SPION coated with covalently bound aminopropyl silanes (APTES) were prepared as reported by Hervé et al. (Hervé et al., 2008). MSN were formulated as described previously (David et al., 2013). Briefly, always equal volumes of siRNA solution and water on the one hand and silanised SPION, chitosan aqueous solution and water on the other hand were mixed together. The addition order was (1) water and (2) siRNA solution on the one hand and (1) water, (2) SPION and (3) chitosan on the other hand. Both volumes were vortexed separately and centrifuged with a micro centrifuge (6000 rpm, Model IR, Fischer Scientific, Illkirch, France), then mixed together using a micropipette. The quantity of each component was calculated upon mass ratio of iron (from SPION) to siRNA (MR = m(Fe)/m(siRNA)) and the charge ratio (CR) of positive chitosan charges to negative siRNA charges. MSN studied were prepared with siRNA concentration of 30 µg/mL, MR of 10 and CR of 44.

MSN purification was done *via* centrifugation (Sigma 3–30 K, Sigma laboratory centrifuges, Germany). After centrifugation at 6000*g* for 15 min, the supernatant was removed and replaced by the same volume of water (Milli-Q) then both supernatant and sediment were redispersed by vortexing for a few seconds.

2.3. MSN and siRNA analysis by capillary electrophoresis (CE)

2.3.1. Instrumentation

CE analysis was carried out using PACE MDQ (Beckman Coulter capillary electrophoresis system, USA) controlled by 32 Karat software (Version 8.0). This apparatus is equipped with a LIF detector with excitation by an air-cooled argon ion laser at a wavelength of 488 nm. The emission intensities were measured at a wavelength of 520 nm filtered by a band pass interference filter. Fused silica capillaries from Agilent technology, (USA) were used and they were 60 cm effective length and 75 µm ID. Capillaries were thermostated at 25 °C. The machine is also equipped with a diode array detector (DAD). UV detection took place at 220 nm for MSN and 272 nm for Fl.siRNA.

2.3.2. Capillaries preparation and coating

Uncoated capillaries were washed with NaOH 1 M for 5 min, followed by washing with water for 5 min before the first analysis. All washing were made at 20 p.s.i. For coated capillaries, the method described by Alejandro (Cifuentes et al., 1999) was used, etching was made by NaOH 1 M for 30 min, then leaching with HCl 0.1 M for 2 h at 20 p.s.i. After that, washing with water and methanol for 30 min and 10 min respectively was made at 20 p.s.i. Capillaries were then dried twice by air for 10 min at 20 p.s.i. Silylation solution was prepared by mixing 2 mL of 3-(trimethoxysilyl)propyl methacrylate, 2 mL methanol and 20 µL acetic acid. Capillary was exposed to the silylation solution for 30 min at 20 p.s.i and then allowed to stand within the solution for 16 h, then washed twice with methanol and water each for 10 min at 20 p.s.i. Coating solution was prepared by adding 7.5 µL ammonium

persulphate (APS)10% w/v and 7.5 µL *N,N,N′,N′*-tetramethyl ethylene diamine (TEMED) 10% v/v to a 3 mL of acrylamide solution 1% w/v. Capillaries were exposed to the coating solution for 30 min at 20 p.s.i and then allowed to stand within the solution for 6 h. Washing with water and buffer each for 1 min was made before each sample injection.

2.3.3. Analysis of nanocarriers before and after purification

Detection of MSN before and after purification was carried out using polyacrylamide coated capillaries. Citrate-phosphate buffer (pH 5, 5 mM) was used as the separation buffer. Samples were injected hydrodynamically for 5 s at 0.5 p.s.i by anodic injection at the short end of the capillary (− 25 kV, 10 cm). Fluorescence and UV detection were used.

2.3.4. Quantification of free Fl.siRNA in nanocarriers

For quantification of free Fl.siRNA in MSN before and after purification, citrate-phosphate buffer (pH 7, 2.5 mM) was used as the separation buffer. MSN were injected hydrodynamically for 5 s at 0.5 p.s.i by cathodic injection at the short end of the capillary (+ 25 kV, 10 cm), LIF detection. A linear calibration curve was obtained between 0.5 and 10 µg/mL as peak area = $2{\cdot}10^6 * \text{Concentration} - 1 * 10^6$, with $R^2 = 0.9974$. At the lowest concentration, the relative standard deviation for peak area variability is about 3.6%, this concentration being then established as the limit of quantification (LOQ = 0.5 µg/mL = $3.6 * 10^{-8}$ M). The precision of the method is demonstrated by RSD of peaks areas < 10% for each concentration level.

2.3.5. MSN colloidal stability assessment

The behavior of purified MSN (pMSN) at different pH ranging between 5 and 8.5 was studied. pMSN were always mixed with the buffer in the ratio of (1: 2, buffer: pMSN) by pipetting followed by vortexing for a few seconds. Citrate-phosphate buffer at a concentration of 25 mM was used for pH 5, 6 and 7.4, while Tris/acetate/EDTA (TAE) 1 × buffer was used for the pH 8.5. The samples were then characterized by capillary electrophoresis to study their aggregation profile as described in Section 2.3.3, and confirmed by size measurements.

2.3.6. In vitro siRNA release determination

The release kinetics of siRNA from pMSN suspended in citrate-phosphate buffer pH 7.4 (25 mM) and Dulbecco's Modified Eagle Medium (DMEM) pH 7.4 were studied. pMSN were always mixed with the buffer or the cell culture medium in the ratio of (1: 2, buffer or culture medium: pMSN) by pipetting followed by vortexing for a few seconds. The mixture was then divided into four aliquots and incubated at 37 °C for 1, 2, 4 and 24 h. After incubation, samples were centrifuged at 6000G for 15 min and the supernatant was analyzed for siRNA content using CE. Released siRNA was detected indirectly through complexation with chitosan by addition of a few microliters of concentrated chitosan solution (20 g/L) to the supernatant. Detection of Fl.siRNA chitosan complex was carried out using uncoated capillary. Sodium-phosphate buffer (pH 2, 10 mM) was used as separation buffer. Samples were injected hydrodynamically for 5 s at 0.5 p.s.i by anodic injection at the short end of the capillary (− 25 kV, 10 cm), LIF detection. A linear calibration curve for the Fl.siRNA chitosan complex was obtained at the concentration of Fl.siRNA between 0.5 and 30 µg/mL as Peak area = 443311 * Concentration + 34525, $R^2 = 0.9991$. At the lowest concentration, the relative standard deviation for peak area variability is 6%, this concentration being then established as the limit of quantification (LOQ = 0.5 µg/mL = $3.6 * 10^{-8}$ M). The precision of the method is demonstrated by RSD of peaks areas < 10% for each concentration level. The amount of the Fl.siRNA released at each condition was calculated as a percentage referring to the initial quantity used for formulation (corresponding to 30 µg/mL).

2.3.7. Study of siRNA degradation by ribonuclease enzymes

Purified MSN were studied for their ability to protect siRNA from degradation by ribonuclease A enzymes. The enzyme (1.2 µg/mL) was added to pMSN in the ratio of (1: 2, enzyme: pMSN) and mixed by pipetting followed by vortexing for a few seconds. The mixture was then divided into four aliquots and incubated at 37 °C for 1, 2, 4 and 24 h. Samples were analyzed by CE-LIF as described in Section 2.3.3 and confirmed by AGE.

The percentage of protection efficiency was calculated as follow:

$$\text{Protection efficiency} = \frac{\textbf{Average peak area of pMSN at time } (t)}{\textbf{Average peak area of pMSN before addition of the enzyme}} \times 100$$

2.4. MSN size and surface charge determination

Mean hydrodynamic diameter (D_H) of the samples was measured using a High Performance Particle Sizer (HPPS) (Malvern Instruments, Malvern, UK). Before measurement, the nanocarriers were diluted in $NaNO_3$ 0.01 M at a ratio of 1:25. The pH of the media was 6.1. The D_H measurements of the nanocarriers were done in triplicate with automatic setting of the measurement parameters. The position of the laser was fixed at 2.0 mm for a better comparison of the measurements.

The surface charge of the nanocarriers, in term of their zeta potential, was measured using a Malvern NanoZ zetameter (Malvern Instruments, Malvern, UK) using the same samples as for the D_H measurements. Each measurement was done in triplicate.

2.5. Analysis of siRNA complexation by agarose gel electrophoresis (AGE)

10 µL of sample and 5 µL of water or 5 µL of KOH (0.1 M) were mixed before adding 1.5 µL of Agarose gel loading dye 6 ×. (Fisher Bioreagents®, Illkirch, France). KOH was added to liberate siRNA from the complexes to verify their integrity after formulation.

The prepared samples were then deposited on 1% agarose gel containing 0.01% ethidium bromide, prepared with pure agarose and a Tris/acetate/EDTA 1 × buffer, to migrate for about 15 min at 100 V. Images were taken using Fusion Solo. S6® imager (WL. Vilber Lourmat, Marne la Vallée, France) and analyzed with the Evolution Capt Software. Before analysis of the samples used in the study of siRNA protection against RNAse A, RNAse activity was inhibited by heating the sample for 30 min at 70 °C.

2.6. Quantification of MSN components by UV–visible spectrophotometry

UV–visible spectra of MSN before and after purification and the different MSN components were acquired with a GENESYS® 10s, UV–visible spectrophotometer (Thermo Scientific, Illkirch, France). Treatment of spectra were performed with LABSPEC 4.04 software. Each experimental spectrum was fitted using the classical least-squares method to a sum of the two reference spectra of siRNA and SPION-chitosan. In parallel, a linear calibration curve was obtained between 0.0039 and 0.011 µg/mL as Absorbance = 0.0024 * Concentration + 0.0027, with $R^2 = 0.999$ for Fl.siRNA. For SPION, linear calibration curve was obtained from SPION chitosan mixture between 0.015 and 0.03 mg/mL as Absorbance = 44.4 * Concentration + 0.211, with $R^2 = 0.999$.

3. Results and discussion

3.1. Capillary electrophoresis (CE) – an interesting analytical tool for MSN characterization

Capillary electrophoresis (CE) is a separation method based on the different electrophoretic mobilities of charged molecules under the effect of an electric field. Typically, separation takes place in a capillary of small diameter (usually 50–100 µm), requiring small amount of

samples for the analysis. Previously, we have used this method in our research on the distribution of doxorubicin drug-loaded magnetic nanovectors in cancer cells (Gautier et al., 2015). CE is a method of high efficiency and the use of laser-induced fluorescence as detection method provides high sensitivity. However, the main problem to be overcome in CE is usually the potential interactions of the analyte with the surface of the capillary. In order to reduce these interactions, various modifications of the capillary inner wall surface are available but need to be optimized (Cifuentes et al., 1999). In the present work, we have used CE to characterize nanoparticles made of several constituents associated by electrostatic interactions. One of the major component is chitosan biopolymer which constitutes the external coating layer of the nanoparticles. At pH range of 5 to 6 used to formulate MSN, chitosan is positively charged and contributes in electrostatic interactions of the MSN with the negative surface of the capillary. In order to reduce these interactions, we chemically modified the capillary wall with neutral polyacrylamide molecules.

Moreover, CE analysis of nanoparticles is more challenging and quite different from study of molecules in solution. Indeed, CE requires to use background buffers to provide separation medium. If the ionic strength of the buffer is too high, ionic cloud surrounding nanoparticles can be compressed and the stability of the system can be affected (López-Lorente et al., 2011). We investigated various separation buffer systems in terms of their composition and pH. The results showed that the optimal MSN analysis conditions were obtained with citrate-phosphate buffer at a low concentration (pH 5, 2.5 mM) whereas the same buffer at a concentration of 5 mM was optimal for MSN formulated with Fl.siRNA. Two methods of detection were used: diode array detector (DAD) is implemented in every commercial CE system for its simplicity. However, its sensitivity is limited. On the other hand, laser induced fluorescence (LIF) detection is known to have nearly 1000 fold higher sensitivity and better selectivity compared to UV–vis detection. UV detection of MSN was based on the light scattering-related absorbance of SPION core of the nanovectors at 220 nm, while LIF-based detection was possible only for MSN loaded with the Fl.siRNA. After analysis of Fl.MSN, typical spectra of SPION (data not shown) was observed for a peak at 2.12 ± 0.14 min while a signal of fluorescence was detected at a similar migration time with CE-LIF detection (Fig. 1A and B). The agreement in the migration time of these two peaks by UV and fluorescence demonstrates that these signals can be assigned to the nanocarriers.

These results were in agreement with the agarose gel electrophoresis (AGE) data (Fig.1D). During the AGE analysis, ethidium bromide incorporated in agarose gel intercalates free siRNA molecules and produces a fluorescence band upon UV excitation. Complexed siRNA molecules are less accessible to ethidium bromide and do not migrate in the agarose gel. For the MSN, a fluorescence band observed in the gel was very weak compared to siRNA solution. This indicates that the major part of siRNA in MSN was bound to the nanoparticles. An increase of the pH, by addition of KOH, suppressed the chitosan positive charges, destabilized MSN and liberated siRNA. As a result, an intense fluorescence band, comparable to that of the control siRNA, was observed, indicating high siRNA payload in MSN.

3.2. Physical and chemical characteristics of MSN

Pharmaceutical quality and safety requirements for MSN as potential nanomedicine treatment involves control of several parameters, like the medium purity in terms of possible presence of residual free components, nanoforms structure and composition and their colloidal and chemical stability (Itoh et al., 2015).

CE results for MSN before and after purification by centrifugation showed that a first centrifugation at 6000*g* yields the required purity for MSN remaining in the supernatant (thereafter called pMSN) with few aggregates being in the sediment (Fig. 1A and B). This was even more apparent when LIF detector was used (Fig.1B). These results are in

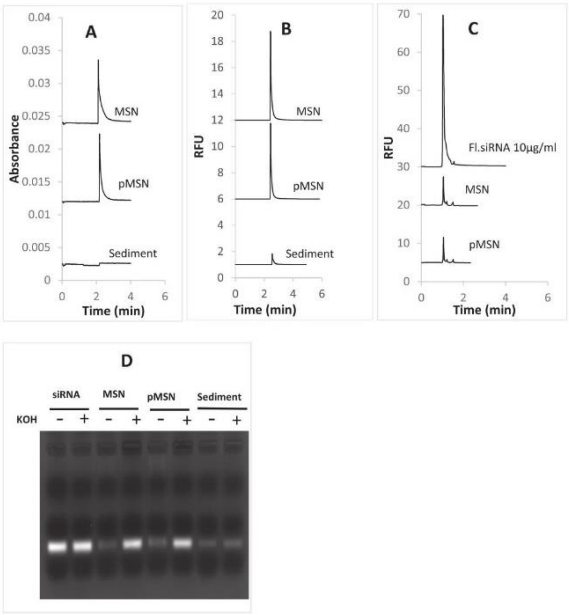

Fig. 1. Purification of MSN: Electropherograms showing: (**A**) UV detection of Fl.MSN at 220 nm. (**B**) LIF detection of Fl.MSN. (**C**) LIF detection of free Fl.siRNA. CE conditions: Polyacrylamide coated capillary 75 µm ID × 60 cm, hydrodynamic injection for 5 s. at 0.5 p.s.i, 25 °C. (**A** and **B**) Citrate phosphate buffer pH 5 (5 mM), applied voltage − 25 kV, anodic injection. (**C**) Citrate phosphate buffer pH 7 (2.5 mM), applied voltage + 25 kV, cathodic injection. (**D**) Agarose gel electrophoresis of MSN before and after purification. The first condition of the sample (−) is without KOH indicating free siRNA in this condition, the second condition of the sample (+) is with KOH indicating the total amount of siRNA in the sample.

agreement with the hypothesis that the centrifugation at low speed removed larger MSN and/or SPION aggregates while less dense individual small MSN remained in the supernatant. A second centrifugation was made at higher strength (20,000*g*), to precipitate individual MSN in the second sediment while allowing residual free molecular components (if found) to remain in the second supernatant. However, because of the high colloidal stability of MSN, such separation was not achieved: MSN were still present in the second supernatant and only few MSN in the second sediment (data not shown). These results confirm that the protocol of MSN formulation was already well optimized. After purification, the values of D_H, measured in aqueous medium (pH 6.1 and ionic strength 0.01 mol/L), decreased from *ca.*100 nm to *ca.* 80 nm (Table 1). The polydispersity index (PDI), indicating if the sample has a monomodal size distribution or if there are several populations in the sample, diminished slightly after purification from 0.33 to 0.29. This is in agreement with the elimination of bigger aggregates or free SPION. The zeta potential (*i.e.* the surface charge of MSN represented by the ions forming an electrical double layer around MSN) decreased from *ca.* + 20 mV to *ca.* + 15 mV, probably due to elimination of free SPION carrying a lot of positive charges due to their aminosilane-modified surface. This hypothesis was supported by the brown color of the sediment and confirmed by atomic absorption

Table 1
Comparison between the nanovectors before (**MSN**) and after purification (**pMSN**).

Formulation	MSN	pMSN
D_H (nm)	93.71 ± 20.56	79.16 ± 6.82
PDI	0.33 ± 0.05	0.29 ± 0.05
Zeta potential (mV)	20.49 ± 13.46	14.92 ± 12.42
Mass ratio (m_{Fe}/m_{siRNA})	9.4	6.5

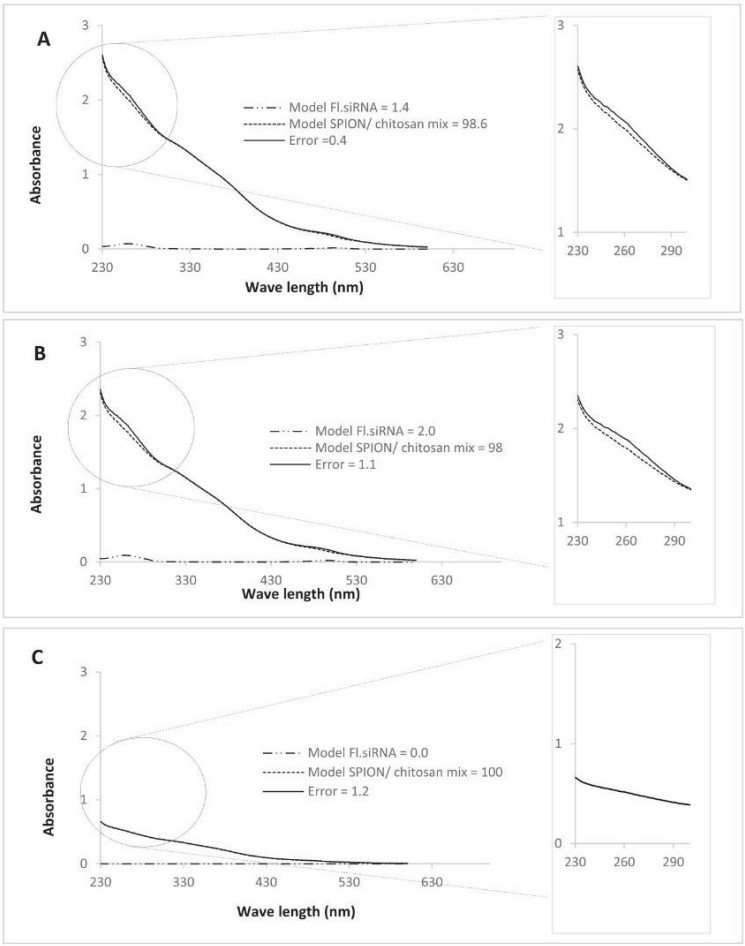

Fig. 2. Quantification of MSN components, representative curve fitting of (**A**) MSN (**B**) pMSN and (**C**) the sediment. The contribution of each component is represented.

spectroscopy (data not shown).

CE technique has also been used to check the presence or absence of free siRNA in pMSN. In that case, MSN were loaded with Fl.siRNA for CE-LIF analysis. The optimum analysis medium was the citrate-phosphate buffer at pH 7 (2.5 mM). Fl.siRNA migration time was 1.05 ± 0.02 min (Fig. 1C). As described in the experimental section, the analytical methodology validation included calibration curve from which the limit of quantification was deduced. Quantification of Fl.siRNA from the electropherograms of MSN and pMSN showed that they contain 1.69 and 1.41 µg/mL of free Fl.siRNA, respectively. In comparison to the theoretical concentration of 30 µg/mL, these results allow to demonstrate that free siRNA content is about 5%. The free Fl.siRNA content determined with CE is in agreement with the intensity of the fluorescence bands observed in AGE (Fig. 1D).

The siRNA loading within pMSN was estimated from their UV–vis spectra, by fitting them with separately recorded spectra of Fl.siRNA and of SPION & chitosan mixture (Fig.2). The fitting errors were typically below 2% of the total spectral area. The obtained results indicated that no Fl.siRNA was found in the sediment of the purification step. Calibration curve obtained from the UV–vis absorption of Fl. siRNA in aqueous solution enabled us to establish that: the concentration of siRNA in MSN before purification (29.3 ± 1.44 µg/mL) was logically similar to that used for formulation (30 µg/mL) and corresponding to the mass of 5.87 ± 0.29 µg. Similar calculations for SPION gave a mass of 55 ± 2.5 µg of iron instead of 60 µg. Thus the mass ratio (MR) calculated as iron content of SPION to siRNA corresponds to 9.4. For pMSN, the mass of Fl.siRNA and iron were found 6.4 ± 0.3 µg and 41.8 ± 3.89 µg respectively (MR: 6.5). The Fl.siRNA loading rate was the same before and after the MSN purification. However, the MR decreased from 9.4 to 6.5 due to the loss of some SPION as aggregates in the sediment after purification. This is in agreement with previous results indicating that a MR between 5 and 7.5 is needed for a complete siRNA complexation with SPION (David et al., 2013). However, smaller MSN sizes were obtained when a MR of 10 was used for the MSN formulation.

In summary, these results show that the centrifugation applied as a method of purification lead to a higher siRNA proportion in pMSN compared to non-purified MSN and especially no valuable raw material loss. The purification could be very useful for a future *in vivo* application as the aim is to carry a sufficient amount of siRNA in pMSN. Thereafter, for further MSN development we will study only the purified MSN (pMSN).

3.3. Influence of pH on colloidal stability

CE was also used, to analyze the colloidal stability of pMSN. Throughout the process of manufacture and storage, pMSN should be stable over a wide pH range to ensure the robustness of the method on the one hand and the safe siRNA delivery on the other hand. CE data (Fig. 3A) indicated that pMSN were resistant against aggregation at

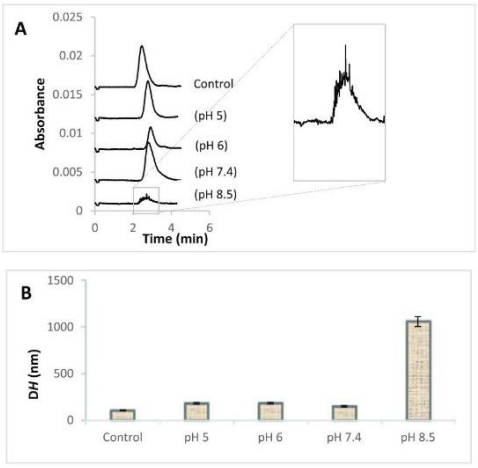

Fig. 3. Colloidal stability of purified MSN at different pH. (**A**) Electropherograms showing behavior of the purified MSN at different pH. CE conditions: Polyacrylamide coated capillary 75 μm ID × 60 cm, Citrate phosphate buffer pH 5 (2.5 mM), applied voltage − 25 kV, anodic hydrodynamic injection for 5 s. at 0.5 p.s.i 25 °C,UV detection at 220 nm. (**B**) Hydrodynamic diameter of purified MSN at different pH. Control = pMSN.

pH 5, 6 and 7.4 since no modifications in the peaks shape and migration time were noticed. At pH 8.5, the nanovectors were immediately prone to aggregation as indicated by presence of spikes. In the past, CE was used to analyze iron oxide nanoparticles and it has been shown that, if instability occurs, groups of spikes are visible on the electropherogram instead of the Gaussian-shaped peaks (Vanifatova et al., 2005). The CE results were concomitant with the hydrodynamic diameter values of pMSN (Fig. 3B): pMSN size was similar at pH 5, 6 and 7.4 while it increased at pH 8.5. The instability of pMSN at pH 8.5 is probably due to the loss of balance of attractive-repulsive forces between nanoparticles. Indeed, the pKa of chitosan is 6.5 (Buchman et al., 2013; M. et al., 2012) indicating that it should be less charged at pH above 6.5. The good colloidal stability of MSN at pH up to 7.4 was encouraging for their biological evaluation.

3.4. Release of siRNA at pH 7.4 and its protection against ribonuclease enzymes

The *in vitro* release profiles of Fl.siRNA from pMSN were established for 24 h at pH 7.4, in both citrate-phosphate buffer and in cell culture medium DMEM. After incubation, we noticed that, pMSN started to separate into two phases with a clear supernatant. We expected a concomitant release of chitosan followed by complexation with siRNA. This hypothesis was confirmed by analysis of siRNA-chitosan complex solution and observation of reproducible peaks for this complex using uncoated capillaries with sodium-phosphate buffer pH 2, 10 mM as separation buffer, by CE-LIF detection. Thus, we decided to add concentrated chitosan solution to the each supernatant obtained from release experiments to ensure detection of the whole siRNA quantity.

siRNA release was found higher in the DMEM cell culture medium (10%) than in the citrate-phosphate buffer (3%) after 1 h. With time, the quantity of released siRNA decreased and may be undetectable in citrate phosphate buffer (Fig. 4A). The siRNA release in the first hour can be explained by diffusion of siRNA bound near the particles surfaces due to dilution. This behavior is similar to that described by A.G. Raja et al. using crosslinked chitosan-siRNA nanoparticles (Abdul Ghafoor Raja et al., 2015). However, in our case, the siRNA release is decreased at later stage which could be explained by a supposable re-inclusion of released siRNA to the (aggregated) MSN.

Efficient gene delivery system is also dependent upon the ability of the carrier to protect its payload from nuclease degradation. For

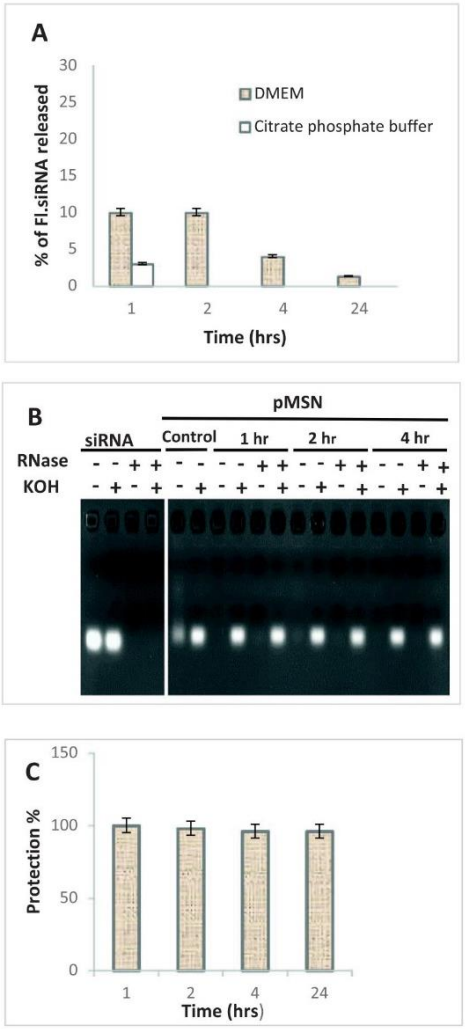

Fig. 4. siRNA release and protection against ribonuclease enzymes (**A**) Histograms showing the *in vitro* release profile of Fl.siRNA from the purified MSN at pH 7.4. The % amount of Fl.siRNA released was determined using CE-LIF detection. CE conditions: uncoated capillary 75 μm ID × 60 cm, 25 °C, hydrodynamic injection for 5 s. at 0.5 p.s.i. Na-phosphate buffer pH 2 (10 mM)), applied voltage − 25 kV, anodic injection. (**B**) Agarose gel electrophoresis of purified MSN in presence (+) or absence (−) of ribonuclease A (RNAse) and KOH. Control = pMSN without addition of RNAse. (**C**) Histograms showing protection of Fl.siRNA against ribonuclease A by MSN using capillary electrophoresis. CE conditions: Polyacrylamide coated capillary 75 μm ID × 60 cm, 25 °C, hydrodynamic injection for 5 s. at 0.5 p.s.i. Citrate phosphate buffer pH 5 (5 mM), applied voltage − 25 kV, anodic injection, LIF detection.

maximal activity in the cells, siRNA must be protected from digestion by nucleases as free siRNA are rapidly degraded (< 30 min) by RNAse (Haupenthal et al., 2006). Fig. 4B shows the siRNA integrity study by AGE indicating a highly efficient siRNA protection toward degradation by ribonucleases. A weak fluorescent band was observed with the initial pMSN as already seen above. The control free siRNA were rapidly degraded by RNAse, as there was no fluorescence band observed after 30 min of incubation. However, for purified MSN both in presence and in absence of ribonuclease, there was no fluorescence in absence of KOH. In contrast, after addition of KOH to the samples, there was an intense band of fluorescence, similar to that of the control sample (siRNA alone). In addition, CE data for pMSN (Fig. 4C) show that the

siRNA enzymatic degradation was hindered up to 24 h, with protection efficiency of 96%. Interestingly, the purification step did not interfere with this protection. In the literature, depending on the type of nanocarriers, one finds that the duration of the siRNA protection against serum or RNAse A *in vitro* (at 37 °C) varied from few minutes to 48 h (Resnier et al., 2013). The result obtained in our study with pMSN is encouraging. Further experiments with pMSN in serum and *in vivo* will be made in the close future.

4. Conclusion

Based on the findings of the present study, we conclude that stable purified magnetic siRNA nanovectors (MSN) possess properties potentially suitable for their systemic administration. In addition, the study includes the optimization of analytical conditions for MSN characterization by CE with DAD detector and CE-LIF. Purification by centrifugation allowed to remove free SPION and therefore to increase the siRNA/SPION ratio in MSN. Purified MSN had smaller sizes, lower PDI and lower zeta potential. At pH 7.4, < 10% of loaded siRNA were released in 24 h, while no MSN aggregation was observed. The nanovectors efficiently protected siRNA against degradation by RNAse A. In summary, MSN demonstrated promising properties for their further evaluation *in vitro* and/or *in vivo* as well as for a perspective of their application in cancer theranosis. However, pMSN stability and efficacy may be improved by addition of polymers and/or targeting ligands.

Conflict of interest

The authors confirm that this article content has no conflicts of interest.

Acknowledgements

The authors would like to thank the “Institut National du Cancer (INCa)”, the “Fondation ARC” and the “Ligue nationale contre le cancer (LNCC)” (ARC_INCa_LNCC_7636) for the financial support and Didier Bedin (EA6295, “Nanomédicaments et Nanosondes”, University François Rabelais of Tours) for technical support.

References

Abdul Ghafoor Raja, M., Katas, H., Jing Wen, T., 2015. Stability, intracellular delivery, and release of siRNA from chitosan nanoparticles using different cross-linkers. PLoS One 10. http://dx.doi.org/10.1371/journal.pone.0128963.

Ban, E., Choi, O.-K., Ryu, J.-C., Yoo, Y.S., 2001. Capillary electrophoresis of high-molecular chitosan: the natural carbohydrate biopolymer. Electrophoresis 22, 2217–2221. http://dx.doi.org/10.1002/1522-2683(20017)22:11<2217::AID-ELPS2217>3.0.CO;2-R.

Bennett, K.M., Jo, J., Cabral, H., Bakalova, R., Aoki, I., 2014. MR imaging techniques for nano-pathophysiology and theranostics. Adv. Drug Deliv. Rev. 74, 75–94. http://dx.doi.org/10.1016/j.addr.2014.04.007.

Buchman, Y.K., Lellouche, E., Zigdon, S., Bechor, M., Michaeli, S., Lellouche, J.-P., 2013. Silica nanoparticles and polyethyleneimine (PEI)-mediated functionalization: a new method of PEI covalent attachment for siRNA delivery applications. Bioconjug. Chem. 24, 2076–2087. http://dx.doi.org/10.1021/bc4004316.

Buschmann, M.D., Merzouki, A., Lavertu, M., Thibault, M., Jean, M., Darras, V., 2013. Chitosans for delivery of nucleic acids. Adv. Drug Deliv. Rev. 65, 1234–1270. http://dx.doi.org/10.1016/j.addr.2013.07.005.

Chen, B., Bartlett, M.G., 2012. Determination of therapeutic oligonucleotides using capillary gel electrophoresis. Biomed. Chromatogr. 26, 409–418. http://dx.doi.org/10.1002/bmc.1696.

Chen, F.T., Evangelista, R.A., 1998. Profiling glycoprotein n-linked oligosaccharide by capillary electrophoresis. Electrophoresis 19, 2639–2644. http://dx.doi.org/10.1002/elps.1150191512.

Cifuentes, A., Canalejas, P., Diez-Masa, J.C., 1999. Preparation of Linear Polyacrylamide-Coated Capillaries - Study of the Polymerization Process and Its Effect on Capillary Electrophoresis Performance. http://dx.doi.org/10.1016/S0021-9673(98)00923-6.

David, S., Marchais, H., Hervé-Aubert, K., Bedin, D., Garin, A.-S., Hoinard, C., Chourpa, I., 2013. Use of experimental design methodology for the development of new magnetic siRNA nanovectors (MSN). Int. J. Pharm. 454, 660–667. http://dx.doi.org/10.1016/j.ijpharm.2013.05.051.

David, S., Marchais, H., Bedin, D., Chourpa, I., 2014. Modelling the response surface to predict the hydrodynamic diameters of theranostic magnetic siRNA nanovectors. Int. J. Pharm. 478, 409–415. http://dx.doi.org/10.1016/j.ijpharm.2014.11.061.

Devarasu, T., Saad, R., Ouadi, A., Frisch, B., Robinet, E., Laquerrière, P., Voegel, J.-C., Baumert, T., Ogier, J., Meyer, F., 2013. Potent calcium phosphate nanoparticle surface coating for in vitro and in vivo siRNA delivery: a step toward multifunctional nanovectors. J. Mater. Chem. B 1, 4692–4700. http://dx.doi.org/10.1039/C3TB20557F.

Estelrich, J., Sánchez-Martín, M.J., Busquets, M.A., 2015. Nanoparticles in magnetic resonance imaging: from simple to dual contrast agents. Int. J. Nanomedicine 10, 1727–1741. http://dx.doi.org/10.2147/IJN.S76501.

Gautier, J., Munnier, E., Soucé, M., Chourpa, I., Douziech Eyrolles, L., 2015. Analysis of doxorubicin distribution in MCF-7 cells treated with drug-loaded nanoparticles by combination of two fluorescence-based techniques, confocal spectral imaging and capillary electrophoresis. Anal. Bioanal. Chem. 407, 3425–3435. http://dx.doi.org/10.1007/s00216-015-8566-9.

Haupenthal, J., Baehr, C., Kiermayer, S., Zeuzem, S., Piiper, A., 2006. Inhibition of RNAse A family enzymes prevents degradation and loss of silencing activity of siRNAs in serum. Biochem. Pharmacol. 71, 702–710. http://dx.doi.org/10.1016/j.bcp.2005.11.015.

Haussecker, D., 2014. Current issues of RNAi therapeutics delivery and development. J. Control. Release 195, 49–54. http://dx.doi.org/10.1016/j.conrel.2014.07.056.

Hervé, K., Douziech-Eyrolles, L., Munnier, E., Cohen-Jonathan, S., Soucé, M., Marchais, H., Limelette, P., Warmont, F., Saboungi, M.L., Dubois, P., Chourpa, I., 2008. The development of stable aqueous suspensions of PEGylated SPIONs for biomedical applications. Nanotechnology 19, 465608. http://dx.doi.org/10.1088/0957-4484/19/46/465608.

Itoh, N., Santa, T., Kato, M., 2015. Rapid and mild purification method for nanoparticles from a dispersed solution using a monolithic silica disk. J. Chromatogr. A 1404, 141–145. http://dx.doi.org/10.1016/j.chroma.2015.05.047.

Juliano, R., Alam, M.R., Dixit, V., Kang, H., 2008. Mechanisms and strategies for effective delivery of antisense and siRNA oligonucleotides. Nucleic Acids Res. 36, 4158–4171. http://dx.doi.org/10.1093/nar/gkn342.

Li, Z., Liu, C., Yamaguchi, Y., Ni, Y., You, Q., Dou, X., 2014. Capillary electrophoresis of a wide range of DNA fragments in a mixed solution of hydroxyethyl cellulose. Anal. Methods 6, 2473–2477. http://dx.doi.org/10.1039/C3AY41965G.

Limayem, I., Charcosset, C., Fessi, H., 2004. Purification of nanoparticle suspensions by a concentration/diafiltration process. Sep. Purif. Technol. 38, 1–9. http://dx.doi.org/10.1016/j.seppur.2003.10.002.

López-Lorente, A.I., Simonet, B.M., Valcárcel, M., 2011. Electrophoretic methods for the analysis of nanoparticles. TrAC Trends Anal. Chem. 30, 58–71. http://dx.doi.org/10.1016/j.trac.2010.10.006.

Malmo, J., Sørgård, H., Vårum, K.M., Strand, S.P., 2012. siRNA delivery with chitosan nanoparticles: Molecular properties favoring efficient gene silencing. J. Control. Release 158, 261–268. http://dx.doi.org/10.1016/j.jconrel.2011.11.012.

Matczuk, M., Aleksenko, S.S., Matysik, F.-M., Jarosz, M., Timerbaev, A.R., 2015. Comparison of detection techniques for capillary electrophoresis analysis of gold nanoparticles. Electrophoresis 36, 1158–1163. http://dx.doi.org/10.1002/elps.201400597.

Meister, G., Tuschl, T., 2004. Mechanisms of gene silencing by double-stranded RNA. Nature 431, 343–349.

Pedro, L., Soares, S.S., Ferreira, G.N.M., 2008. Purification of bionanoparticles. Chem. Eng. Technol. 31, 815–825. http://dx.doi.org/10.1002/ceat.200800176.

Resnier, P., Montier, T., Mathieu, V., Benoit, J.-P., Passirani, C., 2013. A review of the current status of siRNA nanomedicines in the treatment of cancer. Biomaterials 34, 6429–6443. http://dx.doi.org/10.1016/j.biomaterials.2013.04.060.

Song, L., Liang, D., Chen, Z., Fang, D., Chu, B., 2001. DNA sequencing by capillary electrophoresis using mixtures of polyacrylamide and poly(*N*,*N*-dimethylacrylamide). J. Chromatogr. A 915, 231–239. http://dx.doi.org/10.1016/S0021-9673(01)00593-3.

Vanifatova, N.G., Spivakov, B.Y., Mattusch, J., Franck, U., Wennrich, R., 2005. Investigation of iron oxide nanoparticles by capillary zone electrophoresis. Talanta 66, 605–610. http://dx.doi.org/10.1016/j.talanta.2004.12.016.

Wang, Q., Xu, X., Dai, L., 2006. A new quasi-interpenetrating network formed by poly(N-acryloyl-tris-(hydroxymethyl))aminomethane and polyvinylpyrrolidone: separation matrix for double-stranded DNA and single-stranded DNA fragments by capillary electrophoresis with UV detection. Electrophoresis 27, 1749–1757. http://dx.doi.org/10.1002/elps.200500597.

Xu, C., Wang, J., 2015. Delivery systems for siRNA drug development in cancer therapy. Asian J. Pharm. Sci. 10, 1–12. http://dx.doi.org/10.1016/j.ajps.2014.08.011.

Yu, R.Z., Geary, R.S., Monteith, D.K., Matson, J., Truong, L., Fitchett, J., Levin, A.A., 2004. Tissue disposition of 2′-O-(2-methoxy) ethyl modified antisense oligonucleotides in monkeys. J. Pharm. Sci. 93, 48–59. http://dx.doi.org/10.1002/jps.10473.

Annexe 3 : Stealth magnetic nanocarriers of siRNA as platform for breast cancer theranostics

Publié dans International Journal of Pharmaceutics, 2017

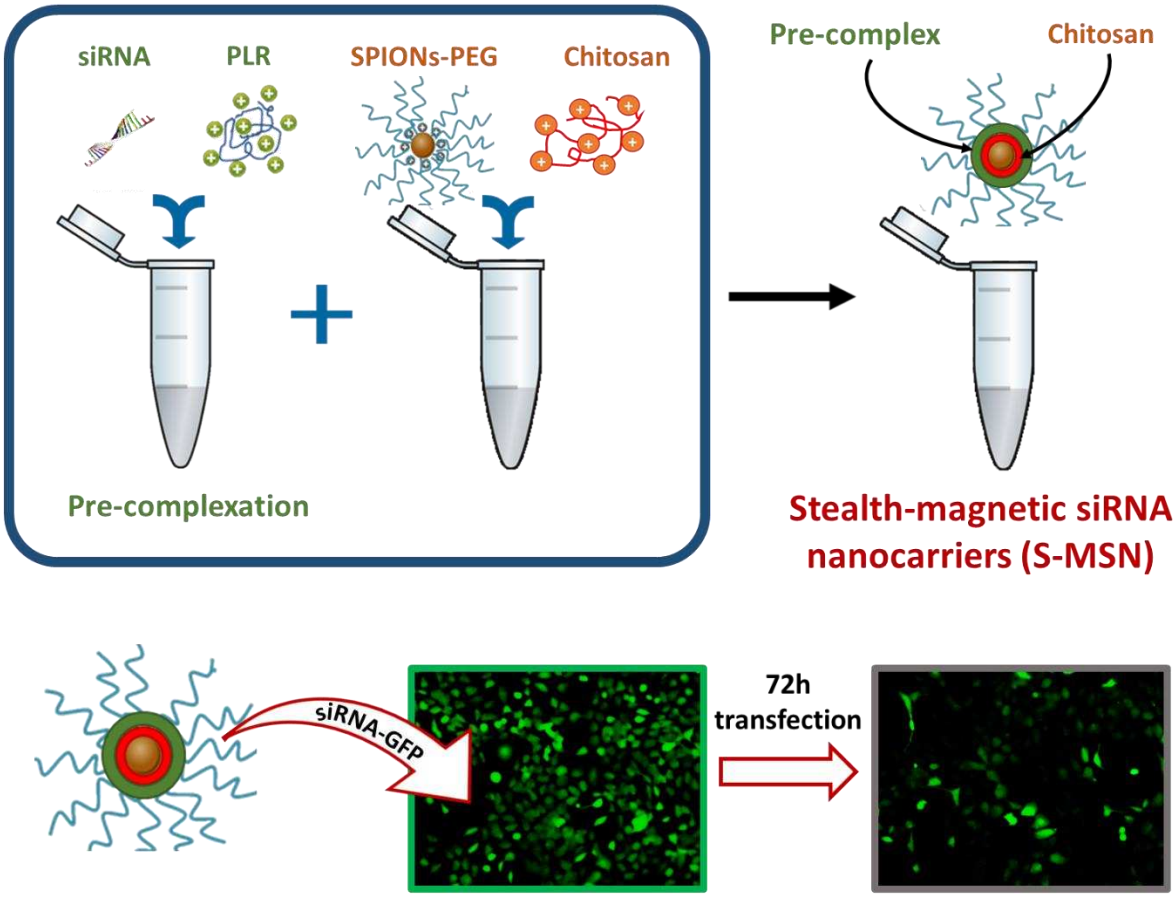

International Journal of Pharmaceutics 532 (2017) 660–668

Contents lists available at ScienceDirect

International Journal of Pharmaceutics

journal homepage: www.elsevier.com/locate/ijpharm

Stealth magnetic nanocarriers of siRNA as platform for breast cancer theranostics

J. Bruniaux, S. Ben Djemaa, K. Hervé-Aubert, H. Marchais, I. Chourpa, S. David*

Université François-Rabelais, EA6295 « Nanomédicaments et Nanosondes », Tours, 37200, France

ARTICLE INFO

Article history:
Received 20 January 2017
Received in revised form 9 May 2017
Accepted 10 May 2017
Available online 12 May 2017

Keywords:
Chitosan
Poly-L-arginine
siRNA
SPION
Transfection

ABSTRACT

The endogenous mechanism of RNA interference is more and more used in research to obtain specific down-regulation of gene expression in diseases such as breast cancer. Currently, despite the new fields of study open up by RNA interference, the rapid degradation of siRNA by nucleases and their negative charges prevent them from crossing cell membranes. To overcome these limitations, superparamagnetic iron oxide nanoparticles (SPIONs) represent a promising alternative for nucleic acid delivery. Previously, we reported the magnetic siRNA nanovectors (MSN) formulation using electrostatic assembly of (1) SPIONs, also able to act as contrast agents for magnetic resonance imaging (MRI), (2) siRNA and (3) chitosan aiming at their protection and enhancing their transfection efficacy. However, these nanoparticles displayed low stability in biological suspensions and inefficient transfection of active siRNA.

This work aimed at upgrading MSN to Stealth MSN (S-MSN) by adding a polyethylene glycol coating to ensure colloidal stability and stealth properties. Furthermore, another polymer (poly-L-arginine) was added for efficient siRNA transfection and the quantitative composition of the formulation was adapted for biological purposes. Results showed that S-MSN provide high siRNA complexation and protection against enzymatic degradation. Green fluorescent protein (GFP) specific down-regulation on MDA-MB231/GFP cells was comparable to that of commercially available reagents, without observable cytotoxicity. According to our works, S-MSN appears as an effective formulation for *in vitro* siRNA specific delivery.

© 2017 Elsevier B.V. All rights reserved.

1. Introduction

Breast cancer is the leading cause of mortality in women worldwide, and the second most common cancer overall (Ferlay et al., 2015). In recent years, significant progress has been made in the development of diagnostic tools and surgical treatments. However, treatment of resistant and recurrent metastatic breast cancers still needs a substantive improvement (Kennecke et al., 2010). Actually, about 80 genetic mutations can be identified in an individual breast tumor, including a dozen that are considered to be actively driving oncogenesis (Schlabach et al., 2008; Wood et al., 2007; Zhang et al., 2014). A unique individual profile of gene mutations may be established for each patient allowing a personalized treatment that takes advantage of the high specificity of small interfering RNA (siRNA). These siRNA are able to down-regulate genes responsible for tumorigenesis, including those driving oncogenesis, proliferation, angiogenesis, metastasis and resistance to treatment (Resnier et al., 2013).

siRNA are double-stranded RNA molecules composed of 19-24 pairs of nucleotides that naturally take part in an endogenous post-transcriptional inhibition mechanism used to regulate gene expression: RNA interference (RNAi) (Fire et al., 1998). siRNA interact with a cytosolic RNA-induced silencing complex (RISC) that recognizes a targeted complementary mRNA with high specificity. This action leads to the inhibition of gene expression through mRNA degradation or hindrance in ribosome activity (Meister and Tuschl, 2004).

However, siRNA have a poor ability to cross plasma membranes and reach RNAi intracellular sites of action. siRNA transfection to

Abbreviations: CR_{CS}, charge ratio (chitosan/siRNA); CR_{PS}, charge ratio (poly-L-arginine/siRNA); DLS, dynamic light scattering; GFP, green fluorescent protein; MR, mass ratio (iron content of SPIONs/siRNA); MRI, magnetic resonance imaging; $NaNO_3$, sodium nitrate; PEG, polyethylene glycol; PLR, poly-L-arginine; RISC, RNA induced silencing complex; SFP, stealth fluorescent particles; (S-)MSN, (stealth) magnetic siRNA nanovectors; SPIONs, superparamagnetic iron oxide nanoparticles.

* Corresponding author at: EA 6295 Nanomédicaments et Nanosondes, Laboratoire de pharmacie galénique, Faculté de pharmacie, 31 avenue Monge, 37200 Tours, France.
E-mail address: stephanie.david@univ-tours.fr (S. David).

http://dx.doi.org/10.1016/j.ijpharm.2017.05.022
0378-5173/© 2017 Elsevier B.V. All rights reserved.

cells is limited by their physico-chemical properties: molecular weight and anionic charge restrain considerably their transport across the plasma membrane (De Fougerolles and Novobrantseva, 2008; Juliano et al., 2008; Layzer et al., 2004; Santel et al., 2006). Moreover, siRNA are relatively vulnerable due to degradation by nucleases and their biodistribution after intravenous injection does not allow targeting cancer cells and/or tumors. To overcome these limitations, different strategies have been developed, including the use of delivery systems (Ozcan et al., 2015; Urban-Klein et al., 2005; Yu et al., 2012).

Among delivery systems developed in the last 10 years, nanocarriers based on superparamagnetic iron oxide nanoparticles (SPIONs) appear to be a promising tool (Medarova et al., 2007; Veiseh et al., 2010). Composed of magnetite and maghemite, SPIONs are superparamagnetic: they are highly magnetized in a magnetic field, but lose their magnetization when the field is switched off. SPIONs provide enhanced negative contrast in magnetic resonance imaging (MRI) and their loading with siRNA could allow to combine MRI-mediated diagnostic and therapeutic functions, in a so-called theranostic approach. Anti-cancer theranostic is expected to permit tailored treatment for individual patients, considering the inter-individual variability of therapeutic response.

We have recently described the formulation of magnetic siRNA nanovectors (MSN) (David et al., 2015, 2013) assembled by electrostatic force-stabilized deposition of siRNA (polyanion) and chitosan (polycation) on SPIONs pre-coated with positively charged amino groups. Experimental design approaches were used to optimize physico-chemical properties of MSN (David et al., 2015, 2013). Chitosan is a biodegradable and biocompatible natural polymer consisting of repeating units of D-glucosamine and N-acetyl-D-glucosamine. Chitosan is known to bind negatively charged nucleic acids, enabling this polymer to be used as a gene delivery vehicle (Howard et al., 2006; Techaarpornkul et al., 2010). The nanoparticles developed in our previous work were not stable in culture medium containing fetal bovine serum. The present study aimed at developing a new generation of stealth magnetic siRNA nanovectors (S-MSN). In addition, MSN were also formulated according to the previously described protocols, characterized and used as control samples to be compared with different S-MSN formulations. Compared to MSN, the S-MSN formulation was based on SPIONs labeled with deep red-fluorescent dye sulfocyanine and coated with biocompatible polymer, polyethylene glycol (PEG, MW 5 kDa), both attached covalently. These precursor particles will hereafter be referred to as stealth fluorescent particles (SFP). Moreover, the synthetic cationic polypeptide poly-L-arginine (PLR) (pKa >12) was added in order to compensate the low stability of the siRNA-chitosan complex and to increase transfection efficiency at physiological pH (Lavertu et al., 2006; Mao et al., 2010; Opanasopit et al., 2011). S-MSN formulations were first optimized by adjusting the quantitative composition and characterized to demonstrate their potential for a future administration *in vivo*. Finally, we compared these S-MSN formulations with a commercially available reagent in terms of their siRNA transfection to breast cancer cells, by measuring (i) down-regulation of green fluorescent protein (GFP) expression in MDA-MB231-GFP cells and (ii) cytotoxicity against MDA-MB231 cells.

2. Materials and methods

2.1. Materials

For physico-chemical characterization, model siRNA (targeted against PCSK9, sense sequence GGAAGAUCAUAAUGGACAGdTdT with lower case letters representing deoxyribonucleotides) were provided by Eurogenetec (Angers, France). Poly-L-arginine (MW 15.000-70.000) and high purity chitosan (MW 110.000-150.000; degree of acetylation: ≤40 mol. %), used for MSN and S-MSN formulation, were from Sigma–Aldrich Chemie GmbH (Schnelldorf, Germany). For transfection assay, commercial transfection reagent Oligofectamine® and siRNA were purchased from Life Technologies (Paisley, UK). For gel retardation assays, loading buffer, agarose and ethidium bromide were purchased from Fisher Bioreagents® (Illkirch, France). All the culture media and supplements for cell culture were supplied by life technologies (Paisley, UK).

2.2. MSN and S-MSN preparation

MSN were prepared based on a protocol previously described by David et al. (2015). In contrast to MSN, S-MSN were formulated using SPIONs covalently modified with sulfocyanine fluorescent label and PEG_{5000} polymer (SFP) (Alric et al., 2016; Perillo et al., 2017). Three different formulation protocols were tested: for protocols 1 and 2, siRNA in DPBS 1 × buffer was pre-complexed with an aqueous solution of chitosan or PLR, respectively, before being mixed with SFP suspensions, to obtain S-MSN_1 and S-MSN_2. For protocol 3, siRNA were pre-complexed with PLR, then added to a solution containing SFP and chitosan, to obtain S-MSN_3. The amount of SPIONs (quantified by its iron content) was defined as iron/siRNA mass ratio (MR). For preliminary experiments, the MR was fixed at 10 (David et al., 2015), then optimized with variation from 10 to 70. Chitosan or PLR content was expressed by the charge ratio (CR) of positive polymer charges to negative siRNA charges. For preliminary experiments, the CR of chitosan/siRNA (CR_{CS}) was set to 44 to formulate S-MSN_1 (David et al., 2015), and then adapted with modification from 10 to 100 to obtain optimized S-MSN_3. In the same way, different CR of PLR/siRNA (CR_{PS}) were tested for S-MSN_2 (from 1 to 44) and S-MSN_3 (from 10 to 50).

2.3. Physico-chemical characterization

2.3.1. DLS and zeta potential measurements

The mean hydrodynamic diameter (HD) and zeta potential (ZP) of S-MSN in suspension were determined using a Malvern HPPS instrument (Malvern Instruments, Malvern, UK). Before measurement, the S-MSN preparations were diluted in $NaNO_3$ 0.01 M at a ratio 1:25 to obtain a constant ionic strength (pH = 5.6) (n = 3). The mean values of HD given were based on intensity.

2.3.2. Agarose gel electrophoresis

S-MSN were formulated with a constant final siRNA concentration of 3 μM before addition of water (Milli-Q system, Millipore, Paris, France) or 10 mg/mL heparin sodium used as control (Sigma-Aldrich, Chemie GmbH, Schelldorf, Germany). With its strong negative charge, heparin is used to displace siRNA from its complex prior to electrophoretic analysis of liberated siRNA. Samples were mixed with 1.5 μL loading buffer (Agarose gel loading dye 6X) prior to deposit on 1% agarose gel containing ethidium bromide. A 100 V voltage was applied for about 15 min in a Tris/acetate/EDTA buffer (TAE 1X, 40 mM acetate, EDTA 1 mM, pH 7.6). Gels were visualized and analyzed with EvolutionCapt software on a Fusion-Solo.65.WL imager (Vilbert Lourmat, Marne-la-Vallée, France).

2.3.3. Stability in culture media

S-MSN (20 nM) were added to solution containing equal parts of OptiMEM serum-free medium and Dulbecco's modified Eagle medium (DMEM) supplemented with 10% fetal calf serum to mimic transfection conditions. After 0 to 4 hours incubation, the hydrodynamic diameter was determined by DLS as described in

2.3.1. In parallel, siRNA retention in S-MSN was studied by gel retardation assay as described in 2.3.2.

2.3.4. siRNA protection assay

A S-MSN solution containing 0.4 μg of siRNA was incubated with 2 ng ribonuclease A (Sigma-Aldrich, Chemie GmbH, Schelldorf, Germany) for 2 or 4 hours at 37 °C. Afterwards, ribonuclease A was inactivated by heating the solutions at 70 °C for 30 min. siRNA was released by adding 5 μL of a 10 mg/mL heparin sodium solution and run on agarose gel as described previously. An equivalent amount of free siRNA was used as a positive control to check the ribonuclease A activity.

2.4. Cell culture

Breast cancer cells, MDA-MB231-GFP (Euromedex, Souffelweyersheim, France) and MDA-MB231 (a kind gift from INSERM UMR 1069 Nutrition, Croissance et Cancer (N2C)), were routinely cultured in Dulbecco's modified Eagle medium (DMEM) supplemented with 10% fetal calf serum, non-essential amino acid 1X and 1% penicillin/streptomycin. Cells were maintained at 37 °C in an atmosphere containing 5% CO_2. Culture medium was changed every 48 hours and the cells were harvested using trypsin as soon as 80% confluency was reached.

2.5. siRNA transfection

At 24 h before transfection, 25.10^3 cells/wells were seeded in a 12-well plate containing equal parts OptiMEM serum-free medium and DMEM supplemented with 10% fetal calf serum. Transfections of 20 nM siRNA were carried out by adding a suspension of S-MSN in DPBS representing 8% of final volume.

2.6. Down-regulation efficiency

Transfection was performed on MDA-MB231-GFP cells with anti-GFP siRNA which specifically down-regulate GFP protein expression. The cells were incubated for 72 hours with the different carriers containing 10 to 50 nM of siRNA per well before removing them using trypsin. For statistical analysis, the level of GFP expression was determined by flow cytometry analysis on a FACScalibur flow cytometer (BD Bioscience). Cells that do not express GFP were used to calibrate flow cytometer. As a nonspecific control, siRNA that has no homology to any known mammalian gene was used for transfection with the different nanocarriers. At least 10^4 events were collected and analyzed using the WinMDI 2.9 software.

2.7. Cytotoxicity

Cell viability was measured through the net metabolic activity using a colorimetric assay for 96-well plates with 2-(4-iodophenyl)-3-(4-nitrophenyl)-5-(2,4-disulfophenyl)-2H-tetrazolium monosodium salt (WST-1) reagent (Roche, France). MDA-MB231 cells were seeded at 4.10^4 cells/well (0.2 mL per well) and allowed to grow 24 h in an incubator in standard cell culture conditions. On the day of the experiment, different concentrations of siRNA (from 1 to 100 nM) included in S-MSN were incubated with the cells for 24 h. Then, the culture medium was removed and fresh complete medium without phenol red was added for further 24 h incubation. 10% WST-1 reagent was added to the culture medium and kept in the incubator for 3 hours. Cells without S-MSN were used as negative controls whereas cells incubated with H_2O_2 (20 mM) were used as positive controls. Absorbance was recorded at 450 nm (to detect the reaction product formazan) and 690 nm (background subtraction) using a microplate reader. The absorbance difference ($A_{450nm} - A_{690nm}$) was directly proportional to the number of viable cells and the percentage cell viability was determined using the following equation: Viability (%) = $(A_S\text{-}A_{PC})/(A_{NC}\text{-}A_{PC}) \times 100$; where A_S, A_{PC} and A_{NC} represent absorbances of the sample, the positive control and negative control respectively.

2.8. Statistical analysis

Data are expressed as mean ± SD of the variables and are compared among groups by using one-way ANOVA followed by Fisher's protected Least Significance Difference test.

3. Results

3.1. From MSN to S-MSN: Stealth fluorescent particles (SFP) as precursors

MSN suspensions in aqueous buffers have a HD of 70 nm (intensity average) and a ZP of +20 mV (Table 1), similarly to previously reported studies (David et al., 2015, 2013). Compared to initial aminosilane treated SPIONs, MSN coated with siRNA and chitosan have an increased HD (+23 nm), but nearly the same ZP (Table 1). Incubation of MSN in complete cell culture medium containing 5% fetal calf serum at 37 °C triggered a large increase of their hydrodynamic diameter over time (data not shown). Thus, in the presence of serum proteins, MSN did not assure an appropriate colloidal stability.

Prior to S-MSN formulations, aminated SPIONs were covalently labeled with sulfocyanine and coated with PEG 5 kDa (Alric et al.,

Table 1
Physico-chemical characterization of MSN and S-MSN: S-MSN_1 contained SFP, chitosan and siRNA; S-MSN_2 were formulated with SFP, PLR and siRNA, whereas S-MSN_3 were optimized with both cationic polymers chitosan and PLR. Measures were performed with siRNA concentrations of 20 nM in $NaNO_3$ 0.01 M by dynamic light scattering on Malvern ZetaSizer. Conductivity was constant between 1.1 and 1.2 mS/cm (n = 3).

	Hydrodynamic diameter (HD) *nm*	Polydispersity (PDI)	Zeta potential (ZP) *mV*
Spion *PEG−/sulfocyanine−*	47 ± 4	0.15 ± 0.03	22 ± 5
SFP *PEG+/sulfocyanine+*	60 ± 3	0.16 ± 0.02	2 ± 3
MSN *with Spion*	70 ± 6	0.27 ± 0.05	20 ± 5
S-MSN_1 *with SFP*	76 ± 4	0.25 ± 0.03	12 ± 2
S-MSN_2 *with SFP*	61 ± 3	0.22 ± 0.02	3 ± 1
S-MSN_3 *with SFP*	64 ± 3	0.17 ± 0.03	5 ± 1

2016; Perillo et al., 2017), to generate SFP. At a hydrodynamic diameter of about 60 nm, the SFP are bigger than SPIONs, which is consistent with the presence of the PEG coating around nanoparticles. Moreover, the PEG shell apparently hides the positive charges of aminosilanes, reducing the ZP to close to neutral charge (Table 1).

3.1.1. Protocol 1 (synthesis of S-MSN_1): replacement of SPIONs by SFP to increase the colloidal stability

The S-MSN_1 were generated by loading SFP with a mixture of siRNA (50 nM) and chitosan (CR_{CS} = 44) in DPBS 1 × buffer. The HD and ZP of S-MSN_1 were 76 nm and 12 mV (Table 1). Thus, the addition of chitosan and siRNA led to an increase in HD (+ 16 nm) and ZP (+ 10 mV) (Table 1). Compared to MSN, the S-MSN_1 have a slightly bigger HD, as well as lower polydispersity and ZP (Table 1). These values are consistent with the presence of a PEG layer in S-MSN_1. In contrast to MSN of the same CR_{CS} (= 44) and MR (= 10), S-MSN_1 suspensions were colloidally stable for at least 4 hours of incubation in a serum-containing cell culture medium at 37 °C (Fig. 1A). In such conditions, S-MSN_1 displayed an increase of hydrodynamic diameter (about 40 nm after incubation with cell culture medium), then remained stable whatever the tested incubation duration. In this study, a minor population was observed around 13 nm in every incubation time: this population represents serum proteins from culture medium (Fig. 1A). The polydispersity, however, decreases significantly over four hours, probably due to the higher ionic strength in culture media.

Despite a better colloidal stability in culture medium, complexation with S-MSN_1 was not completely effective (Fig. 1B). A gel retardation assay was performed in order to determine the amount of siRNA complexed on S-MSN_1: compared to the condition with heparin allowing a complete siRNA release, about 75% siRNA were complexed within S-MSN_1 (Fig. 1B). This lack of complexation was coherent with the results obtained for the complexation between chitosan and siRNA (Fig. 1B).

In order to study transfection efficiency, MDA-MB231-GFP cells are used that normally produce a fluorescent protein GFP. The fluorescence intensity of individual cells is measured by flow cytometry, and the number of cells displaying a certain fluorescence intensity is plotted as a function of intensity (Supplementary data Fig. 1A). When cells, incubated for 72 hours with S-MSN_1 carrying 20 nM siRNA are analyzed, a practically identical profile with untreated cells is obtained, which proves that no transfection occurred with these nanocarriers. Either the nanoparticles do not penetrate into the cells or the siRNA is released prematurely. In order to improve complexation we tried to immobilize the siRNA with a different cationic polymer in our second protocol.

3.1.2. Protocol 2 (synthesis of S-MSN_2): replacement of chitosan with PLR to increase complexation

In the formulation of S-MSN_2, we proceeded first to a complexation of anionic siRNA with cationic PLR, which possesses a significantly higher cationic charge than chitosan at physiologically relevant pH and should thus enhance transfection efficiency (Ragelle et al., 2013). The pre-formed siRNA-PLR molecular complex was then incubated with SFP. The optimal quantity of PLR was determined through its ability to prevent the release of siRNA from nanocarriers during a gel retardation assay (Fig. 2). For a constant amount of siRNA and SFP (MR = 10), the charge ratio between PLR and siRNA (CR_{PS}) was increased from 1 to 44. Concentration of free siRNA diminished with increasing CR_{PS}: compared to a control, only 0.2% of siRNA was released with a CR_{PS} of 24. From CR_{PS} of 28, the totality of the loaded siRNA remained on S-MSN (Fig. 2).

Compared to S-MSN_1, the hydrodynamic diameter of the optimized charge ratio (CR = 28) S-MSN_2 was 15 nm smaller (Table 1). This difference was probably due to the PLR molecules that may produce a more compact complex with siRNA, in line with the lower polydispersity (Table 1). Unexpectedly, the zeta potential of S-MSN_2 was around 3 mV, i.e. 3.7 times lower than that of S-MSN_1 and close to that of SFP (Table 1). The siRNA-PLR complex compaction into S-MSN_2 could enable more efficient shielding of the siRNA-PLR charges within the PEG coating.

Despite a better complexation with these optimized S-MSN_2 (MR = 10 and CR_{PS} = 28), GFP expression was not significantly down-regulated after 20 nM siRNA transfection (Supplementary data Fig. 1B). Therefore, a third protocol of the S-MSN formulation has been developed and described below.

3.1.3. Protocol 3 (synthesis of S-MSN_3): loading of siRNA together with both PLR and chitosan to reach the transfection efficiency of commercially available transfection reagent Oligofectamine®

From the previous experiments, S-MSN_3 was developed. The protocol comprised the siRNA/PLR pre-complexation prior to adding them to a mixture of SFP and chitosan. According to previous protocols, the initial formulation of S-MSN_3 was characterized by MR of 10, CR_{CS} of 44, and CR_{PS} of 28. In order to optimize the biological response, each of these three parameters was varied individually, maintaining the other two constant. The results of transfection with S-MSN_3 of different quantitative composition on MDA-MB231-GFP are shown in Fig. 3.

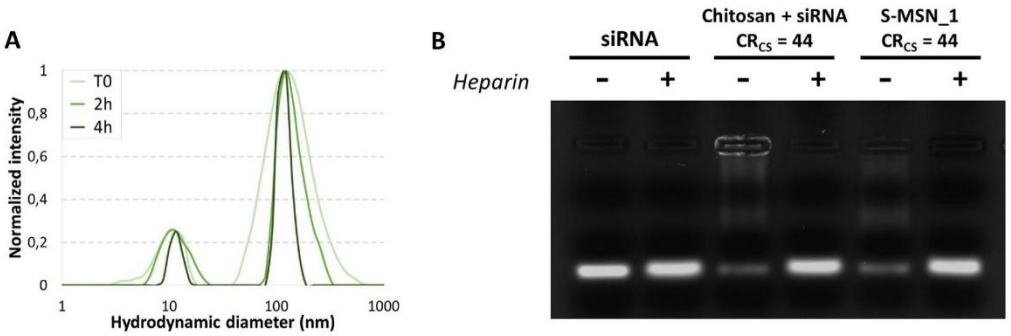

Fig. 1. S-MSN_1. (A) Stability in culture media. S-MSN_1 containing siRNA (20 nM), SFP (MR = 10) and chitosan (CR_{CS} = 44) were studied for colloidal stability in complete culture medium through dynamic light scattering (n = 3). (B) Complexation. Gel retardation assay on chitosan-siRNA polyplex and S-MSN_1 with a constant concentration of siRNA (3 μM) and CR_{CS} (44).

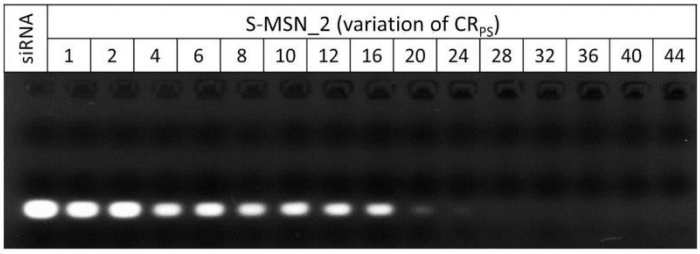

Fig. 2. S-MSN_2. Complexation. Gel retardation assay on S-MSN_2 with a constant concentration of siRNA (3 μM) and CR_{PS} varying from 1 to 44.

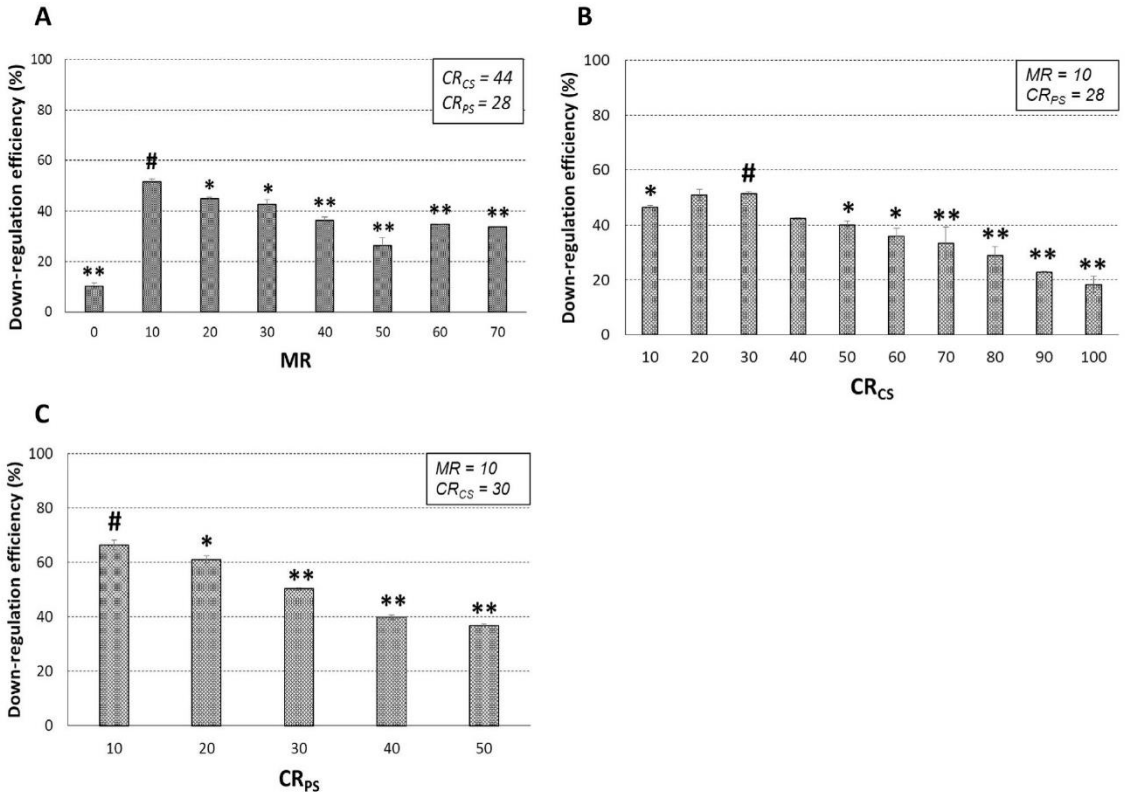

Fig. 3. Optimization of S-MSN_3 for down-regulation efficiency: Fluorescence intensity of MDA-MB231/GFP after 72 hours incubation with 0.13 μg siRNA-GFP included into S-MSN_3. Different components were optimized: (A) MR (B) CR_{CS} and (C) CR_{PS}. #: reference value for statistics; *: $p < 0.05$; **: $p < 0.01$ (mean +/− SD, n = 6).

(i) With a constant siRNA quantity (10 nmol), CR_{CS} (= 44) and CR_{PS} (= 28), the quantity of SPION was adjusted according to a MR from 10 to 70 (Fig. 3A). A control condition of chitosan-PLR-siRNA polyplexes (MR = 0) demonstrated a major contribution of SPION for functional siRNA transfection as this condition led to low GFP down-regulation efficiency (10.3%). However, an increase in SPION concentration ($MR \geq 10$) was correlated with a lowered GFP down-regulation efficiency, from 52.3% to 28.6% (Fig. 3A). Thus, a MR of 10 was chosen as the optimal formulation condition for further experiments.

(ii) With fixed MR (= 10), CR_{PS} (= 28) and siRNA quantity (10 nmol), the chitosan concentration was varied corresponding to a CR_{CS} from 10 to 100 (Fig. 3B). Up to a CR_{CS} of 30, GFP down-regulation efficiency increased with the amount of chitosan, reaching a maximum of around 52% (Fig. 3B). For higher chitosan content, the GFP down-regulation was less pronounced (Fig. 3B), demonstrating the impact of chitosan on siRNA transfection. The optimal amount of chitosan used for further experiments was considered to be a CR_{CS} of 30.

(iii) With fixed MR (= 10), CR_{CS} (= 30) and siRNA quantity (10 nmol), the CR_{PS} was varied from 10 to 50 (Fig. 3C). Unexpectedly, GFP down-regulation efficiency was directly reduced with the increase of PLR (Fig. 3C), showing the need to reduce CR_{PS} to 10 in order to obtain optimal results. Compared to results obtained with CR_{PS} at 30 (Fig. 3C), GFP down-regulation was improved up to 67% with optimum balance between the various components. CR_{PS} of 10 was chosen as optimal formulation condition for further experiments.

(iv) With optimal data defined previously (CR_{CS} = 30; CR_{PS} = 10; MR = 10), the concentration of siRNA incorporated into the

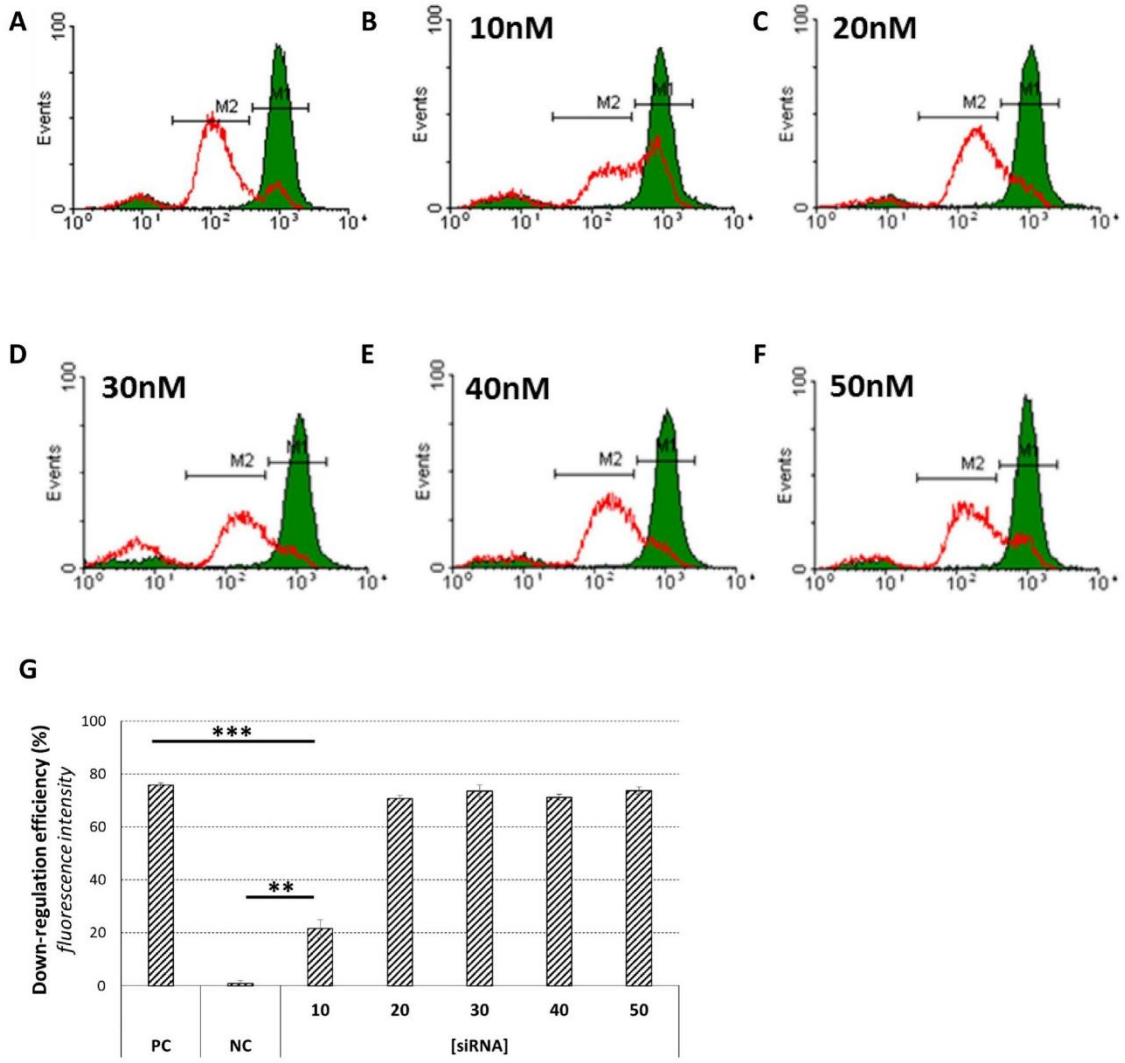

Fig. 4. Optimization of siRNA concentration with S-MSN_3 for down-regulation efficiency. Fluorescence intensity of MDA-MB231/GFP cells after 72 hours transfection with (A) Positive control (PC): transfection with commercially available reagent Oligofectamine® (20 nM siGFP). (B – F) S-MSN_3 with different siGFP concentrations (10, 20, 30, 40 and 50 nM for B, C, D, E, F, respectively). (G) Down-regulation efficiencies (conditions (A – F)) represented as decrease in fluorescence intensity. S-MSN_3 formulation with negative control siRNA (NC) was assessed at 20 nM. Green spectra with a black line represent MDA-MB231/GFP cells without transfection, whereas red line spectra are obtained after S-MSN_3 or Oligofectamine® transfection. ***: $p < 0.001$ (mean +/− SD, n = 3). For interpretation of the references to color in this figure legend, the reader is referred to the web version of the article.

formulation of S-MSN_3 was also varied from 10 nM to 50 nM (Fig. 4). The fluorescence intensity of individual cells is measured by flow cytometry, and the number of cells displaying a certain fluorescence intensity is plotted as a function of intensity. For non-transfected cells, the green curve is obtained showing a relatively homogeneous population of fluorescing cells (at about 10^3 units). A sub-population of particles with a 100-fold lower fluorescence intensity is also observed that corresponds to cellular debris and/or cells that do not express GFP protein. After successful transfection, the expression of GFP should be down-regulated, leading to cells with a lower fluorescence intensity (the main peak in the graph should be shifted to the left). For all siRNA concentrations above 20 nM (Fig. 4C), the peak of fluorescence intensity is shifted to about $2 \cdot 10^2$ units, which means that GFP content in most cells has decreased by a factor of 5: high specific GFP down-regulation was observed with 71% decrease in fluorescence intensity compared to negative control (NC) (Fig. 4G). S-MSN_3 containing from 20 to 50 nM siRNA showed comparable down-regulation efficiency displaying high ability to carry active siRNA. However, S-MSN_3 with only 10 nM siRNA reduced the down-regulation efficiency by a factor of 3 (Fig. 4B and G).

Compared to S-MSN_3, the commercially available reagent Oligofectamine® displayed a similar GFP down-regulation efficiency (Fig. 4A and G). The main difference was in the GFP distribution: with this commercial lipoplex, two distinct populations appeared, cells with or without GFP (Fig. 4A). On the contrary, with S-MSN_3 at 20 nM siRNA concentration, only one cell population with homogeneous GFP expression was observed

(Fig. 4C). With higher siRNA concentration of 50 nM (Fig. 4F), the GFP expression profile was significantly close to Oligofectamine®: 20 nM siRNA was therefore considered as optimum with S-MSN_3.

3.2. Safety, retention and protection required for in vivo adaptation of optimized S-MSN formulation

Among the features required for these nanocarriers with a view to *in vivo* adaptation, low S-MSN cytotoxicity as well as high siRNA retention and protection have to be provided. Cytotoxicity was assessed via the mitochondrial activity reduction depending on siRNA concentration in S-MSN_3 (Fig. 5). In 24 hours incubation with S-MSN_3, their cytotoxic effects seemed to be limited up to a siRNA concentration of 100 nM where cell viability remained as high as 87% (Fig. 5). This high safety could allow the increase of S-MSN_3 concentrations for certain conditions such as hard-to-transfect cells.

Complexation of siRNA with optimal S-MSN_3 formulation was assessed through gel retardation assay (supplementary data Fig. 2): no siRNA release was observed for S-MSN_3, displaying that all siRNA used for the formulation were complexed within S-MSN_3. In the same way, the siRNA retention in S-MSN incubated for various duration in a cell culture medium containing 5% fetal calf serum at 37 °C was monitored using a gel retardation assay (Fig. 6A). For each condition, a control with 10 mg/mL heparin was used in order to release siRNA. Immediately after the contact with the complete culture medium, less than 7% of siRNA had been released (Fig. 6A) and no additional release was observable till 4 hours demonstrating a high retention by S-MSN_3. Even by increasing the amount of fetal calf serum to 50%, the siRNA integrity remained significant (60-70%), with 80% of non-degraded siRNA retained in S-MSN_3 after 4 hours incubation (Supplementary data Fig. 3).

These results was consistent with the siRNA protection against ribonuclease A (Fig. 6B). While free siRNA was totally degraded after 30 minutes of incubation with the enzyme, S-MSN_3 protected siRNA even after 4 hours. More than 90% of siRNA kept their integrity upon the siRNA release stimulated using heparin sodium (Fig. 6B).

4. Discussion

S-MSN_1 have demonstrated promising results concerning their colloidal stability and complexation with siRNA. However, the use of chitosan as unique cationic polymer in the formulation did not allow reaching an efficient GFP down-regulation in MDA-MB231-GFP cells treated with the S-MSN_1 (Fig. 1). Similar limitations of chitosan as agent for *in vitro* and *in vivo* siRNA transfection have been previously described (Mao et al., 2001; Ragelle et al., 2013). Indeed, each deacetylated subunit of chitosan contains a primary amine group with a pKa value of about 6.5. S-MSN formulation occurred at a pH below the chitosan pKa enabling efficient complexation: at pH 5.5-5.7, about 90% of the amino groups were protonated (Mao et al., 2001). However, pH increase to 7.2-7.4 in the cell culture media may reduce the cationic nature of chitosan (Mao et al., 2001). Nevertheless, the role of chitosan remains essential during siRNA transfection to cells *in vitro*, probably for endosomal escape in order to reach cytoplasmic compartment after internalization through vesicles. In such cases, within the acidic endosomal environment, the protonation of chitosan amine groups results to an increased influx of Cl^- ions and water: the combination of the osmotic swelling (called proton-sponge effect) and a swelling of the chitosan because of repulsion between protonated amine groups (called umbrella effect) causes the rupture of the lysosomal membrane with subsequent release of its contents into the cytoplasm (Nguyen and Szoka, 2012).

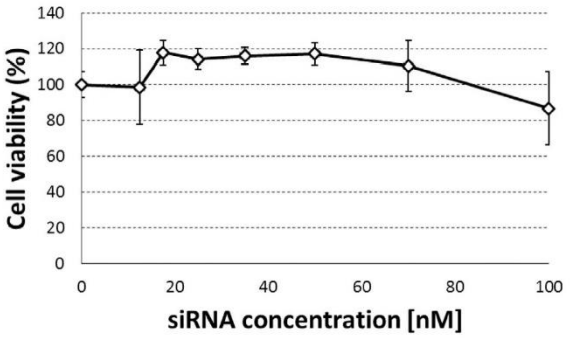

Fig. 5. Cytotoxicity assay on breast cancer cells MDA-MB231 with S-MSN_3. Metabolic activity from WST-1 assay after 24 hours incubation at different siRNA concentrations (with $CR_{CS} = 30$, $CR_{PS} = 10$ and MR = 10) (mean +/− SD, n = 6).

Addition of other cationic polymers represents an interesting approach to overcome the chitosan-related limitation described above. For example, poly-ethylene imine (PEI) (Akinc et al., 2005) and PLR (Kim et al., 2009; Veiseh et al., 2011) have been used in combination with chitosan to promote siRNA transfection. After PEI grafting onto chitosan using an imine reaction, these polymers allowed 55% silencing of GFP expression on adenocarcinomic human alveolar basal epithelial cells A549 after transfection with 50 nM siRNA (Jere et al., 2009). Nevertheless, PEI is generally described to exhibit significant *in vitro* and *in vivo* toxicity in addition to a lack of stability (Merkel et al., 2009). Another polymer, poly-L-arginine (PLR) and its derivatives, seems to be more promising and was shown to lead to the effective down-regulation of targeted genes on different cell lines (Noh et al., 2010). The pKa of PLR is about 12, which favors its cationic nature and its electrostatic interactions with siRNA at physiological pH. In our study, addition of PLR to siRNA and chitosan ($CR_{CS} = 30$) provided a large improvement of GFP down-regulation efficiency when used at a charge ratio CR_{PS} of 10 (Fig. 3).

However, with a larger excess of PLR ($CR_{PS} > 10$), the GFP silencing activity diminished (Fig. 3C). This could be explained with two hypothesis: (1) the strong interaction between PLR and siRNA prevents them from being delivered into cytoplasmic compartment and limits their RISC accessibility. (2) Following the protocol, the pre-complex siRNA/PLR was added to a solution of SPION/Chitosan. Also, during formulation, PLR/siRNA could trap low-charged chitosan on the SFP: this is observable with hydrodynamic diameter comparison between S-MSN_1 and S-MSN_3. Without PLR, S-MSN_1 displayed 76 nm whereas the compaction allowed by PLR in S-MSN_3 led to a hydrodynamic diameter of 63 nm, even with chitosan presence (Table 1). In this hypothesis, when the acidification of the endosome enables the protonation of chitosan amine groups, the electrostatic repulsion between cationic charges triggers polymer expansion and umbrella effect (Nguyen and Szoka, 2012). With a too strong interaction between PLR and siRNA, this effect could be reduced, diminishing endosomal escape and siRNA release into cytoplasm (Fig. 3C).

The optimization of different formulation parameters and the comprehension of their interaction enable to achieve 70% gene silencing efficiency on MDA-MB231-GFP cells using S-MSN_3 (see the flow cytometry data in Figs. 3 and 4). This efficiency was close to that of commercially available lipoplexe Oligofectamine® (Fig. 4). Previous studies have already reported the efficient siRNA transfection by SPION combined to chitosan and other molecules: with linoleic acid, Cheong et al. demonstrated strong down-regulation of GFP in hepatocytes (Cheong et al., 2009). However, nature of molecules associated to inorganic nanoparticles remains

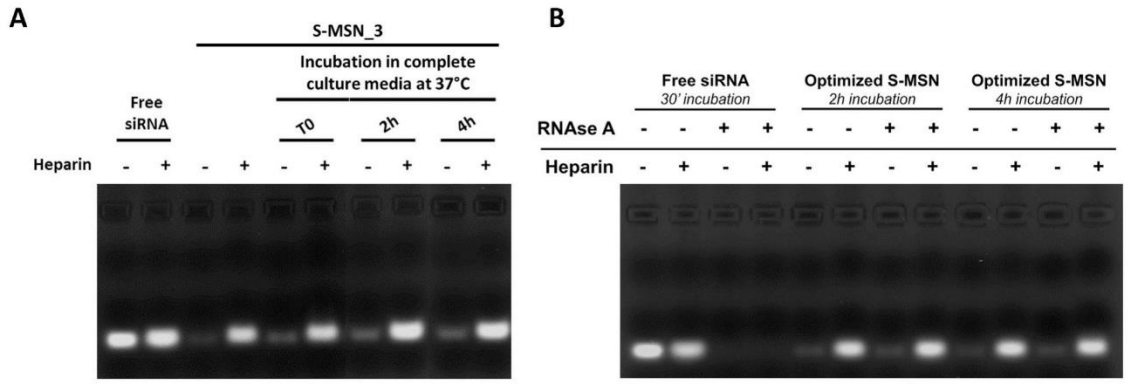

Fig. 6. Protection and retention of siRNA on S-MSN_3. Gel retardation assay with constant concentration of S-MSN_3 ([siRNA] 3 μM) after incubation from 0 to 4 h (A) in complete culture medium or (B) with ribonuclease A (400 ng/mL). Heparin sodium (10 μg/mL) was used to release siRNA from S-MSN complex as a control condition.

a key issue, especially for internalization and endosomal escape. Many studies have shown weak silencing activity attributed to a major accumulation of nanocarriers in endosomes (Ding et al., 2014; Perche et al., 2016; Wu et al., 2014) and required strategies to overcome this limitation, such as endosomal escape enhancer (Perche et al., 2016). Thus, Perche et al. had shown that transfection with high siRNA concentration (up to 200 nM) resulted in a down-regulation efficiency close to that obtained with commercially available lipoplexes (Perche et al., 2016). Our results demonstrate that S-MSN_3 favor siRNA transfection into cytoplasm of cancer cells and results in a strong down-regulation of targeted gene, even at concentration of 20 nM (Fig. 5).

Efficient siRNA nanocarriers have to protect siRNA against degradation from enzymes such as ribonucleases. Moreover, siRNA release need to be avoided until they reach targeted cells or tissues. In the literature, inorganic nanoparticles modified with positively charged L-arginine have already been reported to provide effective protection of siRNA from enzymatic degradation (Li et al., 2011). Besides, other molecules used in formulation could induce some steric hindrance limiting siRNA accessibility to RNAses (Li et al., 2011). With S-MSN_3, chitosan and PLR prevent siRNA from degradation even after several hours of incubation with RNAse A (Fig. 6B). Furthermore, the S-MSN_3 prevented siRNA release in culture media containing fetal bovine serum (Fig. 6A). These results could be explained through a better compaction of siRNA/PLR onto SFP allowing protection by PEG. Nevertheless, a balance between protection and release of siRNA is required to allow the siRNA to act in the cellular cytoplasm. Excessive siRNA protection may hinder their endosomal escape and result in its total degradation into lysosome (Zeller et al., 2015). S-MSN_3 appear to be in line with all the necessary requirements since the down-regulation of the targeted gene was observed after siRNA transfection (Fig. 4).

5. Conclusion

In this study, stealth magnetic siRNA nanocarriers S-MSN_3 were able to provide effective siRNA transfection to the cytosol of breast cancer cells MDA-MB231. Down-regulation of GFP protein by transfected siRNA was confirmed by strong reduction of cytosolic fluorescence intensity. According to their size below 100 nm, nearly neutral surface and their ability to protect siRNA from enzymatic degradation, the S-MSN_3 appear as promising nanomedicine form. In the close future, we will start their evaluation *in vivo*. In parallel, we will advance this nanomedicine form with antibody fragments grafted onto the PEG shell, for active and specific targeting of breast cancer cells.

Acknowledgments

This work is supported by the "Institut National du Cancer (INCa)", the "Fondation ARC" and the "Ligue Nationale Contre le Cancer (LNCC)" (ARC_INCa_LNCC_7636). We are thankful to the "Région Centre-Val de Loire" (NCIS Project). The authors would like to thank Isabelle Dimier-Poisson and Nathalie Moire (UMR INRA 1282, team of "Infectiologie et Santé Publique", University François Rabelais of Tours) for her help with flow cytometry experiments and Didier Bedin (EA6295, "Nanomédicaments et nanosondes", University François Rabelais of Tours) for technical support.

Appendix A. Supplementary data

Supplementary data associated with this article can be found, in the online version, at http://dx.doi.org/10.1016/j.ijpharm.2017.05.022.

References

Akinc, A., Thomas, M., Klibanov, A.M., Langer, R., 2005. Exploring polyethylenimine-mediated DNA transfection and the proton sponge hypothesis. J. Gene Med. 7, 657–663. doi:http://dx.doi.org/10.1002/jgm.696.

Alric, C., Aubrey, N., Allard-Vannier, E., di Tommaso, A., Blondy, T., Dimier-Poisson, I., Chourpa, I., Hervé-Aubert, K., 2016. Covalent conjugation of cysteine-engineered scFv to PEGylated magnetic nanoprobes for immunotargeting of breast cancer cells. RSC Adv . 6, 37099. doi:http://dx.doi.org/10.1039/c6ra06076e.

Cheong, S.J., Lee, C.M., Kim, S.L., Jeong, H.J., Kim, E.M., Park, E.H., Kim, D.W., Lim, S.T., Sohn, M.H., 2009. Superparamagnetic iron oxide nanoparticles-loaded chitosan-linoleic acid nanoparticles as an effective hepatocyte-targeted gene delivery system. Int. J. Pharm. 372, 169–176. doi:http://dx.doi.org/10.1016/j.ijpharm.2009.01.009.

David, S., Marchais, H., Bedin, D., Chourpa, I., 2015. Modelling the response surface to predict the hydrodynamic diameters of theranostic magnetic siRNA nanovectors. Int. J. Pharm. 478, 409–415. doi:http://dx.doi.org/10.1016/j.ijpharm.2014.11.061.

David, S., Marchais, H., Hervé-Aubert, K., Bedin, D., Garin, A.-S., Hoinard, C., Chourpa, I., 2013. Use of experimental design methodology for the development of new magnetic siRNA nanovectors (MSN). Int. J. Pharm. 454, 660–667. doi:http://dx.doi.org/10.1016/j.ijpharm.2013.05.051.

De Fougerolles, A., Novobrantseva, T., 2008. siRNA and the lung: research tool or therapeutic drug? Curr. Curr. Opin. Pharmacol. 8, 280–285. doi:http://dx.doi.org/10.1016/j.coph.2008.04.005.

Ding, Y., Jiang, Z., Saha, K., Kim, C.S., Kim, S.T., Landis, R.F., Rotello, V.M., 2014. Gold nanoparticles for nucleic acid delivery. Mol. Ther. 22, 1075–1083. doi:http://dx.doi.org/10.1038/mt.2014.30.

Ferlay, J., Soerjomataram, I., Dikshit, R., Eser, S., Mathers, C., Rebelo, M., Parkin, D.M., Forman, D., Bray, F., 2015. Cancer incidence and mortality worldwide: Sources, methods and major patterns in GLOBOCAN 2012. Int. J. Cancer 136, E359–E386. doi:http://dx.doi.org/10.1002/ijc.29210.

Fire, A., Xu, S., Montgomery, M.K., Kostas, S.A., Driver, S.E., Mello, C.C., 1998. Potent and specific genetic interference by double-stranded RNA in Caenorhabditis elegans. Nature 391, 806–811. doi:http://dx.doi.org/10.1038/35888.

Howard, K.A., Rahbek, U.L., Liu, X., Damgaard, C.K., Glud, S.Z., Andersen, M.Ø., Hovgaard, M.B., Schmitz, A., Nyengaard, J.R., Besenbacher, F., Kjems, J., 2006. RNA interference in vitro and in vivo using a novel chitosan/siRNA nanoparticle system. Mol. Ther. 14, 476–484. doi:http://dx.doi.org/10.1016/j.ymthe.2006.04.010.

Jere, D., Jiang, H.-L., Kim, Y.-K., Arote, R., Choi, Y.-J., Yun, C.-H., Cho, M.-H., Cho, C.-S., 2009. Chitosan-graft-polyethylenimine for Akt1 siRNA delivery to lung cancer cells. Int. J. Pharm. 378, 194–200. doi:http://dx.doi.org/10.1016/j.ijpharm.2009.05.046.

Juliano, R., Alam, M.R., Dixit, V., Kang, H., 2008. Mechanisms and strategies for effective delivery of antisense and siRNA oligonucleotides. Nucleic Acids Res. 36, 4158–4171. doi:http://dx.doi.org/10.1093/nar/gkn342.

Kennecke, H., Yerushalmi, R., Woods, R., Cheang, M.C.U., Voduc, D., Speers, C.H., Nielsen, T.O., Gelmon, K., 2010. Metastatic behavior of breast cancer subtypes. J. Clin. Oncol. 28, 3271–3277. doi:http://dx.doi.org/10.1200/JCO.2009.25.9820.

Kim, E.-J., Shim, G., Kim, K., Kwon, I.C., Oh, Y.-K., Shim, C.-K., 2009. Hyaluronic acid complexed to biodegradable poly L-arginine for targeted delivery of siRNAs. J. Gene. Med. 11, 791–803. doi:http://dx.doi.org/10.1002/jgm.1352.

Lavertu, M., Méthot, S., Tran-Khanh, N., Buschmann, M.D., 2006. High efficiency gene transfer using chitosan/DNA nanoparticles with specific combinations of molecular weight and degree of deacetylation. Biomaterials 27, 4815–4824. doi:http://dx.doi.org/10.1016/j.biomaterials.2006.04.029.

Layzer, J.M., McCaffrey, A.P., Tanner, A.K., Huang, Z., Kay, M.A., Sullenger, B.A., 2004. In vivo activity of nuclease-resistant siRNAs. RNA 10, 766–771. doi:http://dx.doi.org/10.1261/RNA.5239604.

Li, J.M., Zhao, M.X., Su, H., Wang, Y.Y., Tan, C.P., Ji, L.N., Mao, Z.W., 2011. Multifunctional quantum-dot-based siRNA delivery for HPV18 E6 gene silence and intracellular imaging. Biomaterials 32, 7978–7987. doi:http://dx.doi.org/10.1016/j.biomaterials.2011.07.011.

Mao, H.Q., Roy, K., Troung-Le, V.L., Janes, K. a., Lin, K.Y., Wang, Y., August, J.T., Leong, K.W., 2001. Chitosan-DNA nanoparticles as gene carriers: Synthesis, characterization and transfection efficiency. J. Control. Release 70, 399–421. doi:http://dx.doi.org/10.1016/S0168-3659(00)00361-8.

Mao, S., Sun, W., Kissel, T., 2010. Chitosan-based formulations for delivery of DNA and siRNA. Adv. Drug Deliv. Rev. 62, 12–27. doi:http://dx.doi.org/10.1016/j.addr.2009.08.004.

Medarova, Z., Pham, W., Farrar, C., Petkova, V., Moore, A., 2007. In vivo imaging of siRNA delivery and silencing in tumors. Nat. med 13, 372–377. doi:http://dx.doi.org/10.1038/nm1486.

Meister, G., Tuschl, T., 2004. Mechanisms of gene silencing by double-stranded RNA. Nature 431, 343–349. doi:http://dx.doi.org/10.1038/nature02873.

Merkel, O.M., Librizzi, D., Pfestroff, A., Schurrat, T., Buyens, K., Sanders, N.N., De Smedt, S.C., Behe, M., Kissel, T., 2009. Stability of siRNA polyplexes from poly(ethylenimine) and poly(ethylenimine)-g-poly(ethylene glycol) under in vivo conditions: effects on pharmacokinetics and biodistribution measured by luorescence Fluctuation Spectroscopy and Single Photon Emission Computed Tomography (SPECT) imaging. J. Control. Release. 138, 148–159. doi:http://dx.doi.org/10.1016/j.jconrel.2009.05.01.

Nguyen, J., Szoka, F.C., 2012. Nucleic acid delivery: the missing pieces of the puzzle? Acc. Chem. Res. 45, 1153–1162. doi:http://dx.doi.org/10.1021/ar3000162.

Noh, S.M., Park, M.O., Shim, G., Han, S.E., Lee, H.Y., Huh, J.H., Kim, M.S., Choi, J.J., Kim, K., Kwon, I.C., Kim, J.-S., Baek, K.-H., Oh, Y.-K., 2010. Pegylated poly-l-arginine derivatives of chitosan for effective delivery of siRNA. J. Control. Release 145, 159–164. doi:http://dx.doi.org/10.1016/j.jconrel.2010.04.005.

Opanasopit, P., Tragulpakseerojn, J., Apirakaramwong, A., Ngawhirunpat, T., Rojanarata, T., 2011. Chitosan enhances transfection efficiency of cationic polypeptides/DNA complexes. Int. J. Pharm. 410, 161–168. doi:http://dx.doi.org/10.1016/j.ijpharm.2011.03.008.

Ozcan, G., Ozpolat, B., Coleman, R.L., Sood, A.K., Lopez-Berestein, G., 2015. Preclinical and clinical development of siRNA-based therapeutics. Adv. Drug Deliv. Rev. 87, 108–119. doi:http://dx.doi.org/10.1016/j.addr.2015.01.007.

Perche, F., Yi, Y., Hespel, L., Mi, P., Dirisala, a., Cabral, H., Miyata, K., Kataoka, K., 2016. Hydroxychloroquine-conjugated gold nanoparticles for improved siRNA activity. Biomaterials 90, 62–71. doi:http://dx.doi.org/10.1016/j.biomaterials.2016.02.027.

Perillo, E., Hervé-Aubert, K., Allard-Vannier, E., Falanga, A., Galdiero, S., Chourpa, I., 2017. Synthesis and in vitro evaluation of fluorescent and magnetic nanoparticles functionnalized with a cell penetrating peptide for cancer theranosis. J. Colloid Interface Sci. 499, 209–217. doi:http://dx.doi.org/10.1016/j.jcis.2017.03.106.

Ragelle, H., Vandermeulen, G., Préat, V., 2013. Chitosan-based siRNA delivery systems. J. Control Release 172, 207–218. doi:http://dx.doi.org/10.1016/j.jconrel.2013.08.005.

Resnier, P., Montier, T., Mathieu, V., Benoit, J.P., Passirani, C., 2013. A review of the current status of siRNA nanomedicines in the treatment of cancer. Biomaterials 34, 6429–6443. doi:http://dx.doi.org/10.1016/j.biomaterials.2013.04.060.

Santel, a, Aleku, M., Keil, O., Endruschat, J., Esche, V., Fisch, G., Dames, S., Löffler, K., Fechtner, M., Arnold, W., Giese, K., Klippel, a, Kaufmann, J., 2006. A novel siRNA-lipoplex technology for RNA interference in the mouse vascular endothelium. Gene Ther. 13, 1222–1234. doi:http://dx.doi.org/10.1038/sj.gt.3302777.

Schlabach, M.R., Luo, J., Solimini, N.L., Hu, G., Xu, Q., Li, M.Z., Zhao, Z., Smogorzewska, A., Sowa, M.E., Ang, X.L., Westbrook, T.F., Liang, A.C., Chang, K., Hackett, J.A., Harper, J.W., Hannon, G.J., Elledge, S.J., 2008. Cancer proliferation gene discovery through functional genomics. Science 319, 620–624. doi:http://dx.doi.org/10.1126/science.1149200.

Techaarpornkul, S., Wongkupasert, S., Opanasopit, P., Apirakaramwong, A., Nunthanid, J., Ruktanonchai, U., 2010. Chitosan-mediated siRNA delivery in vitro: effect of polymer molecular weight, concentration and salt forms. AAPS PharmSciTech 11, 64–72. doi:http://dx.doi.org/10.1208/s12249-009-9355-6.

Urban-Klein, B., Werth, S., Abuharbeid, S., Czubayko, F., Aigner, a, 2005. RNAi-mediated gene-targeting through systemic application of polyethylenimine (PEI)-complexed siRNA in vivo. Gene Ther. 12, 461–466. doi:http://dx.doi.org/10.1038/sj.gt.3302425.

Veiseh, O., Kievit, F.M., Mok, H., Ayesh, J., Clark, C., Fang, C., Leung, M., Arami, H., Park, J.O., Zhang, M., 2011. Cell transcytosing poly-arginine coated magnetic nanovector for safe and effective siRNA delivery. Biomaterials 32, 5717–5725. doi:http://dx.doi.org/10.1016/j.biomaterials.2011.04.039.

Veiseh, O., Gunn, J.W., Zhang, M., 2010. Design and fabrication of magnetic nanoparticles for targeted drug delivery and imaging. Adv. Drug Deliv. Rev. 62, 284–304. doi:http://dx.doi.org/10.1016/j.addr.2009.11.002.

Wood, L.D., Parsons, D.W., Jones, S., Lin, J., Sjöblom, T., Leary, R.J., Shen, D., Boca, S.M., Barber, T., Ptak, J., Silliman, N., Szabo, S., Dezso, Z., Ustyanksky, V., Nikolskaya, T., Nikolsky, Y., Karchin, R., Wilson, P.A., Kaminker, J.S., Zhang, Z., Croshaw, R., Willis, J., Dawson, D., Shipitsin, M., Willson, J.K., Sukumar, S., Polyak, K., Park, B.H., Pethiyagoda, C.L., Pant, P.V., Ballinger, D.G., Sparks, A.B., Hartigan, J., Smith, D.R., Suh, E., Papadopoulos, N., Buckhaults, P., Markowitz, S.D., Parmigiani, G., Kinzler, K.W., Velculescu, V.E., 2007. The genomic landscapes of human breast and colorectal cancers. Science. 318, 1108–1113. doi:http://dx.doi.org/10.1126/science.1145720.

Wu, X.A., Choi, C.H.J., Zhang, C., Hao, L., Mirkin, C.A., 2014. Intracellular Fate of Spherical Nucleic Acid Nanoparticle Conjugates. J. Am. Chem. Soc. 136, 7726–7733. doi:http://dx.doi.org/10.1021/ja503010a.

Yu, Y.H., Kim, E., Park, D.E., Shim, G., Lee, S., Kim, Y.B., Kim, C.-W., Oh, Y.-K., 2012. Cationic solid lipid nanoparticles for co-delivery of paclitaxel and siRNA. Eur. J. Pharm. Biopharm. 80, 268–273. doi:http://dx.doi.org/10.1016/j.ejpb.2011.11.002.

Zeller, S., Choi, C.S., Uchil, P.D., Ban, H.S., Siefert, A., Fahmy, T.M., Mothes, W., Lee, S.K., Kumar, P., 2015. Attachment of cell-binding ligands to arginine-rich cell-penetrating peptides enables cytosolic translocation of complexed sirna. Chem. Biol. 22, 50–62. doi:http://dx.doi.org/10.1016/j.chembiol.2014.11.009.

Zhang, J., Li, X., Huang, L., 2014. Non-viral nanocarriers for siRNA delivery in breast cancer. J. Control. Release 190, 440–450. doi:http://dx.doi.org/10.1016/j.jconrel.2014.05.037.

Annexe 4 : Magnetic nanocarriers for the specific delivery of siRNA: Contribution of breast cancer cells active targeting for down-regulation efficiency

Publié dans International Journal of Pharmaceutics, 2019

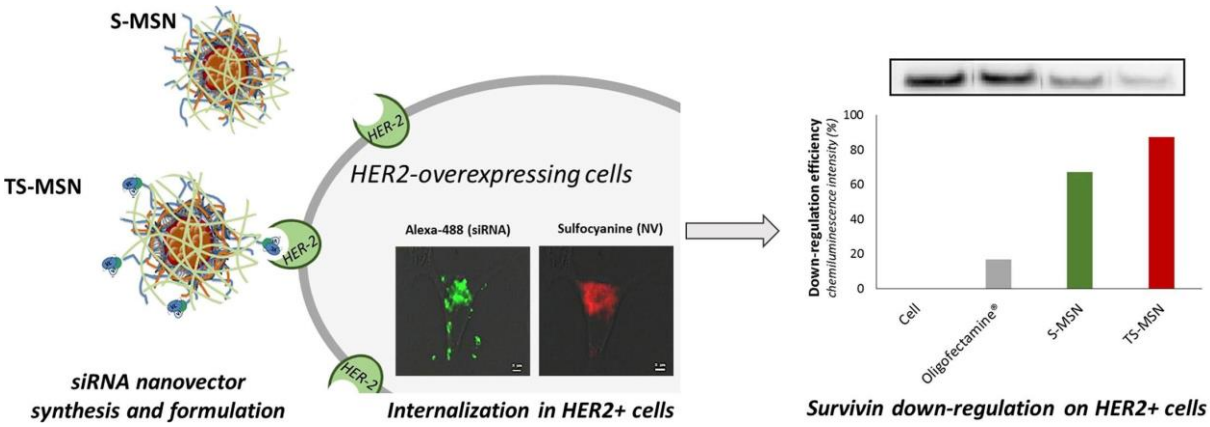

International Journal of Pharmaceutics 569 (2019) 118572

Contents lists available at ScienceDirect

International Journal of Pharmaceutics

journal homepage: www.elsevier.com/locate/ijpharm

Magnetic nanocarriers for the specific delivery of siRNA: Contribution of breast cancer cells active targeting for down-regulation efficiency

J. Bruniaux[a], E. Allard-Vannier[a], N. Aubrey[b], Z. Lakhrif[b], S. Ben Djemaa[a], S. Eljack[a], H. Marchais[a], K. Hervé-Aubert[a], I. Chourpa[a], S. David[a,*]

[a] Université de Tours, EA6295 «Nanomédicaments et Nanosondes», Tours 37200, France
[b] Université de Tours, UMR1282, INRA, «Infectiologie et Santé Publique», équipe BIOMAP, Tours 37200, France

ARTICLE INFO

Keywords:
Small interfering RNA (siRNA)
Superparamagnetic iron oxide nanoparticles (SPION)
scFv anti-HER2
Survivin

ABSTRACT

The association between superparamagnetic iron oxide nanoparticles (SPION), carrying small interfering RNA (siRNA) as therapeutic agents and humanized anti- human epidermal growth factor receptor-2 (HER2) single-chain antibody fragments (scFv) for the active delivery into HER2-overexpressing cells appears as an interesting approach for patients with HER2-overexpressing advanced breast cancer. The obtained Targeted Stealth Magnetic siRNA Nanovectors (TS-MSN) are formulated by combining: (i) the synthesis protocol of Targeted Stealth Fluorescent Particles (T-SFP) which form the core of TS-MSN and (ii) the formulation protocol allowing the loading of T-SFP with polyplexes (siRNA and cationic polymers). TS-MSN have suitable physico-chemical characteristics for intravenous administration and protect siRNA against enzymatic degradation up to 24 h. The presence of HER2-targeting scFv on TS-MSN allowed an improved internalization (3–4 times more compared to untargeted S-MSN) in HER2-overexpressing breast cancer cells (BT-474). Furthermore, anti-survivin siRNA delivered by TS-MSN in HER2-negative breast-cancer control cells (MDA-MB-231) allowed significant down-regulation of the targeted anti-apoptotic protein of about 70%. This protein down-regulation increased in HER2+ cells to about 90% (compared to 70% with S-MSN in both cell lines) indicating the contribution of the HER2-active targeting. In conclusion, TS-MSN are promising nanocarriers for the specific and efficient delivery of siRNA to HER2-overexpressing breast cancer cells.

1. Introduction

Breast cancer is the most common cancer and the leading cause of cancer mortality in women worldwide. In 2012, 25% of all cancers recorded worldwide are represented by new breast cancer cases (Ferlay et al., 2015). Approximately 20% of breast cancer are caused by over-expression of the human epidermal growth factor receptor 2 (HER2) (Anhorn et al., 2008; Slamon et al., 1989; Steinhauser et al., 2006). This HER2 overexpression is currently associated with more aggressive tumor behavior and poorer clinical outcomes (Slamon et al., 1989). Treatment strategies for patients with HER2 positive advanced breast cancer have progressed significantly over the past few decades. The outcome of these patients has been improved with the introduction of multiple successful anti-HER2 therapies, including anti-HER2 monoclonal antibody (mAb, trastuzumab) (Swain et al., 2015; Verma et al., 2012), antibody-drug conjugate (ado trastuzumab emtansine or T-DM1) and tyrosine kinase inhibitor (lapatinib). The market introduction of four trastuzumab biosimilars in 2018 underlines the great interest of this humanized monoclonal antibody for the targeting of HER2 receptors (Santos et al., 2019). However, many HER2-overexpressing breast cancer patients do not respond to anti-HER2 mAb treatment alone (Marty et al., 2005) and development of resistance and disease recurrence continue to be the major clinical challenges as it occurs in more than 50% of treated patients. These clinical problems underline the need of alternative therapeutic strategies combined to anti-HER2 therapies.

Abbreviations: CR, Charge ratio of positive polymer's amino groups to negative siRNA's phosphate groups; DMEM, Dulbecco's Modified Eagle Medium; EPR, Enhanced Permeability and Retention; HER2, human epidermal growth factor receptor-2; mAb, monoclonal antibody; NP, nanoparticle; scFv, single-chain antibody fragments; SFP, Stealth Fluorescent Particles; siRNA, small interfering RNA; S-MSN, Stealth Magnetic siRNA Nanovectors; SPION, superparamagnetic iron oxide nanoparticles; T-SFP, Targeted Stealth Fluorescent Particles; TS-MSN, Targeted Stealth Magnetic siRNA Nanovectors

* Corresponding author at: Université de Tours, EA 6295 Nanomédicaments et Nanosondes, Laboratoire de pharmacie galénique, Faculté de pharmacie, 31 avenue Monge, 37200 Tours, France.
E-mail address: stephanie.david@univ-tours.fr (S. David).

https://doi.org/10.1016/j.ijpharm.2019.118572
Received 30 March 2019; Received in revised form 17 July 2019; Accepted 25 July 2019
Available online 26 July 2019
0378-5173/ © 2019 Elsevier B.V. All rights reserved.

RNA interference strategy using small interfering RNA (siRNA) is an attractive and innovative strategy to inhibit targeted proteins involved in treatment resistance. The first RNA interference drug based on siRNA, Patisiran, was approved by the US Food and Drug Administration in 2018 and other siRNA drugs are already used in clinical trials (Kaczmarek et al., 2017; Ledford, 2018). However, their development as therapeutics is limited by several hurdles including (i) weak biostability as a consequence to nucleases digestion, (ii) poor uptake in cancer cells and, (iii) non-specific biodistribution. Therefore, the effective, targeted and safe delivery of siRNA across the cell membrane to the cytoplasm remains a main obstacle that could be overcome by the complexation of siRNA with a nanosized cargo called nanoparticle (NP) (Wang et al., 2017, Ben Djemaa et al., this issue).

Passive targeting is known as accumulation of NP at the tumor site at high concentrations due to the pathophysiological differences between normal tissues and tumor tissues (Enhanced Permeability and Retention (EPR) effect) (Jee et al., 2012). In addition, active targeting is investigated through molecular recognition by conjugation of targeting moieties onto NP to obtain targeted delivery to specific cells, tissues or organs (Chattopadhyay et al., 2012; Slavoff and Saghatelian, 2012). Cancer cells express different molecular targets (antigens and/or receptors) than do normal cells and tissues. While some of these molecules are down-regulated, others are either newly expressed or significantly up-regulated on the surface of target cells, thus offering possibility of targeting strategies (Allen, 2002). Therefore, biological ligands such as antibodies are associated to nanovectors (Tatiparti et al., 2017). For the NP targeting function, a single-chain variable fragment (scFv) of trastuzumab offers several advantages over the whole antibody, mainly lower immunogenicity due to its reduced size (~27 kDa compared to 150 kDa for the whole mAb) (Alric et al, 2018).

The purpose of this study was to develop Targeted Stealth Magnetic siRNA Nanovectors (TS-MSN) as a novel approach in breast cancer diagnosis and treatment to achieve maximal therapeutic benefit of anticancer siRNA. To combine targeted cancer imaging and therapy, we used superparamagnetic iron oxide nanoparticles (SPION) that can provide imaging ability through MRI. SPION were covalently conjugated to a near-infrared fluorophore, sulfocyanine 5 (sCy5), for optical imaging and to polyethylene glycol (PEG) for improved immune stealthiness (prolonged lifetime in blood). These Stealth Fluorescent Particles (SFP) were conjugated with anti-HER2 scFv of trastuzumab in order to target HER2-overexpressing cells, such as SK-BR3 and BT-474 human breast cancer cells (Alric et al., 2018). Finally, these targeted SFP (T-SFP) were loaded with siRNA polyplexes (complexes with polycations such as chitosan and poly-L-arginine) using a protocol previously developed by our laboratory (Bruniaux et al., 2017). In addition to enabling siRNA complexation, the polycations favore endosomal escape of siRNA in order to reach its cytoplasmic targets (Bruniaux et al., 2017). The therapeutic target aimed in this study was survivin, a chemotherapy-induced anti-apoptotic gene. Survivin is highly and selectively expressed in a majority of human cancers, including breast cancer, representing a potential biomarker (Jha et al., 2012; Lv et al., 2010; Nassar et al., 2008). In addition, high survivin expression is correlated with chemo- and radio-resistance in multiple tumor types whereas low expression enhances cell death (Guan et al., 2006; Kunze et al., 2012). In this way, survivin down-regulation through siRNA specific delivery could be considered as a therapeutic approach.

The final Targeted Stealth Magnetic siRNA Nanovectors (hereafter called TS-MSN) and the control non-targeted Stealth Magnetic siRNA Nanovectors (S-MSN) were both characterized and evaluated *in vitro*, in terms of their ability to down regulate survivin in HER2+ (SK-BR3 and BT-474 cell lines) and HER2- (MDA-MB-231 cell line) breast cancer models. In particular, we investigated the HER2 protein binding, their cellular uptake in HER2+/HER2- cells the siRNA transfection potential. The latter was determined using anti-GFP siRNA delivery to the GFP-producing cells or anti-survivin siRNA delivery to the non-fluorescent cancer cells.

2. Materials and methods

2.1. Materials

NHS-PEG-Maleimide (NHS-PEG-Mal, Mw 5000 Da) and sulfocyanine 5 NHS ester were obtained from Rapp Polymer GmbH (Tübingen, Germany) and Lumiprobe (Hannover, Germany) respectively.

Poly-L-arginine (MW 15.000–70.000) and high purity chitosan (MW 110.000–150.000), used for S-MSN and TS-MSN formulation, were provided by Sigma–Aldrich Chemie GmbH (Schnelldorf, Germany).

For physico-chemical characterization, model siRNA (targeted against PCSK9, sense sequence GGAAGAUCAUAAUGGACAGdTdT with lower case letters representing deoxyribonucleotides) were provided by Eurogentec (Angers, France). Poly-L-arginine (MW 15.000–70.000) and high purity chitosan (MW 110.000–150.000; degree of acetylation: ≤ 40 mol%), used for MSN and S-MSN formulation, were from Sigma–Aldrich Chemie GmbH (Schnelldorf, Germany). For transfection assay, commercial transfection reagent Oligofectamine® and siRNA control were purchased from Life Technologies (Paisley, UK). siRNA against survivin was purchased from Sigma Aldrich Chemie GmbH (St. Quentin Fallavier, France, sense sequence GUCUGGACCUCAUGUU GUUdTdT with lower case letters representing deoxyribonucleotides). For gel retardation assays, loading buffer, agarose and ethidium bromide were purchased from Fisher Bioreagents® (Illkirch, France). All the culture media and supplements for cell culture were supplied by life technologies (Paisley, UK).

2.2. Nanocarriers preparation

2.2.1. Stealth fluorescent nanoparticle (SFP) and targeted SFP (T-SFP) synthesis

T-SFP were synthesized using previously developed protocols. Briefly, SPIONs obtained using the Massart protocol were first silanized (Hervé et al., 2008). Then, silanized SPION were labelled with the fluorochrome sulfocyanine 5 NHS and functionalized with PEG leading to SFP (Alric et al., 2018; Perillo et al., 2017). In parallel, scFv anti HER2 were produced in E.coli and purified using affinity chromatography (Alric et al., 2016). Finally, SFP were functionalized with purified scFv leading to T-SFP (Alric et al., 2018, 2016). SFP as control were treated in the same conditions (reaction and purification conditions) as T-SFP.

2.2.2. Stealth magnetic siRNA nanovector (S-MSN) and targeted S-MSN (TS-MSN) preparation

TS-MSN were prepared based on a protocol previously described by Bruniaux et al. (2017). Briefly, siRNA were pre-complexed with poly-L-arginine (PLR), then added to a suspension containing T-SFP and chitosan. The amount of T-SFP (quantified by its iron content) was defined as iron/siRNA mass ratio and fixed at 10. Chitosan and PLR content were expressed by the charge ratio (CR) of positive polymer charges to negative siRNA charges. CR of chitosan/siRNA (CR_{CS}) and CR of PLR/siRNA (CR_{PS}) were respectively set to 30 and 10. S-MSN, as control, were prepared in the same conditions using SFP instead of T-SFP.

2.3. Nanocarriers' characterization

2.3.1. Size and zeta potential measurements

The mean hydrodynamic diameter and zeta potential of S-MSN and TS-MSN in suspension were determined using a Malvern Nanosizer ZS (Malvern Instruments, Malvern, UK). Before measurement, the S-MSN and TS-MSN preparations were diluted in $NaNO_3$ 0.01 M at a ratio 1:25 to obtain a constant ionic strength (pH = 5.6) (n = 3).

2.3.2. siRNA protection assay

To analyze the siRNA protection, S-MSN and TS-MSN (at an initial siRNA concentration of 2.5 μM) were incubated with an aqueous ribonuclease A solution (1.2 μg/ml, Sigma-Aldrich, Chemie GmbH, Schelldorf, Germany) at a ratio of 2:1 for 8 to 24 h at 37 °C. Afterwards, ribonuclease A was inactivated by heating the suspensions at 70 °C for 30 min. An equivalent amount of free siRNA was incubated for 30 min and used as a positive control to check the ribonuclease A activity.

To analyze the amount of free siRNA, samples were diluted in water (Milli-Q system, Millipore, Paris, France) or aqueous heparin sodium solution (10 mg/ml, Sigma-Aldrich, Chemie GmbH, Schnelldorf, Germany) and mixed with loading buffer (Agarose gel loading dye 6X) in order to deposit 20 mol of siRNA per well on 1% agarose gel containing ethidium bromide. With its strong negative charge, heparin is used as control to displace complexed siRNA from S-MSN or TS-MSN. A 100 V voltage was applied for about 15 min in a Tris/acetate/EDTA buffer (TAE 1X, 40 mM acetate, EDTA 1 mM, pH 7.6). Gels were visualized and analyzed with EvolutionCapt software on a Fusion-Solo.65.WL imager (Vilbert Lourmat, Marne-la-Vallée, France).

2.3.3. Antigen-binding analysis through ELISA assay

The functionality of SFP in S-MSN formulation, and functionalized SPION (T-SFP) in TS-MSN formulation, were checked by indirect enzyme-linked immunosorbent assays (ELISA) using the HER2 protein (Sino Biologicals, Beijing, P. R. China) as a target. scFv fragments were detected by protein L-peroxidase in the presence of chromatic substrate, 3, 30, 5, 50-tetramethylbenzidine (TMB), through the high affinity of protein L to the κ light chain of scFv. Briefly, HER2 protein was coated in a 96-well plate at 1 μg/mL and incubated at 37 °C during 1 h. The wells were then saturated with 3% BSA-PBS for 1 h at 37 °C and washed with PBS prior to incubation with an increasing concentrations of S-MSN and TS-MSN (ranging from 0 to 50 mg/L iron, 0 to 376 nM siRNA) during 1 h at 37 °C. Wells were then washed and incubated with 100 μL/wells of protein L-peroxidase (Life Technologies) for 1 h at 37 °C before addition to TMB substrate (Sigma-Aldrich). Enzymatic reactions were stopped with the addition of 1 M H_2SO_4 and the absorbance was measured at 450 nm using a microplate reader (Biotek). Wells coloration correlated to the presence of scFv and the absorbance at 450 nm was then proportional to scFv content.

2.3.4. Immunofluorescence imaging

SK-BR3 cells, overexpressing HER2, grown on cover glasses were fixed in 4% paraformaldehyde solution for 20 min at room temperature. The cover glasses surface was saturated with a 20% fetal calf serum solution in PBS for 1 h at 37 °C. The fixed cells were then incubated with 40 μL of PBS, S-MSN or TS-MSN (at an iron concentration of 267 mg/l which is equivalent to a siRNA concentration of 2000 nM) all day night at 4 °C in a humidified chamber box. The cover glasses were washed three times with PBS and incubated for 1 h at 37 °C with protein-L-FITC (ACROBiosystems, Newark, USA) at 5 $\mu g.mL^{-1}$ for 1 h at 37 °C. Cells were finally washed with PBS and placed between slide and slip cover with 10 μL of Fluoromount G® mounting medium. Observations were then made with a fluorescent inverted microscope (Olympus, IX51).

2.4. In vitro evaluation

2.4.1. Cell culture

BT-474 and SK-BR3 human breast carcinoma cell lines with HER2 overexpression were purchased from Cell Lines Service (CLS Eppelheim, Germany). BT-4747 cells grow in compact, slowly growing multilayered colonies which rarely become confluent and are tumorigenic in mice. In contrast, SK-BR3 cells form monolayer colonies but are not tumorigenic in mice. MDA-MB231-GFP (Euromedex, Souffelweyersheim, France), MDA-MB231 (ECACC, Salisbury, UK) cell lines were used as negative controls as they express a low level of HER2 receptors (Alric et al., 2018). SK-BR3 cells were grown at 37 °C/5% CO_2 in Dulbecco's Modified Eagle Medium (DMEM) supplemented with 10% fetal calf serum and 1% penicillin/streptomycin. BT-474 cells were grown (37 °C/5% CO_2) in DMEM:Ham's F12 (1:1 mixture) supplemented with insulin 1X, 10% fetal bovine serum and 1% penicillin/streptomycin. MDA-MB231 cells expressing or not GFP were routinely cultured in DMEM supplemented with 10% fetal calf serum, non-essential amino acid 1X and 1% penicillin/streptomycin. Culture medium was changed every 48 h and the cells were harvested using trypsin as soon as 80% confluency was reached.

2.4.2. Internalization studies

2.4.2.1. Flow cytometry. 24 h before transfection, 25.10^3 BT-474 cells (over-expressing HER2 receptor)/wells were seeded in a 12-well plate. Transfections of 20 nM siRNA were carried out by adding a suspension of (T)S-MSN diluted in DPBS into 12-well plate containing equal parts OptiMEM serum-free medium and culture medium conventionally used for this cell line. Cells were treated with the prepared suspensions and maintained in normal growth conditions for different time points from 2 to 48 h. Cells were analyzed using a FACSCalibur flow cytometer (BD Bioscience, Franklin Lakes, NJ). At least 10^4 events were collected and analyzed using the WinMDI 2.9 software.

2.4.2.2. Confocal spectral imaging (CSI). For multispectral confocal imaging, the analysis of nanocarrier distribution was performed on cell-adherent cover slips. Cover glasses treated with poly-D-lysine were placed in 24-well plates. They were seeded with BT-474 cells and placed for 48 h in culture medium. The cells were then incubated with S-MSN and TS-MSN at an iron concentration of 2.66 mg/L (=20 nM siRNA concentration) for 24 h and washed three times with PBS. The cover glasses were then placed between a microscope slide and a cover slip to be scanned for CSI using a LabRAM laser scanning confocal microspectrometer (Horiba SA, Villeneuve d'Ascq, France), equipped with a 300 ‘/mm diffraction grating and a CCD detector air-cooled by Peltier effect. The sulfocyanine fluorescence was excited using a 633 nm line of a built-in He-Ne laser, under a 50 ˣ long focal microscope objective. The laser light power at the sample was approximately 0.1 mW and the acquisition time was 20 ms per spectrum. For the analysis of adherent cells, an optical section (x-y plane) situated at half-thickness of the cell was scanned with a step of 0.8 μm that provided maps containing typically 2500 spectra. Both acquisition and treatment of multispectral maps were performed with LabSpec software version 5.

2.4.2.3. Co-culture experiment. For co-culture experiment 30.10^3 cells/wells and 10^4 cells/wells were respectively seeded for BT-474 and MDA-MB231/GFP considering their growth difference. Transfections of 20 nM siRNA were carried out by adding a suspension of (T)S-MSN diluted in PBS into 12-well plate containing equal parts OptiMEM serum-free medium and culture medium conventionally used for these cell lines. GFP expression of MDA-MB231 promote their discrimination with flow cytometry (FL-1 canal) in order to differentiate (T)S-MSN interaction with each cell line. Cells were treated with the prepared suspensions and maintained in normal growth conditions for different time points from 2 to 48 h. Cells were analyzed using flow cytometry as described above (n = 5).

2.4.3. Efficacy studies

2.4.3.1. siRNA transfection. 24 h before transfection, 25.10^3 cells/well were seeded in a 12-well plate. The day of transfection, TS-MSN (at an initial siRNA concentration of 0.25 μM) were prepared and diluted in a mix of OptiMEM serum-free medium and the culture medium conventionally used for the studied cell line (1:1 v/v) in order to obtain a final siRNA concentration of 20 nM. S-MSN and Oligofectamine™ (Invitrogen, Thermo Fisher Scientific, Paisley, UK) were used as controls and prepared according to the protocol described above and the manufacture recommendation, respectively. Cells were treated with the prepared suspensions and maintained in normal

growth conditions for 72 h.

To validate the down-regulation functionality of siRNA formulated in TS-MSN, transfection was performed on MDA-MB231-GFP cells with anti-GFP siRNA which specifically down-regulate GFP protein expression. For statistical analysis, the level of GFP expression was determined by flow cytometry analysis as described above.

To determine the down-regulation efficacy of our target protein survivin, BT-474 cells (overexpressing HER2 receptor) and MDA-MB231 (control) cells were transfected with TS-MSN containing anti-survivin siRNA as described above. The level of survivin protein expression was determined by Western Blotting as described below.

2.4.3.2. Western Blot (WB). After transfection of siRNA down-regulating survivin with the different nanocarriers for 72 h, transfected cells were washed with cold PBS and total proteins were extracted on ice by RIPA buffer supplemented with anti-protease (Sigma-Aldrich Chemie GmbH, Schnelldorf, Germany). After 15 min centrifugation (10 000 G, 4 °C) to collect supernatant, protein concentrations were determined using a bicinchoninic acid (BCA) protein assay kit (Bio-rad, Hercules, CA). The cell lysate (30 µL protein for each sample) was boiled for 5 min in SDS sample buffer and subjected to SDS-polyacrylamide gel electrophoresis (PAGE). The proteins are transferred to nitrocellulose membrane using an iBlot® 2 dry blotting system (Thermo Fisher Scientific, Illkirch, France). After blocking with 5% nonfat milk at room temperature for 1 h, the membrane was incubated with the primary antibody against survivin (anti-rabbit, 1:1000, Life technologies), or glyceraldehyde-3-phosphate dehydrogenase (GAPDH, anti-rabbit, 1:1000, Life technologies) at 4 °C overnight. After incubating with the peroxidase conjugated secondary antibody (HRP goat to rabbit, 1:1000, Life technologies), the protein was visualized via an enhanced chemiluminescence (ECL) kit (Thermo Pierce) on a Fusion-Solo.65.WL imager (Vilbert Lourmat, Marne-la-Vallée, France) using EvolutionCapt software.

2.5. Statistical analysis

Data are expressed as mean ± SD of the variables and are compared among groups by using one-way ANOVA followed by Fisher's protected Least Significance Difference test calculated with GraphPad Prism7 software.

3. Results and discussion

3.1. Formulation and physico-chemical characterization of targeted stealth magnetic siRNA nanovectors

Targeted Stealth Magnetic siRNA Nanovectors (called TS-MSN) were formulated combining two previously developed protocols: the synthesis protocol of Targeted Fluorescent Particles (T-SFP,(Alric et al., 2018)) and the formulation protocol of Stealth Magnetic siRNA Nanovectors (S-MSN,(Bruniaux et al., 2017)). Briefly, T-SFP, siRNA and the cationic polymers (chitosan and poly-L-arginine) were mixed together in well-defined ratio to self-assembly via electrostatic interactions and form TS-MSN. HER2-targeting scFv incorporation into S-MSN formulation using T-SFP led to an increase in physico-chemical characteristics: the hydrodynamic diameter of formulated TS-MSN doubled almost compared to S-MSN to attain about 160 nm for TS-MSN and the zeta potential value of the formulation in aqueous buffer tripled almost to attain about + 17 mV for TS-MSN (Table 1). Both have an acceptable polydispersity index for self-assembled nanocarriers, i.e. below or around 0.3. Even if the formulation process is easy, the formulation parameters have to be carefully chosen and optimized to obtain reproducible physico-chemical parameters. Results showed that the modification of SFP with HER2 antibody fragment did not affect the formulation parameters and led to reproducible sizes and zeta potential. Despite the increase in size and zeta potential for TS-MSN compared to S-MSN, they are still acceptable considering a future intravenous administration as the size is below 200 nm and the zeta potential below 20 mV in aqueous buffer (pH5.6).

Table 1
Physico-chemical characteristics of S-MSN and TS-MSN.

	Hydrodynamic diameter *nm*	Polydispersity	Zeta potential *mV*
TS-MSN	157 ± 22	0.30 ± 0.04	+17 ± 4
S-MSN	73 ± 6	0.17 ± 0.03	+5 ± 2

To verify the protection of siRNA by our nanocarriers against enzymatic degradation, a gel electrophoresis experiment using RNAse A was performed. An aqueous siRNA solution (control) and samples of S-MSN or TS-MSN were incubated in presence and absence of RNAse A and/or heparin for 30 min, 8 h or 24 h (Fig. 1). Heparin was added as control to liberate siRNA of the nanocarriers and to visualize complexed siRNA. Unprotected siRNA is completely degraded within 30 min by RNAse A as no fluorescence band is visible. In absence of RNAse A and heparin, the fluorescence intensity of free siRNA is similar in the lanes containing the control solution and in the lanes containing S-MSN (Fig. 1A) and TS-MSN (Fig. 1B). In contrast, in absence of RNAse A and heparin, no fluorescence intensity is visible for S-MSN and TS-MSN indicating complete retention of siRNA in the nanocarriers. After 8 and 24 h incubation, in presence and absence of RNAse A, samples with heparin show the same fluorescence intensity of free siRNA for S-MSN and TS-MSN indicating no siRNA degradation up to 24 h. These results are consistent with previous published work (Abdelrahman et al., 2017; Bruniaux et al., 2017) indicating that the modification of the SPION core with HER2-targeting scFv antibodies did not alter the siRNA protection.

To validate the specific HER2 receptor recognition by TS-MSN, an ELISA assay was performed on an immobilized recombinant protein. Results are presented in Fig. 2A. With S-MSN, there is no absorbance measured for iron concentrations up to 8 mg/L. For iron concentrations greater than 8 mg/L the absorbance increase slightly (absorbance of 0.38 for 50 mg/L iron). This increase is related to the absorbance of the SPION and not to the association with HER2. In contrast, with TS-MSN, the absorbance start to increase for iron concentrations about 0.8 mg/L. At iron concentration of 2 mg/L the absorbance is about 1 indicating a high receptor recognition. The absorbance increase in correlation with iron concentration up to a maximum absorbance for iron concentration of 50 mg/L (absorbance about 1.7), displaying the specific recognition of HER2 receptor with formulations containing HER2 antibody fragments. These results show that TS-MSN containing HER2-targeting scFv were efficiently bound to immobilized HER2 receptor while S-MSN demonstrate no association with HER2 receptor

In parallel, immunofluorescence images were realized after the incubation of S-MSN and TS-MSN with SK-BR3 cells overexpressing HER2 receptors located at the plasmic membrane (Alric et al., 2018). HER2-targeting scFv were recognized by the specific interaction between κ light chain of scFv and FITC-labeled protein L (PpL-FITC) and are represented by a green fluorescence in the images (Fig. 2B). Samples treated with TS-MSN showed an intense green fluorescence distribution on the plasma membrane demonstrating the presence of antibody fragments interacting with the HER2 proteins. In contrast, samples treated with S-MSN showed only low green fluorescence on the plasma membrane. These results are in accordance with previous results obtained with T-SFP (Alric et al., 2018). Thus, the immunofluorescence images proved that the anti-HER2 targeting with TS-MSN is still efficient even after formulation of T-SFP with siRNA and cationic polymers.

These results confirmed that TS-MSN have appropriated physico-chemical characteristics for systemic administration and that the combination of the two protocols did not affect the characteristics of the

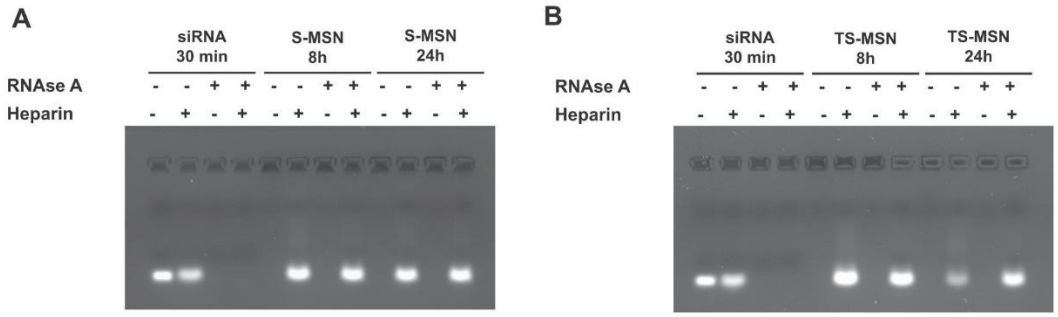

Fig. 1. Gel retardation assay demonstrating the siRNA protection against enzymatic degradation. siRNA formulated in S-MSN (A) or TS-MSN (B) in presence or absence of RNAse A and/or heparin after 8 and 24 h incubation compared to naked siRNA incubated for 30 min. Lanes without heparin show free siRNA amount and lanes with heparin show total siRNA amount in the sample.

initial properties: siRNA protection and HER2 receptor recognition.

3.2. The improved internalization through active targeting

The specific recognition of HER2 receptor with TS-MSN should improve the specific distribution inside cancer cells overexpressing this receptor. The results of internalization experiments on BT-474 cell line over-expressing HER2 receptor using flow cytometry are represented in Fig. 3A. Results showed that TS-MSN did not induce more interaction with cells for incubation time below 4 h compared to S-MSN. Nevertheless, whereas S-MSN fluorescence with cells remained constant above 24 h incubation, TS-MSN fluorescence continued to increase displaying a better interaction with this cell line until 48 h. After 24 and 48 h incubation, the amount of TS-MSN found inside the BT-474 cells is respectively 1.4 and 2.2 times higher compared to the amount of S-MSN in the same cell line. This result was confirmed and completed with multispectral confocal imaging. After 24 h incubation, TS-MSN had a massive internalization into cytoplasmic compartment with a homogenous distribution (Fig. 3B). T-SFP (red) and siRNA-alexa488 (green) were represented with high intensity signal suggesting that the nanovectors allow the delivery of siRNA inside the cells with high efficacy. In the same conditions with S-MSN, despite an accumulation into cytoplasmic compartment, the intensity signal remained weaker confirming the contribution of active targeting with TS-MSN.

To ensure the privileged TS-MSN distribution into cell lines over-expressing HER2 receptor, internalization studies on cellular co-culture were performed (Fig. 4). S-MSN and TS-MSN were incubated for increasing incubation times into a mixed culture of MDA-MB231/GFP (HER2-) and BT-474 (HER2+) cells. The different cell lines were discriminated through the green fluorescent protein (GFP) expression of MDA-MB231/GFP in order to compare nanocarrier interactions with cells depending on their HER2 receptor expression (Fig. 4A).

For TS-MSN, the fluorescence signal increased significantly over time in MDA-MB231/GFP cells up to 4 h ($p < 0.001$) with a threshold between 4 and 24 h and a slight increase between 24 and 48 h ($p < 0.01$). In BT-474 cells, the fluorescence signal increased continuously between 2 and 48 h but without any threshold ($p < 0.001$ up to 24 h and $p < 0.01$ between 24 and 48 h) (Fig. 4B, left). These results displayed more interaction between cells overexpressing HER2 receptors and nanocarriers with active targeting (TS-MSN). In contrast, with S-MSN the fluorescence signal increased significantly in both cell lines between 2 and 24 h with a threshold after 24 h ($p < 0.001$ for all points except at 24 h for MDA-MB231/ GFP cells where $p < 0.01$), indicating that the entry of S-MSN inside both cell lines is similar (Fig. 4B, right).

However, at all time points the fluorescence signal intensity measured on cells incubated with TS-MSN is significantly higher than that measured on cells incubated with S-MSN indicating more interaction

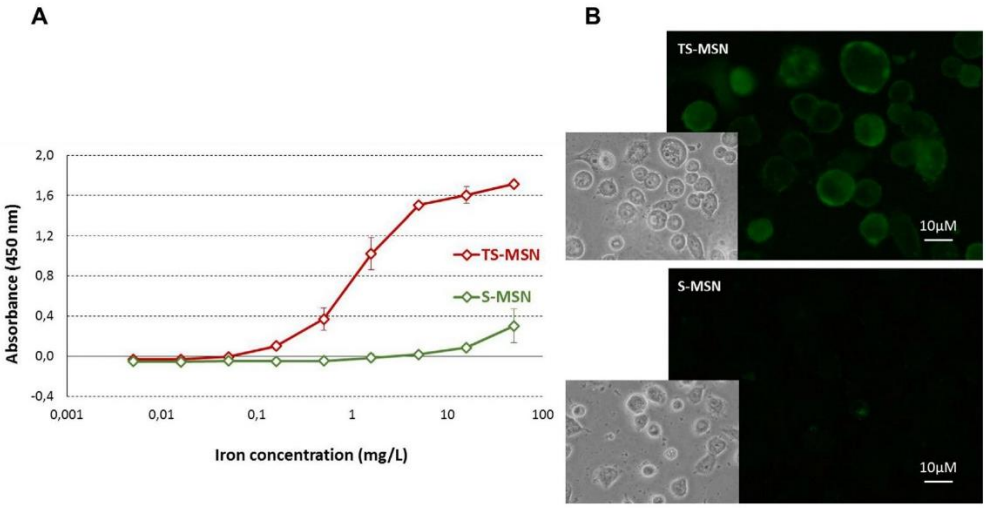

Fig. 2. HER2 protein recognition of S-MSN and TS-MSN. A: Indirect ELISA test of the immunoreactivity of TS-MSN (red curve) and S-MSN (green curve). B: Immunofluorescence images of SK-BR3 breast cancer cells incubated with TS-MSN and S-MSN (detection with PpL-FITC) and white light images to visualize the cells.

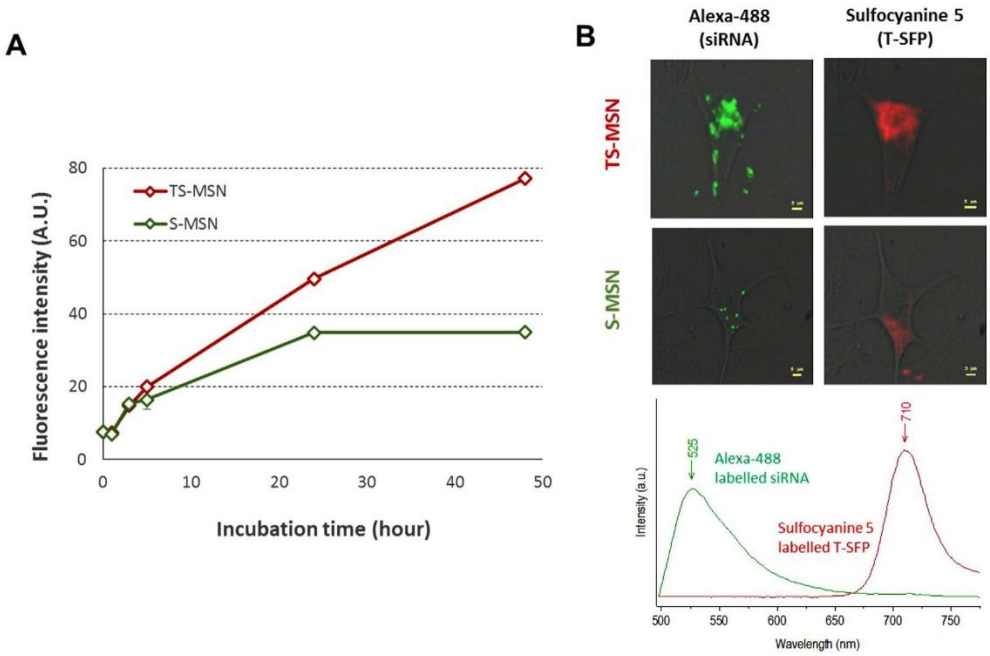

Fig. 3. Uptake of TS-MSN and S-MSN in BT-474 (HER2 +) cells. A: Uptake kinetics of TS-MSN (red curve) and S-MSN (green curve). B: Confocal spectral imaging data showing the fluorescence of the sulfocyanine labelled nanosystems (red) and the Alexa-488 labelled siRNA (green) after 24 h of incubation. Representative spectra of both fluorochromes (emission maximum: 525 for Alexa-488 and 710 nm for Sulfocyanine-5) are shown below.

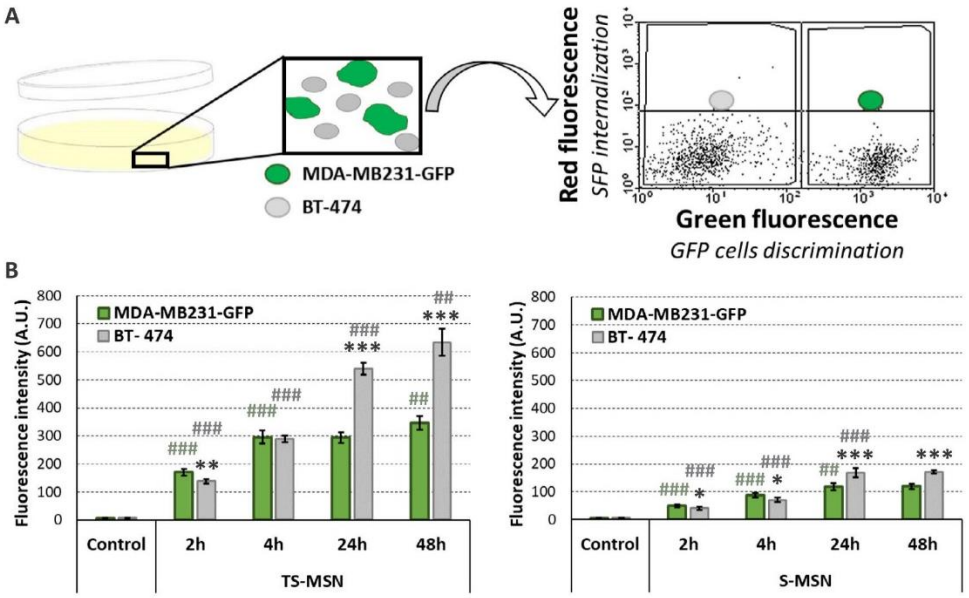

Fig. 4. Uptake kinetics of TS-MSN and S-MSN in a co-culture of BT-474 and MDA-MB231-GFP cells. A. Schematic representation of the co-culture and cytometry separation of the two cell lines according to green fluorescence intensity. B. Representation of the sulfocyanine fluorescence ratio found in BT-474 versus MDA-MB231-GFP cell lines after incubation of TS-MSN (left) and S-MSN (right) according time (2–48 h). *: $p < 0.05$; **: $p < 0.01$; ***: $p < 0.001$ correspond to the comparison between MDA-MB231/GFP and BT-474 for a same incubation time. ##: $p < 0.01$; ###: $p < 0.001$ correspond to the comparison with the previous incubation time for the same cell line.

between TS-MSN with cells. The difference between TS-MSN and S-MSN was the same in both cell lines after 2 h incubation (3.4 times). This phenomenon can be explained by the highly positive zeta potential value of TS-MSN compared to S-MSN allowing stronger interaction with the plasmic membrane (Table 1). However, this difference appeared to be higher after longer incubation: a fluorescence intensity 4 times higher for 4 h incubation, and respectively 3.2 and 3.7 times higher for 24 h et 48 h indicating a more pronounced internalization of TS-MSN in BT-474 thanks to the overexpression of the HER2 receptor.

In summary, TS-MSN containing HER2-targeting scFv showed (i) the specific HER2 receptor recognition in BT-474 cells while S-MSN demonstrated no visible distinction between both cell lines, (ii) an enhanced internalization in BT-474 (HER2 +) cells compared to MDA-MB231/GFP (HER2-) control cells for long term incubation (greater than 24 h).

These results are in accordance with our previous study performed on T-SFP (Alric et al., 2018) and with other studies that have previously reported the improved delivery of nanocarriers to the tumor sites by conjugation of HER2 antibody to the delivery carriers. Kievit *et al.* developed multifunctional superparamagnetic iron oxide nanoparticles containing trastuzumab antibody for active targeting and displayed the efficient targeting effect on HER2 expressing mouse mammary carcinoma (MMC) cells *in vitro* and *in vivo* in a transgenic mouse model (Kievit et al., 2012). In this study on HER2 expressing MMC, nanocarriers (50 µg/mL nanoparticles) containing trastuzumab antibodies led to an internalization two times higher after 2 h of treatments compared to non-functionalized nanoparticles (Kievit et al., 2012). In the same way, *Choi et al.* described that the extent of cellular uptake of anti-HER2 antibody-conjugated iron oxide nanoparticles (150 µg/mL iron) was approximately 5 times higher in HER2-positive cells than in HER2-negative cells at all time points (Choi et al., 2015). Despite a considerably lower iron concentration (ca. 2.67 µg/mL), our study reports an impact of active targeting on HER2-overexpressed BT-474 cells after comparison with MDA-MB231/GFP (HER2-) control cells.

3.3. The impact of active targeting on down-regulation efficiency after siRNA transfection

To verify the down-regulation efficiency of TS-MSN, flow cytometry experiments were performed on a MDA-MB231/GFP model using nanocarriers formulated with siRNA against GFP (Fig. 5A). Results demonstrated GFP down-regulation efficiency about 60% after siRNA transfection with TS-MSN, at the same level than S-MSN or commercial lipoplex formulation, Oligofectamine®. These results are in accordance with previous obtained results for S-MSN (Bruniaux et al., 2017).

To check the down-regulation efficiency of survivin by TS-MSN, Western Blot experiments were performed on MDA-MB231 cells using nanocarriers formulated with siRNA against survivin (Fig. 5B). Results demonstrated survivin down-regulation efficiency about 70% after siRNA transfection with TS-MSN, at a similar level as S-MSN. Surprisingly, commercial lipoplex formulation, Oligofectamine® inhibited the survivin expression only about 15%.

These results indicate that modification of SFP by antibody fragments grafting , in order to upgrade S-MSN to TS-MSN, did not alter the down-regulation efficiency on this HER2 negative model.

To verify the impact of the observed active targeting of TS-MSN on the specific down-regulation, transfection on BT-474 (HER2 +) cells was performed in order to down-regulate survivin expression. After 72 h transfection of siSurvivin with Oligofectamine®, S-MSN and TS-MSN, survivin protein level was analyzed through western-blot and compared to transfection with siControl (Fig. 5C). As expected, transfection with siControl did not provide any survivin protein down-regulation. As in the previous experiment on MDA-MB231 cells, siSurvivin transfection with Oligofectamine® enabled only about 15% survivin down-regulation whereas S-MSN induced about 70% down-regulation in the same conditions. With active targeting allowed by TS-MSN, survivin down-regulation was improved to about 90% demonstrating a direct contribution of HER2-targeting scFv integration in the formulation. Thus TS-MSN provide efficient down-regulation efficiency of survivin on BT-474 cells *in vitro*.

The study was performed with siRNA targeting GFP and survivin showing significant protein down-regulation and indicating the

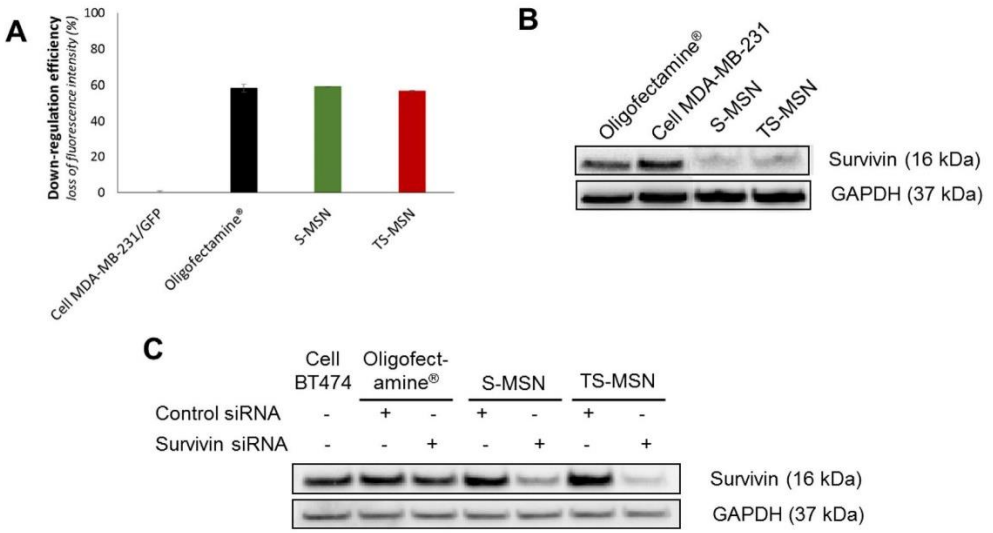

Fig. 5. Down-regulation efficiency of S-MSN and TS-MSN. A. GFP fluorescence expression in MDA-MB-231/GFP cells either untreated (Cell MDA-MB-231/GFP) or treated with oligofectamine®, S-MSN or TS-MSN formulated with anti GFP siRNA. B. Western Blot membranes of survivin expression in MDA-MB-231 cells either untreated (Cell MDA-MB-231) or treated with oligofectamine®, S-MSN or TS-MSN formulated with anti-survivin siRNA. C. Survivin down-regulation in BT474 cells. Western Blot membranes of survivin expression in BT474 cells either untreated (Cell BT474) or treated with oligofectamine®, S-MSN or TS-MSN formulated with either anti-survivin siRNA or a control siRNA.

adaptability of the delivery system to many target genes. Additionally, results show that the functionalization of T-SFP with scFv did not disturb the optimized formulation protocol of S-MSN indicating the adaptability of the delivery system to other cell types.

The correlation between selective targeting and down-regulation efficiency was also demonstrated by Jiang *et al.*: siRNA transfection (from 10 to 40 nM) with e23sFv-9R protein, allowing specific HER2 recognition, induced significant CXCR4 expression decrease in BT-474 cells (HER2 +) whereas no obvious change in MDA-MB231 cells (HER2-) was observed (Jiang et al., 2015). Despite the difference in both delivery system and siRNA target, the same behavior were observed with the specific antibody fragment grafting. Such a correlation was also observed with other targeting ligands on other cell types using nanovectors more similar to ours. For example, Veiseh *et al.* used SPION coated with PEG-grafted chitosan and PEI which were functionalized with siRNA and the tumor-targeting ligand, chlorotoxin (CTX). They showed that CTX-targeted nanovectors were internalized by C6 tumor cells 2-fold more than untargeted nanovectors and that the gene knockdown was correlated (35% reduction in GFP expression with non-targeted nanovectors vs 62% with CTX-targetd nanovectors) (Veiseh et al., 2010). However, to achieve this down-regulation efficiency, they have to use 7.5 times more siRNA, compared to the present study. Another example is the publication of Yang *et al.* who functionalized their SPION via electrostatic absorption of PEI and Gal-PEG-NH_2 (using galactose as targeting ligand) and loaded the obtained Gal-PEI-SPION with siRNA via electrostatic interactions. They emphasized the importance of nanoparticles protecting cargo siRNA from nuclease degradation during *in vivo* siRNA delivery. Their serum stability study showed no siRNA degradation up to 48 h. Furthermore, cy5-siRNA loaded Gal-PEI-SPIO nanoparticles were still observed with strong fluorescence intensity 24 h after intravenous injection into C57BL/6 tumor-bearing mice showing the successful complexation of the siRNA into Gal-PEI-SPIO nanoparticles with high protection efficiency. They showed that the tumor volume, the liver/body weight ratio and the mRNA levels were significantly reduced using siRNA against c-Met compared to a negative control siRNA after repeated intravenous administration in an orthotopic hepatocellular carcinoma mouse model (Yang et al., 2018). However, they did not compare their formulation with a non-targeted formulation.

The main advantage of using SPION as delivery system is related to their theranostic properties, i.e. their possible monitoring using imaging techniques such as MRI thus allowing to combine their diagnostic and their therapeutic functions. The above cited examples and the promising results presented here (physico-chemical characteristics of the nanocarriers compatible with an intravenous administration, siRNA protection against nuclease degradation up to 24 h, active targeting and efficient down-regulation *in vitro*) encourage us to continue towards *in vivo* preclinical assays. Moreover, *in vivo*, active cancer targeting through HER2 recognition, combined to an enhanced permeability and retention (EPR) effect in tumor environment, should promote specific biodistribution and improved down-regulation efficiency compared to control non-targeted nanovectors.

4. Conclusion

In this study, Targeted Stealth Magnetic siRNA Nanovectors (TS-MSN), were developed as alternative to existing HER2 cancer therapies in the objective to achieve a maximal therapeutic benefit. Therefore T-SFP functionalized with trastuzumab scFv (targeting HER2) were combined with S-MSN (for efficient siRNA delivery) and loaded with siRNA targeting survivin (highly expressed in cancers such as HER2 breast cancer). The main conclusions of our developed delivery system are that: 1) the formulation is rapid and simple 2) this delivery system can be adapted to many target genes, 3) the transfection efficacy is very high even if the nanovector is not targeted (S-MSN), 4) the active targeting with anti-HER2 antibody fragment increased the uptake of TS-MSN into the cells and especially in HER2 overexpressing cells, 5) the gene silencing effect of anti-survivin siRNA is even stronger for TS-MSN on cells that overexpressed the HER2 receptor.

Declaration of Competing Interest

The authors declare that they have no known competing financial interests or personal relationships that could have appeared to influence the work reported in this paper.

Acknowledgments

This work was supported by the “Institut National du Cancer (INCa)”, the “Fondation ARC” and the “Ligue Nationale Contre le Cancer (LNCC)” (ARC_INCa_LNCC_7636), France, the “Région Centre-Val de Loire” (NCIS Project) and the “Cancéropole Grand Ouest” , France. “This work has been funded with support from the French Higher Education and Research ministry under the program “Investissements d’avenir” Grant Agreement: LabEx MAbImprove ANR-10-LABX-53–01.”The authors would like to thank Isabelle Dimier-Poisson and Nathalie Moire (UMR INRA 1282, team of “Infectiologie et Santé Publique”, University François Rabelais of Tours) for their help with flow cytometry experiments and Lizzy Angevin for skillful technical support with cells.

References

Abdelrahman, M., Douziech Eyrolles, L., Alkarib, S.Y., Hervé-Aubert, K., Ben Djemaa, S., Marchais, H., Chourpa, I., David, S., 2017. siRNA delivery system based on magnetic nanovectors: characterization and stability evaluation. Eur. J. Pharm. Sci. Off. J. Eur. Fed. Pharm. Sci. 106, 287–293. https://doi.org/10.1016/j.ejps.2017.05.062.

Allen, T.M., 2002. Ligand-targeted therapeutics in anticancer therapy. Nat. Rev. Cancer 2, 750–763. https://doi.org/10.1038/nrc903.

Alric, C., Aubrey, N., Allard-Vannier, É., di Tommaso, A., Blondy, T., Dimier-Poisson, I., Chourpa, I., Hervé-Aubert, K., 2016. Covalent conjugation of cysteine-engineered scFv to PEGylated magnetic nanoprobes for immunotargeting of breast cancer cells. RSC Adv. 6, 37099–37109. https://doi.org/10.1039/C6RA06076E.

Alric, C., Hervé-Aubert, K., Aubrey, N., Melouk, S., Lajoie, L., Même, W., Même, S., Courbebaisse, Y., Ignatova, A.A., Feofanov, A.V., Chourpa, I., Allard-Vannier, E., 2018. Targeting HER2-breast tumors with scFv-decorated bimodal nanoprobes. J. Nanobiotechnology 16, 18. https://doi.org/10.1186/s12951-018-0341-6.

Anhorn, M.G., Wagner, S., Kreuter, J., Langer, K., von Briesen, H., 2008. Specific targeting of HER2 overexpressing breast cancer cells with doxorubicin-loaded trastuzumab-modified human serum albumin nanoparticles. Bioconjug. Chem. 19, 2321–2331. https://doi.org/10.1021/bc8002452.

Bruniaux, J., Djemaa, S.B., Hervé-Aubert, K., Marchais, H., Chourpa, I., David, S., 2017. Stealth magnetic nanocarriers of siRNA as platform for breast cancer theranostics. Int. J. Pharm. https://doi.org/10.1016/j.ijpharm.2017.05.022.

Chattopadhyay, N., Fonge, H., Cai, Z., Scollard, D., Lechtman, E., Done, S.J., Pignol, J.-P., Reilly, R.M., 2012. Role of antibody-mediated tumor targeting and route of administration in nanoparticle tumor accumulation in vivo. Mol. Pharm. 9, 2168–2179. https://doi.org/10.1021/mp300016p.

Choi, W.I., Lee, J.H., Kim, J.-Y., Heo, S.U., Jeong, Y.Y., Kim, Y.H., Tae, G., 2015. Targeted antitumor efficacy and imaging via multifunctional nano-carrier conjugated with anti-HER2 trastuzumab. Nanomedicine Nanotechnol. Biol. Med. 11, 359–368. https://doi.org/10.1016/j.nano.2014.09.009.

Ferlay, J., Soerjomataram, I., Dikshit, R., Eser, S., Mathers, C., Rebelo, M., Parkin, D.M., Forman, D., Bray, F., 2015. Cancer incidence and mortality worldwide: Sources, methods and major patterns in GLOBOCAN 2012. Int. J. Cancer 136, E359–E386. https://doi.org/10.1002/ijc.29210.

Guan, H.-T., Xue, X.-H., Dai, Z.-J., Wang, X.-J., Li, A., Qin, Z.-Y., 2006. Down-regulation of survivin expression by small interfering RNA induces pancreatic cancer cell apoptosis and enhances its radiosensitivity. World J. Gastroenterol. 12, 2901–2907.

Hervé, K., Douziech-Eyrolles, L., Munnier, E., Cohen-Jonathan, S., Soucé, M., Marchais, H., Limelette, P., Warmont, F., Saboungi, M.L., Dubois, P., Chourpa, I., 2008. The development of stable aqueous suspensions of PEGylated SPIONs for biomedical applications. Nanotechnology 19, 465608. https://doi.org/10.1088/0957-4484/19/46/465608.

Jee, J.-P., Na, J.H., Lee, S., Kim, S.H., Choi, K., Yeo, Y., Kwon, I.C., 2012. Cancer targeting strategies in nanomedicine: design and application of chitosan nanoparticles. Curr. Opin. Solid State Mater. Sci. Polymeric Nanomedicine 16, 333–342. https://doi.org/10.1016/j.cossms.2013.01.002.

Jha, K., Shukla, M., Pandey, M., 2012. Survivin expression and targeting in breast cancer. Surg. Oncol. 21, 125–131. https://doi.org/10.1016/j.suronc.2011.01.001.

Jiang, K., Li, J., Yin, J., Ma, Q., Yan, B., Zhang, X., Wang, Lei, Wang, Lifeng, Liu, T., Zhang, Y., Fan, Q., Yang, A., Qiu, X., Ma, B., 2015. Targeted delivery of CXCR4-siRNA by scFv for HER2(+) breast cancer therapy. Biomaterials 59, 77–87. https://doi.org/

10.1016/j.biomaterials.2015.04.030.
Kaczmarek, J.C., Kowalski, P.S., Anderson, D.G., 2017. Advances in the delivery of RNA therapeutics: from concept to clinical reality. Genome Med. 9, 60. https://doi.org/10.1186/s13073-017-0450-0.
Kievit, F.M., Stephen, Z.R., Veiseh, O., Arami, H., Wang, T., Lai, V.P., Park, J.O., Ellenbogen, R.G., Disis, M.L., Zhang, M., 2012. Targeting of primary breast cancers and metastases in a transgenic mouse model using rationally designed multifunctional SPIONs. ACS Nano 6, 2591–2601. https://doi.org/10.1021/nn205070h.
Kunze, D., Erdmann, K., Froehner, M., Wirth, M.P., Fuessel, S., 2012. siRNA-mediated inhibition of antiapoptotic genes enhances chemotherapy efficacy in bladder cancer cells. Anticancer Res. 32, 4313–4318.
Ledford, H., 2018. Gene-silencing technology gets first drug approval after 20-year wait. Nature 560, 291–292. https://doi.org/10.1038/d41586-018-05867-7.
Lv, Y.-G., Yu, F., Yao, Q., Chen, J.-H., Wang, L., 2010. The role of survivin in diagnosis, prognosis and treatment of breast cancer. J. Thorac. Dis. 2, 100–110.
Marty, M., Cognetti, F., Maraninchi, D., Snyder, R., Mauriac, L., Tubiana-Hulin, M., Chan, S., Grimes, D., Antón, A., Lluch, A., Kennedy, J., O'Byrne, K., Conte, P., Green, M., Ward, C., Mayne, K., Extra, J.-M., 2005. Randomized phase II trial of the efficacy and safety of trastuzumab combined with docetaxel in patients with human epidermal growth factor receptor 2-positive metastatic breast cancer administered as first-line treatment: the M77001 study group. J. Clin. Oncol. Off. J. Am. Soc. Clin. Oncol. 23, 4265–4274. https://doi.org/10.1200/JCO.2005.04.173.
Nassar, A., Sexton, D., Cotsonis, G., Cohen, C., 2008. Survivin expression in breast carcinoma: correlation with apoptosis and prognosis. Appl. Immunohistochem. Mol. Morphol. AIMM 16, 221–226. https://doi.org/10.1097/PAI.0b013e3180c317bc.
Perillo, E., Hervé-Aubert, K., Allard-Vannier, E., Falanga, A., Galdiero, S., Chourpa, I., 2017. Synthesis and in vitro evaluation of fluorescent and magnetic nanoparticles functionalized with a cell penetrating peptide for cancer theranosis. J. Colloid Interface Sci. 499, 209–217. https://doi.org/10.1016/j.jcis.2017.03.106.
Santos, S.B., Sousa Lobo, J.M., Silva, A.C., 2019. Biosimilar medicines used for cancer therapy in Europe: a review. Drug Discov. Today 24, 293–299. https://doi.org/10.1016/j.drudis.2018.09.011.
Slamon, D.J., Godolphin, W., Jones, L.A., Holt, J.A., Wong, S.G., Keith, D.E., Levin, W.J., Stuart, S.G., Udove, J., Ullrich, A., 1989. Studies of the HER-2/neu proto-oncogene in human breast and ovarian cancer. Science 244, 707–712.
Slavoff, S.A., Saghatelian, A., 2012. Discovering ligand-receptor interactions. Nat. Biotechnol. 30, 959–961. https://doi.org/10.1038/nbt.2373.
Steinhauser, I., Spänkuch, B., Strebhardt, K., Langer, K., 2006. Trastuzumab-modified nanoparticles: optimisation of preparation and uptake in cancer cells. Biomaterials 27, 4975–4983. https://doi.org/10.1016/j.biomaterials.2006.05.016.
Swain, S.M., Baselga, J., Kim, S.-B., Ro, J., Semiglazov, V., Campone, M., Ciruelos, E., Ferrero, J.-M., Schneeweiss, A., Heeson, S., Clark, E., Ross, G., Benyunes Cortés, M.C.J., CLEOPATRA Study Group, 2015. Pertuzumab, trastuzumab, and docetaxel in HER2-positive metastatic breast cancer. N. Engl. J. Med. 372, 724–734. https://doi.org/10.1056/NEJMoa1413513.
Tatiparti, K., Sau, S., Kashaw, S.K., Iyer, A.K., 2017. siRNA Delivery Strategies: A Comprehensive Review of Recent Developments. Nanomater. Basel Switz. 7. https://doi.org/10.3390/nano7040077.
Veiseh, O., Kievit, F.M., Fang, C., Mu, N., Jana, S., Leung, M.C., Mok, H., Ellenbogen, R.G., Park, J.O., Zhang, M., 2010. Chlorotoxin bound magnetic nanovector tailored for cancer cell targeting, imaging, and siRNA delivery. Biomaterials 31, 8032–8042. https://doi.org/10.1016/j.biomaterials.2010.07.016.
Verma, S., Miles, D., Gianni, L., Krop, I.E., Welslau, M., Baselga, J., Pegram, M., Oh, D.-Y., Diéras, V., Guardino, E., Fang, L., Lu, M.W., Olsen, S., Blackwell, K., EMILIA Study Group, 2012. Trastuzumab emtansine for HER2-positive advanced breast cancer. N. Engl. J. Med. 367, 1783–1791. https://doi.org/10.1056/NEJMoa1209124.
Wang, T., Shigdar, S., Shamaileh, H.A., Gantier, M.P., Yin, W., Xiang, D., Wang, L., Zhou, S.-F., Hou, Y., Wang, P., Zhang, W., Pu, C., Duan, W., 2017. Challenges and opportunities for siRNA-based cancer treatment. Cancer Lett. 387, 77–83. https://doi.org/10.1016/j.canlet.2016.03.045.
Yang, Z., Duan, J., Wang, J., Liu, Q., Shang, R., Yang, X., Lu, P., Xia, C., Wang, L., Dou, K., 2018. Superparamagnetic iron oxide nanoparticles modified with polyethylenimine and galactose for siRNA targeted delivery in hepatocellular carcinoma therapy. Int. J. Nanomedicine 13, 1851–1865. https://doi.org/10.2147/IJN.S155537.

Sanaa BEN DJEMAA

Nanovectorisation de siRNA pour le traitement du cancer du sein triple négatif

Résumé

Dans l'optique d'améliorer le traitement du cancer du sein triple négatif (CSTN), les objectifs de ces travaux de thèse sont : i) d'optimiser la formulation d'un nanovecteur de siRNA fonctionnalisé par un peptide membranotrope (CS-MSN) pour augmenter son efficacité de transfection et pour avoir des caractéristiques compatibles avec une administration par voie systémique, ii) étudier ses voies d'internalisation et son trafic et devenir intracellulaire et iii) valider son efficacité sur un modèle cellulaire de CSTN. L'optimisation de la formulation des CS-MSN a abouti à un nanovecteur d'une taille d'environ 170 nm avec une charge de surface légèrement positive. Les CS-MSN ont montré une capacité à protéger les siRNA contre la dégradation en présence de sérum sans toxicité remarquable sur les cellules. L'entrée des CS-MSN dans les cellules est augmentée par la présence du peptide gH625 à leur surface et elle implique une voie d'endocytose clathrines et cavéoles dépendante. Les CS-MSN ont montré une capacité à échapper à la dégradation par les vésicules endo-lysosomales, cet échappement étant facilité par la présence du peptide gH625. Cet échappement résulte en une inhibition de 73 % de l'expression de la protéine GFP et une réduction significative de l'ARNm et de la protéine Bcl-xL.

Mots clés : nanovecteur, siRNA, transfection, trafic intracellulaire, peptide gH625, polymères

Abstract

In order to improve the treatment of triple negative breast cancer (TNBC), the objectives of this work are: i) to optimize the formulation of a siRNA nanovector (CS-MSN) functionalized by a cell-penetrating peptide to increase its transfection efficiency and to obtain features compatible with a systemic administration, ii) to investigate its internalization mechanisms and pathways and its intracellular trafficking and iii) to validate its efficiency on a TNBC cell model. The optimization of CS-MSN formulation resulted in a nanovector with a size of about 170 nm with a slightly positive surface charge. CS-MSN showed an ability to protect siRNA against degradation in the presence of serum without remarkable cell toxicity. The entry of CS-MSN in cells is enhanced by the presence of the membranotropic peptide gH625 on their surface and involves clathrin- and caveolae-mediated endocytosis pathway. CS-MSN showed an ability to escape degradation in endo-lysosomal vesicles, facilitated by the gH625 peptide. This endosomal escape results in 73% of inhibition of the GFP protein expression and a significant reduction of Bcl-xL mRNA and protein.

Keywords: nanovecteor, siRNA, transfection, intracellular trafficking, gH625 peptide, polymers